

DOTTORATO DI RICERCA IN
Area del farmaco e trattamenti innovativi

CICLO XXXIV

COORDINATORE Prof.ssa Ghelardini Carla

*Application of Quality by Design and innovative
technologies to the production and control of
pharmaceutical dosage forms*

Settore Scientifico Disciplinare CHIM/09

Dottorando

Dott.ssa Biagi Diletta

Diletta Biagi

Tutore

Prof.ssa Mura Paola Angela

Paola Mura

Coordinatore

Prof.ssa Ghelardini Carla

Carla Ghelardini

Anni 2018/2021

The current work was carried out during the three years of Research Doctorate in “Area of Drugs and Innovative Treatments”, Curriculum in “Pharmaceutical Sciences”, with a scholarship funded by A. Menarini M.L.S., Florence, Italy.

This work is the result of collaboration between the Pharmaceutical Technology Laboratory of the University of Florence, under the supervision of Prof. Paola Mura and the Pharmaceutical Technology Laboratory of A. Menarini M.L.S., Florence, under the supervision of Dr. Maurizio Valleri.

The presented project consisted in the application of Quality by Design (QbD) and its principles to the manufacturing process of bilastine tablets. Most of the experimental and research work was performed at the Pharmaceutical Technology Laboratory of A. Menarini M.L.S., which is endowed of all necessary equipment and software.

The manufacturing process of bilastine tablets has already been developed and it is currently used for manufacturing of commercial product. The present work was not aimed at criticizing the previous process development; rather, it was intended to acquire an increased knowledge and understanding, in order to better control the steps of the process and to assure a constant quality of the final product.

More and more often international authorities call for a change in the product design. In particular, the concept that quality should not be *tested* in the final product, but should be *built-in* can be accomplished following the QbD philosophy.

During this work, innovative tools have been employed for process monitoring and quality control. In particular, the NIR technology has been widely applied as fast, simple, real time and non-destructive analysis.

Contents

1. INTRODUCTION ABOUT QUALITY	1
1.1 ICH Guidelines	2
1.1.1 Quality by Design (QbD)	3
1.1.2 Quality Risk Management (ICH Q9).....	7
1.1.3 Design of Experiment (DoE).....	8
1.2 Process Analytical Technology (PAT)	12
1.2.1 Principles	12
1.2.2 PAT tools.....	13
References	15
2. NIR SPECTROSCOPY	19
2.1 Fundamentals and theory	21
2.2 Instrumentation.....	24
2.3 Chemometrics.....	27
2.3.1 Generalities.....	27
2.3.2 Development of a NIR-based analytical method.....	27
References	34
3. MANUFACTURING PROCESS.....	37
3.1 Powder mixing.....	38
3.1.1 Mixing mechanism.....	38
3.1.2 Mixing evaluation	39
3.2 Tableting	43
3.2.1 Tableting mechanism and physics of compression	43
3.2.2 Mathematical description of physics of compression.....	45
3.3 Tablet coating	54
3.3.1 Tablet coating mechanism.....	54
3.3.2 Tablet coating evaluation and controls	55
3.4 Tablet controls.....	57
References	61
4. BILASTINE CASE STUDY	67
4.1. INTRODUCTION	68
4.1.1 Case study presentation	68
4.1.2 Tablet's characteristics	68
4.1.3 Bilastine manufacturing process	69

4.2. MATERIALS AND METHODS.....	71
4.2.1 Materials.....	71
4.2.2 Instruments and Methods.....	71
4.2.2.1 MicroNIR spectral acquisitions.....	71
4.2.2.2 Mixing process.....	72
4.2.2.3 Tableting process.....	72
4.2.2.4 Coating process	73
4.2.2.5 Data elaboration.....	74
4.3. RESULTS AND DISCUSSION	75
4.3.1 Process Risk Assessment	75
4.3.2 Analytical methods development and control strategy definition	81
4.3.2.1 NIR analytical method for mixing monitoring: Moving Block of Standard Deviation	83
4.3.2.2 NIR analytical method for drug assay determination in mixture	85
4.3.2.3 NIR analytical method for drug assay determination in tablets.....	93
4.3.2.4 NIR analytical method for tablet crushing strength determination.....	100
4.3.2.5 NIR analytical method for coating process monitoring.....	105
4.3.3 Study of the process	109
4.3.3.1 Mixing	109
4.3.3.2 Tableting.....	120
4.3.3.3 Coating.....	130
Conclusions.....	133
References.....	134
5. DEXKETOPROFEN TROMETAMOL PROJECT.....	136
References.....	146

1. INTRODUCTION ABOUT QUALITY

1.1 ICH Guidelines

The International Council for Harmonisation of Technical Requirements for Pharmaceuticals for Human Use (ICH) is a non-profit association whose mission is *“to achieve greater harmonisation worldwide to ensure that safe, effective, and high quality medicines are developed and registered in the most resource-efficient manner”*¹. During past years, an always increasing number of countries realised the need of having an organization capable of evaluating the safety, quality and efficacy of medicinal product. Such evaluation should have been independent from the national regulations, but equally accepted by different nations. The need of an independent organization came up because of the expansion and internationalization of pharmaceutical market. In fact, the globalization of pharmaceutical market clashed with the different requirements, imposed by each country. Such situation obliged to repeat test procedures, with loss of time and money, when selling a product in a new country. It was, therefore, necessary to harmonise the regulations required for product commercialization².

European Community started to harmonise regulatory requirements since 1980s, as the concept of “international product” came up, but ICH was officially founded in 1990, by regulatory agencies and authorities of Europe, US and Japan. The ICH Steering Committee divided the topics selected for harmonisation into Safety, Quality and Efficacy, which are the three basic criteria, for authorising the commercialisation of new pharmaceutical products. Therefore, the ICH guidelines are mainly divided into the three categories of Quality (Q), Safety (S) and Efficacy (E); an additional fourth category exists, which is called “Multidisciplinary (M)” and contains those guidelines that do not fit uniquely to one of the previous three main categories. The guidelines divided into four categories are reported in Table 1.

Efficacy Guidelines		Quality Guidelines	
E1	Clinical Safety for Drugs used in Long-Term Treatment	Q1A-Q1F	Stability
E2A-E2F	Pharmacovigilance	Q2	Analytical Validation
E3	Clinical Study Reports	Q3A-Q3E	Impurities
E4	Dose-Response Studies	Q4A-Q4B	Pharmacopoeias
E5	Ethnic Factors	Q5A-Q5E	Quality of Biotechnological Products
E6	Good Clinical Practice	Q6A-Q6B	Specifications
E7	Clinical Trials in Geriatric Population	Q7	Manufacturing Practice
E8	General Considerations for Clinical Trials	Q8	Pharmaceutical Development
E9	Statistical Principles for Clinical Trials	Q9	Quality Risk Management
E10	Choice of Control Group in Clinical Trials	Q10	Pharmaceutical Quality System
E11-E11A	Clinical Trials in Pediatric Population	Q11	Development and Manufacturing of Drug Substances
E12	Clinical Evaluation by Therapeutic Category	Q12	Lifecycle Management
E14	Clinical Evaluation of QT	Q13	Continuous Manufacturing of Drug Substances and Drug Products
E15	Definition in Pharmacogenetics/Pharmacogenomics	Q14	Analytical Procedure Development
E16	Qualification of Genomic Biomarkers		
E17	Multi-Regional Clinical Trials		
E18	Genomic Sampling		
E19	Safety Data Collection		
E20	Adaptive Clinical Trials		
Safety Guidelines		Multidisciplinary Guideline	
S1A-S1C	Carcinogenicity Studies	M1	MedDRA Terminology
S2	Genotoxicity Studies	M2	Electronic Standards
S3A-S3B	Toxicokinetics and Pharmacokinetics	M3	Nonclinical Safety Studies
S4	Toxicity Testing	M4	Common Technical Document
S5	Reproductive Toxicology	M5	Data Elements and Standards for Drug Dictionaries
S6	Biotechnological Products	M6	Gene Therapy
S7A-S7B	Pharmacology Studies	M7	Mutagenic impurities
S8	Immunotoxicology Studies	M8	Electronic Common Technical Document (eCTD)
S9	Nonclinical Evaluation for Anticancer Pharmaceuticals	M9	Biopharmaceutics Classification System-based Biowaivers
S10	Photosafety Evaluation	M10	Bioanalytical Method Validation
S11	Nonclinical Paediatric Safety	M11	Clinical electronic Structured Harmonised Protocol (CeSHaP)
S12	Non-clinical Biodistribution Considerations for Gene Therapy Products	M12	Drug Interaction Studies
		M13	Bioequivalence for Immediate-Release Solid Oral Dosage Forms

Table 1 – List of ICH Guidelines, divided into categories of Quality (Q), Safety (S), Efficacy (E), and Multidisciplinary (M).

A new paradigm for product quality can be found into the Quality guidelines. This new systematic and science-based approach is called Quality by Design (QbD) and its principles are mainly exposed in guidelines Q8³, Q9⁴ and Q10⁵. These three guidelines are complementary to each other⁶. ICH Q8 is focused on QbD pharmaceutical development; ICH Q9 is focused on Quality Risk Management (QRM), which is a basic tool for an effective QbD development, but, in turn, QRM uses results of experiments performed during the pharmaceutical development itself. Moreover QRM gives guidance about tools and principles for effective risk-based decisions about the quality, throughout the product lifecycle; therefore, “*QRM is integral to an effective pharmaceutical quality system*”⁵. ICH Q10 is focused on the aforementioned Pharmaceutical Quality System (PQS) and it gives instructions for the management of a quality system throughout the lifecycle of a product; QRM gives guidance about changes within the design space. From previous explanation, it can be concluded that all the three guidelines are at the base of the QbD approach. Nadpara et al., 2012⁷, graphically represented this founding relationship (Figure 1).

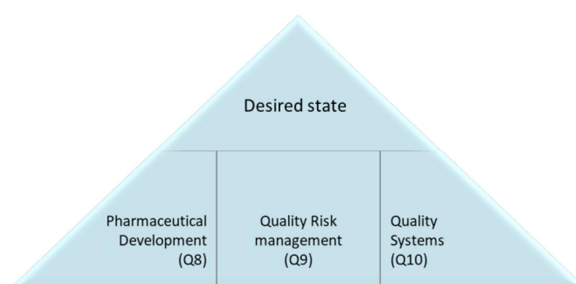


Figure 1 – ICH guidelines are at the base of Quality by Design. Picture inspired by Nadpara et al., 2012⁷.

1.1.1 Quality by Design (QbD)

In recent years the QbD principles reported in ICH guidelines have been more and more used. The aim of QbD is to build the quality into the product from the beginning of its pharmaceutical development, instead of testing it into the product. The product and its manufacturing process are designed to meet a predefined quality and to maintain it, throughout the product lifecycle. In doing so, QbD needs to investigate and understand the effect of the formulation and the process, on the quality of the final product; all the available knowledge (prior knowledge or results of Design of Experiment studies), the knowledge management (reported in ICH Q10) and the QRM are used with this purpose. QbD process development follows some steps, which are illustrated in Figure 2.

- 1- Defining the Quality Target Product Profile (QTPP), i.e. all the characteristics of the final product. QTPP is defined as “*a perspective summary of the quality characteristics of a drug product that ideally will be achieved to ensure the desired quality, taking into account safety and efficacy of the drug product*”³. As the Food and Drug Administration (FDA)⁸ said: “*by beginning with the end in mind, the result of development is a robust formulation and manufacturing process with a control strategy that ensures the performance of the drug product*”. In fact, the QTPP is the basis for the design of quality, during development. As reported by ICH Q8³, the QTPP should include elements such as the intended clinical use, route of administration, delivery systems, dosage form, dosage strength, container closure system, information about pharmacokinetic and drug product quality criteria. However, the elements of QTPP depend on the pharmaceutical form. The QTPP is not the same as product specification; in fact, QTPP includes elements not part of product specification and vice versa. The QTPP should include elements relevant for patients⁹



Figure 2 – Steps for a QbD development approach.

2- Identifying the potential Critical Quality Attribute (CQAs), i.e. the final product properties which could have an impact on QTPP. CQAs are defined as *“a physical, chemical, biological or microbiological property or characteristic that should be within an appropriate limit, range, or distribution to ensure the desired product quality. CQAs are generally associated with the drug substance, excipients, intermediates (in-process materials) and drug product”*³. Every CQA has got a range of acceptable values; if the CQAs do not respect those values, the target is not reached and the product is not a quality product. A CQA is an attribute which directly affects the product quality, or affects another CQA of the product.

3- Performing a risk analysis. The QTPP and the prior knowledge are fundamental to define an initial list of CQAs. The more relevant CQAs are then evaluated, following a priority criterion.

A CQA with a greater impact on the safety and efficacy is more

critical to quality; in fact, as reported by the FDA⁸, *“The identification of a CQA from the QTPP is based on the severity of harm to a patient, should the product fall outside the acceptable range for that attribute”*.

- 4- Determining the Critical Material Attributes (CMAs) and the Critical Process Parameters (CPPs) i.e. attributes of the input materials and process parameters that could have an effect on CQAs. They should be controlled, to achieve the required product quality. CMAs and CPPs identification is carried out with an early risk assessment evaluation, which is a science-based tool of the QRM. As new knowledge is gained, the risk assessment evaluation can be repeated and updated. A robust process is able to give a quality product and it is tolerant to CMAs and CPPs variability, at the same time. Therefore, CMAs and CPPs values are varied to evaluate their robustness and their possible effect on CQAs. From this kind of studies, the CPPs and CMAs that really affect product quality are identified and the limits, within which the quality of the product is assured, are established.
- 5- Determining the design space, by finding a link between CMAs and CQAs, and between CPPs and CQAs. The relationship between the process inputs (material attributes and process parameters) and the critical quality attributes is described by the design space. The design space is the *“multidimensional combination and interaction of input variables (e.g. material attributes) and process parameters that have been demonstrated to provide assurance of quality”*³. Design of Experiment (DoE) is a widely used tool to study the relationship between inputs and CQAs, and to define the design space. An individual design space can be defined for each unit operation of a process, or a single design space can be defined for the entire process. The first case is easier to perform, but the second one provides a wider flexibility.
- 6- Defining a control strategy, to ensure the consistent production of a product, with the required quality. The comprehension of product and process is the basis for the control strategy: *“sources of variability that can impact product quality should be identified, appropriately understood, and subsequently controlled”*³. The comprehension of the variability sources and their consequences on the final quality gives the opportunity to shift controls, directly at the sources of variability; it also allows the use of alternative methods to perform controls, such as real time control, which can support the Real Time Release Testing (RTRT). The RTRT would ideally replace the traditional end-product testing, by

monitoring the quality from the beginning of the process. However, the control strategy can include different controls approaches at the same time: *“one element of the control strategy could rely on end-product testing, whereas another could depend on real-time release testing”*³. An efficient control strategy includes:

- the control of input material attributes and unit operations, that have an impact on downstream;
- the definition of product specifications;
- the in-process controls and real time release testing;
- a program of monitoring.

QbD has two fundamentals: the product knowledge and the process understanding. The first one is made of prior knowledge and acquisition of new data and experience about the product performance. The whole knowledge is rationalized with the application of two instruments: DoE and QRM. They are the connection between product knowledge and process understanding, in both directions: they use the knowledge to reach a deep process understanding and, at the same time, extrapolate new knowledge from it (the process understanding). Only with a deep process understanding it is possible to define a design space and apply a really effective control strategy, which uses in-process controls and lead to a robust process. Such a greater understanding concretizes in a higher regulatory flexibility, always keeping in mind that the more is the knowledge, the more flexible can be the regulatory approach. In fact, as the ICH Q8 states, *“working within the design space is not considered as a change. Movement out of the design space is considered to be a change”*³; this makes perfect sense, considering that the design space can be defined only if a certain level of knowledge is gained.

The QbD process development envisages an effective control strategy. Knowing a process also means to know all the sources of variability that could have an impact on the product quality. The carried out control strategy allows to identify, understand and control the variability sources. In particular, if the effect of certain variability downstream is well known, an opportunity exists to shift controls upstream, reducing the importance of end product testing. In fact, the final goal of QbD development consists in designing adaptive process steps, i.e. responsive to the input variability, so to guarantee a consistent product quality. This requires an appropriate process controls strategy, based on in-process controls. An in-process control, in fact, can constantly monitor the process performance in real time, ensuring that it is as expected and predicted by the design space. If a deviation from the expected performance occurs, it is immediately seen and corrected, by adjusting the process parameters; the quality of final product is thus kept constant.

“The aim of pharmaceutical development is to design a quality product and its manufacturing process” – says ICHQ8³, and this can be reached with both, a traditional empirical and a more systematic, science-based QbD approach. The objective of the traditional approach is to have a reproducible process, which gives the same quality product every time that it is performed. In order to get it, all the process parameters and the input characteristics must be rigidly fixed. The quality control system checks the quality mainly on the final product, by checking its quality against the approved specifications. It turns out if the product has the right quality or not, only at the end of the process. If the quality does not meet the specifications (out-of-specification at batch testing), the batch must be rejected or reworked; this requires an effort of resources, time and money. This traditional approach is called Quality by Testing (QbT)⁹. QbD stands as an alternative to this traditional approach. Instead of fixing the whole process, it is possible to define a design space, which is the multidimensional combination and interaction of input variables (e.g. material attributes) and process parameters, which have been demonstrated to provide assurance of quality. Moreover, QbD controls are performed at different levels and this makes it possible to perfectly control the particular noise that always comes into the process, but never in the same way. When the

variability input is known, understood and controlled, the process is robust, which means flexible and responsive to input materials. A robust process always gives the same reproducible quality product. However, having a reproducible quality does not mean having a reproducible process too; in fact, a reproducible process is always the same, it is fixed and it has, for example, a time-defined end-point. In case of robust process, the end-point would, rather, be based on the time requested to reach the predefined quality¹⁰. A robust process is possible because of the different control approach of QbD. Controls at the end of the process are replaced by controls made directly at the source of variability, which means by in-process control. Such type of control uses the data generated during the process, to control and monitor the process itself; this new control approach is called Process Analytical Technology (PAT), and it is consistent with the idea that quality cannot be tested into products, but rather should be built-in or should be by design¹⁰.

In conclusion, the QbD pharmaceutical development differs from a more traditional approach on some points, bringing numerous advantages. A comparison of the two possible approaches is proposed in the Appendix 1 of the ICH Q8³ and it is reported below (Table 2). It is important to underline that, in the pharmaceutical industry a middle ground between this two approaches is often used.

Aspect	Minimal Approaches	Enhanced, Quality by Design Approaches
Overall Pharmaceutical Development	<ul style="list-style-type: none"> • Mainly empirical • Developmental research often conducted one variable at a time 	<ul style="list-style-type: none"> • Systematic, relating mechanistic understanding of material attributes and process parameters to drug product CQAs • Multivariate experiments to understand product and process • Establishment of design space • PAT tools utilised
Manufacturing Process	<ul style="list-style-type: none"> • Fixed • Validation primarily based on initial full-scale batches • Focus on optimisation and reproducibility 	<ul style="list-style-type: none"> • Adjustable within design space • Lifecycle approach to validation and, ideally, continuous process verification • Focus on control strategy and robustness • Use of statistical process control methods
Process Controls	<ul style="list-style-type: none"> • In-process tests primarily for go/no go decisions • Off-line analysis 	<ul style="list-style-type: none"> • PAT tools utilised with appropriate feed forward and feedback controls • Process operations tracked and trended to support continual improvement efforts post-approval
Product Specifications	<ul style="list-style-type: none"> • Primary means of control • Based on batch data available at time of registration 	<ul style="list-style-type: none"> • Part of the overall quality control strategy • Based on desired product performance with relevant supportive data
Control Strategy	<ul style="list-style-type: none"> • Drug product quality controlled primarily by intermediates (in-process materials) and end product testing 	<ul style="list-style-type: none"> • Drug product quality ensured by risk-based control strategy for well understood product and process • Quality controls shifted upstream, with the possibility of real-time release testing or reduced end-product testing
Lifecycle Management	<ul style="list-style-type: none"> • Reactive (i.e., problem solving and corrective action) 	<ul style="list-style-type: none"> • Preventive action • Continual improvement facilitated

Table 2 – Comparison between a QbD and a more traditional approach. Source of the table: Appendix 1 of ICH Q8³.

1.1.2 Quality Risk Management (ICH Q9)

Quality Risk Management (QRM) is defined in ICH Q9⁴ as: “a systematic process for the assessment, control, communication and review of risks to the quality of the drug (medicinal) product across the product lifecycle”. Risk is defined as “the combination of the probability of occurrence of harm and the severity of that harm”. However, different counterparts involved in pharmaceutical business could perceive different potential harms and attribute different probability or severity to the same harm. When using a pharmaceutical product, there is always a degree of risk involved; the overall risk has many components, one of which is the risk to quality. The aim of QRM is to guarantee a product quality, by identifying and controlling potential risks to quality (preventive action) and also facilitating the decision making, when an issue arises (reactive action). QRM is based on two principles: the risk evaluation should be based on scientific knowledge, and the general behaviour respect to the considered risk should be proportional to its level. The ICH Q9 presents a schematic view of the QRM elements, as reported in Figure 3.

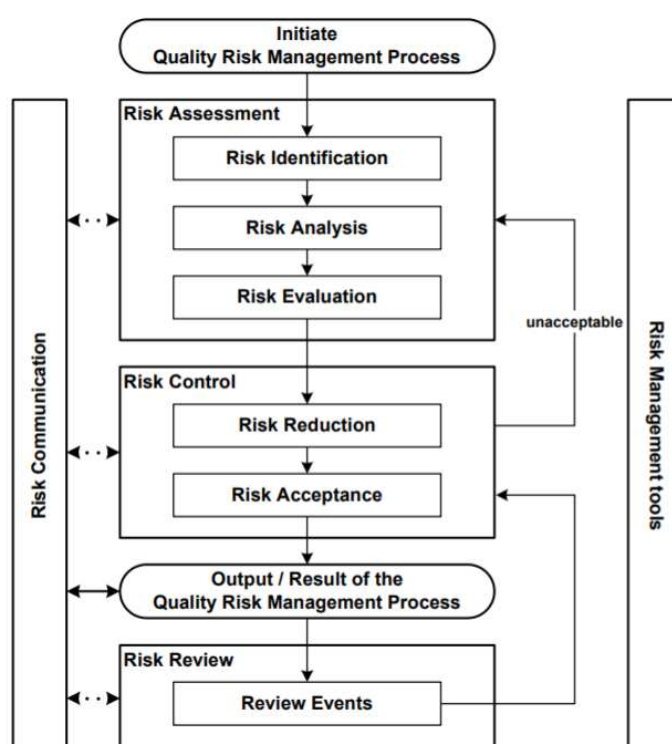


Figure 3 – Schematic representation of a QRM process. Source of figure: ICH Q9⁴.

At the beginning of a QRM process the objective of the investigation must be defined, all the available information and data should be collected, and the necessary resources and time should be decided.

1. Risk Assessment: it “consists of the identification of hazard and the analysis and evaluation of risks associated with exposure to those hazards”. To clearly define the risk, it should be asked: what could go wrong and what are the probability and the severity that it will go wrong. The risk assessment includes: 1) the use of knowledge, to identify the hazards (risk identification), 2) the evaluation of the risk related to the hazard, in terms of probability of occurrence and severity of harm (risk analysis) and 3) comparison of the risk, previously identified and analysed, against predefined criteria (risk evaluation). When performing the risk assessment, it is important to be confident with data and have robust data; in fact, where there is uncertainty, there could be an unexpected variability. Such unexpected variability is due to the process variability, or to a lack of

knowledge. The result of the risk assessment can be provided as a quantification of the risk (as numerical probability) or as a qualitative description (with qualitative descriptors “low”, “medium” and “high”; or with a score of risk, when making a risk ranking).

2. Risk Control: it *“includes decision making to reduce and/or accept risks”*. When a risk is known and has been analysed, there are two possibilities: reducing the risk to an acceptable level, or accepting the risk. Risk reduction is aimed at reducing the probability of risk occurrence, or the severity of the consequences, when the risk happens. When reducing a risk, attention should be paid, as new risks could be introduced, or pre-existing ones could increase in significance. The risk can also be accepted with a formal acceptance, if the risk or the residual risk is well known, or with a passive acceptance; in the latter case, a risk with a low detectability is not known, not evaluated and consequently, passively accepted.
3. Risk Communication: it is fundamental, among the involved counterparts, along all the risk management process.
4. Risk Review: it is important to regularly review the output of the QRM process, in particular, when new knowledge and experience are gained.

QRM principles are applied to development, manufacturing, distribution, inspection and submission/review of a process, through its entire lifecycle.

1.1.3 Design of Experiment (DoE)

It would be difficult to establish a design space with the traditional on-factor-at-a-time (OFAT) approach, as the pharmaceutical development is complex and multivariate in nature. QbD requires to find relationship among the CQAs and the multi-level factors of process and formulation (as previously explained in section 1.1.1. This cannot be done with an OFAT approach. A multivariate approach, such as DoE, is perfect, instead: *“DoE is systematic cost effective tool to rationalize the effect of input variables on the product quality attributes by reducing the number of experiments”*¹¹. As Montgomery states, in his book¹², *“experiments are used to study the performance of processes and systems”*.

A process (graphically represented in Figure 4) transforms the inputs into an output. The process has got some parameters, which can be modulated, thus changing the output characteristics too. Their variation is controllable, as they can be arbitrarily set to known values (or levels); these are called controllable factors, or variables (x_1, x_2, \dots, x_n). At the same time, every process has got some uncontrollable factors or variables (z_1, z_2, \dots, z_n), which bring an unexpected and uncontrolled variability.

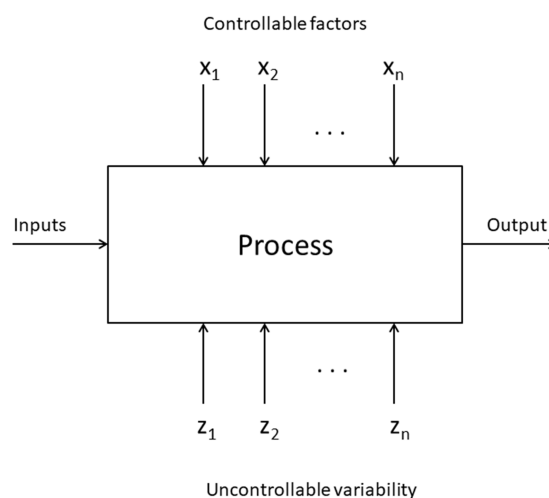


Figure 4 – Scheme of a generic process. Figure inspired by Montgomery, 2001¹².

In order to know the process performance, it is necessary to study the relationship between the process parameters and the output characteristics. The DoE is a valuable tool to gain this knowledge. In fact, its objectives are 1) to determine which are the factors mainly affecting the output characteristics and 2) how do they affect the output characteristics. By exploiting the OFAT strategy it is possible to investigate all the factors singularly, but by doing so the interactions among factors would not be taken into consideration. A more efficient strategy would be following a design, which “consists of a series of experiments performed under different conditions”¹³. For example, a factorial design could be planned, by simultaneously varying factors. The second strategy is properly a DoE strategy. Let’s imagine to perform a mixing process, in order to obtain a homogenous mixture. Let’s assume the main process parameters affecting the powder homogeneity are the mixing time and the mixing speed. Before to start the experiments, the factor’s values (or levels) to be studied are selected. Following an OFAT approach, the two factors are singularly changed and the output characteristic is measured for every level variation. Two distinct relationships are obtained, between the process parameters and the output characteristic, as reported in Figure 5a. Performing a factorial experiment, the factors are simultaneously changed on their levels. In the considered examples, as there are two factors changed on two different levels, a 2^2 factorial design is performed. The relationship obtained from this factorial strategy is graphically represented in Figure 5b. With the same number of experiments a different space is investigated.

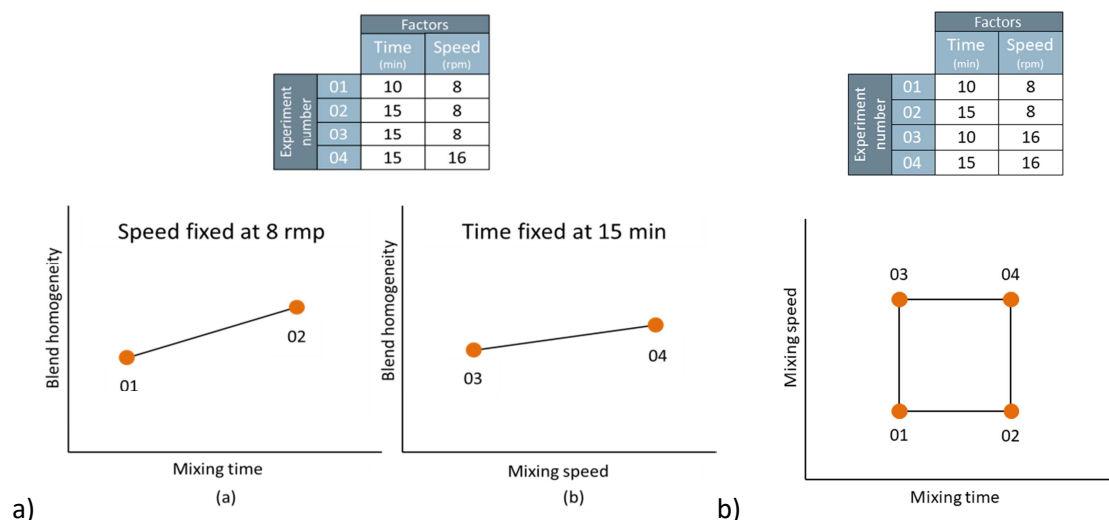


Figure 5 – OFAT approach for powder mixing process (a). Factorial experiments for powder mixing process (b).

The DoE approach starts with the definition of a final goal: screening, optimisation, saving time, quantitative modelling, etc. As it will be further explained, the type of design will be selected on the base of the objective. Then the DoE approach continues, with the following reported steps.

Responses and variables selection

Each manufacturing operation has many input variables affecting the output quality (CQAs). It is not possible to experimentally investigate all of them; for that reason, at this stage, the use of prior experience and prior knowledge and an effective risk management is of fundamental relevance, to identify the input factors that really are critical to output quality. The more critical input variables are, then, investigated with DoE. A factor can be discrete, if it assumes only some values, or continuous, if it can assume all the possible values in a certain interval. For each factor, the range of variation must be defined, as well as the specific values (or levels), that those factor will assume during experiments. 2 levels are used to study a linear relationship, while 3 levels are necessary to study a quadratic relation, in a surface design. At the same

time, the responses of the design, i.e. the product characteristics to be measured, should be selected. An acceptable range of values should be also defined for them. Often, the average and the standard deviation of a measured output characteristic is used as response¹².

Experimental strategy definition and model selection

When planning experiments different types of design can be chosen, depending on the final goal of the DoE. The full factorial design is generally used for screening purpose, to distinguish between significant and not significant factors. A full factorial design allows to study the effect of all the factors, on the product characteristics (the responses); it also allows to study the effect of the first level interactions, between factors. However, a full factorial often requires a large amount of experiments. It is possible to systematically reduce the number of experiments by 1/2, 1/4, 1/8, etc., with the fractional factorial design. Both, the full factorial and the fractional factorial designs, thus far taken into consideration, have a number of experiments equal to a power of two, as they refer to two levels. Such constrain is overcome by the Plackett-Burman and the Taguchi design, which allow to study n factors by performing $n+1$ experiments. These types of design are often used for screening. In fact, as they allow to study a big number of factors, with relatively few experiments, only the main single effect are clearly distinguished; the interactions are confounded instead. When the DoE is performed for optimisation purpose, it is important to provide a more detailed model. The central composite design (or response surface design) is often selected in this case. It provides information on squared terms and interaction, and often requires to replicate some experimental points, thus giving a more detailed model. To estimate the square terms, three levels are required for each factor; while the replicates are used to estimate the experimental error. Other particular type of design can be selected, such as the mixture design, which is used when the value of each factor is constrained by the value of the other factors. This happens when the total sum of the factors is a constant sum. A new type of design, often used by the industry environmental, is the D-Optimal design. Its major advantage is the possibility to offer more customized designs, which are alternatives to the standard models. They can be used when there are particular restrictions and constrains, and allows to simultaneously study variables of different types (continuous and category). Optimal designs necessarily require adequate software, as they are computer-generated experiments¹⁴.

Experimental matrix and experimental plan

Once selected the type of design, an experimental matrix is build, where the rows correspond to the experiments and the columns refer to the investigated factors. In the experimental matrix, each value of a factor is coded, with a recognised language: the lower level is coded as a “-1”, the higher level is coded as a “+1”; if there is a central level, it is coded as a “0”. These value do not have any physical or chemical significance, they are only used to identify the factor’s level. It is, therefore, necessary to “translate” this coded language in the real values used during experimentation, thus obtaining the experimental plan (Figure 6).

		Factors	
		Time (min)	Speed (rpm)
Experiment number	01	-1	-1
	02	+1	-1
	03	-1	+1
	04	+1	+1

(a)

		Factors	
		Time (min)	Speed (rpm)
Experiment number	01	10	8
	02	15	8
	03	10	16
	04	15	16

(b)

Figure 6 – Coded experimental matrix (a) and the corresponding experimental plan (b).

Experiment performance and analysis of data

The performance of experiments provides the experimental data, which are used to build a mathematical relationship, or model: $Y=f(X)$ (where Y is the matrix of responses and X is the matrix of factors). Such model describes the mathematical relationship between factors and response, and explains the response change, when changing factors. A typical equation for two factors is following reported:

$y =$	response
$b_0 +$	intercept
$b_1x_1 + b_2x_2 +$	linear terms for each of the two factor
$b_{11}x_1^2 + b_{22}x_2^2 +$	quadratic terms for each factor
$b_{12}x_1x_2 +$	interaction term between factors
ε	experimental error

Once the model is built, it should be evaluated with statistical analysis of the model, in order to verify its ability in predicting the output characteristics, for given factors values. If the model is good, it can be used for prediction. To evaluate the model, for each variable:

- the regression coefficient is calculated;
- the actual vs predicted plot is made;
- the analysis of variance (ANOVA) is performed;
- the statistical analysis of coefficient is performed;
- the response surface are plotted;
- the residual analysis is done.

The DoE is a fundamental tool of QbD. It can be used with different purposes: for screening the most relevant variables affecting the product quality, during a QRM evaluation, or for defining the design space of a process. The raw materials attributes and the process parameters (factors) could be combined in different ways, but only the combinations that allow the CQAs to be within acceptable ranges of values are part of the design space and this is commonly established with a DoE activity¹⁵.

1.2 Process Analytical Technology (PAT)

1.2.1 Principles

Process Analytical Technology (PAT) was formally introduced through the FDA guidance document in 2004¹⁰. It gives its contribute to build the new science-orientated and risk-based paradigm for quality, together with the cGMP for the 21st century¹⁶ and the aforementioned ICH guidelines. This innovative approach is consistent with the idea that *“quality cannot be tested into the product: it should be built-in or should be by design”*¹⁰. PAT is defined by ICH Q8³ as *“A system for designing, analysing, and controlling manufacturing through timely measurements (i.e., during processing) of critical quality and performance attributes of raw and in-process materials and processes with the goal of ensuring final product quality”*. PAT is present in non-pharma industries since many years, while it entered late in pharmaceutical industries, because of the too much rigorous requirements for the manufacturing⁶. However, the ICH, FDA and cGMP’s for the 21st century recommended new technology implementation. The need of eliminating hesitation about innovation was recognised in 2002, when the Pharmaceutical cGMP’s for the 21st Century were launched, by the FDA¹⁶. The use of PAT in pharmaceutical industry is, therefore, strongly increasing^{17,18}. As reported in ICH Q8, the traditional approach ensures quality, by post-production testing. On the contrary, the current approach is based on science and risks evaluation, efficiency planning, real time quality assurance and, therefore, it allows having tailor made regulatory policies. To realise a regulatory flexibility, new knowledge of product performance, manufacturing process options and process parameters are necessary. *“This understanding can be gained by application of, for examples, formal experimental designs, process analytical technology (PAT) and/or prior knowledge”*³. In ICH Q9, Annex II⁴, the PAT is linked to an efficient QRM. In fact, PAT can be used as a tool of QRM, for control of risks. At the same time, QRM, as part of production, is used to evaluate and justify the use of PAT for in-process sampling and testing. As previously reported, PAT is a system for designing, analysing and controlling; therefore, it plays a role at multiple levels: during the development, as a part of QRM and during the whole product lifecycle. It follows that PAT is strictly connected with all the three previously reported ICH guidelines (see section 1.1). It is evident that PAT is a key aspect of QbD, as it increases the knowledge and process understanding, by allowing in-process measurements, alternative to end-product testing. PAT has the advantages of providing fast real time data, without sample preparation, nor sample destruction¹⁹.

The aim of PAT is to build a process so well understood, to assure a predefined quality product, even before to test it. The extreme consequence of a well performed QbD and PAT approach is the RTRT, which consists in evaluating and assuring quality by real time data, continuously acquired during the process. The RTRT, ideally, would eliminate the need of end-product testing. A process can be considered well understood, if all the variability sources are well known, well controlled, and if the quality attributes of the product can be efficiently predicted over the design space. It is possible to make a reliable prediction only if there is knowledge and the more the knowledge, the more accurate the prediction. A general PAT-based control strategy is well depicted by Johansson et al., 2010²⁰ (see Figure 7).

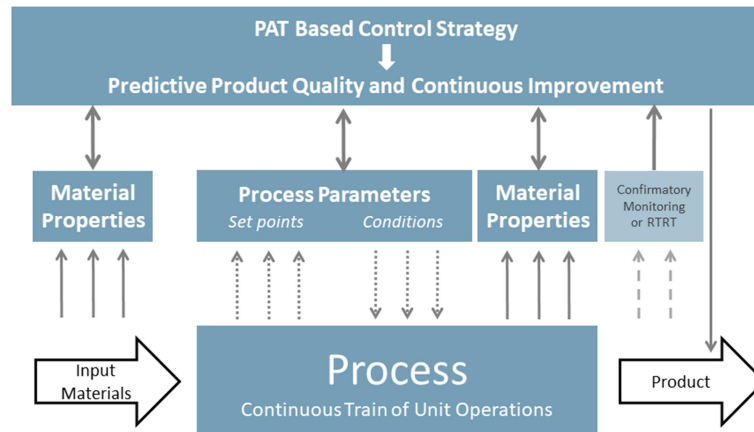


Figure 7 – PAT-based control strategy, in a QbD approach. Figure from Johansson et al., 2010²⁰.

1.2.2 PAT tools

PAT has got many tools to actuate the design, the analysis and the control. They are categorized into four groups¹⁰: 1) multivariate tools for design, data acquisition and analysis, 2) process analysers, 3) process control tools and 4) continuous improvement and knowledge management tools. Each group is used by one of the four main components of PAT²¹, as reported in Figure 8.

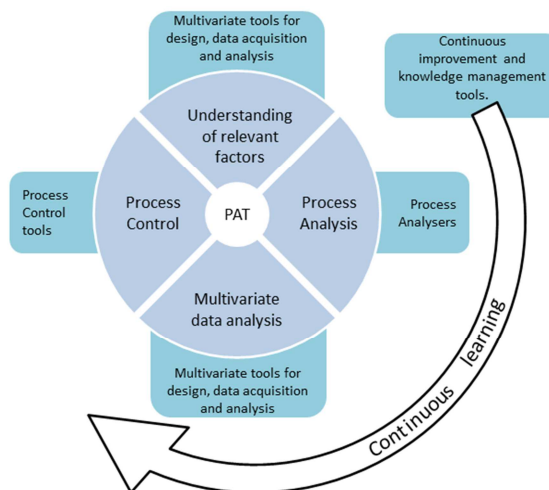


Figure 8 – Four PAT components and four groups of PAT tools. (Figure inspired by Grassi et al., 2018²¹).

- 1) Multivariate tools are necessary to gain the deep knowledge, required for an efficient PAT and QbD approach. The pharmaceutical products and processes are complex system and multi-factorial relationships exist between the inputs (CMAs and CPPs) and the output quality attributes. Only multivariate mathematical approaches have the ability to properly describe and understand such complex systems. The most used multivariate tools are: DoE, response surface methodologies, process simulation and pattern recognition tools.
- 2) Process analysers' origins are related to the petrochemical industry, but they are now rapidly developing in many fields, including the pharmaceutical industry. They are incorporated into processes streams or equipment, to directly monitor the material transformation; thus allowing making real time monitoring possible². A process can be monitored in several ways, by sampling and analysing the sample off-line, at-line and on-line (*operando*), or simply in-line (*in situ*), without sampling (see Figure 9)¹⁸.

- Off-line: a sample is taken from the process and transported to a laboratory, which is physically away from the manufacturing equipment.
- At-line: a sample is taken from the process stream and it is analysed in close proximity of the process equipment.
- On-line: a part of the material under process is diverted from the process via a bypass and it is analysed, with a specialized analyser; afterwards it returns to the process stream.
- In-line: it is not a proper sampling, as the unmodified product under process is measured. The instrument of analysis is able to analyse the material during the manufacturing process, without interfering with it. This particular type of analysis requires being non-destructive.

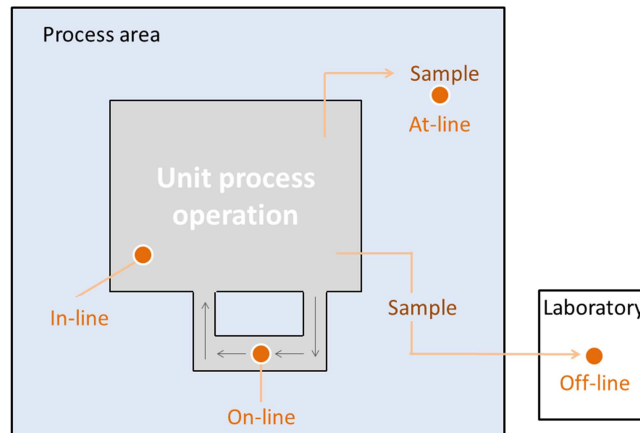


Figure 9 – Different types of controls.

The PAT approach definitely prefers the in-line and on-line analysis, as no manual sampling is required. A continuous real-time measurements is possible, by “*bringing the instrument into the sample*”^{22,23}. In this case, spectroscopic instrumentation (UV-Vis, NIR, MIR and Raman) are the most used process analysers. These kinds of analysis generate a great number of complex and multi-dimensional data, which need to be correctly decoded and interpreted. For this purpose Chemometrics is the tool of choice^{2,24,25}.

- 3) Process control tools. “*Process monitoring and control strategies are intended to monitor the state of a process and actively manipulate it to maintain a desire state*”¹⁰. This automatism of control is possible only if a mathematic relationship exists, that links the measurements of CPPs and CMAs, and the CQA of the final product. The final goal of PAT, in fact, relies on the “*achievement of process endpoint to ensure consistent quality of the output materials and the final product*”¹⁰.
- 4) Continuous improvement and knowledge management tools. Collecting knowledge is fundamental, for the process development and for the control strategy, but it is equally important, to keep collecting data and knowledge throughout all the product lifecycle.

Nowadays PAT has got many applications in pharmaceutical industry, in both, primary manufacturing²⁶ and secondary manufacturing operations¹⁸, such as in hot melt extrusion²⁷, wet granulation²⁸, drying processes²⁹, blending^{30,31} direct compaction tablet manufacturing³² and coating^{33–35}. NIR spectroscopy is the most commonly used process analyser³⁶. The reason of this relies on NIR’s ability of supporting the real-time monitoring of a variety of different quality attributes, such as concentration^{30,31,37–40}, content uniformity⁴¹, homogeneity, residual moisture¹⁷ and physical characteristics, such as blend uniformity^{41–44}, density, powder flow characteristics³⁸ particle size^{17,38}, disintegration time, dissolution, crushing strength⁴⁵ and coating thickness^{17,41}. The NIR technique is deeply explained in chapter 2.

References

- (1) International Council for Harmonisation of Technical Requirements for Pharmaceuticals for Human Use. ICH Harmonisation for better health. <https://www.ich.org/page/mission> (accessed Aug 11, 2021).
- (2) Chew, W.; Sharratt, P. Trends in process analytical technology. *Anal. Methods* **2010**, *2* (10), 1412–1438. <https://doi.org/10.1039/c0ay00257g>.
- (3) ICH Harmonized Tripartite Guideline. Pharmaceutical Development Q8 (R2) [https://database.ich.org/sites/default/files/Q8%28R2%29 Guideline.pdf](https://database.ich.org/sites/default/files/Q8%28R2%29%20Guideline.pdf) (accessed Aug 11, 2021).
- (4) ICH Harmonized Tripartite Guideline. Quality Risk Management Q9 [https://database.ich.org/sites/default/files/Q9 Guideline.pdf](https://database.ich.org/sites/default/files/Q9%20Guideline.pdf) (accessed Aug 11, 2021).
- (5) ICH Harmonized Tripartite Guideline. Pharmaceutical Quality System Q10. <https://database.ich.org/sites/default/files/Q10%20Guideline.pdf> (accessed Aug 11, 2021).
- (6) Karanakov, L.; Tonic-Ribarska, J.; Glavas-Dodov, M.; Trajkovic-Jolevska, S. Analysis and critical review of ICH Q8, Q9 and Q10 from a generic pharmaceutical industry view point. *Maced. Pharm. Bull.* **2012**, *57*, 85–96.
- (7) Nadpara, N. P.; Thumar, R. V.; Kalola, V. N.; Patel, P. B. Quality by Design (QBD): a complete review. *Int. J. Pharm. Sci. Rev. Res.* **2012**, *17* (2), 20–28.
- (8) Food and Drug Administration. Quality by Design for ANDAs: an example for immediate-release dosage forms <https://www.fda.gov/files/drugs/published/quality-by-design-%28QbD%29-for-an-immediate-release.pdf> (accessed Jul 24, 2021).
- (9) Charoo, N. A.; Shamsher, A. A. A.; Zidan, A. S.; Rahman, Z. Quality by design approach for formulation development: a case study of dispersible tablets. *Int. J. Pharm.* **2012**, *423* (2), 167–178. <https://doi.org/10.1016/j.ijpharm.2011.12.024>.
- (10) Food and Drug Administration. *Guidance for Industry, PAT - A Framework for Innovative Pharmaceutical Development, Manufacturing and Quality Assurance*; 2004.
- (11) Mishra, S. M.; Rohera, B. D. An integrated, quality by design (QbD) approach for design, development and optimization of orally disintegrating tablet formulation of carbamazepine. *Pharm. Dev. Technol.* **2016**, *22* (7), 889–903. <https://doi.org/10.1080/10837450.2016.1199566>.
- (12) Montgomery, D. C. *Design and Analysis of Experiments*, 5th edition; John Wiley & Sons, INC., 2001.
- (13) Brereton, R. G. *Chemometrics: Data Analysis for the Laboratory and Chemical Plant*; John Wiley & Sons: Chichester, West Sussex, 2003.
- (14) Johnson, R. T.; Montgomery, D. C.; Jones, B. A. An expository paper on optimal design. *Qual. Eng.* **2011**, *23* (3), 287–301. <https://doi.org/10.1080/08982112.2011.576203>.
- (15) Soans, D.; Chandramouli, R.; Kavitha, A. N.; Roopesh, S. K.; Shrestha, S. Application of design of experiments for optimizing Critical Quality Attributes (CQA) in routine pharmaceutical product development. *J. Pharm. Res.* **2016**, *15* (3), 96–100. <https://doi.org/10.18579/jpcrk/2016/15/3/103041>.
- (16) Food and Drug Administration. Pharmaceutical CGMP's for the 21st Century — A Risk-Based Approach. <https://www.fda.gov/media/77391/download> (accessed Jul 27, 2021).

- (17) Liu, R.; Li, L.; Yin, W.; Xu, D.; Zang, H. Near-infrared spectroscopy monitoring and control of the fluidized bed granulation and coating processes — A Review. *Int. J. Pharm.* **2017**, *530* (1–2), 308–315. <https://doi.org/10.1016/j.ijpharm.2017.07.051>.
- (18) Laske, S.; Paudel, A.; Scheibelhofer, O. A review of PAT strategies in secondary solid oral dosage manufacturing of small molecules. *J. Pharm. Sci.* **2017**, *106*, 667–712. <https://doi.org/10.1016/j.xphs.2016.11.011>.
- (19) Corredor, C. C.; Vikstrom, C.; Persson, A.; Bu, X.; Both, D. Development and robustness verification of an at-line transmission raman method for pharmaceutical tablets using Quality by Design (QbD) principles. *J. Pharm. Innov.* **2018**, *13* (4), 287–300. <https://doi.org/10.1007/s12247-018-9334-0>.
- (20) Johansson, J.; Claybourn, M.; Folestad, S. Raman spectroscopy: a strategic tool in the process analytical technology toolbox. In *Emerging Raman Applications and Techniques in Biomedical and Pharmaceutical Fields.*; Matousek, P., Morris, M., Eds.; Springer: Heidelberg, Berlin, 2010.
- (21) Grassi, S.; Alamprese, C. Advances in NIR spectroscopy applied to process analytical technology in food industries. *Curr. Opin. Food Sci.* **2018**, *22*, 17–21. <https://doi.org/10.1016/j.cofs.2017.12.008>.
- (22) Pu, Y. Y.; O'Donnell, C.; Tobin, J. T.; O'Shea, N. Review of near-infrared spectroscopy as a process analytical technology for real-time product monitoring in dairy processing. *Int. Dairy J.* **2020**, *103*, 104623. <https://doi.org/10.1016/j.idairyj.2019.104623>.
- (23) Cattaneo, T. M. P.; Holroyd, S. E. The use of near infrared spectroscopy for determination of adulteration and contamination in milk and milk powder: updating knowledge. *J. Near Infrared Spectrosc.* **2013**, *21*, 341–349. <https://doi.org/10.1255/jnirs.1077>.
- (24) Pasquini, C. Near infrared spectroscopy: fundamentals, practical aspects and analytical applications. *J. Braz. Chem. Soc.* **2003**, *14* (2), 198–219.
- (25) Pasquini, C. Near infrared spectroscopy: a mature analytical technique with new perspectives – A review. *Anal. Chim. Acta* **2018**, *1026*, 8–36. <https://doi.org/10.1016/j.aca.2018.04.004>.
- (26) Simon, L. L.; Pataki, H.; Marosi, G.; Meemken, F.; Hungerbu, K.; Baiker, A.; Tummala, S.; Glennon, B.; Kuentz, M.; Steele, G.; Kramer, H. J. M.; Rydzak, J. W.; Chen, Z.; Morris, J.; Kjell, F.; Singh, R.; Gernaey, K. V.; Louhi-Kultanen, M.; Reilly, J. O.; Sandler, N.; Antikainen, O.; Yliruusi, J.; Frohberg, P.; Ulrich, J.; Braatz, R. D.; Leyssens, T.; von Stosch, M.; Oliveira, R.; Tan, R. B. H.; Wu, H.; Khan, M.; Grady, D. O.; Pandey, A.; Westra, R.; Delle-Case, E.; Pape, D. Assessment of recent process analytical technology (PAT) trends: a multi-author review. *Org. Process Res. Dev.* **2015**, *19* (1), 3–62.
- (27) Hwang, I.; Renuka, V.; Lee, J.; Weon, K.; Kang, Y.; Lee, B.; Park, J. Preparation of celecoxib tablet by hot melt extrusion technology and application of process analysis technology to discriminate solubilization Effect. *Pharm. Dev. Technol.* **2020**, *25* (5), 525–534. <https://doi.org/10.1080/10837450.2020.1723023>.
- (28) Ryckaert, A.; Stauffer, F.; Funke, A.; Djuric, D.; Vanhoorne, V.; Vervaet, C.; De Beer, T. Evaluation of torque as an in-process control for granule size during twin-screw wet granulation. *Int. J. Pharm.* **2021**, *602*, 120642. <https://doi.org/10.1016/j.ijpharm.2021.120642>.
- (29) Fonteyne, M.; Arruabarrena, J.; de Beer, J.; Hellings, M.; Van Den Kerkhof, T.; Burggraeve, A.; Vervaet, C.; Remon, J. P.; De Beer, T. NIR spectroscopic method for the in-line moisture assessment during drying in a six-segmented fluid bed dryer of a continuous tablet production line: validation of quantifying abilities and uncertainty assessment. *J. Pharm. Biomed. Anal.* **2014**, *100*, 21–27. <https://doi.org/10.1016/j.jpba.2014.07.012>.

- (30) Biagi, D.; Nencioni, P.; Valleri, M.; Calamassi, N.; Mura, P. Development of a Near Infrared Spectroscopy method for the in-line quantitative bilastine drug determination during pharmaceutical powders blending. *J. Pharm. Biomed. Anal.* **2021**, *204*, 1144277. <https://doi.org/10.1016/j.jpba.2021.114277>.
- (31) Vanarase, A. U.; Alcalà, M.; Rozo, J. I. J.; Muzzio, F. J.; Romanach, R. J. Real-time monitoring of drug concentration in a continuous powder mixing process using NIR spectroscopy. *Chem. Eng. Sci.* **2010**, *65* (21), 5728–5733. <https://doi.org/10.1016/j.ces.2010.01.036>.
- (32) Cogoni, G.; Liu, Y. A.; Husain, A.; Alam, M. A.; Kamyar, R. A hybrid NIR-soft sensor method for real time in-process control during continuous direct compression manufacturing operations. *Int. J. Pharm.* **2021**, *602*, 120620. <https://doi.org/10.1016/j.ijpharm.2021.120620>.
- (33) Feng, H.; Mohan, S. Application of process analytical technology for pharmaceutical coating: challenges, pitfalls, and trends. *AAPS PharmSciTech* **2020**, *21* (5), 1–17. <https://doi.org/10.1208/s12249-020-01727-8>.
- (34) Radtke, J.; Kleinebudde, P. Real-time monitoring of multi-layered film coating processes using raman spectroscopy. *Eur. J. Pharm. Biopharm.* **2020**, *153*, 43–51. <https://doi.org/10.1016/j.ejpb.2020.05.018>.
- (35) Radtke, J.; Rehbaum, H.; Kleinebudde, P. Raman spectroscopy as a PAT-tool for film-coating processes: in-line predictions using one PLS model for different cores. *Pharmaceutics* **2020**, *12* (9), 796.
- (36) Corredor, C. C.; Bu, D.; McGeorge, G. Chapter 9 - Applications of MVDA and PAT for drug product development and manufacturing. In *Multivariate Analysis in the Pharmaceutical Industry*; Ferreira, A. P., Menezes, J. C., Toby, M., Eds.; Elsevier Inc., 2018; pp 211–234. <https://doi.org/10.1016/b978-0-12-811065-2.00010-2>.
- (37) Martínez, L.; Peinado, A.; Liesum, L.; Betz, G. Use of near-infrared spectroscopy to quantify drug content on a continuous blending process: influence of mass flow and rotation speed variations. *Eur. J. Pharm. Biopharm.* **2013**, *84*, 606–615. <https://doi.org/10.1016/j.ejpb.2013.01.016>.
- (38) Porfire, A.; Rus, L.; Vonica, A. L.; Tomuta, I. High-throughput NIR-chemometric methods for determination of drug content and pharmaceutical properties of indapamide powder blends for tableting. *J. Pharm. Biomed. Anal.* **2012**, *70*, 301–309. <https://doi.org/10.1016/j.jpba.2012.07.026>.
- (39) Jamrogiewicz, M.; Cal, K.; Gruszecka, M.; Ciesielski, A. Determination of API content in a pilot-scale blending by near-infrared spectroscopy as a first step method to process line implementation. *Polish Pharm. Soc.* **2013**, *70* (3), 419–429.
- (40) Puig-Bertotto, J.; Coello, J.; Maspoch, S. Evaluation of a handheld near-infrared spectrophotometer for quantitative determination of two APIs in a solid pharmaceutical preparation. *Anal. Methods* **2019**, *11*, 327–335. <https://doi.org/10.1039/c8ay01970c>.
- (41) Moes, J. J.; Ruijken, M. M.; Gout, E.; Frijlink, H. W.; Ugwoke, M. I. Application of process analytical technology in tablet process development using NIR spectroscopy: blend uniformity, content uniformity and coating thickness measurements. *Int. J. Pharm.* **2008**, *357* (1–2), 108–118. <https://doi.org/10.1016/j.ijpharm.2008.01.062>.
- (42) Momose, W.; Imai, K.; Yokota, S.; Yonemochi, E.; Terada, K. Process analytical technology applied for end-point detection of pharmaceutical blending by combining two calibration-free methods: simultaneously monitoring specific near-infrared peak intensity and moving block standard

deviation. *Powder Technol.* **2011**, *210* (2), 122–131. <https://doi.org/10.1016/j.powtec.2011.03.005>.

- (43) Fonteyne, M.; Vercruyse, J.; De Leersnyder, F.; Besseling, R.; Gerich, A.; Oostra, W.; Remon, J. P.; Vervaet, C.; De Beer, T. Blend uniformity evaluation during continuous mixing in a twin screw granulator by in-line NIR using a moving F-test. *Anal. Chim. Acta* **2016**, *935*, 213–223. <https://doi.org/10.1016/j.aca.2016.07.020>.
- (44) Storme-Paris, I.; Clarot, I.; Esposito, S.; Chaumeil, J. C.; Nicolas, A.; Brion, F.; Rieutord, A.; Chaminade, P. Near infrared spectroscopy homogeneity evaluation of complex powder blends in a small-scale pharmaceutical preformulation process, a real-life application. *Eur. J. Pharm. Biopharm.* **2009**, *72* (1), 189–198. <https://doi.org/10.1016/j.ejpb.2008.11.002>.
- (45) Blanco, M.; Alcalá, M. Content uniformity and tablet hardness testing of intact pharmaceutical tablets by near infrared spectroscopy: a contribution to process analytical technologies. *Anal. Chim. Acta* **2006**, *557* (1–2), 353–359. <https://doi.org/10.1016/j.aca.2005.09.070>.

2. NIR SPECTROSCOPY

2. NIR SPECTROSCOPY

The electromagnetic spectrum (Figure 10) is divided into seven regions, each one corresponding to a specific range of wavelengths and frequencies. The infrared (IR) portion goes from 750 nm to 100 μm and three different regions can be distinguished: near infrared or NIR region (750-2500 nm), middle infrared or MIR region (2500-25 μm) and far infrared or FIR region (25-100 μm). NIR is so called as it is the nearest portion of infrared spectrum to the visible region¹.

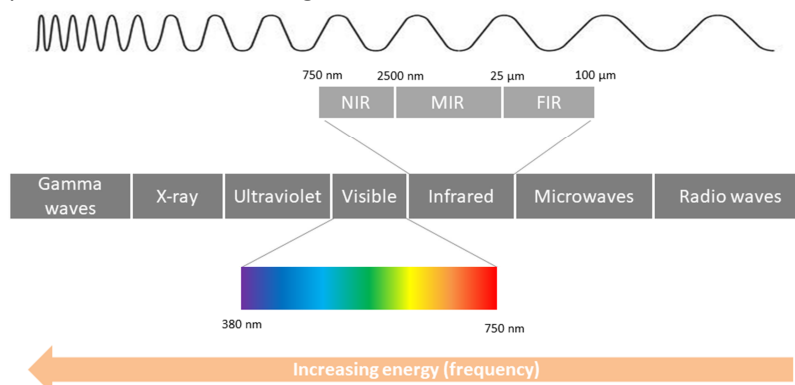


Figure 10 – Electromagnetic spectrum. Figure inspired by Pu et al., 2020¹.

The usefulness of NIR spectroscopy in pharmaceutical industry has been deeply demonstrated^{2,3}. Its use, as an analytical tool, increased in recent years in many different fields⁴: agricultural and food⁵, petrolchemical⁶, environmental⁷, textile, biomedical and clinical⁸, pharmaceutical and cosmetics^{2,9}, and others, thanks to the advantage it offers such as versatility, speed of analysis, non-destructiveness and absence of chemical treatment of samples. In pharmaceutical field NIR is used for many different application, such as incoming material identification¹⁰, powder analysis¹¹, water content determination¹², assay determination¹³, on line monitoring of mixing^{14,15}, granulation¹⁶ and tablet coating process¹⁷. Since its first uses as an analytical technique, NIR has undergone a continuous evolution, thanks to instrumentation improvement and mathematical tools implementation.

The NIR output is a spectrum made of absorption bands. A single absorption band can be identified with two characteristics: the intensity and the frequency (wavelength) at which it occurs. The absorption bands are different from a sample to another, because of different factors, such as atomic and molecular composition (microscopic effects), and macroscopic effects (bulk level). Qualitative and quantitative information are associated to intensity and wavelength of the spectrum of a given sample. The spectral output contains lots of physical and chemical information, really few of which are naked eye visible. In fact, because of its high complexity a NIR spectrum is not directly usable: to extract information data needs to be processed¹⁸. NIR spectrum presents broad and superimposed absorption bands, corresponding to exciting overtones, combination and resonance of fundamental O-H, C-H, N-H and S-H molecular vibrational modes. They are not easily attributed to the presence of a specific functional group, but they can suggest where (which wavelengths) to look at, to find qualitative and quantitative relevant information. Even if the most information is not directly interpretable, there is always a link between sample's attribute and spectral features. As just said, NIR analytical technique needs some tools to interpret spectra and it relies on chemometrics. NIR technology and chemometrics go hand in hand; actually chemometrics is one of three sustaining pillars of NIRS technology, together with the fundamentals of vibrational spectroscopy and the instrumentation, as explained and graphically expressed by Pasquini, 2018¹⁹ (Figure 11).

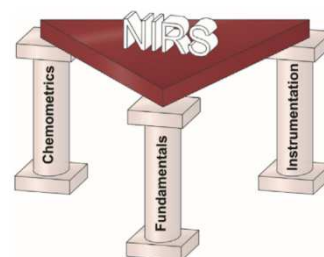


Figure 11 – Three sustaining pillars of Near Infrared Spectroscopy. Figure from Pasquini, 2018¹⁹.

2.1 Fundamentals and theory

NIR spectrum is the result of an energy transfer from the electromagnetic radiation to the sample. Radiation energy is transformed into mechanical energy of vibration among atoms. But, to understand the origin of a NIR spectrum and to be able to interpret it, it is important to be familiar with the fundamentals of vibrational spectroscopy^{4,20,21}.

Spectroscopy studies the matter-radiation interaction. The matter only exists in determinate and quantized states, while the radiation possess energy, which can be exchanged in quantized amount equal to $h\nu$. When matter and radiation interact, there is an energy exchange. The energy transferred is defined by the Einstein-Planck relation:

$$E = h\nu = h\frac{c}{\lambda} \qquad c = \nu\lambda$$

where c is light speed ($3 \cdot 10^8$ m/s), h is the Planck constant ($6,62 \cdot 10^{-34}$ Joule-sec), ν is the frequency and λ is the wavelength.

Transition of a system from one energy level to another is always matched to an energy emission or absorption and it corresponds to a spectroscopic transition.

There are three types of molecular motion²²:

- 1- Translational motion: the whole molecule moves from one place to another, in a three dimensional space. All the atoms move at the same time, in the same direction, maintaining always the same distance respect to the other atoms.
- 2- Rotational motion: the molecule rotates about one of its three axes (through centre of mass). During rotation each atom maintains the same distance from the other atoms of the molecule;
- 3- Vibrational motion: it is an internal motion of the molecule. The molecule does not move in the space, only the atoms move and change their position. The chemical bonds act like a spring, which compresses or extends during vibration along the bond direction (stretching), or bends at an angle to the bond direction, but in the same plane (scissoring).

All the three types of motion are represented in Figure 12.

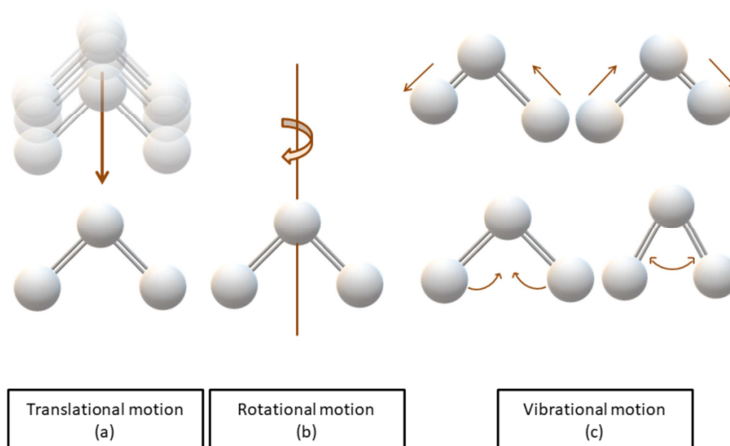


Figure 12 – Molecular motion possibilities: (a) translational motion; (b) rotational motion and (c) vibrational motion.

IR spectroscopy gives information about molecular vibrational modes, i.e. transitions between possible quantized vibrational levels of a molecule. Most of the molecules exist in their fundamental vibrational energy levels at room temperature and atoms have a vibration of certain amplitude, which can

be increased, if additional energy is transferred to the molecule. However, IR radiation does not have enough energy to promote electronic transitions; therefore, the absorbance is limited to the rotational and vibrational levels inside of the fundamental electronic state. Vibrational transitions give important information about the functional groups and flexibility of the molecule, that is, ease of lengths and angles of bonding change respect to equilibrium configuration.

A diatomic molecule is the easiest vibrating system to study. It is depicted as two spherical point masses (m_1 and m_2) held together by a chemical bond that acts like a spring, with a given force constant (k) (Figure 13).

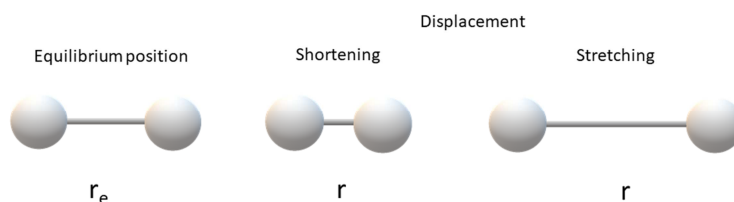


Figure 13 – Diatomic molecule acting like a spring.

During vibration, the bond stretches and shortens, obeying the Hook's law^{23,24}. It states that, when a mass moves away from the equilibrium position, a force (F) is created, which tends to bring the mass back to its equilibrium position. The force is proportional to the movement (x) done.

$$F = -kx$$

where k is the force proportionality constant.

In an equilibrium condition (no vibration) the two atoms of the diatomic molecule have an equilibrium internuclear distance (r_e). During vibration, the internuclear distance changes (r). The movement, therefore, corresponds to the difference between r_e and r , which is called displacement coordinate ($q=(r-r_e)$). Such classical mechanic approach is not completely correct. A molecular systems cannot assume a continuous energy profile, as predicted by the classical spring model; rather it can only have some discrete energy levels.

As said before, vibration is to be intended as a displacement from the equilibrium position. Depending on the entity of the movement, a vibrating system can be described with approximation⁴:

1. by the **harmonic oscillator** for small displacement from the equilibrium position;
2. by the **anharmonic motion** for large displacement (Figure 14).

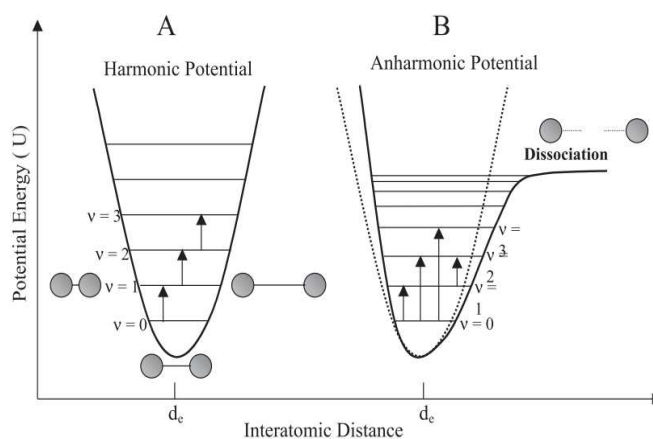


Figure 14 – Potential energy curve for harmonic and anharmonic oscillator. Figure from Pasquini, 2003⁴

The potential energy curve of an harmonic oscillator is described by⁴:

$$V = \frac{1}{2}k(r - r_e)^2$$

where r is the internuclear distance during the vibration, r_e is the equilibrium internuclear distance, k is the force proportionality constant.

The potential energy curve has a parabolic shape and it is symmetrical about the equilibrium bond length r_e (minimum energy). According to the harmonic oscillator approximation, the vibrational levels are infinite and separated from each other by the constant quantity $h\nu$. The harmonic oscillator well describes the vibration, but only for small displacement from the equilibrium position. In a real molecule, when two atoms get too close, repulsion between electronic clouds occurs, while an over-displacement of the atomic nuclei causes molecule bond rupture. Such behaviours are not described by the parabolic curve. Anharmonic molecular potentials may be represented by approximate functions, such as Morse function²⁰:

$$V = D_e(1 - e^{-a(r-r_e)})^2$$

where r is the internuclear distance during the vibration, r_e is the equilibrium internuclear distance, D_e is the spectral dissociation energy and a is a constant depending on the molecule.

In this case, the energetic levels are a finite number and have a variable distance; in particular, they get closer, as the quantum number (and the energy) increase. This is the consequence of the mechanical anharmonicity.

2.2 Instrumentation

According to Pasquini's philosophy¹⁹, instrumentation is one of the three sustaining pillar of NIRS technology. A rapid evolution has involved this field: from the first laboratory-bench filter-based instrumentations, to the micronized hand-portable NIR instruments. All the instruments, despite all the possible differences, consist of four basic elements:

- Light source: originates the light beam that hits or penetrates the sample. An ideal radiation source should have a wide wavelength range and a strong and stable intensity of the light.
- Dispersing element or monochromator: allows to select the desired wavelength range and separate the single wavelengths that will interact with the sample.
- Sample holder: keeps the sample in the right place and position.
- Detector: receives the non-absorbed light by the sample as an intensity signal and converts it in the spectral output.

The spatial localization of these four elements into the instrumentation depends on the desired light-matter interaction mode (Figure 15). NIR instruments prevalently work in transmittance, reflectance or transreflectance mode.

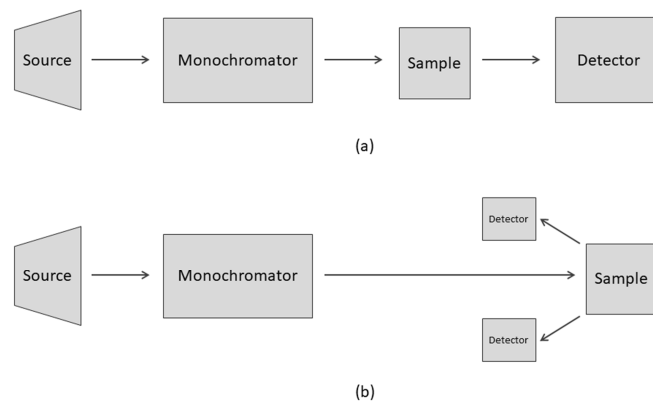


Figure 15 – Possible interaction modes in NIR spectroscopy: (a) transmittance and (b) reflectance mode. Figure inspired by Handbook of Near-Infrared-Analysis 3rd edition²⁵.

When using transmittance mode, the light penetrates through the sample, which absorbs part of the radiation. The non-absorbed radiation reaches the detector. In reflectance mode, the light hits the surface of the sample, with only a small penetration inside it. A part of the radiation is absorbed, while the amount of not absorbed light is reflected back, reaching the detector. Transreflectance is a combination of reflectance and transmittance mode. The light passes through the sample, as in the transmittance mode, but it is, then, reflected back, with a mirror, as for the reflectance mode. In any case, the information revealed by the detector is the amount of non-absorbed light. Therefore, to express the information in terms of absorbance, the transmittance and reflectance information must be converted, using the following expressions, respectively²⁵:

$$A = \log \frac{1}{\text{Transmittance}}; \quad A = -\log_{10} \text{reflectance}$$

NIR instruments differ for the type of radiation source, the optical configuration, the detector used and also for other criteria^{1,26}.

Source type distinction

Basing on the emitting mechanism, the sources can be divided into continuum and line sources. A continuum source emits light with a continuous intensity and over a wide range of wavelengths; a line source emits only a narrow band of wavelengths, with an intensity that depends on the type of emitted wavelength.

Optical configuration distinction

The optical configuration concerns the mechanism of separation of light, which can occur with different mechanisms:

- Filter based instruments use filters mounted on rotating plate for wavelength selection.
- Acousto-Optical Tunable Filters (AOTF) based instruments are a particular type of filters, called electronically tunable filters. They do not contain any moving part, have high speed scan and use radio frequency to select the wavelength.
- Dispersive spectrometer or monochromators are based on optical prisms or diffracting grating elements as monochromator. The polychromatic beam hits a grating element or a prism, which disperses the radiation into its monochromatic wavelengths, by reflecting them with a different angle.
- Fourier-transform (FT) spectrometers are based on the interference theory of Michelson. The light beam is focused on a beam splitter, which divides the light in two different beams, one reflected by a fixed mirror and the other reflected by a moving mirror. The two beams are then reunited, to hit the sample.
- Diode-array instruments have a grating system to separate the wavelengths, which are measured all at the same time, as there is a diode detector for each wavelength. This type of instrument shows a high speed of analysis.
- Micro-electro-mechanical system (MEMS) are small devices based on semi-conductor technologies. They are generally used for portable and small instruments, employed for the on-site measuring.

Detector type distinction

Single or multi-channels detectors can be employed. The latter presents several elements organized in rows (diode array) or planes, in order to record many wavelengths at the same time and increasing the speed. Basing on the principles of operation, two types of detectors can be distinguished: thermal detectors and photon-sensitive detectors (or photodiodes). The best quality detector consists in cooled InGaAs semiconductor, which shows a fast response and has a high detectivity.

There is a specific category of NIR instruments used for the on-line and in-line process monitoring. This type of instrumentation requires an operational autonomy and a speed of response. Some FT instruments have been used, especially for on-line process controls, even if they are particularly sensible to vibrations. Respect to previous consideration, the solid-state NIR instruments without moving parts can be employed for on-line and also in-line process control more easily, as they are not sensible to vibrations. In order to remove all the moving parts, the solid-state instruments couple diffraction grating to a InGaAs, Si, PbS or HgCdTe sensor or employ the AOFT technology¹⁹.

Another special group of equipment are the miniaturized and handheld instruments. They are characterized by a small size and light weight (for that reason they are also called “micro” instruments) and employ microelectronics and micro-electro-mechanical systems (MEMS)¹⁹. One of the aforementioned instrument is the MicroNIR developed by Viavi Solutions^{27,28} and used by many authors^{14,29,30}. It is a small dimension, about 100 g, solid-state instrument, tolerant to vibration. It has two small tungsten filaments, as radiation source and contains a Linear Variable Filter (LVF)-based optical train, as dispersing element, which

is located on top of an InGaAs array detector. The innovative element of this optical train is the LVF, which is a bandpass filter. A bandpass filter is a special type of dichroic optical filter which only allows a “band” of wavelengths to pass through, while the other wavelengths around it are attenuated³¹. The LVF works as a Fabry-Perot filter, which is made of two quarter-wave stacks divided by a “spacer” (the whole structure is called Fabry-Perot cavity). A quarter wave stack is made of an alternating series of thin film layers of high and low-index materials. They are called “quarter”, because the thickness of each layer corresponds to a quarter of a specific wavelength. The “spacer” is a layer with a thickness equal to a half of the specific wavelength. Such type of filter gives a particular type of spectrum, containing a central zone, called stopband, where there is no transmission. At the centre of the stopband, the light constructively interferes, thus transmitting a very narrow band, corresponding to the specific wavelength. However, the LVF used in the MicroNIR linearly changes the thickness of the cavity along its length, moving in one direction, resulting in an infinite number of Fabry-Perot cavities³². The thickness of the cavities determines the wavelength that is transmitted in the correspondent filter position. A schematic representation of the LVF principle is shown in Figure 16.

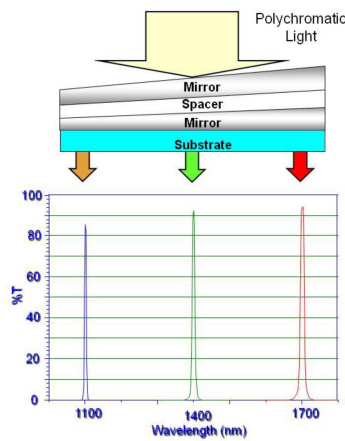


Figure 16 – Working principle of Linear Variable Filter (LVF) component. Image from Friedrich et al., 2014²⁸.

The LVF is deposited with a vapour deposition process, that makes it stable at high temperature and for long time. Generally, a LVF-based instrument has a very short optical train, because the dispersive element directly translates position to wavelength, at the plane of the filter. In order to make an instrument not sensible to vibration, Viavi Solutions chose to couple the LVF to the detector array, rather than incorporating moving parts, which could increase size, decrease ruggedness, and increase power consumption. A cross sectional view of the instrument configuration is shown in Figure 17.

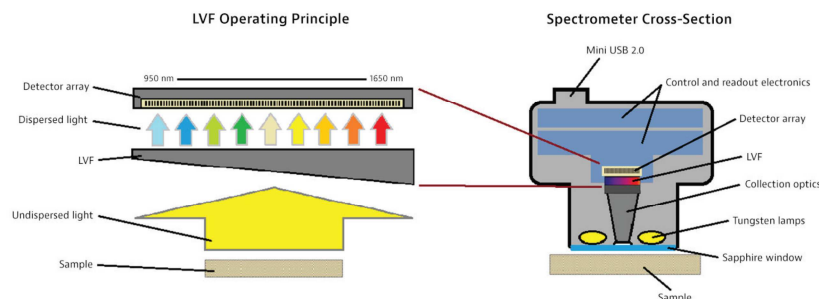


Figure 17 – Cross sectional view of the optical train. Image from Viavi Solutions official website²⁷.

Prior to perform the sample acquisition two reference measurement are taken: the acquisition of a Teflon material, called spectralon, with the 99% reflectance and the acquisition of a reference with 0% reflectance²⁷.

2.3 Chemometrics

2.3.1 Generalities

Numerous definitions of chemometrics can be found in literature. Kramer defined chemometrics as “the art of processing data with various numerical techniques in order to extract useful information”³³; according to Gemperline “Chemometrics is an interdisciplinary field that combines statistics and chemistry”³⁴; Pasquini defined it as “the use of mathematical and statistical techniques for extracting relevant information from analytical data” (the NIR spectra)⁴. Miller defines chemometrics as “the chemical discipline that uses mathematical, statistics and formal logic a) to design or select optimal experimental procedures b) to provide maximum relevant chemical information by analysing chemical data and c) to obtain knowledge about chemical systems”³⁵. NIR spectroscopy is used for analytical purpose, as it gives information about one or more chemical and/or physical properties (concentration, content uniformity, homogeneity, residual moisture and physical characteristics) of the studied system. The chemical and physical information are contained inside the acquired spectrum, which is the direct output of the spectroscopic measurement. Therefore, the physical and chemical information are not directly available; they need to be extracted from the spectral output. A single property is generally correlated to many spectral variables, not just one; for that reason multivariate analysis is required, to classify and identify data (qualitative multivariate analysis) or for properties prediction of new samples, by calibration models (quantitative multivariate analysis)³⁶. With this premises, it is necessary a multivariate tool, for correctly interpreting the spectral data and linking a specific physical or chemical characteristic of the analysed sample to the spectral features. Chemometrics is employed with this exact purpose: linking sample properties to spectra.

2.3.2 Development of a NIR-based analytical method

NIR spectroscopy is used for qualitative and quantitative analytical purpose and, in both cases, “the critical step is the development and validation of a classification or regression model based on multivariate analysis”¹⁹.

When performing NIR spectroscopic analysis a large amount of data is acquired. They are organized in multivariate data set, where the columns correspond to the variables and the rows to the samples, or the single spectrum acquisition (Table 3).

Spectrum number	Variable 1	Variable 2	...	Variable m
1	X_{11}	X_{21}
2	X_{12}
...
n	X_{1n}	X_{mn}

Table 3 – Data matrix of spectroscopic data.

Multivariate data sets can be very large and complex and, as mentioned before, such complexity requires the use of specific instruments to extract information. When applying chemometrics to extract information from NIR spectra, there are three aspects to consider: spectra pre-treatment, variable selection and choice of the multivariate analytical method. As Pasquini said “the analytical information present in NIR spectra is very complex, self-correlated, and usually not promptly available for analytical purpose. Most of the time the information is dispersed all over the spectrum”¹⁹. For that reason, a raw data set, generally, undergoes a pre-treatment and a variable selection, so that only “clear” data are used for the analytical purpose.

The data pre-treatment is useful to reduce the spectral noise and also the physical information, in those samples where this is not important, in order to build a robust model³⁴. The data pre-treatment can be applied on both, columns and rows.

The column pre-processing consists in centering and scaling the data, in order to obtain a homogeneous data set. For each variable, the average (\bar{X}) and the standard deviation (SD) are calculated. To center the data, a new matrix is obtained, by subtracting the calculated average to each value of the corresponding column. For each column m the new values are calculated as follows:

$$X'_n = X_n - \bar{X}_m.$$

where n indicates the row, m indicates the column and \bar{X} is the column mean value.

The mean-centering pre-processing option graphically corresponds to a shift in the plot origin. The variance scaling is another possibility for column pre-treatment. To scale the data a new matrix is obtained, by dividing each value for the standard deviation (SD) of the corresponding variable. For each column:

$$X'_n = \frac{X_n}{SD_m}.$$

where n indicates the row, m indicates the column and SD is the standard deviation on the corresponding column.

The variance scaling is always performed after the mean-centering. It makes sure that every variable has the same importance, respect to other variables, as graphically represents in Figure 18. Centering and scaling the data is useful, especially when the signal-to-noise ratio is considerably different from variable to variable. However, as the measurement error is uniform along the whole spectral wavelength, it is not particularly useful in case of NIR spectral data³⁴. When performing such matrix transformations, the new obtained values do not possess a chemical meaning, but the relation among data and the inner structure is maintained and no information is lost.

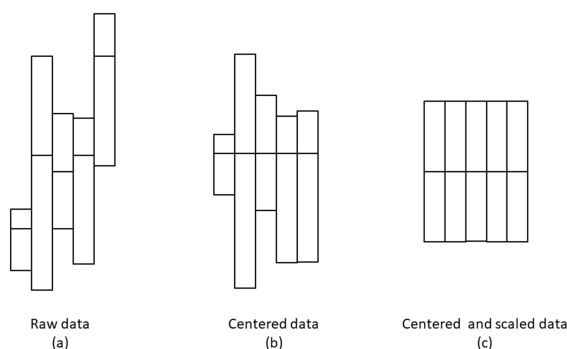


Figure 18 – Column pre-treatment. (a) not pre-treated raw data; (b) centered data, after mean centering; (c) centered and scaled data, after performing variance scaling.

Row pre-treatment is aimed at removing the instrumental noise and increasing the resolution, i.e. the signal-to-noise ratio. The first aspect to consider when applying the row pre-treatment is whether replicates measurements of a single sample are present. If it is so, they should be averaged as first thing. When acquiring spectra, the noise is always present and it can appear as a baseline shift, or as the noise of a single spectrum. Both type of noise are represented in Figure 19a. The baseline shift is due to the light scattering; this type of noise can be reduced with the baseline correction or with the Standard Normal Variate (SNV) transformation³⁷, as applied in Figure 19b.

For baseline transformation following equation is used:

$$X'_n = X_n - \min_m$$

where n indicates the row, m indicates the column X'_n is the new calculated value and \min_m is the minimum value of the column.

For SNV transformation the following equation is used:

$$X'_n = \frac{X_n - \bar{X}_m}{SD_m}$$

where n indicates the row, m indicates the column, X'_n is the new calculated value, \bar{X}_m is the column mean value and SD_m is the standard deviation of the column.

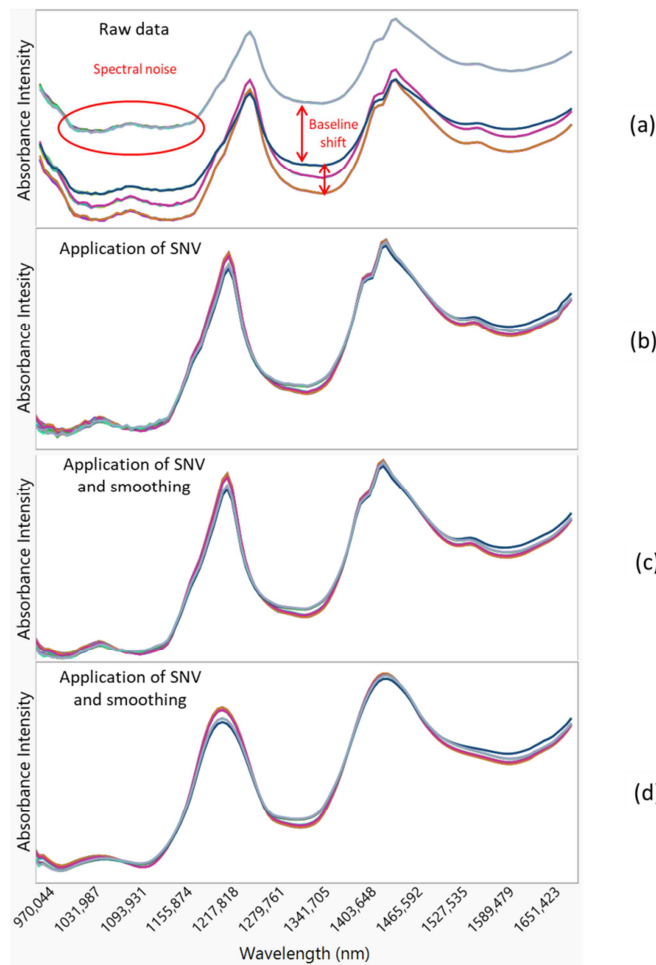


Figure 19 – Noise reduction with row spectra pre-treatment. (a) The raw spectra contain noise due to baseline shift and instrumental noise. (b) Application of SNV reduces the baseline shift noise. (c) Application of smoothing pre-treatment to the SNV spectra reduces the instrumental noise. (d) Excessive smoothing is applied and some information is lost.

The noise present in a single spectrum appears as irregularities and little sharp edges on the spectrum line, as indicated in the left portion of the spectra in Figure 19a. A smoothing function can be used to reduce this type of noise. There are different possibilities for smoothing a spectrum: the simplest method is calculating the moving average of a narrow window of points; smoothing filters (smoothing median filter and smoothing Gaussian filter) can be used; but the most used method is the polynomial smoothing, called Savitzky-Golay³⁸. It is important to remember that the spectrum is not a continuous

mathematical curve, rather it is a series of measured values of absorbance³⁹. To calculate the polynomial Savitzky-Golay smoothing, a moving window of a certain width w (generally equal to an odd number) is defined and it contains w measurements or points. A polynomial function is then calculated, to fit the w points of the selected window. The midpoint of the polynomial function generates a smoothed point. Then, the window moves to the right, losing its first point and adding the newest available one, thus always maintaining the same width. A new polynomial function is fitted to the points inside the new window and the midpoint is estimated. The process goes on, until the last point is included inside a window and the whole spectrum is smoothed^{34,38}. An example of smoothed spectra is reported in Figure 19c, where the smoothed function is applied together with the SNV pre-treatment, in order to reduce both types of noise. However, attention should be paid, when applying a smoothing function; if the smooth is too deep, some information could be removed together with noise, as showed in Figure 19d. In addition to noise reduction, it is possible to increase the spectral resolution with derivatives. The most common algorithms used to calculate derivatives are three: the Savitzky-Golay algorithm³⁸, the Norris algorithm and the Hruschka algorithm. In addition to this most common pre-treatment, some other pre-processing techniques exist, such as Multiplicative Signal Correction (MSC), Extended Multiplicative Signal Correction (EMSC), Detrending (DT)^{37,5}, baseline correction and normalization. Overviews of the pre-treatment techniques are available^{40,34}. More pre-treatment types can be simultaneously applied and combined, in order to extrapolate as much information as possible. There is not a precise order to follow, as every sample is different from the others.

As concern the variable selection, it is necessary to consider only those wavelengths that really contain useful information, for the model to build. The spectral region is defined by the instrument characteristics, therefore not all the wavelengths necessarily contain information about the sample. Moreover, for complex samples' spectrum, some variables could contain little information about the component of interest and many more information about the others components; therefore, a proper variable selection is an important step, for the development of a robust and simpler model. A review of variable selection methods is available^{41,19}.

The third aspect of applying chemometrics regards the choice of the multivariate analysis method. Its goals are: firstly, building a model, which links samples property of interest to spectral characteristics; secondly, using it to predict the same property of an unknown sample. There are a lot of different qualitative and quantitative modelling methods to be used for this purpose^{34,42}, as illustrated in Figure 20 by Blanco and Villaroya, 2002¹⁸.

trends in analytical chemistry, vol. 21, no. 4, 2002

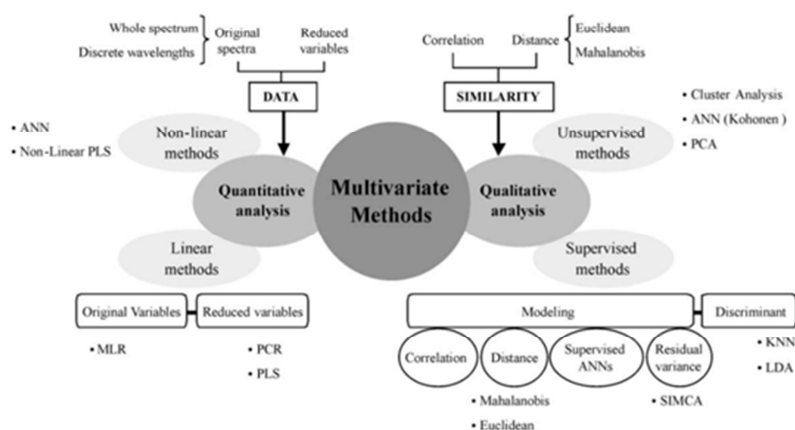


Figure 20 – Multivariate methods for qualitative and quantitative analytical purpose. Figure from Blanco and Villaroya, 2002¹⁸.

Qualitative application

Qualitative NIR analytical methods are, generally, used for identification and classification purpose and are based on libraries of known substances. Qualitative analysis uses methods known as “pattern-recognition methods”, based on differences and similarities between samples. There are several groups of pattern recognition methods^{4,18,34,43}: Exploratory Data Analysis (EDA), Principal Component Analysis (PCA), unsupervised pattern recognition methods (cluster analysis) and supervised pattern recognition methods.

Quantitative application

NIR can also be used for quantitative application, proposing itself as an alternative to other quantitative (and generally destructive) analytical methods, such as HPLC (High Performance Liquid Chromatography). The objective of a quantitative analytical method is to build a *model*, in order to establish a relationship between a sample’s property and the NIR spectrum⁴³. A training set, called calibration set is used to build the model; then, its quality is assessed on an independent test set, called validation set. Once verified the model’s quality, the model can be used to predict the property of an unknown sample. When performing calibration, a spectroscopic information (called “x” block) is used to predict a sample property (called “c” block). If performing a univariate calibration, the x and c block are both single variable blocks; therefore, the sample property is predicted by one single variable. In a multivariate calibration, on the contrary, the sample property is contemporarily determined by many variables. The difference between the two methods is graphically represented in Figure 21.

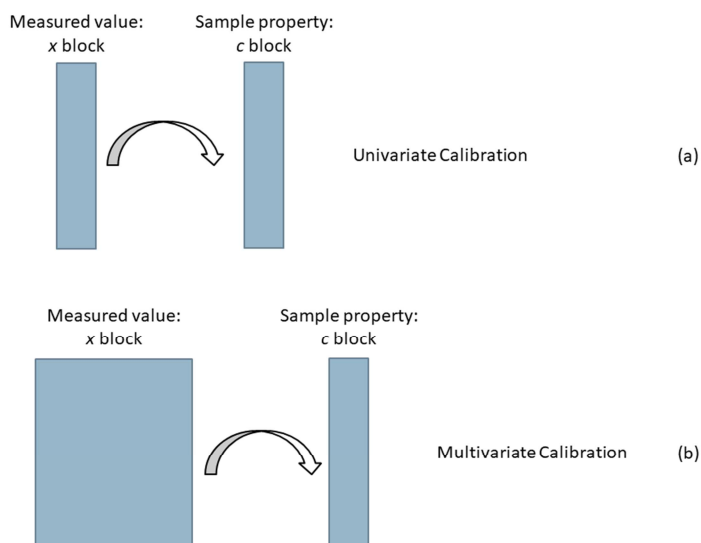


Figure 21 – Univariate and multivariate calibration. Figure inspired by Breton, 2007⁴³.

As a first distinction, a calibration method can be univariate and multivariate; a second distinction is between the linear and non-linear methods. A linear method is used when the property is linearly correlated to the measured value; if it is not, a non-linear method should be used. A linear method relates spectroscopic peak intensity (x) to a sample property, such as concentration (c) and it can be done with a direct or an inverse method. Therefore, it is possible to distinguish among direct (or classic) and inverse linear methods. A direct linear method expresses the instrumental response (x) as a function of concentration (c), as reported in Figure 22a. An inverse method, on the contrary, expresses the concentration, as a function of the spectral intensity, with the equation reported in Figure 22b. The aim of a direct method is to use the peak intensity (x) to predict the concentration (c); it assumes all sources of error to be in the x block. The inverse method starts from the concentration (c), to predict the instrumental response (x) and assume the errors to be in the c block.

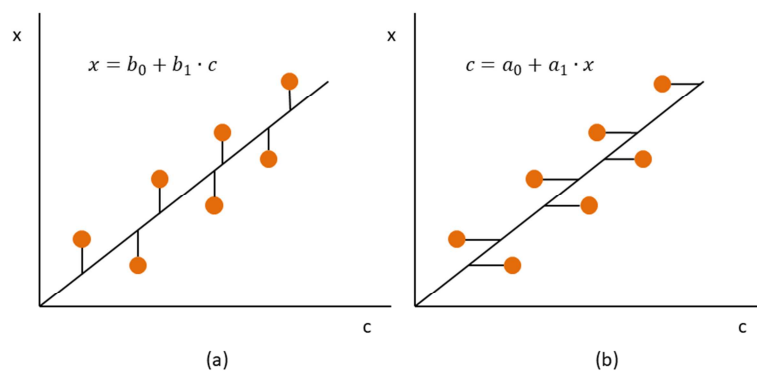


Figure 22 – Possible calibration modes. Figure (a) direct (or classical) calibration; figure (b) inverse calibration.

Different algorithms can be used for linear multivariate calibration, such as Multilinear Regression (MLR), Partial Least Square (PLS)⁴⁴ and Principal Component Regression (PCR).

The development of a quantitative NIR method can be divided into several phases, which are graphically represented in Figure 23⁴:

Design and experiments

The model development is planned and the calibration and validation set of samples are selected and prepared. For selection of calibration and validation set a DoE strategy can be followed. Samples should be of the same nature of the prediction samples, so that the calibration set will include all the usual variability of process and concentration (physical and chemical variability, respectively). The chemical variability is related to the drug concentration. In order to keep it into account the calibrations set should cover an adequate concentration range. The physical variability comes from those manufacturing operations that affect physical characteristics, such as density, particle size, shape, etc. The number of samples employed in the calibration set should depend on the complexity and variability of the sample itself. A laboratory calibration set is optimal to predict other laboratory batches, because it represents the whole variability of the laboratory scale. The same is not for production batches; in this case, for a better prediction some alternatives should be considered, such as including production batches in the calibration set, using pilot scale samples, underdosing/overdosing industrial samples or calculating and adding a manufacturing spectrum to the laboratory ones. Once the calibration and validation sets are prepared, the actual sample's concentration is determined with a reference method. Finally, the NIR spectra of the samples are collected. This step itself could introduce a lot of variability and noise, if not correctly executed: it is fundamental that all the samples (calibration, validation and prediction ones) are acquired under the same experimental conditions.

Data elaboration and model building

The mathematical calibration model is built and optimized. For this step, it is important to previously perform an adequate spectral pre-processing, i.e. correctly select pre-treatment type and the number of variables of NIR spectra, as previously described (see section 2.3). Data processing helps in reducing information related to physical phenomena; therefore, it is of primary importance when interested only in chemical information. The model's performance is estimated from the Root Mean Square Error of Calibration (RMSEC) and the coefficient of multiple regression (R^2) of calibration.

Model verification

The predictive ability of the selected model must be evaluated. Validation can be performed as a cross validation or, with a more realistic results, as an external validation. The predictive ability of the

model is evaluated using statistical figure of merits, such as the Root Mean Square Error of Prediction (RMSEP) and the coefficient of multiple regression (R^2) of prediction, the bias, the Standard Error of Prediction (SEP) and the Ratio of Prediction to Deviation (RPD)^{1,45,46}.

Use and maintenance of the model

The model can be used, to predict the property of an unknown sample. It can also be improved and upgraded with other additional data.

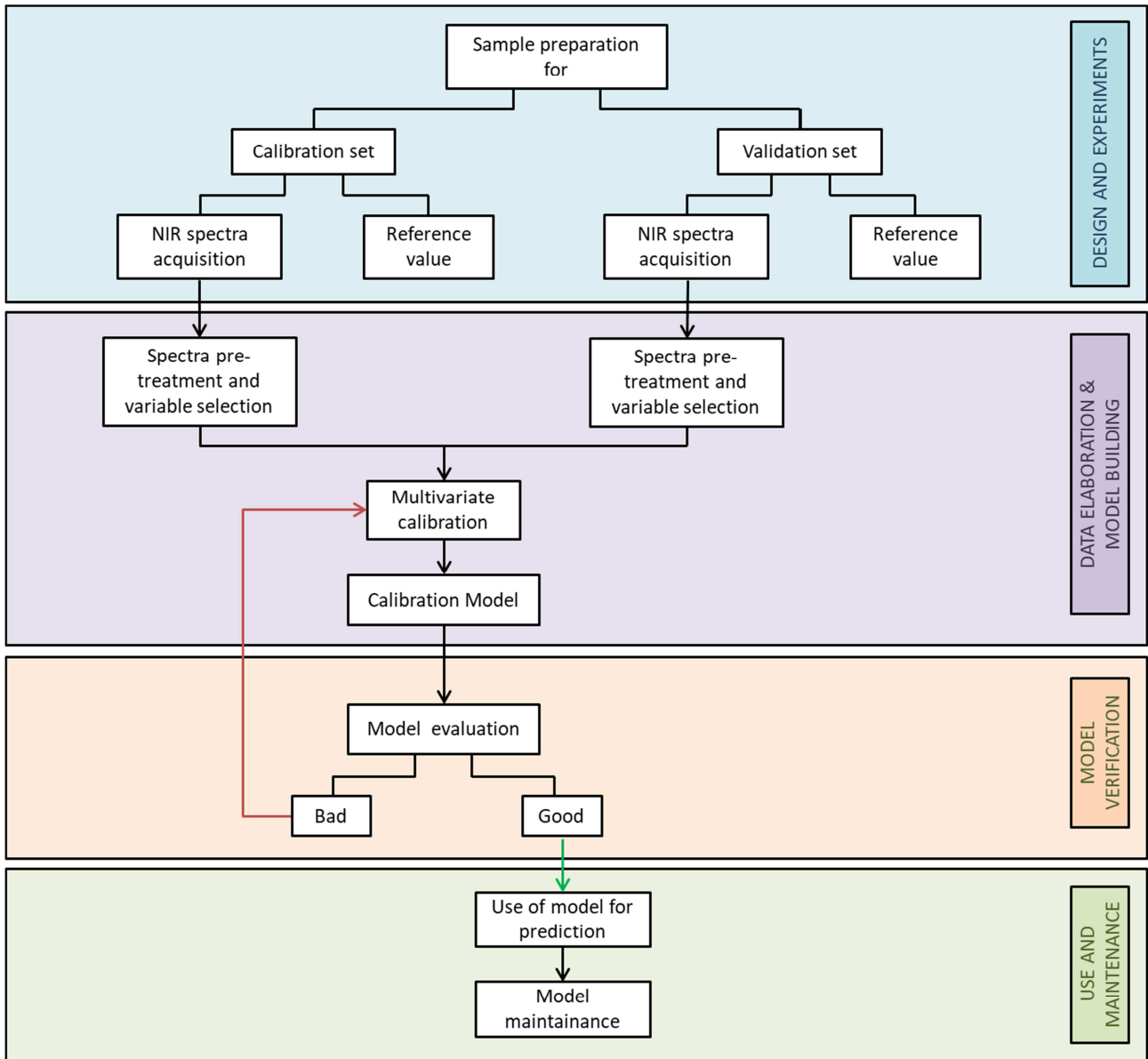


Figure 23 – Schematic representation of a development of a NIR quantitative method. Figure inspired by Pu et al., 2020¹.

References

- (1) Pu, Y. Y.; O'Donnell, C.; Tobin, J. T.; O'Shea, N. Review of near-infrared spectroscopy as a process analytical technology for real-time product monitoring in dairy processing. *Int. Dairy J.* **2020**, *103*, 104623. <https://doi.org/10.1016/j.idairyj.2019.104623>.
- (2) Luybaert, J.; Massart, D. L.; Vander Heyden, Y. Near-infrared spectroscopy applications in pharmaceutical analysis. *Talanta* **2007**, *72* (3), 865–883. <https://doi.org/10.1016/j.talanta.2006.12.023>.
- (3) Roggo, Y.; Chalus, P.; Maurer, L.; Lema-Martinez, C.; Edmond, A.; Jent, N. A review of near infrared spectroscopy and chemometrics in pharmaceutical technologies. *J. Pharm. Biomed. Anal.* **2007**, *44*, 683–700. <https://doi.org/10.1016/j.jpba.2007.03.023>.
- (4) Pasquini, C. Near infrared spectroscopy: fundamentals, practical aspects and analytical applications. *J. Braz. Chem. Soc.* **2003**, *14* (2), 198–219.
- (5) Shi, H.; Lei, Y.; Louzada Prates, L.; Yu, P. Evaluation of near-infrared (NIR) and Fourier transform mid-infrared (ATR-FT/MIR) spectroscopy techniques combined with chemometrics for the determination of crude protein and intestinal protein digestibility of wheat. *Food Chem.* **2019**, *272*, 507–513. <https://doi.org/10.1016/j.foodchem.2018.08.075>.
- (6) Mancini, M.; Duca, D.; Toscano, G. Laboratory customized online measurements for the prediction of the key-parameters of biomass quality control. *J. Near Infrared Spectrosc.* **2019**, *27* (1), 15–25. <https://doi.org/10.1177/0967033518825341>.
- (7) Gredilla, A.; Fdez-Ortiz de Vallejuelo, S.; Elejoste, N.; de Diego, A.; Madariaga, J. M. Non-destructive spectroscopy combined with chemometrics as a tool for green chemical analysis of environmental samples: a review. *TrAC - Trends Anal. Chem.* **2016**, *76*, 30–39. <https://doi.org/10.1016/j.trac.2015.11.011>.
- (8) Barnea, Z. H.; Abookasis, D. Determination of creatinine level in patient blood samples by fourier NIR spectroscopy and multivariate analysis in comparison with biochemical assay. *J. Innov. Opt. Health Sci.* **2019**, *12* (6), 1950015. <https://doi.org/10.1142/S1793545819500159>.
- (9) Martínez, L.; Peinado, A.; Liesum, L.; Betz, G. Use of near-infrared spectroscopy to quantify drug content on a continuous blending process: influence of mass flow and rotation speed variations. *Eur. J. Pharm. Biopharm.* **2013**, *84*, 606–615. <https://doi.org/10.1016/j.ejpb.2013.01.016>.
- (10) Blanco, M.; Romero, M. A. Near-infrared libraries in the pharmaceutical industry: a solution for identity confirmation. *Analyst* **2001**, *126* (12), 2212–2217. <https://doi.org/10.1039/b105012p>.
- (11) O'Neil, A. J.; Jee, R. D.; Moffat, A. C. The Application of multiple linear regression to the measurement of the median particle size of drugs and pharmaceutical excipients by near-infrared spectroscopy. *Analyst* **1998**, *123* (11), 2297–2302. <https://doi.org/10.1039/a806001k>.
- (12) Zhou, X.; Hines, P.; Borer, M. W. Moisture Determination in hygroscopic drug substances by near infrared spectroscopy. *J. Pharm. Biomed. Anal.* **1998**, *17* (2), 219–225. [https://doi.org/10.1016/S0731-7085\(97\)00182-9](https://doi.org/10.1016/S0731-7085(97)00182-9).
- (13) Nikolich, K.; Sergides, C.; Pittas, A. The Application of Near Infrared Reflectance Spectroscopy (NIRS) for the quantitative analysis of hydrocortisone in primary materials. *J. Serbian Chem. Soc.* **2001**, *66* (3), 189–198. <https://doi.org/10.2298/jsc0103189n>.

- (14) Biagi, D.; Nencioni, P.; Valleri, M.; Calamassi, N.; Mura, P. development of a Near Infrared Spectroscopy method for the in-line quantitative bilastine drug determination during pharmaceutical powders blending. *J. Pharm. Biomed. Anal.* **2021**, *204*, 1144277. <https://doi.org/10.1016/j.jpba.2021.114277>.
- (15) Berntsson, O.; Danielsson, L.; Lagerholm, B.; Folestad, S. Quantitative in-line monitoring of powder blending by near infrared reflection spectroscopy. *Powder Technol.* **2002**, *123*, 185–193.
- (16) Alcalà, M.; Blanco, M.; Bautista, M.; González, J. M. On-line monitoring of a granulation process by NIR spectroscopy. *J. Pharm. Sci.* **2010**, *99* (1), 336–345. <https://doi.org/10.1002/jps.21818>.
- (17) Andersson, M.; Josefson, M.; Langkilde, F. W.; Wahlund, K. G. Monitoring of a film coating process for tablets using near infrared reflectance spectrometry. *J. Pharm. Biomed. Anal.* **1999**, *20* (1–2), 27–37. [https://doi.org/10.1016/S0731-7085\(98\)00237-4](https://doi.org/10.1016/S0731-7085(98)00237-4).
- (18) Blanco, M.; Villarroya, I. NIR spectroscopy: a rapid-response analytical tool. *TrAC - Trends Anal. Chem.* **2002**, *21* (4), 240–250. [https://doi.org/10.1016/S0165-9936\(02\)00404-1](https://doi.org/10.1016/S0165-9936(02)00404-1).
- (19) Pasquini, C. Near infrared spectroscopy: a mature analytical technique with new perspectives – a review. *Anal. Chim. Acta* **2018**, *1026*, 8–36. <https://doi.org/10.1016/j.aca.2018.04.004>.
- (20) *Infrared and Raman Spectroscopy*; Schrader, B., Ed.; Wiley-VCH: Weinheim, 1995.
- (21) Atkins, P.; Paula, D. *Atkins' Physical Chemistry*, 8th Edition.; Oxford University Press, 2006.
- (22) Oldenberg, O.; Frost, A. A. Molecular translation, rotation, and vibration in chemical activation. *Chem. Rev.* **1937**, *20* (1), 99–129.
- (23) Hooke, R. *De Potentia Restitutiva, or of Spring. Explaining the Power of Springing Bodies*; London, 1678.
- (24) Ciurczak, E. W.; Drennen, J. K. *Pharmaceutical and Medical Applications of Near-Infrared Spectroscopy*; Marcel Dekker Inc., 2002.
- (25) *Handbook of Near-Infrared Analysis*, 3rd ed.; Burns, D. A., Ciurczak, E. W., Eds.; CRC Press Taylor & Francis, 2007.
- (26) *Infrared Spectroscopy for Food Quality Analysis and Control*; Sun, D. W., Ed.; Academic Press, Elsevier Inc.: Belfield, Dublin, 2009.
- (27) Viavi Solutions Inc, MicroNIR PAT-W <https://www.viavisolutions.com/en-us/osp/products/micronir-pat-w#technical> (accessed Sep 16, 2021).
- (28) Friedrich, D. M.; Hulse, C. A.; von Gunten, M.; Williamson, E. P.; Pederson, C. G.; O'Brien, N. A. miniature near-infrared spectrometer for point-of-use chemical analysis. *Photonic Instrum. Eng.* **2014**, *8992*, 899203. <https://doi.org/10.1117/12.2040669>.
- (29) Sierra-Vega, N. O.; Román-Ospino, A.; Scicolone, J.; Muzzio, F. J.; Romañach, R. J.; Méndez, R. Assessment of blend uniformity in a continuous tablet manufacturing process. *Int. J. Pharm.* **2019**, *560*, 322–333. <https://doi.org/10.1016/j.ijpharm.2019.01.073>.
- (30) Puig-Bertotto, J.; Coello, J.; Maspoch, S. Evaluation of a handheld near-infrared spectrophotometer for quantitative determination of two APIs in a solid pharmaceutical preparation. *Anal. Methods* **2019**, *11*, 327–335. <https://doi.org/10.1039/c8ay01970c>.
- (31) Angstrom Engineering. Optical Filters <https://angstromengineering.com/applications/introduction->

optical-coatings/optical-filters/ (accessed Sep 12, 2021).

- (32) Emadi, A.; Wu, H.; de Graaf, G.; Wolffenbuttel, R. Design and implementation of a sub-nm resolution microspectrometer based on a Linear-Variable Optical Filter. *Opt. Express* **2012**, *2*, 489–507. <https://doi.org/10.1364/OE.20.000489>.
- (33) Kramer, R. *Chemometrics Techniques for Quantitative Analysis*; Marcel Dekker Inc., 1998.
- (34) Gemperline, P. *Practical Guide to Chemometrics*; CRC/Taylor & Francis: Boca Raton, FL, 2006.
- (35) Miller, C. Chemometrics in Process Analytical Technology (PAT). In *Process Analytical Technology: Spectroscopic Tools and Implementation Strategies for the Chemical and Pharmaceutical Industries*; John Wiley & Sons, Ltd, 2010; pp 353–438.
- (36) Cárdenas, V. Development of new analytical methods using near infrared and chemometrics for pharmaceutical quality control: enhancement of modelling strategies towards a better product understanding, Universitat Autònoma de Barcelona, 2015.
- (37) Barnes, R. J.; Dhanoa, M. S.; Lister, S. J. Standard normal variate transformation and de-trending of near-infrared diffuse reflectance spectra. *Appl. Spectrosc.* **1989**, *43* (5), 772–777.
- (38) Savitzky, A.; Golay, M. J. E. Smoothing and differentiation of data by simplified least squares procedures. *Anal. Chem.* **1964**, *36* (8), 1627–1639. <https://doi.org/10.1021/ac60214a047>.
- (39) Næs, T.; Isaksson, T.; Fearn, T.; Davies, T. *Multivariate Calibration and Classification*; NIR Publications, 2004.
- (40) Rinnan, A.; van den Berg, F.; Engelsen, S. B. Review of the most common pre-processing techniques for near-infrared spectra. *Trends Anal. Chem. Chem.* **2009**, *28* (10), 1201–1222. <https://doi.org/10.1016/j.trac.2009.07.007>.
- (41) Yun, Y.; Li, H.; Deng, B.; Cao, D. An overview of variable selection methods in multivariate analysis of near-infrared spectra. *Trends Anal. Chem.* **2019**, *113*, 102–115. <https://doi.org/10.1016/j.trac.2019.01.018>.
- (42) Brereton, R. G. *Chemometrics: Data Analysis for the Laboratory and Chemical Plant*; John Wiley & Sons: Chichester, West Sussex, 2003.
- (43) Brereton, R. G. *Applied Chemometrics for Scientists*; John Wiley & Sons, Ltd, 2007.
- (44) Garthwaite, P. H. An Interpretation of Partial Least Squares. *J. Am. Stat. Assoc.* **1994**, *89* (425), 122–127.
- (45) Porep, J. U.; Kammerer, D. R.; Carle, R. On-line application of near infrared (NIR) spectroscopy in food production. *Trends Food Sci. Technol.* **2015**, *46* (2), 211–230. <https://doi.org/10.1016/j.tifs.2015.10.002>.
- (46) Croce, R.; Malegori, C.; Oliveri, P.; Medici, I.; Cavaglioni, A.; Rossi, C. Prediction of quality parameters in straw wine by means of FT-IR spectroscopy combined with multivariate data processing. *Food Chem.* **2020**, *305* (September 2019), 125512. <https://doi.org/10.1016/j.foodchem.2019.125512>.

3. MANUFACTURING PROCESS

3.1 Powder mixing

Powder blending is a process operation commonly performed, when manufacturing solid oral dosage forms. In fact, almost every manufacturing process of a solid oral dosage form depends on a mixing operation, whose final aim is to produce a uniform mixture of powders or granulates¹.

3.1.1 Mixing mechanism

Mixing of solid materials is not a spontaneous event, it requires the action of an external force². However mixing of solids is reversible: de-mixing and segregation phenomena commonly occur, often as a problem. The mixing event can follow three mechanisms^{3,4}: convection, when groups of adjacent particles move from a place to another (macro-mixing)⁵; diffusion, when individual particles randomly move on new formed surfaces (micro-mixing); shear, when slipping planes originate within the powder³ (Figure 24).

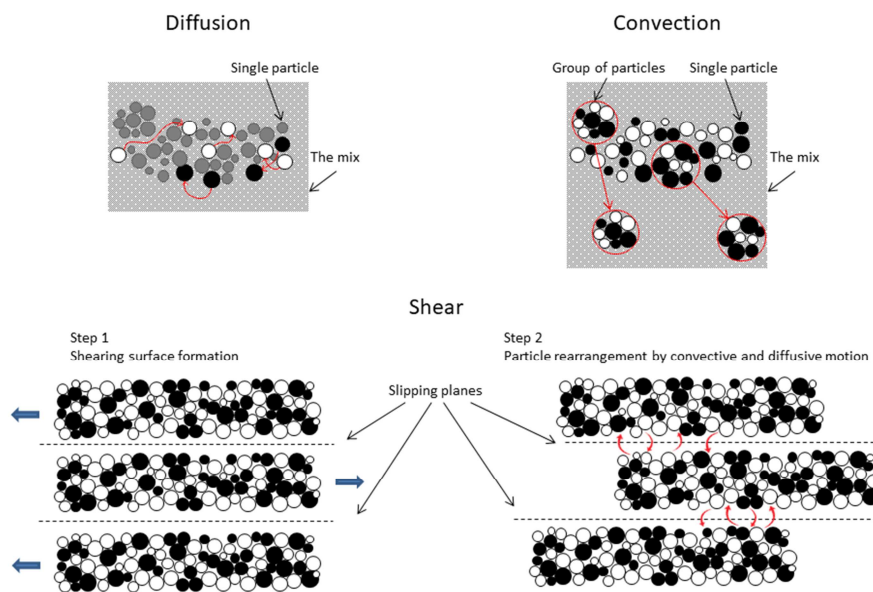


Figure 24 – Mixing mechanisms: diffusion, convection and shear.

These three mechanisms always occur during mixing, but not all have the same importance. The convective motion is strictly dependent on mixer geometry, while the diffusive motion is mainly influenced by the flow characteristics of the powder. For free-flowing powders, the single particle micro-mixing occurs quite rapidly, while for cohesive powders the external shear force plays a key role.

The solid-solid mixing consists of four steps:

- 1) Bed expansion. As the solid material is loaded, it forms a static bed. When the mixing begins, the bed expands, increasing the voids between particles and incorporating air. This is a necessary requirement, to allow the inter-particulate movement.
- 2) Activation of shear forces. They are necessary to activate particle movements. The forces induce a random and turbulent movement in all the three dimensions.
- 3) Proper mixing. Mixing for an adequate time, in order to generate a true randomization of particles. The mixing process can be described by a mathematical law, proposed by Fisher.

$$M = A(1 - e^{-kt})$$

where M is the resistance to mixing, t is the time, A is the initial resistance of the dry powder or granules and k is the rate at which fine powders disperse through the system¹.

The mathematical equation shows that mixing is a time dependent process and that the majority of the process occurs during the initial minutes, when the rate is very rapid.

- 4) Maintaining of particle randomization after the mixing has stopped. It is always desired, even if segregation could take place at this stage.

Segregation is the consequence of a difference in the mobility of particles, due to differences in particle characteristics, such as size, shape and density. Large particles, generally, has a better flow, than smaller ones. In fact, the smaller is the particle, the greater is the surface area; this could generate electrostatic and van der Waals cohesive forces, thus obstaculating the mixing process. The bad flow properties of cohesive powders reduce the mobility of single particles and also the tendency to segregate. However, an excessive cohesiveness can end up in agglomerate formation, which segregates from the rest of the powders in turn. Segregation can also be induced when transferring and handling powder, for example, by pouring the powder to empty the mixer, when it is charged in a capsule-filling machine or in a tablet press or when it is poured by a loading hopper, and in particular during sampling procedure. A review on sampling is available⁶. The most used sampling methodology consists in employing a volumetric sample thief, which possesses one or more cavity to accommodate the powder. It is inserted into the powder bed and, as the cavity opens, the powder particles flow into it. This procedure implies some criticism: when the thief is inserted into the powder bed, it disturbs and alters the bed micro-structure⁷ and the powders tend to segregate, when flowing into the cavity. It has been highly demonstrated that the sampling procedure is biased, regardless of the design of sampling⁸⁻¹¹. The NIR methods is non-invasive and does not require any sampling, thus it is a great alternative to reduce the error due to sampling.

3.1.2 Mixing evaluation

The mixing process step is critical to the manufacturing of tablet, as blend uniformity affects the content uniformity, one of the final product CQAs. The objective of powder mixing process is to obtain a uniform blend, which currently is reached with a fixed and validate process. However, this kind of approach does not take into account the unexpected variability of raw materials and environmental conditions, which always come into the process. The performance of mixing step depends on physical properties of the raw materials, type and geometry of blender and operating conditions (process parameters). In a QbD approach all the factors affecting the mixing process should be identified by the QRM system and deeply investigated¹⁰. The Ishikawa diagram in Figure 25 reports all the factors that could be critical for the blend homogeneity achievement.

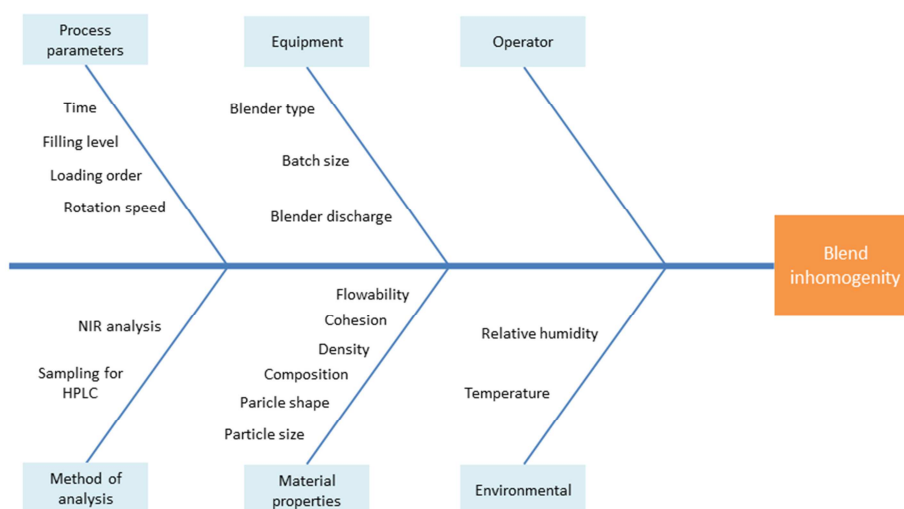


Figure 25 – Ishikawa diagram for identifying the potential critical factors for the mixing process.

The need of testing for blend homogeneity was suggested by FDA in 1996¹² and it is still required for batch release. Since then, criticism about the standard method raised and a new approach of QbD and real time testing has been proposed by ICH and FDA. In a QbD perspective, it is necessary to assess if the CQAs of the final product meet the pre-defined specification, in order to ensure the final quality. The most important CQA for a mixture of powders is its blend uniformity, as it represents a necessary condition for end-point definition. As said before, traditionally, the end-point was time-defined and validated. In a QbD and PAT approach the end-point is not reached after a predefined time of mixing, but rather, when the desired grade of homogeneity in the mixture is achieved. In both cases, however, the blend uniformity needs to be evaluated. The traditional analytical method to estimate blend uniformity is the UV/Vis spectroscopy or the HPLC, which require sampling the material and performing an off-line destructive measurement. Both techniques require time and resources, which need to be disposed after analysis, but above all, introduce a not well estimable error. It is now well known that sampling procedure can cause powder segregation and introduces artefacts in the system⁷⁻¹¹. Alternatives to the traditional analysis exist and one of them is represented by the non-invasive spectroscopic method¹³ (IR, NIR and Raman). Such methods require a previous calibration, but no solvents are used for the analysis and no sampling is performed. Moreover, spectroscopic methods would allow the control shift proposed by QbD, by on-/in-line monitoring the mixing process, instead of just assessing final product quality (see section 1.1.1). Some bibliographic reviews on the available approaches for determination of blend uniformity with NIRS are proposed by: Ciurczak and Drennen, 2002⁶, Blanco et al., 2002¹⁴, Puchert et al., 2011¹⁵, Asachi et al., 2018¹⁶ and Roggo et al., 2007¹⁷. Spectroscopic tools allow to monitor the blending process with two different approaches¹⁸: a qualitative analysis, as proposed by Sekulic et al., 1996¹⁹ and Hailey et al., 1996²⁰ or a quantitative analysis as proposed by Berntsson et al., 2000²¹. Since this two works, many others have been published, proposing both quantitative^{8,10,21-25} and qualitative^{13,18,19,26,27} analytical methods for powder blend uniformity assessment.

Quantitative blend uniformity determination

The spectroscopic supervised quantitative methods use a model previously developed with a calibration set of powder blends. The calibration samples have different concentrations, chosen in a useful range, in order to be able to monitor content variation. The grade of blending of powder mixtures is then evaluated for comparison with the calibration set. Principal Component Analysis (PCA)^{11,24}, Partial Least Square (PLS)^{23,25,28,29}, Classical Least Square (CLS)³⁰, Principal Component Regression (PCR)²² and other techniques can be used for the model building. For a deeper knowledge about the quantitative model development see section 2.3.2.

Qualitative mixing process evaluation

The qualitative methods are based on evaluating the spectral variance, i.e. changes in consecutively collected spectra²⁷. There are many qualitative analysis available^{14,15,17,18,27}, even if the most used is the Moving Block of Standard Deviation (MBSD), first proposed by Sekulic et al., 1996¹⁹ and Hailey et al., 1996²⁰. MBSD evaluates the state of mixing, by checking the decrease of variability in NIR spectra over time, as powders are more and more blended. MBSD is an unsupervised method, therefore it does not require calibration, nor historical or reference data, as it is independent from the formulation. This represents a big advantage respect to other qualitative methods. It is non-invasive, it can be used for in-/on-line evaluations and it requires multivariate statistical analysis techniques and chemometrics.

MBSD consists in the comparison between standard deviation of two adjacent blocks of spectra^{13,19,31}. One NIR spectrum is acquired over a certain number of wavelengths (n_w), at each revolution.

The wavelengths are named as $j=1, 2, \dots, n_w$. m consecutive spectra are grouped into blocks. The m spectra inside a block are identified as $k=1, 2, \dots, m$; the blocks are indicated with the letter i , which is the block number. The MBSD algorithm gives a vector (s_{ij}) , containing the standard deviations of the spectral intensities calculated at each wavelength (j), of the m spectra consecutively recorded and grouped in the i block.

$$s_{ij} = \sqrt{\frac{\sum_{k=1}^m (A_{jk} - \bar{A}_j)^2}{m - 1}}$$

Where A_{jk} is the absorbance of the spectrum k at the wavelength j ; \bar{A}_j is the averaged absorbance of the m spectra at the wavelength j .

For each vector s_{ij} the mean standard deviation over all of the n_w wavelength is calculated, therefore obtaining a single value of standard deviation for each single block $i^{14,27}$:

$$s_i = \frac{\sum_{j=1}^{n_w} s_{ij}}{n_w}$$

When calculating the MBSD, two parameters must be defined:

- The window size (WS): the dimension of each block, i.e. how many contiguous spectra it contains. In the previous equation it is identified with m . It can be arbitrarily chosen.
- The step size (SS): it is the number of spectra the next block is shifted, with respect to the previous one. In fact, each block differs from the others for one or more spectra. Let's imagine to set window size equal to 5, i.e. making blocks of five spectra ($m=5$); the first block ($i=1$) contains spectrum 1 to 5. The second block ($i=2$) contains spectrum 2 to 6, if the step size is equal to 1; in this case the second block loses the spectrum number 1 and takes spectrum number 6, therefore each block contains all the spectra of the previous block, except the first one, which is replaced with the next available spectrum not contained into the block (Figure 26a). If the step size is set equal to 2, each block will contain the same spectra of the previous one, but the first two (Figure 26b). Also the step size can be arbitrarily chosen.

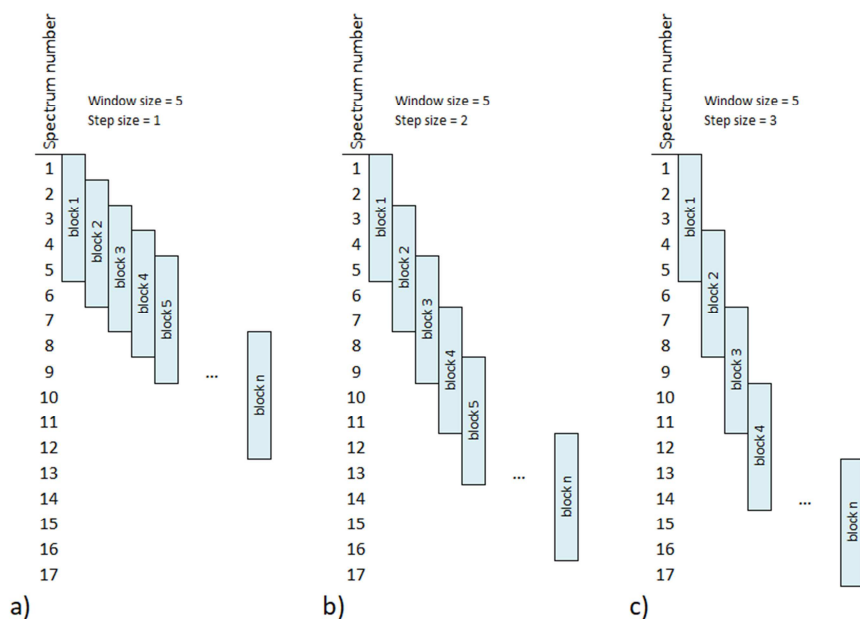


Figure 26 – Criterion for blocks definition in MBSD.

The comparison between two consecutive standard deviations gives information about the status of mixing powder. The standard deviation plotted versus time (Figure 27) gives information about the blend homogeneity and stability over time³². It can be used to track the mixing process and defining its ending-point^{13,26,29}.

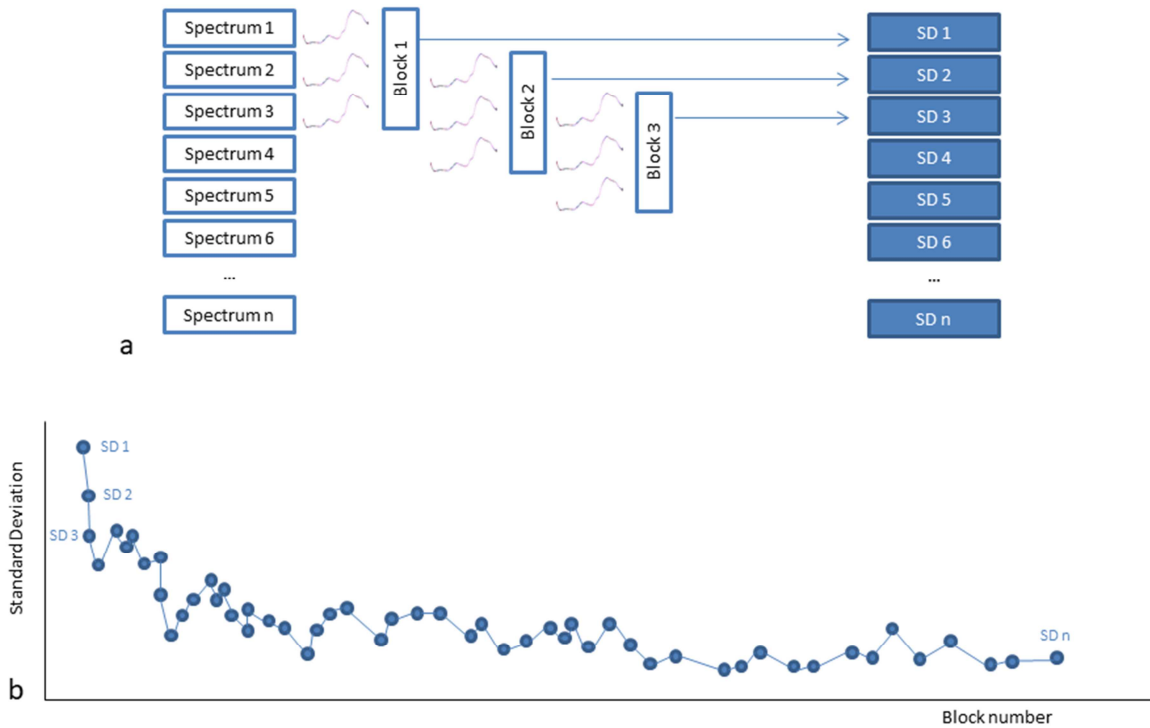


Figure 27 – Criterion for standard deviation calculation (a). Plot of standard deviation versus block number (or time) (b).

The end-point is identified as the time point at which the MBSD versus time profile reaches a minimum value. When the MBSD stabilizes on a minimum value, it corresponds to the repeatability error of the instrument³³. However, MBSD only evaluates the time beyond which the formulation does not change, without any information about the components' concentration.

3.2 Tableting

3.2.1 Tableting mechanism and physics of compression

Tablets are defined by the European Pharmacopoeia as follows: “*Tablets are solid preparations each containing a single dose of one or more active substances. They are obtained by compressing uniform volumes of particles*”³⁴. Tablet can be obtained by direct compression of a powder, or by compression of granules, obtained with wet or dry granulation. The direct compression is seen as the most promising and preferred manufacturing approach, as it is simple, quick and fast³⁵.

A deep knowledge of the whole compression process is really complex, as many simultaneous internal processes are involved, such as particle rearrangement (predominant at the beginning of the process), fracture, plastic deformation (predominant at the end of the process) and, sometimes, also localized melting³⁶. However, for an easier description of the process, a series of events is generally individuated and described as subsequent one to another, even if they actually occurs simultaneously¹:

- a) Transitional repacking and particle rearrangement
- b) Deformation at points of contact
- c) Fragmentation and/or deformation
- d) Bonding
- e) Deformation of the solid body
- f) Decompression
- g) Ejection

a) **Transitional repacking and particle rearrangement**

During compression a mass of powder undergoes some transformations. At the very beginning, when the pressure is still low, a volume reduction occurs, because of particles rearrangement. Particles move over each other, with the finer particles occupying the voids between bigger particles, and thus eliminating the air. This phase is dependent on the particles' shape: spherical particles show a tidier and closer arrangement before the start of the process, therefore undergo less particle rearrangement, respect to the irregular shape particles. The rearrangement phase goes on, until an equilibrium condition is reached. Particles are not able to move, as all the voids have been occupied. However, at this stage the porosity can still be considerable. During the particle rearrangement the first densification phenomenon occurs, leading to an increasing of the initial bulk density.

b) **Deformation at points of contact**

When all the voids are occupied and particles are not able to move and rearrange any further, an increase of compression force causes deformation at the point of contact. The deformation can be elastic or plastic. A plastic deformation is reversible, therefore, if the applied force would be release, the particles would return to their initial shape. On the contrary, a plastic deformation does not completely recover, after the stress release; therefore, it is an irreversible deformation. The type of deformation (elastic or plastic) depends on the material characteristics and, generally, one of the two types predominates. However, the presence of plastic and elastic deformation also depends on the applied force: at low pressure, elastic deformation occurs at first, but when a sufficiently strong stress (yield stress) is applied, the yield point is passes and the deformation becomes plastic (Figure 28).

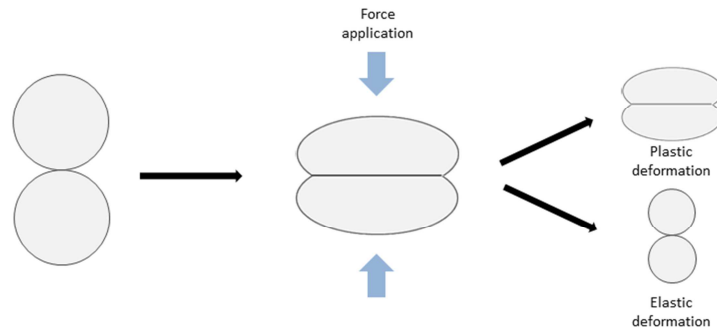


Figure 28 – Elastic and plastic deformation. Image inspired by Sun, 2011³⁷.

c) **Fragmentation and/or deformation**

Some powders, in alternative or after plastic deformation, fragment, creating a bigger number of smaller particles, thus new surfaces and new point of contact with neighbour particles. This new binding surfaces are responsible for the increasing of strength and also of density, as the small fragments occupy the remaining small voids. At the beginning of the fragmentation, the strength rapidly increases, as new surfaces continuously appear and new intermolecular interactions are established. As pressure further increases, the strength increase is slower. Higuchi et al., 1953³⁸ observed the variation of the specific surface area, as a function of the compression force, by measuring the particle dimension and surface before and during compression. The authors observed an increase in specific surface area and a reduction of particles diameter at the beginning of the compaction process, indicating the new surfaces formation, as a consequence of fragmentation. New surfaces mean new areas available for bonding interactions, called *bonding areas*. The fragmentation degree depends on the material: some powders, in fact, do not fragment, as the applied stresses distribute on particle as a plastic deformation.

d) **Bonding**

Going further with compression, a decrease of specific surface area occurs, probably due to cold bonding of neighbour particles³⁸. Different mechanisms of bonding have been proposed. The intermolecular theory attributes the bonding formation to the molecular interaction between neighbour particles and this depends on both *bonding area* and *bonding strength*, as proposed by Sun with his BABS model³⁷. He reported that “*the forces responsible for the strength of a tablet are not different from the familiar interactions that define the form of the physical universe*”. Molecular solid are held together by van der Waals interactions and hydrogen bonding, while ions are held together by ion-dipole, and ion-induced dipole interactions and coulombic forces. The molecule and ions at the surface of a solid, therefore, are able to interact with other particles. However, the magnitude of intermolecular interaction depends on distance³⁹. This is the reason why a not compacted powder does not possess an appreciable strength and particles are easily separable (because neighbour particles are too far from each other), while a compacted powder has a mechanical strength (because particles are sufficiently near to establish intermolecular interactions). The ability of a powder to originate a compact of a sufficient strength is referred to as *tableability* and it is deeply described in the next section (see section 3.2.2).

e) **Deformation of the solid body**

When the solid body is formed, a further increase in applied pressure would cause a plastic or elastic deformation of the whole tablet inside the matrix.

f) **Decompression**

The decompression phase begins when the upper punch moves up and the compaction pressure rapidly passes from the highest value to zero. The deformation previously induced in the solid body and an elastic rebound causes a stress distribution inside the tablet; an elastic recovery releases all the elastic energy accumulated during compression.

g) **Ejection**

After the powder has been compacted in a tablet, it has to be removed from the die. The lower punch rises up pushing the tablet out of the die. As the tablet is removed the lateral pressure, previously experimented by the tablet wall, is released. A further relaxation, plastic recovery and increase of volume occurs.

3.2.2 Mathematical description of physics of compression

To obtain tablets, a powder (or a granulate) is located into a die and a compressive force is applied with punches, causing a reduction of powder volume. What exactly happens during the reduction of the volume has been the subject of numerous studies and there is not a unique way to describe the process. The starting powder has its own characteristics (input characteristics), affecting the tableting process and, in turn, the resulting tablets have some characteristics (output characteristics), depending on the punch and die geometry, on the applied force and also on the powder characteristics (Figure 29).

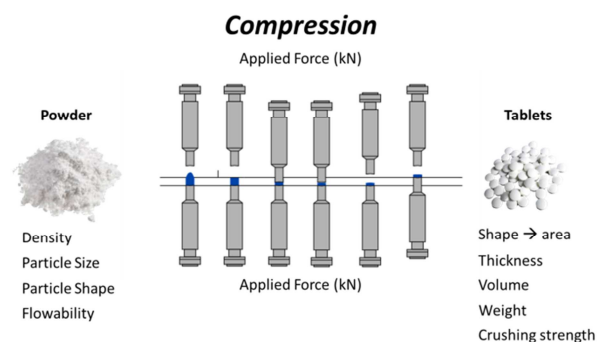


Figure 29 – Schematic representation of the mixing process.

It can be concluded that there are a lot of characteristics affecting the process and resulting from it, which are all interconnected. The relationship between some of these characteristics have been investigated and used to describe and study the compaction behaviour. As stated by Newton and Grant, 1974⁴⁰, when compressing a powder to obtain a tablet “for a given material under given conditions, the variables of pressure, porosity and tensile strength should be related mathematically”. When describing the compression process in terms of pressure, porosity and tensile strength some clarifications are needed: the compaction pressure is used, instead of compression force, the tensile strength, instead of breaking force (or crushing strength) and the porosity is calculated through the powder true density and the solid fraction.

The compaction pressure links the applied force to the cross sectional area of the punch.

$$Pressure = \frac{Applied\ Force}{Area}$$

It is useful for comparing the loading of different size tablet, because it is not possible to directly compare the forces, when the tablets have a different size. In fact, the same compaction force has a different effect on tablets of different dimensions: a smaller tablet would experience a higher pressure, than a bigger tablet, when compressed with the same compaction force and this would result in a different

mechanical strength. For comparison purpose and for tableability, compressibility and compactibility assessment the compaction pressure is used, instead of compaction force³⁷.

The true density “corresponds to the exact volume occupied by the material, without porosity”⁴¹. True density is a material characteristic, necessary for a complete characterization of powder mechanical properties. In fact it is necessary for calculating other properties, such as tablet porosity. However true density is not so easy to quantify. It could be obtained with flotation density measurement⁴², or from single crystal structure⁴³, but the first one is not suitable for powder mixtures and the second one is performed at low-temperature, thus giving error-affected value due to the low-temperature measurement^{44,45}. Other methods have been proposed⁴⁶, but true density is more commonly obtained with helium pycnometry. Such analysis is performed at ambient temperature and consists in measuring the pressure of a known amount of helium gas, located in a test cell, before and after the powder sample loading. As the sample is loaded, helium penetrates into the smallest pores of powder; this causes a difference in pressure, which is used to calculate the volume of the sample. However also this technique is not criticism-free, as literature data show different values reported by different authors⁴¹. This phenomenon depends on the high sensitivity of pycnometry, to many factors, such as operating parameters, powder characteristics and also to water release. In those samples containing water, an error is often made, due to the evaporation of water and the consequent alteration of the pressure in the test cell. In fact, in this case the measured pressure is not only due to the helium, but also to the water evaporated from the sample. At the same time, it is not possible to dry a hydrated form, as it would alter the crystal structure. For that reason Sun⁴⁴ sustained that helium pycnometry is not suitable for water-containing powders, such as hydrates, amorphous and most formulations. Significant errors and different values can be obtained, because of the water release during analysis⁴⁴. He proposed an alternative method, for mathematically calculating the true density, by fitting the compaction data. This mathematical method is based on the existing relation between the compaction pressure and the tablet porosity, described by the Heckel equation⁴⁷:

$$\ln\left(\frac{1}{1-D}\right) = KP + A$$

where D is the relative density, P the pressure, $1-D$ is the pore fraction, K a proportionality constant and A is a constant.

The tablet porosity is related to the true density, by the following equation:

$$\text{Tablet porosity} = 1 - \frac{\text{Tablet Density}}{\text{True Density}}$$

Therefore the true density can be expressed in terms of tablet density and tablet porosity, as follows:

$$\text{True Density} = \frac{\text{Tablet density}}{1 - \text{Tablet porosity}}$$

The method proposed by Sun calculates the true density using the equation derived from the modified Heckel equation⁴⁴:

$$P = \frac{1}{C} \left[(1 - \varepsilon_c) \frac{\rho_{\text{tablet}}}{\rho_{\text{true}}} - \varepsilon_c \ln \left(\frac{1 - \frac{\rho_{\text{tablet}}}{\rho_{\text{true}}}}{\varepsilon_c} \right) \right]$$

where P is the compaction pressure, C is a constant indicating the deformability of the powder sample, ε_c is the critical porosity, ρ_{true} is the true density, ρ_{tablet} is the tablet density.

The tablet density of a powdered material approaches its corresponding true density, when increasing the pressure⁴⁸.

The solid fraction is the ratio of tablet's apparent density and the true density and it is related to the porosity.

$$\text{Solid Fraction} = \frac{\text{Tablet Density}}{\text{True Density}}$$

$$\text{Porosity} = 1 - \text{Solid Fraction}$$

Numerous authors⁴⁹⁻⁵¹ stated the importance of solid fraction, when characterizing tablet compaction properties. In particular, Tye et al, 2005⁵² demonstrated that tablet solid fraction is the primary responsible for tablet strength. Amidon et al., 2017⁴⁵ reported that “a change in solid fraction of 0.01 (i.e., a change in SF from 0.85 to 0.86) can result in a mechanical property change of 10-20%. For this reason, it is critical to compare the properties of a material at a “reference” solid fraction. The reference value for solid fraction can be arbitrarily chosen, but is important to be in the typical range for tablet compaction.

The tablet mechanical strength is important to produce tablets with the correct strength, considering all the subsequent processing, packing, transport and handling⁵³. An excess in tablet strength could cause a too slow disintegration time and drug release, and difficulties in breaking the tablet, for patients who need dosage flexibility or cannot swallow the entire tablet. However, a tablet should be hard enough to resist further processing, packing, transport and handling. A too high friability, in fact, would affect the visual aspect, besides causing a dosage reduction³⁷. The tablet mechanical strength is commonly quantified by the force necessary to break the tablet, with a diametral-compression test⁵⁴ (see section 3.4). The obtained measured value is commonly, and erroneously, called “tablet hardness”; more correctly it represents the “breaking force”. A so called “compression profile” can be made, by plotting the breaking force vs the compaction force. However, the breaking force is strictly dependent on the tablet shape and size. In fact, tablets of the same formulation, but different dimensions do not exhibit the same mechanical strength^{37,55}. Newton et al., 1971⁵⁵ demonstrated that the tensile strength is a property of the compacted material and proposed it as a new parameter, to maintain constancy of properties for tablets of different size, but same composition. In fact, tensile strength normalizes the force dividing it by the longitudinal section of the tablet.

$$T_s = \frac{2 \cdot F}{\pi D t}$$

where F is the breaking force, D is the tablet diameter and t is the thickness⁵⁴.

The conversion of breaking force to tensile strength is different for tablets of different geometry. The equation previously reported is valid for round and flat tablets. Newton et al., 1972⁵⁶ developed an equation for deep concave tablets; Stanley and Newton, 1980⁵⁷ for capsule-shaped; Pitt et al., 1988⁵⁸ for convex-faced round tablets, while Pitt and Heasley, 2013⁵⁹ for elongated tablets. Compacts of the same tensile strength show almost the same mechanical properties, while the same is not, when talking about breaking force. This was demonstrated by Newton et al., 1971⁵⁵, by plotting the tablet strength (as breaking load or as tensile strength) against the compaction pressure of tablets of different size. When the tablet strength was expressed in terms of breaking load, an individual regression line was found for each tablet dimension. When expressing the tablet strength as tensile strength, on the contrary, a common regression line was obtained, despite the tablet size (Figure 30). For pharmaceutical tablets, tensile strength should be major than 1 MPa; the typical range is (0.1 – 4 MPa)⁴⁵.

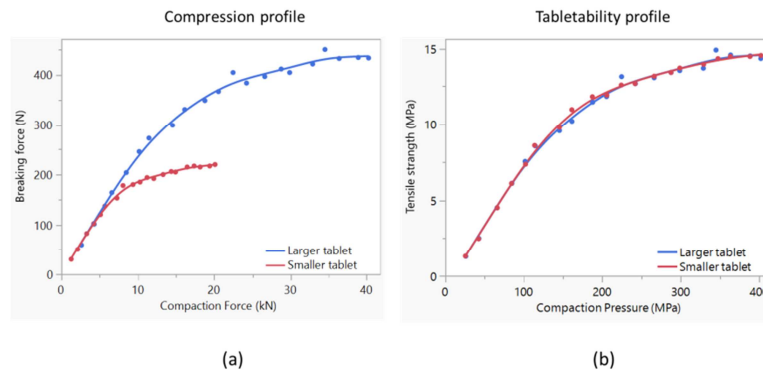


Figure 30 – Figure (a) shows the compression profile, which depends on the tablet dimensions. Figure (b) shows the tableability profile, which is independent from tablet dimensions.

The speed rate is a critical parameter for compression. The compression process has been highly demonstrated to be time dependent^{45,49,52}. The time dependency of the compaction phenomenon derives from the stress relaxation of materials undergoing plastic deformation, after compression. Materials with a plastic behaviour are the most time-dependent, while brittle materials are expected to be less sensible to time variation. In fact, once the fragmentation is finished, a prolonged applied force has a limited effect on increasing strength, because all the possible interactions have already been established⁵². Powder characteristics, such as particle size, can influence the speed dependency. A different rotation speed can cause a different porosity reduction, which reflects on the final tablet tensile strength, as demonstrated by Armstrong and Palfrey, 1989⁴⁹.

Compression profiles

As explained by Tye et al., 2005, compaction pressure, tensile strength and solid fraction are related, with a direct or an indirect cause-effect relationship. “The solid fraction of a compact is the direct result of the application of compaction pressure. Similarly, the tensile strength of a compact is the direct result of its solid fraction. However, the relationship between compaction pressure and the resulting tensile strength is more indirect”⁵². This concept was also graphically represented (Figure 31).

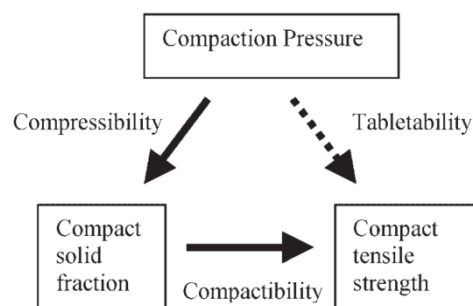


Figure 31 – Relationship existing between compaction pressure, porosity and tablet strength. Figure from Tye et al., 2005⁵².

Kuentz and Leuenberger, 1999⁶⁰ defined a tablet as “a special type of dispersion” where “the solid fraction and the air in pores constitute two phases of the system”. The properties of a low packing compact and a tablet obtained at higher pressure can be very different, as in the first case particles maintain a certain grade of individuality and possess minimum movement ability, while in the second case the individuality disappears, as the tablet resembles a continuum of solid fraction. This makes clear that the systems characteristics are different as a function of the relative density. This is the reason why a big effort has been made by many authors, in describing the whole compression process in terms of volume

reduction, i.e. increase of density. However, it is nearly impossible to describe the densification process with a single monovariate equation⁶¹. Rather, the three variables (compaction pressure, tensile strength and porosity, or solid fraction) can be plotted one versus another in three different ways, obtaining three different relationships, respectively named: compressibility, compactibility and tabletability. The previous relationships are used for describing the compression behaviour of a material and, then, to predict its ability to form tablets. Tabletability represents the relationship between tensile strength and compaction pressure. However, it does not give a full understanding of the relationship, because the tablet mechanical strength depends on both, bonding area and bonding strength per unit bonding area, (as described by the BABS model proposed by Sun, 2011³⁷). At the same time, the single contribution of each of the two factors cannot be deduced from the tabletability relationship alone. The bonding area and bonding strength contribution should be singularly evaluated, with two additional relationships. Bonding area is assessed by powder compressibility, while bonding strength is quantified using compactibility^{37,62}. In conclusion, a total of three relationships are used to describe the tableting performance of powdered materials:

- Compressibility → porosity vs compaction pressure
- Compactibility → porosity vs tensile strength
- Tabletability → tensile strength vs compaction pressure

In literature there are highly numerous relationships expressing the compressibility, a quite abundant number of expressions for compactibility, but only a few expressions for the tabletability profile. Anyway, there is not a single and unique relationship between pressure and volume reduction (thus porosity), nor between pressure and tensile strength, therefore, any relationship among these three parameters depends on the method of compaction and on the starting material⁴⁰.

Tabletability

*“Tabletability is the capacity of a powdered material to be transformed into a tablet of specified strength under the effect of compression pressure”*⁶³. Tabletability describes the relationship between tablet tensile strength and compaction pressure^{37,62}. Really different tabletability behaviours exist, as reported in Figure 32.

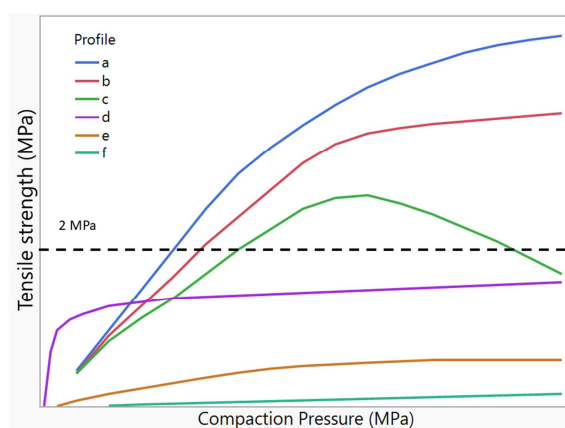


Figure 32 – Different tabletability profiles. Figure inspired by Sun, 2011³⁷.

Profile a and b shows powders which easily compact with low pressure, therefore possessing a good tabletability. Profile c shows a powder with a good tabletability only at low and medium pressure; as pressure increases the tabletability get worst. Profile d, e and f shows powders with a poor tabletability, which will never reach a sufficient strength, regardless of the applied pressure.

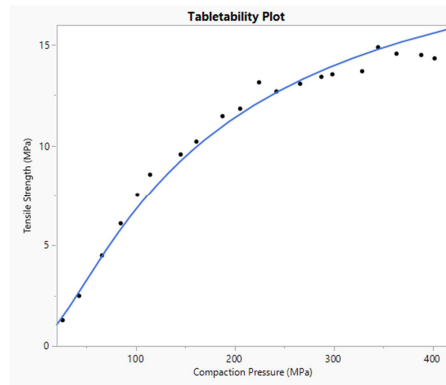


Figure 33 – A generic tabletability profile.

A generic tabletability curve is reported in Figure 33. The tensile strength increases as compaction pressure increases, in a linear way only at the beginning, i.e. for low and medium pressures. For an easier understanding of the process Persson and Alderborn, 2018⁶⁴, defined three regions: a low, an intermediate and a high pressure region. In the first region, the pressure is so low, that no solid compacts are still formed. In the intermediate pressure region, particles pack more closely, reducing pores dimension; a big number of new points of interactions and new bonding sites occur, causing a rapid, and almost linear, increase in tensile strength, up to a critical point. At this point the increasing rate of tensile strength gradually decreases, as pressure increases: only few additional interactions occur, thus resulting in a different and slower rate of tensile strength increase. As pressure is further increased the high pressure region is reached and no more inter particle changes happens, because the maximal tablet strength have already been obtained^{48,64}. In 2011, Sun³⁷ published a review about powder tabletability, with the purpose of deeply describing this phenomenon. He proposed a qualitative model called *BABS model*, based on the concept of inter-particulate *bonding area* and *bonding strength*³⁷. The different tabletability behaviour depends on the combination of bonding area and bonding strength and a classification of tabletability profiles can be made considering the role of them both. The tabletability relationship is speed dependent.

Literature data report a few equations for tabletability relationship, which are listed in Table 4.

Equation	References
$\sigma = kP + C$	Newton et al., 1971 ⁵⁵ ; Mallik, 2014 ⁶¹ , Joiris et al., 1998 ⁶³ ; Sun and Grant, 2001 ⁶²
$\sigma = k \log P + C$	Higuchi et al., 1953 ³⁸
$\log \sigma = k \log P + C$	Newton and Grant, 1974 ⁴⁰
$\sigma = kP^{T_f/2}$	Kuentz and Leuenberger, 2000 ⁶⁵
$\ln(-\ln(1-CS/CS_{max}))=a\ln P+b$	Castillo and Villafuerte, 1995 ⁶⁶
$SCS = C_p \cdot P + b$	Sonnergard, 2006 ⁶⁷

Table 4 – Some of the equations for tabletability profile, available in literature.

Where σ is the tensile strength, P is the applied pressure, T_f is the critical fracture exponent, k , a , b and C are constants, SCS is the specific crushing strength and C_p is a constant called compactibility parameter.

Compressibility

“The compressibility of a material is its ability to be reduced in volume as a result of an applied pressure”⁶³. When applying a pressure to a powder material, a densification phenomenon occurs. However, tablet density can be significantly different for different materials; therefore, the plot of tablet density versus pressure is not useful for comparison purpose. What can be compared among different materials are the tablet porosity and the solid fraction. The first one is the ratio of tablet density and true density and it always has a value ranged between 0 and 1; the solid fraction is directly calculated from the porosity, with the equation⁴⁸:

$$\text{Solid Fraction} = 1 - \text{Porosity}$$

The simplest method to compare the compressibility of a set of substances consists in representing the gradual change in tablet porosity as a function of any increase in compaction pressure⁶³, as proposed in Figure 34. A decreasing of powder porosity corresponds to an increase in solid fraction and also of bonding area. In fact, the closer are the particles, the more abundant are the points of contact among neighbour particles. Therefore, it can be concluded that bonding area increases when increasing pressure³⁷.

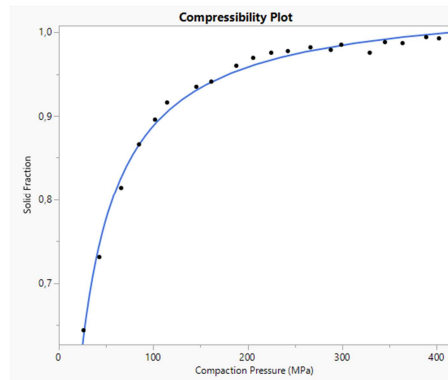


Figure 34 – A generic compressibility profile.

The volume reduction can be expressed in terms of porosity^{35,48,52,62,63}, solid fraction⁶⁸, or apparent density³⁸. Several equations, expressing the relation between the pressure and the volume reduction of a powdered material under compression, can be found in literature. The two most used equations are reported in Table 5. A comparative review was proposed by Kawakita and Ludde, 1970⁶⁹ and by Kawakita and Tsutsumi, 1966⁷⁰.

Reported Equation or Plot	References	Volume reduction expression
Porosity vs log Compaction Pressure	Higuchi et al., 1953 ³⁸	Porosity
$\ln \frac{1}{1-\rho} = kP + A$	Heckel, 1961 ⁴⁷	Relative density
$\frac{P}{C} = \frac{P}{a} + \frac{1}{ab}$	Kawakita and Ludde, 1970 ⁶⁹	Volume reduction

Table 5 – Most used equation for compressibility profile.

Where P is the compaction pressure, ρ is relative density, C is relative volume decrease i.e. = $(V_0 - V_p)/V_0$, with V_0 the initial powder bed volume and V_p the powder volume upon compression. a , b , k and A are constants.

The so called Heckel's analysis is often associated to the compressibility, as the Heckel equation has been highly used to study the densification behaviour^{63,71}. Such equation expresses porosity (ϵ)-compaction pressure (P) relationship in a linear way⁴⁸:

$$-\ln(\epsilon) = KP + A$$

where K, the reciprocal of the slope, is the mean yield pressure and A is a constant.

Heckel plot has been widely used to assess the mechanism of deformation and as a tool to estimate yield pressure⁵². Heckel considered the powder compaction as a first-order chemical reaction, where the pores are the reactant and the densification is considered to be the product of the "reaction". According to first-order kinetics, the density variation (dD) is proportional to the pore fraction (1-D), as pressure (P) varies:

$$\frac{dD}{dP} = K \cdot (1 - D)$$

Solving the equation:

$$\frac{dD}{(1-D)} = K \cdot dP \quad \rightarrow \quad \int_{D_0}^D \frac{dD}{(1-D)} = K \int_0^P dP \quad \rightarrow \quad \ln(1 - D_0) - \ln(1 - D) = KP$$

where D_0 is the relative density at zero pressure.

It is finally obtained the well-known Heckel's equation:

$$\ln\left(\frac{1}{1-D}\right) = KP + \ln\left(\frac{1}{1-D_0}\right) \quad \text{or} \quad -\ln(1 - D) = KP + A$$

If $\ln(1/1-D)$ is plotted versus the compaction pressure, the relationship appears to be not linear, over the whole pressure scale. In particular, a curvature can be observed for low pressure. Heckel attributed such deviation from linearity to the rearrangement of particle at the beginning of the compaction process. The curvature is due to the term $\ln(1/1-D_0)$ in the equation. As the deviation from linearity is only at low pressure, this term is usually substituted with a constant A, thus obtaining a quantitatively valid equation, except at the lowest pressure⁴⁷. The constant A is derived from the linear portion of the plot. Since 1961, a number of modifications have been made to the original equation, as described by Kuentz and Leuenberger, 1999⁶⁰ and by Sonnergard, 2006⁶⁷.

Compactibility

"Compactibility is the ability of a material to produce tablets with sufficient strength under the effect of densification", when volume is reduced or, in another words when the porosity decreases (i.e. solid fraction increases)⁶³. A generic compactibility profile is reported in Figure 35.

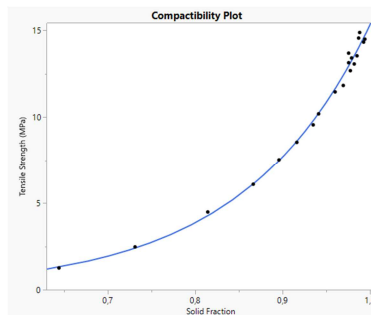


Figure 35 – A generic compactibility profile.

Different equations exist in literature, to relate the tensile strength to the porosity (i.e. solid fraction); some have been reported in Table 6.

Reported equation or plot	References	Volume reduction expression
$\sigma = \sigma_0 e^{-b\varepsilon}$	Ryshkewitch, 1953 ⁷²	Porosity
Crushing strength vs Porosity	Higuchi et al., 1953 ³⁸	Porosity
$\sigma = \frac{1}{C} \left[\rho_c - \rho - (1 - \rho_c) \ln \left(\frac{1 - \rho}{1 - \rho_c} \right) \right]$	Kuentz and Leuenberger, 1999 ⁶⁰	Relative density
$\sigma = k(\rho - \rho_c)^{T_f}$	Kuentz and Leuenberger, 2000 ⁶⁵	Relative density
$\sigma^{1/T_f} = k^{1/T_f}(\rho - \rho_c)$	Kuentz and Leuenberger 2000 ⁶⁵	Relative density
$\sigma = k(\rho - \rho_c)^{T_f} + \sigma_0$	Ramirez et al., 2004 ⁷³	Relative density
$\sigma = k\rho^{T_f}$	Ramirez et al., 2004 ⁷³	Relative density
Log(Tensile strength) vs Porosity	Tye et al., 2005 ⁵²	Porosity
$\ln \sigma = \ln \sigma_0 + kSF$	Mallick, 2014 ⁶¹	Solid fraction

Table 6 – Some of the equations for compactibility profile, available in literature.

σ is the tensile strength, σ_0 is the tensile strength at zero porosity, ρ is the relative density, ρ_c is the critical relative density, T_f is the fracture exponent, SF is the solid fraction, ε is the tablet porosity and C , k , a and b are constants.

The densification process can be described in terms of relative density⁶⁰, reduction of volume or porosity⁷⁴, or as an increase of solid fraction^{61,68}. The compactibility profile relates the increase of tensile strength to the decrease of porosity with an exponential trend. Among all the reported equation, the most used is the Ryshkewitch equation⁷²:

$$\sigma = \sigma_0 e^{-b\varepsilon}$$

where σ is the tensile strength, σ_0 the tensile strength at zero porosity and ε the tablet porosity.

As previously explained, the bonding area depends on particle size and shape, but it is related to porosity decrease too. Therefore, it could be assumed that, “for powder of the same particle size and dimension, the same porosity corresponds to the same bonding area. If so, the relative bonding strength can be derived from the ratio of tensile strengths at an identical porosity, e.g., zero porosity”³⁷. In other words, the compactibility reports the tensile strength normalized by the tablet porosity⁶².

The tensile strength has been demonstrated to be speed dependent⁴⁹: in fact, tablets with the same composition, but compressed with different speed have shown a differences in tensile strength value. As the strength of tablets is the result of a porosity reduction, it is reasonable to attribute the observed difference to a difference of tablet porosity. This has a confirmation in the work of Hancock et al, 2003⁵⁰. The authors observed that the strength of different tablets was comparable only when the solid fraction was comparable too. However, Tye et al., 2005⁵² demonstrated that the compactibility plot is independent of process parameters, such as speed, because only measured tablet properties are used in the equation.

As final conclusion, with tableting, compressibility and compactibility plots it is possible to understand and compare the tableting performance of powder materials. The understanding of the compression process is necessary, for the development of a robust tablet formulation and it is necessary for the scale up of a laboratory formulation.

3.3 Tablet coating

Coating is a unit operation commonly performed during the tablet manufacturing process. Unfortunately, it is also one of the more critical, as it suffers of a lack of understanding of the process complexity, as highlighted by Feng and Mohan, 2020⁷⁵ and by Suzzi et al., 2010⁷⁶. It consists in a thin-layer deposition of a polymer-based film, over the tablet surface. There are three different types of coating^{77,78}:

- non-functional coating, used for aesthetic and compliance purpose (ease of swallowing, etc.) and to protect the tablet from environmental effects;
- functional coating, used for taste masking, gastric protection, or to control the API release;
- active coating, which consists of application of a coating layer containing the API.

Coated tablets can show three different types of release profile⁷⁹:

- immediate release;
- modified release;
- controlled or sustained release.

If a coated tablet has an immediate release profile, thus the coating can have an aesthetic (dosage strength or brand identification and visual attractiveness) or a compliance function (facilitates the assumption, taste masking), thus it, generally, consists of a non-functional coating, with the exception of taste masking. A modified release coated tablet has a specific type of functional coating, also called enteric coating, which gives the tablet a protection from the gastric environmental and releases the API in the intestine. Controlled or sustained release tablets have a well-defined release profile: the API release occurs at a predefined time interval, or it is gradually released over an extended period of time. The applied coating in this case is a functional-coating.

3.3.1 Tablet coating mechanism

Coating is applied by spraying tablets with a coating suspension. The most used equipment for tablet coating is the rotating pan, which can be perforated or not perforated. The pan coating consists in spraying a coating suspension on top of a moving bed of tablets, thanks to one or more spray guns, which are mounted on an arm inside the pan. The spraying suspension is composed by a solvent, a polymer and a plasticizer; in case of coloured coating a pigment is also added. When the tablets are located inside the pan, the spray guns are orientated, in order to have a spray direction perpendicular to the tablets' bed. The speed of pan rotation should let the tablets move in a continuous and fluid way, so that they remain under the spraying zone not too much time, nor too little. Discontinuous movement should always be avoided. During the pan rotation the coating suspension is sprayed on top of tablets. The nozzle dimension of the guns should be selected on the base of the amount of suspension sprayed per minute. It is important not to have big drops falling on the bed of tablets. As the coating suspension is sprayed, small droplets deposit on tablet's surface and the solvent evaporates. The droplets formation depends on many variables, such as the nozzle type (hydraulic airless or pneumatic air-blast atomizer), the pump speed and the characteristics of the coating suspension. As a droplet deposits on a tablet surface, the solvent evaporates under the effect of the hot temperature of the air and the insoluble materials adhere to the tablet. The solvent evaporation is controlled by the inside temperature of the pan, which in turn, depends on the in-air temperature. The evaporation should be fast enough not to excessively wet the tablet bed, thus causing sticking of tablets with the nearby ones. However, a too fast solvent evaporation could dry part of the droplets before they reach the tablets, leading to the formation of an heterogeneous film, accentuating intra- and inter-tablets variability. Ideally a droplet should be dried before the application of the next one⁷⁶.

The coating process consists of three distinct phases:

- heating: the tablet bed is heated until the desired temperature is reached;
- spraying: as the bed of tablet has reached the desired temperature, the spraying phase starts. The suspension is sprayed on top of the tablet. The temperature and the air flow must be continuously controlled, in order to ensure a constant process;
- drying: once the coating suspension has been sprayed, the tablets continue to move, until they are completely dry. Attention should be paid, in order to avoid an excessive drying.

3.3.2 Tablet coating evaluation and controls

The coating process is complex, still not well understood and, as previously emerged, the final coating layer can be influenced by numerous variables (equipment geometry, coating suspension properties) and process parameters (inlet and outlet air temperature, bed temperature, pan speed, atomizing air pressure, spray rate, tablet-nozzle distance and spraying guns orientation, etc.). The coating should ensure that tablet CAQs (such as content uniformity, drug assay and dissolution) meet the quality specifications. Therefore the coating thickness and the coating uniformity should equally be monitored, as they could have an impact on tablets CQAs⁷⁵. The risk evaluation for coating process is graphically reported in Figure 36.

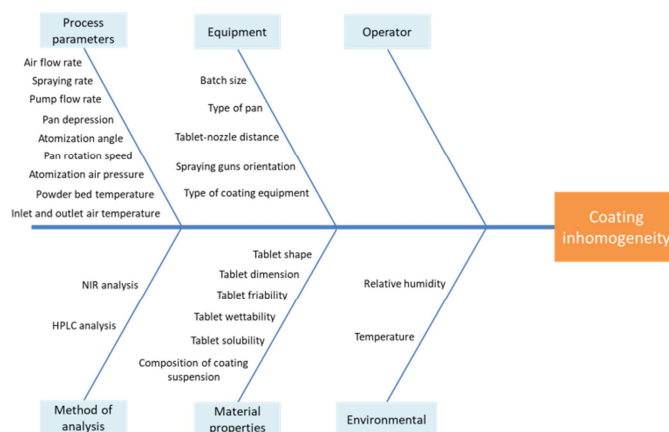


Figure 36 – Ishikawa diagram for identifying the potential critical factors for the coating process.

The coating uniformity needs to meet quality standards and it is quantified with a coefficient of variation (Cv). It is possible to distinguish among an intra- and inter-tablet uniformity. The first one is the uniformity of the coating of each single tablet, while the second one represents the uniformity of the coating, among different tablets and it is the most critical one. The coating thickness is relevant for functional and active coating. As concern the active coating, alteration of the thickness would have a repercussion on the API amount⁸⁰. As for functional coating, a too thin layer could be ineffective for tablet protection against gastric acid in enteric-coated tablets; or it could cause alterations of the dissolution rate, in sustained release coated tablets. At the same time, a too thick layer could increase the dissolution time. It can be concluded that, in any case, an erroneous film thickness would have an effect on tablet CQAs, thus bringing to undesired consequences. Some of the reference methods for thickness measurements available in literature are⁷⁷:

- consumption of coating suspension during the coating process;
- weight gain of tablets: the tablets are weighted before and after coating and the average weight gain is calculated;
- estimation of tablet dimensions with a micrometer gauge;
- cutting of a tablet of halves under a microscope.

However, all these reference methods do not provide any other information about the homogeneity and uniformity of coating. For that reason it is of particular importance to develop an effective quality control, based on PAT approach⁸¹. Different PAT tools can be used for coating monitoring, such as visual imaging, terahertz pulsed technology, optical coherence tomography and in particular Raman^{78,81} and NIR spectroscopy^{32,75,79,82,83}. A brilliant summary of NIR, Raman and Terahertz spectroscopy application in coating process from 1995 to 2019 is reported in Feng et al., 2020⁷⁵. Spectroscopic measurements are considered indirect methods⁷⁷, as the provided output is a spectrum, and only extracting information from it, data relative to coating thickness or coating uniformity becomes available. The coating monitoring with NIR spectroscopy is based on spectral changes, which are related to a variation in coating thickness⁸². Two different types of change can be seen: a quantitative change in peak intensity and a physical change. The chemical composition of coating layer differs from the core composition. As the API is progressively coated, it is not visible to the NIR anymore (with the exception of active coating). Consequently, the API peaks should reduce and peaks relative to coating components should be seen instead. At the same time, the thickness increase shows up as a change in the reflectance spectra, which does not affect the intensity, but rather, it causes an up or down shift of the entire profile. Such differences in spectra are related to the progression in coating process, by a quantitative model. For quantitative model building, see section 2.3.2. The model for tablet coating monitoring can be developed as an individual coating thickness model, as made by Moes et al., 2008³², or by scanning the whole bed of tablets.

3.4 Tablet controls

Tablets are the final product of the manufacturing process. A list of elements (such as the intended clinical use, route of administration, delivery systems, dosage form, dosage strength, esthetical aspect, container closure system, information about pharmacokinetic and drug product quality criteria), which must be respected, defines the tablet QTPP. The achievement of the QTPP depends on the CQAs, which for tablets are drug assay, content uniformity, dissolution, disintegration time, identity, microbial limits, impurities, crushing strength and appearance. However, in turn, they depend on other tablet characteristics, which are equally monitored in order to assure the tablets quality.

Appearance

The first information about the quality of the tablet comes from the visual appearance. A tablet should appear not dusty, with a smooth and homogeneous surface. Alteration of the visual aspect is often connected with tableting issues. The visual inspection can be done with no instrumentation, or via imaging analysis, with an optical or scanning electron microscopy.

Weight

The control of weight of tablets should be performed as reported in the European Pharmacopoeia: individually weigh 20 units taken at random and determine the averaged mass. No more than 2 of the individual masses should deviate from the average mass by more than the percentage deviation reported in Table 7 and none deviates by more than twice that percentage⁸⁴.

Pharmaceutical Form	Average Mass (M)	Percentage Deviation
Tablet (uncoated and film-coated)	$M \leq 80 \text{ mg}$	10
	$80 \text{ mg} < M < 250 \text{ mg}$	7.5
	$M \geq 250 \text{ mg}$	5

Table 7 – Control of weight, as reported in the European Pharmacopoeia.

The weight control is performed with an analytical balance. The average weight is always coupled with a measure of dispersion of data, generally the standard deviation (SD), the relative standard deviation (RSD) or Coefficient of Variation (CV). The weight variation or mass variation, in some cases, is a recognised method for the assessment of uniformity of dosage units. The weight control is also an important feedback about the tableting process: a high weight variation could indicate an insufficient powder flow, a wrong filling of the die cavity, tableting issue such as sticking, capping or lamination, or an equipment issue. The weight measurement is also used for coating assessment.

Thickness and diameter

Thickness, diameter and all the other tablet dimensions are measured with a digital caliper. Thickness and diameter are necessary parameters of some equations, such as the tensile strength (see section 3.2.2); they are also necessary to calculate the volume of the tablet and consequently the tablet porosity. The diameter is defined by the die geometry and does not change during compression. On the contrary, the tablet thickness is not a pre-defined and fixed parameter, but it can change, as response of compression force. The thickness variation is also correlated to weight variation.

Tablet crushing strength

The importance and the role of tablet crushing strength have been previously described in section 3.2.2. The diametral-compression test is carried out by placing the tablet between two flat metal platens, which move, approaching each other. When they touch the tablet, some forces develop inside it, causing it

to break, as shown in Figure 37. The point A and B are touched by the two platens, therefore are the points of external force application (points of loading). σ_1 , σ_2 and τ are the forces developed inside the tablet, as response to the external applied forces and can be calculated by elastic theory. σ_1 is defined tensile stress and causes the tablet to break perpendicularly to the external force direction. σ_2 is called compressive stress, while τ is the shear stress⁵⁴.

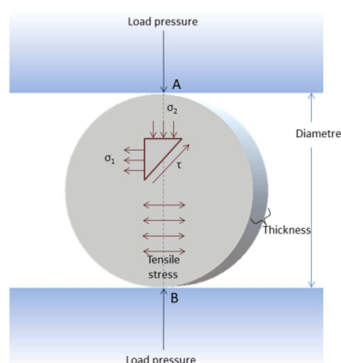


Figure 37 – Diametral compression test.

An alternative method for tablet crushing strength determination is represented by the NIR spectroscopy. Drennen, 1991⁸⁵ was the first presenting data about the crushing strength determination with NIR. One of the advantages of using NIR, instead of the classical diametral-compression test, relies on the non-destructiveness of the spectroscopic analysis. In order to be able to predict tablet crushing strength with NIR, a qualitative or quantitative model should be built. A different tablet crushing strength affect the NIR spectrum mainly as baseline shift, even if other phenomena could occur, such as peak shift⁸⁶. When developing a calibration model, tablets made at different compaction pressure are analysed with NIR and their spectra are used to build a quantitative model, which can be a PLS model⁸⁷, a PCR model⁸⁸ or others⁸⁹. For quantitative model development read section 2.3.2. Kirsch and Drennen, 1999⁸⁶ used a different approach for correlation of spectral features to tablet crushing strength. From the comparison of NIR spectra of tablet of different crushing strength, they observed a change in the slope of the spectral baseline. The authors determined the “*best-fit line through each spectrum, thereby reducing the spectrum to slope and intercept values*”⁸⁶. Then, they used a least-square calibration method to build a regression model, which regresses the slope and intercept previously obtained, versus the measured crushing strength.

Friability

Friability is an indirect measure of the tablet strength. Tablets should have a sufficient strength, in order to resist to handling without damaging the surface, losing fragments and becoming dusty. The friability test quantifies the amount of powder and fragments lost during tablet handling, under defined conditions. The test is described in the European Pharmacopoeia⁹⁰. The friability is expressed as the amount of mass lost, which should be lower than 1.0%.

Disintegration time

Disintegration test is aimed at measuring the time needed to completely disintegrate the tablet; this does not necessarily imply its dissolution. The disintegration is considered to be concluded, as there is not a hard core and no residue remains on the screen. The apparatus used for disintegration consists of a rigid basket supporting six cylindrical tubes, where the tablets are placed. The bottom of each tube is

placed on top of a stainless net, with 2.0 x 2.0 mm holes, which do not allow a tablet to pass, but allow the passage of tablet's fragments. The basket is held by a mechanic arm, which moves up and down inside a beaker full of thermostated water.

If the final product is the uncoated tablet the drug assay, content uniformity and dissolution test are evaluated at this stage, otherwise they are evaluated after coating.

Drug assay

The drug assay is aimed at evaluating the correct amount of API contained in a single unite dose. It can be performed with different techniques, the most used are the HPLC and the Uv-Vis spectroscopy. The amount of API contained into a single unit can be expressed as the actual mg quantified, or as the percentage, respect to the theoretical expected amount, which is the 100%. The variability should be as less as possible; however, an interval of accepted variability, such as the $\pm 2.5\%$ or $\pm 5\%$ is generally specified. The traditional reference methods for drug assay determination are destructive; for that reason, non-destructive spectroscopic analysis is a promising alternative.

Content uniformity

The content uniformity evaluates the consistency among different units of the same batch. In fact, each unit should have an API concentration within a narrow range, around the label claim. The European Pharmacopoeia defines the uniformity of dosage unit as *"the degree of uniformity in the amount of the active substance among dosage units."* The content uniformity test consists of individually assaying the API contents of a number of dosage units, to determine if the individual contents are within the limits. For solid dosage forms the indication is to perform the test on 10 units, generally with HPLC or UV-Vis spectroscopy, and then to calculate the acceptance value (AV), as described in Table 8⁹¹. An AV lower than 15 is accepted. However, according to Chalayudth, 2016⁹² values below 8 indicate a very good content uniformity. As previously said for drug assay, since the traditional reference methods are destructive, the spectroscopic analysis is a promising alternative.

Variable	Definition	Conditions	Value
\bar{X}	Mean of individual contents (x_1, x_2, \dots, x_n), expressed as a percentage of the label claim		
x_1, x_2, \dots, x_n	Individual contents of the dosage units tested, expressed as a percentage of the label claim		
n	Sample size (number of dosage units in a sample)		
k	Acceptability constant	If n = 10, then If n = 30, then	2.4 2.0
s	Sample Standard Deviation		$\left[\frac{\sum_{i=1}^n (x_i - \bar{X})^2}{n - 1} \right]^{1/2}$
RSD	Relative Standard Deviation		$\frac{s \cdot 100}{\bar{X}}$
M (case 1) To be applied when $T \leq 101.5$	Reference value	If $98.5\% \leq \bar{X} \leq 101.5\%$, then If $\bar{X} < 98.5\%$, then If $\bar{X} > 101.5\%$, then	$M = \bar{X}$ (AV = ks) $M = 98.5\%$ (AV = $98.5 - \bar{X} + ks$) $M = 101.5\%$ (AV = $\bar{X} - 101.5 + ks$)
M (case 2) To be applied when $T > 101.5$	Reference value	If $98.5\% \leq \bar{X} \leq T$, then If $\bar{X} < 98.5\%$, then If $\bar{X} > T$, then	$M = \bar{X}$ (AV = ks) $M = 98.5\%$ (AV = $98.5 - \bar{X} + ks$) $M = T\%$ (AV = $\bar{X} - T + ks$)
Acceptance value (AV)			General formula: $ M - \bar{X} + ks$
L1	Maximum allowed acceptance value		L1=15.0 unless otherwise specified

L2	Maximum allowed range for deviation of each dosage unit tested from the calculated value of M	On the low side, no dosage unit result can be less than 0.75 M while on the high side, no dosage unit result can be greater than 1.25 M (This is based on L2 value of 25.0)	L2 = 25.0 unless otherwise specified
T	Target content per dosage unit at time of manufacture, expressed as a percentage of the label claim. Unless otherwise stated, T is equal to 100% or T is the manufacturer's approved target content per dosage unit		

Table 8 – Parameters for Acceptance Value (AV) calculation, as reported in the European Pharmacopoeia.

Dissolution

The dissolution test is an analytical method described by the European Pharmacopoeia⁹³. It is performed to determine the compliance of the analysed product with the dissolution requirements for solid oral dosage forms. It measures the dissolution rate of the API from the tablet. Different instrument setup can be chosen, depending on the type of release to be tested: the paddle apparatus, the basket apparatus, the reciprocating cylinder and the flow-through cell. The tablet is located inside a certain volume of dissolution medium and samplings of the solution are made at different time intervals. The amount of API in every sample is quantified with HPLC or with Uv-Vis spectroscopy and it is plotted versus time, obtaining a dissolution profile.

References

- (1) *Pharmaceutical Dosage Forms: Tablets*; Lieberman, H. A., Lachman, L., Schwartz, B., Eds.; Marcel Dekker Inc.: New York, 1990.
- (2) Hogg, R. Mixing and segregation in powders: evaluation, mechanisms and processes. *KONA Powder Part. J.* **2009**, *27*, 3–17.
- (3) Lacey, P. M. C. Developments in the theory of particle mixing. *J. Appl. Chem.* **1954**, *4*, 257–268.
- (4) Bridgwater, J. Fundamental powder mixing mechanisms. *Powder Technol.* **1976**, *15*, 215–236.
- (5) Cahn, D. S.; Fuerstenau, D. W. Simulation of diffusional mixing of particulate solids by Monte Carlo techniques. *Powder Technol.* **1967**, *1* (3), 174–182.
- (6) Ciurczak, E. W.; Drennen, J. K. *Pharmaceutical and Medical Applications of Near-Infrared Spectroscopy*; Marcel Dekker Inc., 2002.
- (7) Muzzio, F. J.; Robinson, P.; Wightman, C.; Brone, D. Sampling practices in powder blending. *Int. J. Pharm.* **1997**, *155*, 153–178.
- (8) Berntsson, O.; Danielsson, L.; Lagerholm, B.; Folestad, S. Quantitative in-line monitoring of powder blending by near infrared reflection spectroscopy. *Powder Technol.* **2002**, *123*, 185–193.
- (9) Esbensen, K. H.; Román-Ospino, A. D.; Sanchez, A.; Romañach, R. J. Adequacy and verifiability of pharmaceutical mixtures and dose units by variographic analysis (theory of sampling) - A call for a regulatory paradigm shift. *Int. J. Pharm.* **2016**, *499* (1–2), 156–174. <https://doi.org/10.1016/j.ijpharm.2015.12.038>.
- (10) Koller, D. M.; Posch, A.; Hörl, G.; Voura, C.; Radl, S.; Urbanetz, N.; Fraser, S. D.; Tritthart, W.; Reiter, F.; Schlingmann, M.; Khinast, J. G. Continuous quantitative monitoring of powder mixing dynamics by near-infrared spectroscopy. *Powder Technol.* **2011**, *205*, 87–96. <https://doi.org/10.1016/j.powtec.2010.08.070>.
- (11) El-Hagrasy, A. S.; D'Amico, F.; Drennen, J. K. A process analytical technology approach to near-infrared process control of pharmaceutical powder blending. Part I: D-optimal design for characterization of powder mixing and preliminary spectral data evaluation. *J. Pharm. Sci.* **2006**, *95* (2), 392–406. <https://doi.org/10.1002/jps.20467>.
- (12) Food and Drug Administration. Current good manufacturing practice: amendment of certain requirements for finished pharmaceuticals; proposed rule. 1996.
- (13) Storme-Paris, I.; Clarot, I.; Esposito, S.; Chaumeil, J. C.; Nicolas, A.; Brion, F.; Rieutord, A.; Chaminade, P. Near infrared spectroscopy homogeneity evaluation of complex powder blends in a small-scale pharmaceutical preformulation process, a real-life application. *Eur. J. Pharm. Biopharm.* **2009**, *72* (1), 189–198. <https://doi.org/10.1016/j.ejpb.2008.11.002>.
- (14) Blanco, M.; Gozález Bañó, R.; Bertran, E. Monitoring powder blending in pharmaceutical processes by use of near infrared spectroscopy. *Talanta* **2002**, *56*, 203–212. [https://doi.org/10.1016/S0039-9140\(01\)00559-8](https://doi.org/10.1016/S0039-9140(01)00559-8).
- (15) Puchert, T.; Holzhauser, C. V.; Menezes, J. C.; Lochmann, D.; Reich, G. A new PAT/QbD approach for the determination of blend homogeneity: combination of on-line NIRS analysis with PC Scores Distance Analysis (PC-SDA). *Eur. J. Pharm. Biopharm.* **2011**, *78* (1), 173–182. <https://doi.org/10.1016/j.ejpb.2010.12.015>.

- (16) Asachi, M.; Nourafkan, E.; Hassanpour, A. A review of current techniques for the evaluation of powder mixing. *Adv. Powder Technol.* **2018**, *29* (7), 1525–1549. <https://doi.org/10.1016/j.appt.2018.03.031>.
- (17) Roggo, Y.; Chalus, P.; Maurer, L.; Lema-Martinez, C.; Edmond, A.; Jent, N. A review of near infrared spectroscopy and chemometrics in pharmaceutical technologies. *J. Pharm. Biomed. Anal.* **2007**, *44*, 683–700. <https://doi.org/10.1016/j.jpba.2007.03.023>.
- (18) Fonteyne, M.; Vercruyssen, J.; De Leersnyder, F.; Besseling, R.; Gerich, A.; Oostra, W.; Remon, J. P.; Vervaet, C.; De Beer, T. Blend uniformity evaluation during continuous mixing in a twin screw granulator by in-line NIR using a moving F-Test. *Anal. Chim. Acta* **2016**, *935*, 213–223. <https://doi.org/10.1016/j.aca.2016.07.020>.
- (19) Sekulic, S. S.; Ward, H. W.; Brannegan, D. R.; Stanley, E. D.; Evans, C. L.; Sciavolino, S. T.; Hailey, P. A.; Aldridge, P. K. On-line monitoring of powder blend homogeneity by near-infrared spectroscopy. *Anal. Chem.* **1996**, *68* (3), 509–513. <https://doi.org/10.1021/ac950964m>.
- (20) Hailey, P. A.; Doherty, P.; Tapsell, P.; Oliver, T.; Aldridge, P. K. Automated system for the on-line monitoring of powder blending processes using near-infrared spectroscopy part I. System development and control. *J. Pharm. Biomed. Anal.* **1996**, *14* (5), 551–559. [https://doi.org/10.1016/0731-7085\(95\)01674-0](https://doi.org/10.1016/0731-7085(95)01674-0).
- (21) Berntsson, O.; Danielsson, L.; Johansson, M. O.; Folestad, S. Quantitative determination of content in binary powder mixtures using diffuse reflectance near infrared spectrometry and multivariate analysis. *Anal. Chim. Acta* **2000**, *419*, 45–54.
- (22) El-Hagrasy, A. S.; Drennen, J. K. A process analytical technology approach to near-infrared process control of pharmaceutical powder blending. Part III: quantitative near-infrared calibration for prediction of blend homogeneity and characterization of powder mixing kinetics. *J. Pharm. Sci.* **2006**, *95* (2), 422–434. <https://doi.org/10.1002/jps.20465>.
- (23) Jamrogiewicz, M.; Cal, K.; Gruszecka, M.; Ciesielski, A. Determination of API content in a pilot-scale blending by near-infrared spectroscopy as a first step method to process line implementation. *Polish Pharm. Soc.* **2013**, *70* (3), 419–429.
- (24) Vanarase, A. U.; Alcalà, M.; Rozo, J. I. J.; Muzzio, F. J.; Romanach, R. J. Real-time monitoring of drug concentration in a continuous powder mixing process using NIR spectroscopy. *Chem. Eng. Sci.* **2010**, *65* (21), 5728–5733. <https://doi.org/10.1016/j.ces.2010.01.036>.
- (25) Vanarase, A. U.; Järvinen, M.; Paaso, J.; Muzzio, F. J. Development of a methodology to estimate error in the on-line measurements of blend uniformity in a continuous powder mixing process. *Powder Technol.* **2013**, *241*, 263–271. <https://doi.org/10.1016/j.powtec.2013.02.012>.
- (26) Shi, Z.; Cogdill, R. P.; Short, S. M.; Anderson, C. A. Process characterization of powder blending by near-infrared spectroscopy: blend end-points and beyond. *J. Pharm. Biomed. Anal.* **2008**, *47* (4–5), 738–745. <https://doi.org/10.1016/j.jpba.2008.03.013>.
- (27) Besseling, R.; Damen, M.; Tran, T.; Nguyen, T.; van den Dries, K.; Oostra, W.; Gerich, A. An efficient, maintenance free and approved method for spectroscopic control and monitoring of blend uniformity: the moving F-test. *J. Pharm. Biomed. Anal.* **2015**, *114*, 471–481. <https://doi.org/10.1016/j.jpba.2015.06.019>.
- (28) Biagi, D.; Nencioni, P.; Valleri, M.; Calamassi, N.; Mura, P. Development of a Near Infrared Spectroscopy method for the in-line quantitative bilastine drug determination during pharmaceutical powders blending. *J. Pharm. Biomed. Anal.* **2021**, *204*, 1144277.

<https://doi.org/10.1016/j.jpba.2021.114277>.

- (29) Martínez, L.; Peinado, A.; Liesum, L.; Betz, G. Use of near-infrared spectroscopy to quantify drug content on a continuous blending process: influence of mass flow and rotation speed variations. *Eur. J. Pharm. Biopharm.* **2013**, *84*, 606–615. <https://doi.org/10.1016/j.ejpb.2013.01.016>.
- (30) Igne, B.; Zacour, B. M.; Shi, Z.; Talwar, S.; Anderson, C. A.; Drennen, J. K. D. Online monitoring of pharmaceutical materials using multiple NIR sensors — Part I: blend homogeneity. *J. Pharm. Innov.* **2011**, *6*, 47–59. <https://doi.org/10.1007/s12247-011-9099-1>.
- (31) Sekulic, S. S.; Wakeman, J.; Doherty, P.; Hailey, P. A. Automated system for the on-line monitoring of powder blending processes using near-infrared spectroscopy. Part II. Qualitative approaches to blend evaluation. *J. Pharm. Biomed. Anal.* **1998**, *17* (8), 1285–1309. [https://doi.org/10.1016/S0731-7085\(98\)00025-9](https://doi.org/10.1016/S0731-7085(98)00025-9).
- (32) Moes, J. J.; Ruijken, M. M.; Gout, E.; Frijlink, H. W.; Ugwoke, M. I. Application of process analytical technology in tablet process development using NIR spectroscopy: blend uniformity, content uniformity and coating thickness measurements. *Int. J. Pharm.* **2008**, *357* (1–2), 108–118. <https://doi.org/10.1016/j.ijpharm.2008.01.062>.
- (33) Lapointe-Grant, P.P.; Simard, J.S.; Abatzoglou, N. Real-time NIR monitoring of a pharmaceutical blending process through multivariate analysis-derived models. *WSEAS Int. Conf. Proceedings. Math. Comput. Sci. Eng.* **2008**, *7*.
- (34) Tablets. In *European Pharmacopoeia*; 2008; pp 748–750.
- (35) McDonagh, A. F.; Duff, B.; Brennan, L.; Tajber, L. The impact of the degree of intimate mixing on the compaction properties of materials produced by crystallo-co-spray drying. *Eur. J. Pharm. Sci.* **2020**, *154*, 105505. <https://doi.org/10.1016/j.ejps.2020.105505>.
- (36) Hiestand, E. N.; Wells, J. E.; Peot, C. B.; Ochs, J. F. Physical processes of tableting. *J. Pharm. Sci.* **1977**, *66* (9), 510–519.
- (37) Sun, C. C. Decoding powder tableting: roles of particle adhesion and plasticity. *J. Adhes. Sci. Technol.* **2011**, *25* (4–5), 483–499. <https://doi.org/10.1163/016942410X525678>.
- (38) Higuchi, T.; Rao, N. A.; Busse, J. W.; Swintosky, J. V. The physics of tablet compression. II. The influence of degree of compression on properties of tablets. *J. Am. Pharm. Assoc.* **1953**, *42* (4), 194–200.
- (39) Hiestand, E. N. Dispersion forces and plastic deformation in tablet bond. *J. Pharm. Sci.* **1985**, *74* (7), 768–770. <https://doi.org/10.1002/jps.2600740715>.
- (40) Newton, J. M.; Grant, D. J. W. The relation between the compaction pressure, porosity and tensile strength of compacted powders. *Powder Technol.* **1974**, *9*, 295–297.
- (41) Viana, M.; Jouannin, P.; Pontier, C.; Chulia, D. About pycnometric density measurements. *Talanta* **2002**, *57*, 583–593.
- (42) Bettin, H.; Toth, H. Solid density determination by the pressure-of-flotation method. *Meas. Sci. Technol.* **2006**, *17*, 2567–2573. <https://doi.org/10.1088/0957-0233/17/10/006>.
- (43) Richards, F. M.; Lindley, P. F. Determination of the density of solids. In *International Tables for Crystallography*; Prince, E., Ed.; Springer: Dordrecht, Netherlands, 2006; Vol. C, pp 156–159.
- (44) Sun, C. C. A novel method for deriving true density of pharmaceutical solids including hydrates and water-containing powders. *J. Pharm. Sci.* **2004**, *93* (3), 646–653.

- (45) Amidon, G. E.; Meyer, P. J.; Mudie, D. M. Chapter 10. Particle, powder, and compact characterization. In *Developing Solid Oral Dosage Forms*; Qiu, Y., Zhang, G. G. Z., Porter, W. R., Chen, Y., Liu, L., Eds.; Elsevier Inc. Academic Press, 2017; pp 271–294. <https://doi.org/10.1016/B978-0-12-802447-8.00010-8>.
- (46) Cao, X.; Leyva, N.; Anderson, S. R.; Hancock, B. C. Use of prediction methods to estimate true density of active pharmaceutical ingredients. *Int. J. Pharm.* **2008**, *355*, 231–237. <https://doi.org/10.1016/j.ijpharm.2007.12.012>.
- (47) Heckel, R. W. Density-pressure relationships in powder compaction. *Trans. Metall. Soc. Aime* **1961**, *221* (4), 671–675.
- (48) Sun, C. C. A material-sparing method for simultaneous determination of true density and powder compaction properties-aspartame as an example. *Int. J. Pharm.* **2006**, *326* (1–2), 94–99. <https://doi.org/10.1016/j.ijpharm.2006.07.016>.
- (49) Armstrong, N. A.; Palfrey, L. P. The effect of machine speed on the consolidation of four directly compressible tablet diluents. *J. Pharm. Pharmacol.* **1989**, *41* (3), 149–151. <https://doi.org/10.1111/j.2042-7158.1989.tb06418.x>.
- (50) Hancock, B. C.; Colvin, J. T.; Mullarney, M. P.; Zinchuk, A. V. The relative densities of pharmaceutical powders, blends, dry granulations, and immediate-release tablets. *Technology* **2003**, *27* (April), 64–80.
- (51) Van der Voort Maarschalk, K.; Vromans, H.; Groenendijk, W.; Bolhuis, G. K.; Lerk, C. F. Effect of water on deformation and bonding of pregelatinized starch compacts. *Eur. J. Pharm. Biopharm.* **1997**, *44* (3), 253–260. [https://doi.org/10.1016/S0939-6411\(97\)00128-8](https://doi.org/10.1016/S0939-6411(97)00128-8).
- (52) Tye, C. K.; Sun, C. C.; Amidon, G. E. Evaluation of the effects of tableting speed on the relationships between compaction pressure, tablet tensile strength, and tablet solid fraction. *J. Pharm. Sci.* **2005**, *94* (3), 465–472. <https://doi.org/10.1002/jps.20262>.
- (53) Reynolds, G. K.; Campbell, J. I.; Roberts, R. J. A compressibility based model for predicting the tensile strength of directly compressed pharmaceutical powder mixtures. *Int. J. Pharm.* **2017**, *531* (1), 215–224. <https://doi.org/10.1016/j.ijpharm.2017.08.075>.
- (54) Fell, J. T.; Newton, J. M. Determination of tablet strength by the diametral-compression test. *J. Pharm. Sci.* **1970**, *59* (5), 688–691.
- (55) Newton, J. M.; Rowleey, G.; Fell, J. T.; Peacock, D.; Ridgway, K. Computer analysis of the relation between tablet strength and compaction pressure. *J. Pharm. Pharmacol.* **1971**, *23*, 195S–201S.
- (56) Newton, J. M.; Rowley, G.; Fell, J. T. The tensile strength of deep concave tablets. *J. Pharm. Pharmacol.* **1972**, *24* (6), 503–504.
- (57) Stanley, P.; Newton, J. M. The tensile fracture stress of capsule-shaped tablets. *J. Pharm. Pharmacol.* **1980**, *32* (1), 852–854. <https://doi.org/10.1111/j.2042-7158.1980.tb13090.x>.
- (58) Pitt, K. G.; Newton, J. M.; Stanley, P. Tensile fracture of doubly-convex cylindrical discs under diametral loading. *J. Mater. Sci.* **1988**, *23* (8), 2723–2728. <https://doi.org/10.1007/BF00547442>.
- (59) Pitt, K. G.; Heasley, M. G. Determination of the tensile strength of elongated tablets. *Powder Technol.* **2013**, *238*, 169–175. <https://doi.org/10.1016/j.powtec.2011.12.060>.
- (60) Kuentz, M.; Leuenberger, H. Pressure susceptibility of polymer tablets as a critical property: a modified Heckel equation. *J. Pharm. Sci.* **1999**, *88* (2), 174–179.

- (61) Mallick, S. Rearrangement of particle and compactibility, tableability and compressibility of pharmaceutical powder: a rational approach. *J. Sci. Ind. Res.* **2014**, *73*, 51–56.
- (62) Sun, C.; Grant, D. J. W. Influence of crystal structure on the tableting properties of sulfamerazine polymorphs. *Pharm. Res.* **2001**, *18* (3), 274–280.
- (63) Joiris, E.; Di Martino, P.; Berneron, C.; Guyot-Herman, A.M.; Guyot, J.C. Compression behavior of orthorhombic paracetamol. *Pharm. Res.* **1998**, *15* (7), 1122–1130.
- (64) Persson, A.S.; Alderborn, G. A Hybrid approach to predict the relationship between tablet tensile strength and compaction pressure using analytical powder compression. *Eur. J. Pharm. Biopharm.* **2018**, *125*, 28–37. <https://doi.org/10.1016/j.ejpb.2017.12.011>.
- (65) Kuentz, M.; Leuenberger, H. A new theoretical approach to tablet strength of a binary mixture consisting of a well and a poorly compactable substance. *Eur. J. Pharm. Biopharm.* **2000**, *49*, 151–159.
- (66) Castillo, S.; Villafuerte, L. Compactibility of ternary mixtures of pharmaceutical. *Pharm. Acta Helv.* **1995**, *70* (4), 329–337.
- (67) Sonnergaard, J. M. Quantification of the compactibility of pharmaceutical powders. *Eur. J. Pharm. Biopharm.* **2006**, *63*, 270–277. <https://doi.org/10.1016/j.ejpb.2005.10.012>.
- (68) Steffens, K. E.; Wagner, K. G. Improvement of tableability via twin-screw melt granulation: focus on binder distribution. *Int. J. Pharm.* **2019**, *570*, 118649. <https://doi.org/10.1016/j.ijpharm.2019.118649>.
- (69) Kawakita, K.; Ludde, K.H. Some consideration on powder compression equations. *Powder Technol.* **1970**, *4* (2), 61–68.
- (70) Kawakita, K.; Tsutsumi, Y. A comparison of equations for powder compression. *Bull. Chem. Soc. Jpn.* **1966**, *39* (7), 1364–1368.
- (71) Sonnergaard, J. M. A critical evaluation of the Heckel equation. *Int. J. Pharm.* **1999**, *193*, 63–71.
- (72) Ryshkewitch, E. Compression strength of porous sintered alumina and zirconia. *J. Am. Ceram. Soc.* **1953**, *36* (2), 65–68.
- (73) Ramirez, N.; Melgoza, L. M.; Kuentz, M.; Sandoval, H.; Caraballo, I. Comparison of different mathematical models for the tensile strength – relative density profiles of binary tablets. *Eur. J. Pharm. Sci.* **2004**, *22*, 19–23. <https://doi.org/10.1016/j.ejps.2004.02.002>.
- (74) Aleksiev, A.; Kostova, B.; Rachev, D. Technological and biopharmaceutical properties of galantamine hydrobromide based matrix systems. *Int. J. PharmTech Res.* **2015**, *8* (3), 315–324.
- (75) Feng, H.; Mohan, S. Application of process analytical technology for pharmaceutical coating: challenges, pitfalls, and trends. *AAPS PharmSciTech* **2020**, *21* (5), 1–17. <https://doi.org/10.1208/s12249-020-01727-8>.
- (76) Suzzi, D.; Radl, S.; Khinast, J. G. Local analysis of the tablet coating process: impact of operation conditions on film quality. *Chem. Eng. Sci.* **2010**, *65* (21), 5699–5715. <https://doi.org/10.1016/j.ces.2010.07.007>.
- (77) Knop, K.; Kleinebudde, P. PAT-tools for process control in pharmaceutical film coating applications. *Int. J. Pharm.* **2013**, *457* (2), 527–536. <https://doi.org/10.1016/j.ijpharm.2013.01.062>.
- (78) Radtke, J.; Kleinebudde, P. Real-time monitoring of multi-layered film coating processes using raman

spectroscopy. *Eur. J. Pharm. Biopharm.* **2020**, *153*, 43–51.
<https://doi.org/10.1016/j.ejpb.2020.05.018>.

- (79) Wahl, P. R.; Peter, A.; Wolfgang, M.; Khinast, J. G. How to measure coating thickness of tablets: Method comparison of optical coherence tomography, near-infrared spectroscopy and weight-, height- and diameter gain. *Eur. J. Pharm. Biopharm.* **2019**, *142*, 344–352.
<https://doi.org/10.1016/j.ejpb.2019.06.021>.
- (80) Toschkoff, G.; Just, S.; Knop, K.; Kleinebudde, P.; Funke, A.; Djuric, D.; Scharrer, G.; Khinast, J. G. Modeling of an active tablet coating process. *J. Pharm. Sci.* **2015**, *104* (12), 4082–4092.
<https://doi.org/10.1002/jps.24621>.
- (81) Radtke, J.; Rehbaum, H.; Kleinebudde, P. Raman spectroscopy as a PAT-Tool for film-coating processes: in-line predictions using one PLS model for different cores. *Pharmaceutics* **2020**, *12* (9), 796.
- (82) Andersson, M.; Josefson, M.; Langkilde, F. W.; Wahlund, K. G. Monitoring of a film coating process for tablets using near infrared reflectance spectrometry. *J. Pharm. Biomed. Anal.* **1999**, *20* (1–2), 27–37. [https://doi.org/10.1016/S0731-7085\(98\)00237-4](https://doi.org/10.1016/S0731-7085(98)00237-4).
- (83) Pérez-Ramos, J. D.; Findlay, W. P.; Peck, G.; Morris, K. R. Quantitative analysis of film coating in a pan coater based on in-line sensor measurements. *AAPS PharmSciTech* **2005**, *6* (1), 127–136.
- (84) 2.9.5. Uniformity of mass of single-dose preparations. In *European Pharmacopoeia*; 2017; pp 335–336.
- (85) Drennen, J. K. PhD Thesis. University of Kentucky 1991.
- (86) Kirsch, J. D.; Drennen, J. K. Nondestructive tablet hardness testing by near-infrared spectroscopy: a new and robust spectral best-fit algorithm. *J. Pharm. Biomed. Anal.* **1999**, *19* (3–4), 351–362.
[https://doi.org/10.1016/S0731-7085\(98\)00132-0](https://doi.org/10.1016/S0731-7085(98)00132-0).
- (87) Short, S. M.; Cogdill, R. P.; Wildfong, P. L. D.; Drennen, J. K.; Anderson, C. A. A near-infrared spectroscopic investigation of relative density and crushing strength in four-component compacts. *J. Pharm. Sci.* **2009**, *98* (3), 3–8. <https://doi.org/10.1002/jps>.
- (88) Tanabe, H.; Otsuka, K.; Otsuka, M. Theoretical analysis of tablet hardness prediction using chemoinformetric near-infrared spectroscopy. *Anal. Sci.* **2007**, *23*, 857–862.
- (89) Donoso, M.; Kildsig, D. O.; Ghaly, E. S. Prediction of tablet hardness and porosity using near-infrared diffuse reflectance spectroscopy as a nondestructive method. *Pharm. Dev. Technol.* **2003**, *8* (4), 357–366. <https://doi.org/10.1081/PDT-120024689>.
- (90) 2.9.7. Friability of uncoated tablets. In *European Pharmacopoeia*; 2017; pp 336–337.
- (91) 2.9.40. Uniformity of dosage units. In *European Pharmacopoeia*; 2017; pp 398–400.
- (92) Chalayudth, P. Establishing acceptance limits for uniformity of dosage units: part 1. *Pharm. Technol.* **2016**, *40* (12), 34–43.
- (93) 2.9.3. Dissolution test for solid dosage forms. In *European Pharmacopoeia*; pp 326–333.

4. BILASTINE CASE STUDY

4.1. INTRODUCTION

4.1.1 Case study presentation

The case study consists in the application of the QbD approach and its innovative tools, to a process previously developed with a traditional approach. As improving a pre-existing process, many data about the process were already available and they represented an important source of prior knowledge, which is the base of QbD. The present work assumed that the formulation has already been optimized and, therefore, it focused on the study of all the single steps that are part of the process. The selected manufacturing process is that of immediate-release tablets of the antihistaminic drug bilastine, by direct compression. Such process is particularly suitable for this kind of study, because:

- direct compression is a fast, simple and easy process;
- direct compression shows how input has effect on the output better than other processes;
- bilastine was selected as a trial product to perform the drug assay and content uniformity determination by spectroscopic analysis, instead of the more common HPLC determination. In fact, one of the objective is the development of alternative NIR analytical methods;
- bilastine tablets have a simple formulation of only four excipients.

The study is divided into three phases:

- 1- Collection and use of previous knowledge, to identify those aspects critical for the finished product quality and to define a control strategy.
- 2- Development of the analytical NIR method, which will be used to systematically check the product, and to monitor the process.
- 3- Use of the NIR spectroscopic monitoring tools, for the study of each step of the manufacturing process.

4.1.2 Tablet's characteristics

The finished product of the studied process is represented by bilastine tablets, which are immediate release tablets, with an oval biconvex shape and a single score line along the minor axis of the upper face. They appear white and without defects or cracks and they are packaged in Aluminium-Aluminium blisters of 10 tablets each. All the previously reported, and other tablet characteristics are resumed into the bilastine Common Technical Document (CTD). Tablet composition is reported in Table 9; all the batches of the study have this same composition.

Substance	Per tablet (mg)	% w/w	Description
Bilastine	20.0	16.0	Active ingredient
Microcrystalline cellulose (MCC)	103.0	82.4	Diluent
Sodium starch glycolate (Type A)	1.0	0.8	Disintegrant
Colloidal silicon dioxide (SiO₂)	0.5	0.4	Glidant
Magnesium Stearate (MgSt)	0.5	0.4	Lubricant

Table 9 – Bilastine tablet composition for a theoretical tablet weight of 125 mg.

The bilastine tablet dimensions are defined by the tableting punch equipment used during compression. A deep description was made, by observing tablet dimensions with an optical microscopy (Nikon SMZ800), equipped with a camera (Rapitoron KC 25H2PG) and a light source (Photonic PL 2000), and taking dimensional measurements with the software Easy View (Microconsult S.r.l., Florence, Italy). The microscopy top and side view of bilastine tablets are shown in Figure 38. Table 10 reports all the measured dimensional elements.

Element	Dimension
Major axis	10.00 mm
Minor axis	5.00 mm
Cup depth	0.71 mm
Tablet thickness	Variable
Band thickness	Variable
Major side radius	9.00 mm
Minor end radius	1.72 mm
Major cup radius	17.24 mm
Minor axis cup radius	4.41 mm
Land	0.10 mm
Bisect angle	60°
Break radius	0.38 mm

Table 10 – Bilastine tablet dimensions, measured with an optical microscopy.

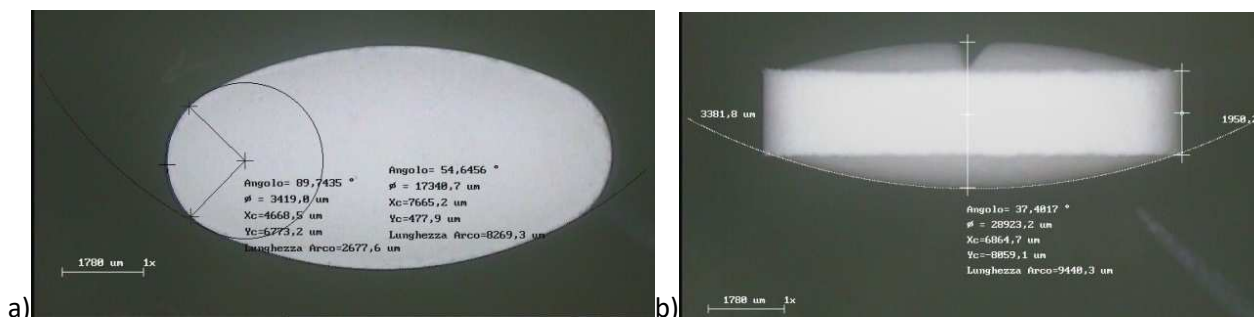


Figure 38 – Bilastine tablet observed with an optical microscopy. Top view (a) and side view (b).

4.1.3 Bilastine manufacturing process

Bilastine tablet manufacturing process is schematized in the workflow of Figure 39. All the raw materials are sieved with a 0.5 mm net size and then added into the mixer, with the exception of MgSt, in the following order:

- half of the total amount of MCC;
- bilastine;
- colloidal silicon dioxide;
- sodium starch glycolate;
- remaining half of the total amount of MCC.

All these ingredients are mixed for 30 min at 15 rpm. Then, MgSt is sieved, with a 1.0 mm net size and added to the rest of the mixture. The final mixture is blended for 5 min at 15 rpm.

The fundamental steps of the process will not be changed in this work, but the process parameters will be varied, in order to deeply study the process performance and defining a design space for all of them.

BILASTINE 20 mg tablet

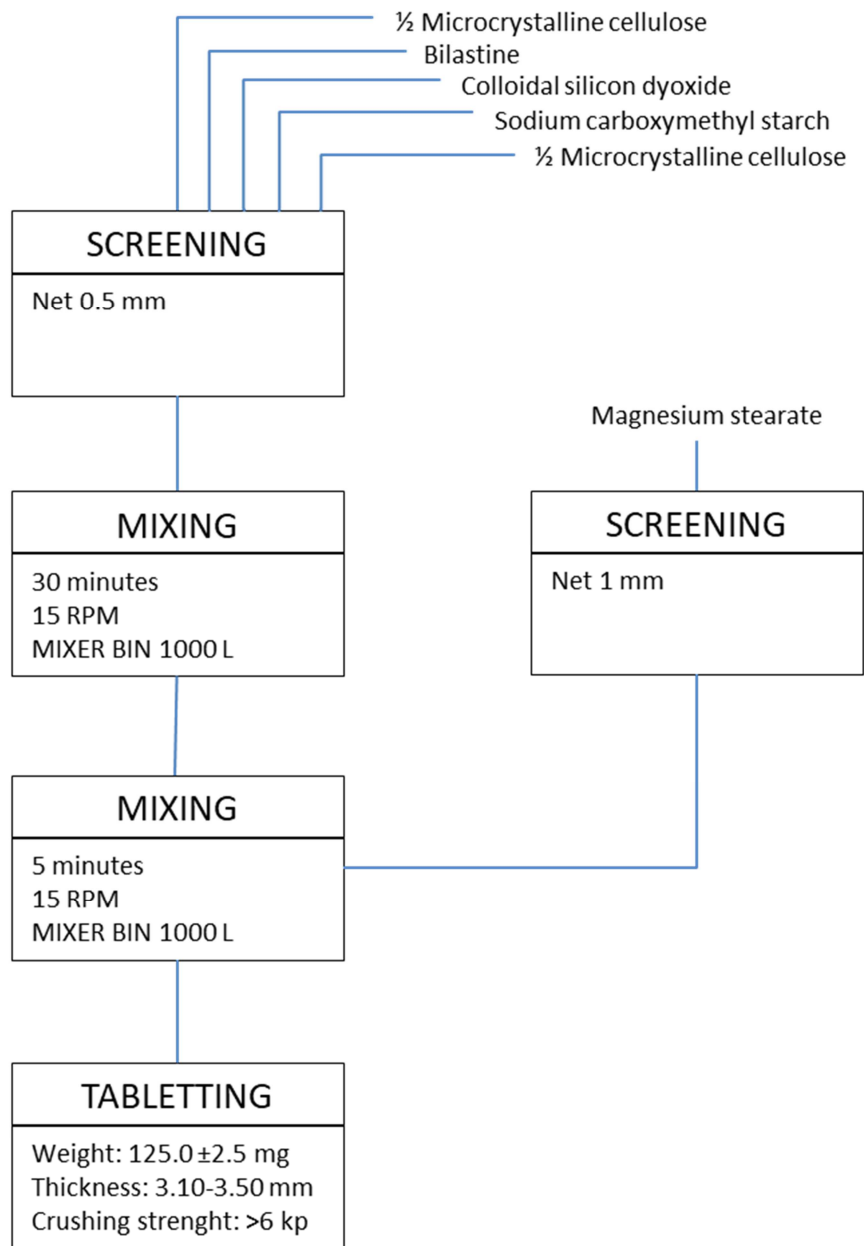


Figure 39 – Work flow of bilastine manufacturing process.

4.2. MATERIALS AND METHODS

4.2.1 Materials

All the raw materials were available at A.M.M.L.S L'Aquila plant, provided by the following suppliers: bilastine was obtained from Neuland Laboratories Ltd (India) and from Sai Life Sciences Ltd (India); MCC (Avicel PH102) was from DuPont de Nemours. Inc. (USA), SiO₂ (Aerosil 200) from Evonik Degussa (USA), sodium starch glycolate (EXPLOTAB) from JRS Pharma GmbH & Co. (Germany) and MgSt from Peter Greven (Germany).

4.2.2 Instruments and Methods

In the following paragraphs, the practical operation and the technical data of the equipment, used for preparing and analysing the batches, are described.

4.2.2.1 MicroNIR spectral acquisitions

To carry out the study, laboratory and production scale batches have been analysed with NIR spectrometer instrument. The NIR instrument used in this work is the MicroNIR™ PAT-W Spectrometer (Viavi Solutions Inc., USA)¹. The small size and low weight of this instrument allows its easy installation on both laboratory and manufacturing equipment, in order to monitor the process, as stated by the PAT approach. It was used for monitoring the mixing and the coating process, to quantify the drug content in mixtures and tablets, and to measure the tablet crushing strength. NIR spectra were acquired in the wavelength range between 900 and 1700 nm, with the diffuse reflectance mode. A panel with a R99 (99% reflectance), supplied with the instrument, was employed as a reference standard of absorbance and measured along all the wavelengths. For long lasting acquisitions, such as the mixing process monitoring, a long time interval passes since the 99% Reference scan was done; in that case, the option "Auto Zero" was enabled on the instrument. When this option is selected, the lamps are turned off and a dark reference is collected, before to collect the sample scan. Different acquisition modes were used for analysing powders, tablets and coated tablets.

For powder samples two methods of spectra acquisition were used, because of the different size of samples.

- A static mode was used for calibration and validation samples set (10g) and for pure raw materials (50g), because of the small dimension of the powder samples. A white PVC container (about 64 mL) was mounted on the MicroNIR window and filled with powder. Each sample was acquired 20 times and every five acquisitions the powder was gently moved manually or the container emptied and filled again. The 20 acquisitions of a single sample were averaged, before analysing data. The spectral acquisition was made using a manual scan mode, with a default configuration: each single spectrum resulted from the average of 200 scans, with an integration time of 7.8 ms.
- A dynamic mode was used to monitor powders during the mixing process, for both, laboratory (2 Kg) and production (250 Kg) scale batches. To make this acquisition mode possible, the rotary bin lid was modified, in order to attach the MicroNIR to it. A gravimetric sensor installed into the MicroNIR, autonomously drives the spectra acquisition. The horizontal position of the instrument is a trigger for the start of the acquisition; setting an appropriate delay causes the instrument to scan when it is in the desired position. In case of automated scan mode, the acquisition setup was personalized, depending on the rotation speed used for mixing. The setups employed in the study are reported in Table 11.

Mixer type	Rotation speed (rpm)	Scan count	Integration time (ms)	Delay (ms)
Cubic 8 L	8	100	7.8	980
Cubic 8 L	11.5	100	7.8	500
Cubic 8 L	15	100	7.8	550
Cubic 8 L	26	100	7.8	0
Manufacturing 1000 L bin	15	100	7.8	600

Table 11 – Acquisition mode setups and parameters.

Tablet acquisition with NIR is sensible to the tablet position; for that reason, a sample holder of the same shape of tablet was employed, in order to avoid any movement during acquisition. The analysis was made only on the unscored face and replicated 10 times on each tablet, by rotating it respect to the NIR detector, after each acquisition and before the next one. Such tablet rotation helps in reducing the noise due to the tablet position respect to the detector, as it affects the acquisition. The spectral acquisition was made using a manual scan mode, with a default configuration: each single spectrum resulted from the average of 200 scans, with an integration time of 7.8 ms.

For coating process monitoring, the acquisitions were performed by opening the coating pan and placing the NIR probe inside the bed of tablet, with a perpendicular orientation respect to it. The process was not stopped during acquisition. The manual scan mode, with a default configuration, was used also in this case.

4.2.2.2 Mixing process

Manufacturing scale batches of 250 kg were prepared following the work flow previously reported (see section 4.1.3), by sieving all the substances, mixing them in a 1000 L tumbling mixer (IMA, Italy), adding MgSt previously sieved with a 1.0 mm net, and mixing it with the other components. On manufacturing scale batches the NIR spectra were only acquired with the dynamic mode, i.e. during the mixing process (see section 4.2.2.1).

Laboratory scale batches of about 2kg were prepared according to the same process used for the industrial production of bilastine tablets. All the substances, except for MgSt, were sieved with a 0.5 mm net (FGS oscillating granulator - Erweka, Germany) and then mixed for 30 min at 15 rpm, in a cubic 8 L mixer (Erweka motor drive, Germany). MgSt was then sieved (1.0 mm net), added to the other ingredients and mixed for 5 min at 15 rpm. NIR acquisitions on laboratory scale batches were made with both, static and dynamic acquisition mode (see section 4.2.2.1).

Laboratory calibration set (25 samples) and laboratory validation set (15 samples) of 10 g each were prepared as follows: all the components were singularly and manually sieved with a 0.5 mm net, accurately weighed and then mixed at 15 rpm for 30 min with RRM Mini-II (J. Engelsmann AG, Germany). The whole samples of both, calibration and validation set, were acquired with NIR, using a static acquisition mode, as previously explained in (see section 4.2.2.1).

4.2.2.3 Tableting process

The entire calibration and validation set, the laboratory scale and the manufacturing scale powder blend batches were compressed in laboratory, to obtain tablets. Two different tableting machines have been used: a manual single station punch press (Natoli NP-RD10A, USA), equipped with the same tooling used at the industrial scale (oblong 10 x 5 mm, concave punches and with a score line on the upper punch) and a rotary machine (Korsch PH103, Germany), equipped with bilastine-dedicated tooling. The tableting

equipment parameters were not fixed, but were changed, depending on the performed experiment; therefore, they will be further specified.

The following technological measurements were performed on tablets: weight (Mettler, PE 160), thickness (Digital Micrometer Mitutoyo, Germany), crushing strength (Schleuniger 6D Tablet Tester, Switzerland) and disintegration time (Erweka ZT 221, Germany). The identity, the drug assay and the content uniformity were also performed on tablets, with reverse phase HPLC, using a C18 column. The used reagents were: methanol (HPLC grade or equivalent), acetonitrile (HPLC grade or equivalent), n-octylamine (analytical grade or equivalent), phosphoric acid 85% (analytical grade or equivalent), HCl 0.1 N (analytical grade or equivalent) and water (Millipore Milli-Q or equivalent). Drug was analytically quantified by an HPLC equipped with an Elite LaChrom L-2400 UV-Vis detector (Merck Hitachi Darmstadt, Germany). The analysis was carried out with an isocratic method using a mobile phase composed of 43% of aqueous phase (phosphoric acid 85% 0.046% v/v; n-octylamine 0.165% v/v adjusted at pH 6.5 with phosphoric acid), 30% of methanol and 28% acetonitrile. The column was an Agilent Zorbax CN (4.6 mm x 150 mm, 5 μ m) and the UV detection was carried out at 275 nm. The injection volume was 20 μ L, the flow rate 1.0 mL/min and the temperature was maintained at 30 \pm 1.0 $^{\circ}$ C. In these conditions the bilastine retention time was 3.10 \pm 0.01 min. The method was validated for linearity in the range of 130.0 – 50.0 μ g/mL ($y=70000000x-411010$; $r^2=0.9957$), LOQ (20.0 μ g/mL) and LOD (6.0 μ g/mL). A bilastine standard solution of 0.1 mg/mL in concentration was prepared, by solubilizing 20 mg of bilastine reference standard, accurately weighted, in 50 mL of HCl 0.1 N and adding the amount of mobile phase necessary to reach 200 mL of volume. The bilastine standard solution was prepared in duplicate. The sample solution was prepared, by placing one bilastine tablet into a 200 mL flask, adding 50 mL of HCl 0.1 N and sonicating for about 35 min; then, the volume was filled to 200 mL with the mobile phase. The suspension was centrifuged for 10 min at 3500 rpm and the supernatant was injected for the analysis by HPLC.

4.2.2.4 Coating process

The coating process was performed only on laboratory scale batches, with a perforated coating pan (MyLab IMA, Italy). The following conditions were used during coating: air flow: 250 m³/h, pan chamber pressure: -30 Pa, pan rotation speed: 20 rpm, atomization 0.8 bar, tablet's bed temperature: 40-45 $^{\circ}$ C, pump speed: 15/20 rpm, pump flow: 15-20 mL/min. A total amount of 995 mL of coating suspension, of the reported composition (see Table 12), was consumed, to achieve the final goal of tablet weight increase equal to 4%. The Opadry-OY 1-700 is a ready to use powder blend for coating, containing hydroxypropylmethylcellulose, titanium dioxide and polyethylene glycol 4000. The bed of tablet was heated with a hot air flow, until the temperature of 45 $^{\circ}$ C was reached; then, the spraying phase started. The pump flow was set to 15 mL/min for the firsts 15 min and, then, it was increased to 20 mL/min, for the remaining time of coating (about 45-50 min). The coated tablets were then cooled, with a cool airflow.

Ingredient	Amount (g)	%
Opadry®-OY 1-700	12	12
Water	88	88

Table 12 – Coating suspension composition.

4.2.2.5 Data elaboration

NIR spectral acquisitions required data pre-processing with chemometric tools, to remove noise and increase resolution. Spectral acquisitions, data pre-processing and model building were performed using the Unscrambler X version software (Camo Software, Oslo, Norway). The spectral pre-processing approach was evaluated every time that a new analysis were made and depended on the analytical model developed. For that reason, it will be specified in detail. NIR data were used to develop quantitative Partial Least Square (PLS) models^{2,3} and the statistics used to assess their validity were the coefficient of multiple regression (R^2), for both calibration and validation, the Root Mean Square Error of Calibration (RMSEC) and the Root Mean Square Error of Prediction (RMSEP)⁴. The NIR data were also used for qualitative analysis (when used for mixing process monitoring). In this case, the Moving Block of Standard Deviation (MBSD)⁵ was calculated. The parameters required to perform MBSD were defined each time, depending on the rotating speed and the mixing time used; therefore they will be further specified.

For data collection, data elaboration and statistical analysis the Software JMP (SAS Institute, North Carolina, USA Inc.) was used.

4.3. RESULTS AND DISCUSSION

4.3.1 Process Risk Assessment

The first part of the work consisted in identification of all the critical aspects for the final product quality, using QRM tools⁶. Following the QbD process development, all the steps proposed by ICH Q8⁷ for pharmaceutical development have been accomplished. For a complete description of them, see section 1.1.1. Once defined the Quality Target Product Profile (QTPP), the Critical Process Parameters (CPPs) having an impact on finished product characteristics (or Critical Quality Attributes: CQAs) were identified. The effect of CPPs on CQAs, has been studied and mathematically described. Some of the above-mentioned elements are shown in Figure 40.

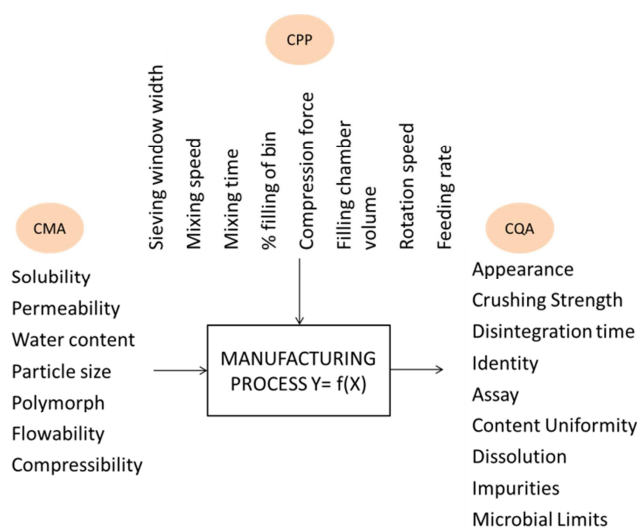


Figure 40 – P-Chart of the bilastine process.

The process assessment accomplished the following steps:

- 1- Defining QTPP, i.e. all the characteristics of the finished product, which need to be achieved, in order to ensure the product quality. It does not necessarily coincide with the product specifications. The bilastine QTPP are listed in Table 13.

QTPP Element	Target
Appearance	White tablets, oval, biconvex, with break-marks on one side. Absence of line or crack on the surface.
Dosage form	Tablet
Pharmacokinetics	Immediate release
Route of administration	Oral
Dosage strength	20 mg
Stability	5 years

Table 13 – Bilastine Quality Target Product Profile.

- 2- Identifying CQAs, which will be studied, in order to evaluate their effect on the finished product quality. The identification of bilastine CQAs is presented in Table 14.

Potential CQA	Target	Is it critical	Justification
Appearance	White tablets, oval, biconvex, with break-marks on one side. Absence of line or crack on the surface	No	It is not related with safety and efficacy
Size	length: 10 mm width: 5 mm thickness: 3.35 mm (Min.: 3.10 mm Max.: 3.5 mm)	No	It is related to the manufacturing operation more than to the patient safety and efficacy
Score configuration	One side scored	No	It is only to facilitate breaking for ease of swallowing and not to divide in equal doses; therefore, it is not critical for the safety and efficacy
Average mass	Average within 125.0 ± 2.5 mg/tablet	Yes	It is related to the dosage
Mass Uniformity	No tablets should be > 6.0% and maximum 2 can be > 3.0%	Yes	It is related with safety and efficacy
Crushing strength	≥ 6 kP	Yes	Crushing strength can have an influence on dissolution rate and therefore on the pharmacokinetics
Disintegration time	≤ 15 min	Yes	Dissolution is influenced by disintegration time
Friability	≤ 1.0% w/w	Yes	A too high friability could bring to an excessive mass variation
Identification	Positive	Yes	It is related with efficacy and safety
Assay	19.0-21.0 mg/tablets (95-105%)	Yes	It is related with efficacy and safety
Content uniformity	None of the results should be out ± 15% of the theoretical content with a RSD ≤ 5.2%	Yes	It is related with efficacy and safety
Dissolution	90% of the theoretical content should be dissolved within 30 min (Q ₃₀ ≥ 85%)	Yes	It is related with efficacy: it has an influence on pharmacokinetics
Impurities	Total impurities < 0.50% w/w	Yes	It is related with safety
Microbial Limits	TAMC < 10 ³ CFU/g	Yes	It is related with safety

Table 14 – Bilastine Critical Quality Attributes definition.

Not all the CQAs have the same importance with respect to safety and efficacy for patient; therefore, it would be useful to understand which are the most relevant CQAs for quality. There are some QRM tools, which help in giving priority to the CQAs. In this case, Pairwise comparison was used (Figure 41). It consists in a direct pair comparison between two different CQAs. In correspondence of the row and column crossing of two CQAs, the identification letter of the more relevant CQA of the couple is reported. A final ranking, made by counting how many times each letter compares, indicated the most relevant CQAs.

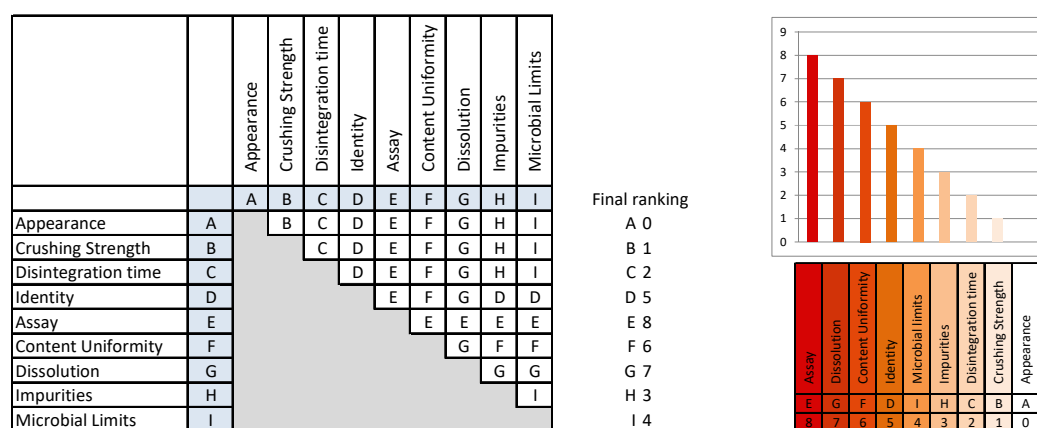


Figure 41 – Pairwise comparison and final ranking to give priority to CQAs.

From the Pairwise comparison, the assay, the dissolution and the content uniformity, resulted to be the most relevant CQAs for safety and efficacy.

3- Determining CMAs. The present study assumed the formulation as unchangeable and focused on the study of process parameters. Nevertheless, a brief overview of the CMA is reported below (Table 15, Table16, Table 17, Table 18, Table 19), for completeness of the risk assessment evaluation. Each ingredient was individually evaluated. All its CMAs are listed in the columns, while the tablet CQAs are

reported in the rows. The effect of each CMA on the CQAs is indicated as low, medium or high and it is highlighted with green, orange or red, respectively. It is reported in the cell corresponding to the crossing of the considered CMA row and CQA column. As an example, the bilastine solubility is not expected to influence the tablet crushing strength, while it surely has a great impact on the disintegration time and dissolution.

	Bilastine CMA						
	Solubility	Permeability	Water content	Particle size	Polymorph	Flowability	Compressibility
Assay	Low	Low	Low	Medium	Low	Low	Low
Dissolution	High	High	Low	Medium	Medium	Low	Low
Content Uniformity	Low	Low	Low	Medium	Low	Medium	Low
Identity	Low	Low	Low	Low	Low	Low	Low
Microbial Limits	Low	Low	Low	Low	Low	Low	Low
Impurities	Low	Low	Medium	Low	Low	Low	Low
Disintegration time	High	High	Low	Low	Low	Low	Low
Crushing strength	Low	Low	Low	Low	Low	Low	Medium
Appearance	Low	Low	Low	Low	Low	Low	Low

Table 15 – Definition of bilastine CMAs.

	Microcrystalline cellulose CMA			
	Water content	Particle Size	Flowability	Compressibility
Assay	Low	Low	Low	Low
Dissolution	Low	Low	Low	Low
Content Uniformity	Low	High	Medium	Low
Identity	Low	Low	Low	Low
Microbial Limits	Low	Low	Low	Low
Impurities	Medium	Low	Low	Low
Disintegration time	Low	Low	Low	Low
Crushing strength	Low	High	Low	Medium
Appearance	Low	Low	Low	Low

Table 16 – Definition of MCC CMAs.

	Sodium Starch Glycolate CMA			
	Water content	Particle Size	Flowability	Compressibility
Assay	Low	Low	Low	Low
Dissolution	Low	Low	Low	Low
Content Uniformity	Low	Medium	Medium	Low
Identity	Low	Low	Low	Low
Microbial Limits	Low	Low	Low	Low
Impurities	Medium	Low	Low	Low
Disintegration time	Low	Low	Low	Low
Crushing strength	Low	Medium	Low	Medium
Appearance	Low	Low	Low	Low

Table 17 – Definition of sodium starch glycolate CMAs.

Colloidal Silicon Dioxide CMA				
	Water content	Particle Size	Flowability	Compressibility
Assay	Low	Low	Low	Low
Dissolution	Low	Low	Low	Low
Content Uniformity	Low	Low	Low	Low
Identity	Low	Low	low	Low
Microbial Limits	Low	Low	Low	Low
Impurities	Low	Low	Low	Low
Disintegration time	Low	Low	Low	Low
Crushing strength	Low	Low	Low	Low
Appearance	Low	Low	Low	Low

Table 18 – Definition of SiO₂ CMAs.

Magnesium Stearate CMA				
	Water content	Particle Size	Flowability	Compressibility
Assay	Low	Low	Low	Low
Dissolution	Low	Low	Low	Low
Content Uniformity	Low	Low	Low	Low
Identity	Low	Low	low	Low
Microbial Limits	Low	Low	Low	Low
Impurities	Low	Low	Low	Low
Disintegration time	Low	Low	Low	Low
Crushing strength	Low	Low	Low	Low
Appearance	Low	Low	Low	Low

Table 19 – Definition of MgSt CMAs.

- 4- Determining CPPs of the manufacturing process. The most critical ones will be studied, in order to evaluate the effect of their variation on the finished tablets. Each step of the process should be considered, to find the correspondent CPPs. It should be evaluated whether if the considered step has direct or indirect impact on the final quality. In particular, a single unit operation has a direct impact on the product quality, if it influences, at least, one of the tablet CQAs. Referring to Figure 39 (see section 4.1.3), the direct/indirect effect of dispensing, sieving, mixing and tableting were evaluated (Table 20).

Single Unit Operation	Direct impact	Indirect impact
Dispensing	X	
Sieving		X
Mixing	X	
Tableting	X	

Table 20 – Evaluation of the impact of a single unit operation on the CQAs of the finished product.

All the “events” which could lead to a not acceptable quality are listed, for each single unit operation, in Table 22. A risk level was associated to each critical step. The risk level can be high, medium or low, depending on the probability of occurrence of such event, its severity and its detectability. A score was attributed to probability, severity and detectability: the value 1 represents the lowest probability and severity and the easiest detectability, while 3 represents the most probable,

the most critical and the hardest event to detect. The attributed score was used to calculate the Risk Index (RI) and the Risk Level, as following reported (Table 21):

$$\text{Risk Index} = \text{Probability} \times \text{Severity} \times \text{Detectability}$$

RI value	Risk Level
1-6	Low
7-13	Medium
14-27	High

Table 21 – Risk Level definition on the base of the RI value.

Step	Criticality	Event	Risk level					Score rationale
			P	S	D	RI	RL	
Dispensing	Storage conditions	Spoiled starting material	1	3	1	3	Low	Probability (1): starting materials are stored within acceptable temperature limits. Severity (3): the step has a direct impact on the finished product specifications. Detectability (1): laboratory analysis ensures the quality of the starting material.
	Quantity weighed	Balance performance is not adequate	1	3	2	6	Low	Probability (1): balances are periodically calibrated and checked. Severity (3): the step has a direct impact on the finished product specifications. Detectability (2): balance controls ensure the reliability, but cannot exclude an accidental event at all.
Sieving	Aggregation of powder	Wrong sieving net size	1	3	2	6	Low	Probability (1): the screen are easily distinguished Severity (1): the event does not directly influence the finished product characteristics. Detectability (2): the laboratory analysis assures the quality.
Mixing	Uniformity of active ingredient distribution	Insufficient mixing time	2	3	2	12	Medium	Probability (2): the timer connected with rotating mixer is calibrated. Severity (3): the event directly influences the finished product specifications. Detectability (2): the operators check the timer during the process.
		Insufficient rotating mixer speed	2	3	2	12	Medium	Probability (2): rotating mixer speed is calibrated. Severity (3): the event directly influences the finished product specifications. Detectability (2): this parameter is not directly checkable during process.
Tableting	Tablets properties do not meet the specifications	Tableting unit performances are not correct	3	3	2	18	High	Probability (3): tableting unit performances are controlled, but the correct setting depends on the characteristics of the powder. Severity (3): the event directly influences the specifications of the finished product. Detectability (2): in process controls ensure the quality of tablets.

Table 22 – Risk analysis for evaluation of the critical manufacturing steps.

From the previous risk analysis, the dispensing and sieving steps present only low risk operations; therefore, they were not be considered as critical, to the finished product quality. On the contrary, the critical process parameters of mixing and tableting process will be investigated and studied and will be monitored with the control strategy, in order to ensure the final quality of the product. The CPP of the

mixing and tableting process are reported in Table 23. Despite the filling chamber volume is a CPP, it was not evaluated. Since no operation affecting the powder physical properties (such as density and particle size) were made on the powder, the chamber was set and fixed before starting tableting operation, in order to obtain the desired tablet weight, in a reproducible way.

Type of process	Process Parameters
Mixing	Mixing speed (rpm)
	Mixing time
	% filling of bin
Tableting	Compression force
	Filling chamber volume
	Rotation speed
	Feeding speed

Table 23 – Critical Process Parameters studied.

5- Finding a correlation between CPPs and CQAs. It was then evaluated the effect of the CPPs reported in Table 23 on the tablet CQAs. The filling chamber volume was excluded, for the aforementioned reason. CPPs are listed in the columns of Table 24, while the tablet CQAs are reported in the rows. The effect of each CPP on the CQAs is indicated as low, medium or high and it is highlighted with green, orange or red, respectively; it is reported in the cell corresponding to the crossing of the considered CMA row and CQA column.

	Mixing speed	Mixing time	% filling of bin	Compression force	Rotation speed	Feeding speed
Assay	Low	Low	Low	Low	Low	Low
Dissolution	Low	Medium	Low	High	Low	Low
Content Uniformity	High	High	High	Low	Medium	Medium
Identity	Low	Low	Low	Low	Low	Low
Microbial Limits	Low	Low	Low	Low	Low	Low
Impurities	Low	Low	Low	Low	Low	Low
Disintegration time	Low	Medium	Low	High	Low	Low
Crushing strength	Low	Medium	Low	High	Medium	Low
Appearance	Low	Low	Low	Medium	Low	Low

Table 24 – CPPs and CQAs correlation.

From the previous CPP-CQAs correlation, the content uniformity resulted to be the CQA most influenced by the considered CPPs, followed by the crushing strength, the disintegration time and the dissolution.

4.3.2 Analytical methods development and control strategy definition

It is important to plan an effective control strategy, in order to assure a reproducible quality during the overall process. Therefore, controls were performed at different levels: on the raw materials, on the intermediate product (the mixture) and on the finished product (the tablets) (Table 25). A schematic view of the bilastine process steps and controls is reported in Figure 42.

	Controls
Raw material	NIR acquisition of raw materials
Intermediate product (mixture)	NIR acquisition for drug assay determination
	NIR in process control
Final product (tablets)	NIR acquisitions for drug assay determination
	Content Uniformity
	Mass Uniformity
	Disintegration time
	Crushing strength
	Thickness

Table 25 – Types of control performed.

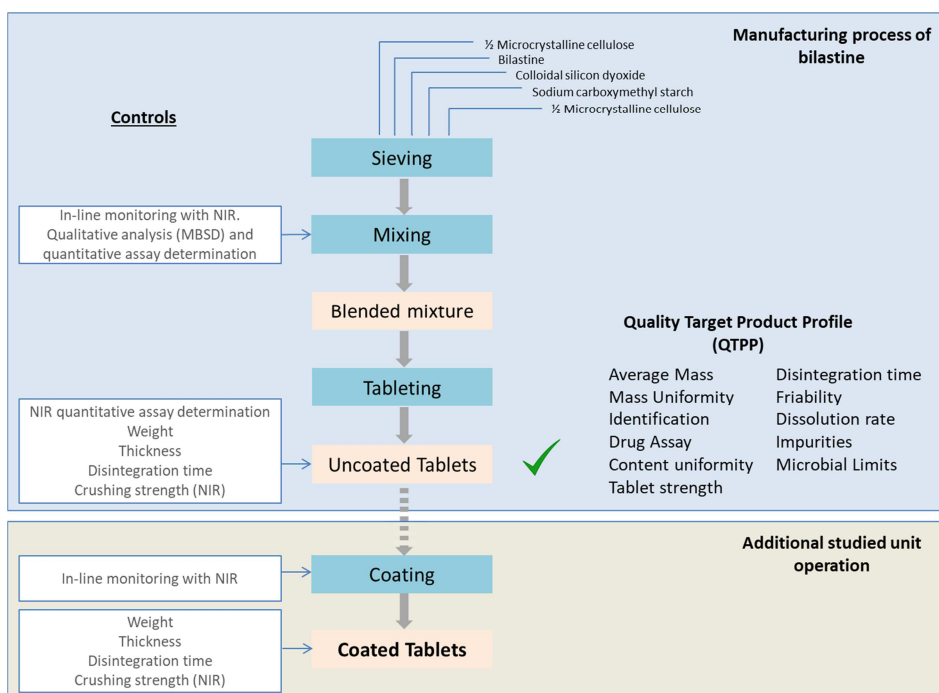


Figure 42 – Bilastine process work flow and controls.

With the aim of improving the process, by applying QbD and PAT elements, some NIR tools have been developed to control the process and the product. Currently, the process is only monitored by testing the finished product quality. Dissolution time, content uniformity and drug assay are required to assure the tablet quality and release the batches. No analysis is performed on the intermediate mixture. In order to imprint a QbD perspective to the process, a new control strategy should be actuated, to in-line monitoring the process step by step and systematically assure the quality. All the controls which are part of the control strategy are reported in Table 25.

With these premises, the NIR spectroscopy was applied to all the possible single unit operations and the following qualitative and quantitative analytical models have been developed:

- a qualitative method for the mixing process monitoring (using the MBSD);
- a quantitative method for drug assay determination in mixture;
- a quantitative method for drug assay determination in tablets;
- a quantitative method for crushing strength measurement on tablets;
- a quantitative method for tablet weight gain determination, during coating process.

The four quantitative model development followed some subsequent stages:

- Design and experiments: consisted in the preparation of samples for calibration and validation. It represented the phase of data generation and acquisition.
- Data elaboration and model building: consisted in the elaboration of the data and generation of the mathematical predictive model.
- Model verification: consisted in the evaluation of the predictive ability of the model.
- Use of the model: consisted in the application of the model for routine analysis.

For a complete description, see section 2.3.2. In the following sections only the model development will be reported, while its use and application will be presented during the study of the process (section 4.3.3).

Raw materials investigation

Before to begin the development of the NIR analytical methods, a preliminary evaluation of the raw materials was made. All the pure raw materials were independently acquired with NIR. The collected spectra were superimposed, to have a better comparison of the maximum absorbance wavelengths of each substance (Figure 43). A Standard Normal Variate (SNV) pre-treatment was performed on raw data to remove the baseline shift noise and improve the spectral visualization.

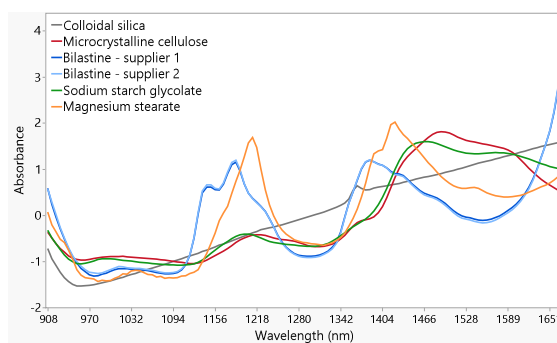


Figure 43 – Spectra of raw materials (MCC, sodium starch glycolate, SiO₂, MgSt, bilastine from both suppliers). A SNV pre-treatment was performed to remove the baseline shift noise.

Spectra of bilastine from suppliers 1 and 2 were very similar: they only presented slightly non-significant differences, for the purpose of our study. Bilastine exhibits a first peak with maximum absorbance at 1100-1270 nm and a second one at 1320-1540 nm. MCC and sodium starch glycolate have only a very weak absorbance, in correspondence of the first API peak, while their characteristic absorbance band was between 1330 and 1600 nm, therefore partially overlapped to the second bilastine peak. MgSt has its maximum absorbance peak at about 1240 nm, partially overlapped to the first bilastine signal and a second one at about 1430 nm. No absorption peaks were shown by SiO₂.

4.3.2.1 NIR analytical method for mixing monitoring: Moving Block of Standard Deviation

One of the easiest and immediate evaluations of the mixture process was done with the Moving Block of Standard Deviation (MBSD), which is based on the observation of the spectral variance. The difference between blocks of consecutive spectra is quantified by calculating the standard deviation (SD). When the difference is minimal, the mixture is considered to be blended. When using the MBSD, two parameters need to be defined: the window size (indicated as WS, in this text) and the step size (indicated as SS, in the text). An investigation was carried out, in order to define the optimal size of the blocks of spectra, i.e. the WS, and the “distance” between two consecutive blocks, that is the SS. For the proper definition of such parameters see section 3.1.2. At this purpose, MBSD was calculated on data differently pre-treated, and using different values of WS and SS. The investigation was carried out on a laboratory batch (TFM1904), prepared as reported in section 4.2.2.2. At first, the SS was fixed at 1 and the WS value was changed from 3 to 30. MBSD results are reported in Figure 44a. When using a small WS (WS=3, WS=5) the MBSD is quite noisy and presents sharp peaks. On the contrary, it becomes smoother and smoother as the WS increases. WS values either too small or too big were excluded. In the first case, eventual inhomogeneity information could be confused with the noise; in the other case, they could be reduced in their intensity. To select the right WS, the rotation speed used for mixing the powder was also taken into account. A preference was given to the WS values that reflected the number of acquisitions made in one minute. The laboratory batch was mixed using a rotation speed of 15 rpm, so a WS of 15 calculates the MBSD using all the acquisitions made during each minute. A WS of 15 was also a good compromise between WS dimensions that are too small or too big. The second evaluation was focused on the selection of the optimal SS. New MBSD were calculated, setting WS at 15 and varying the SS from 1 to 7. Results are reported in Figure 44b. The SS is the number of spectra the first block is displaced, with respect to the second block, and so on. If the SS is small, the two compared blocks will be similar, since they will contain, for the most part, the same spectra. For example, SS=1 means that the two compared blocks differ from each other by only one spectrum. On the contrary, the greater is the number, the more different the blocks will be. In this specific case, despite the similarity of two consecutive blocks for SS=1, we preferred not choosing too big SS; in that case, the MBSD curve would show a lower resolution, as fewer block comparisons are possible. Moreover, a big SS calculates the SD between blocks of spectra related to different moments of the mixing process; therefore, it would be harder to relate the results to a specific minute of mixing. In conclusion, the chosen MBSD parameters values were found to be 15 for the WS and 1 for the SS.

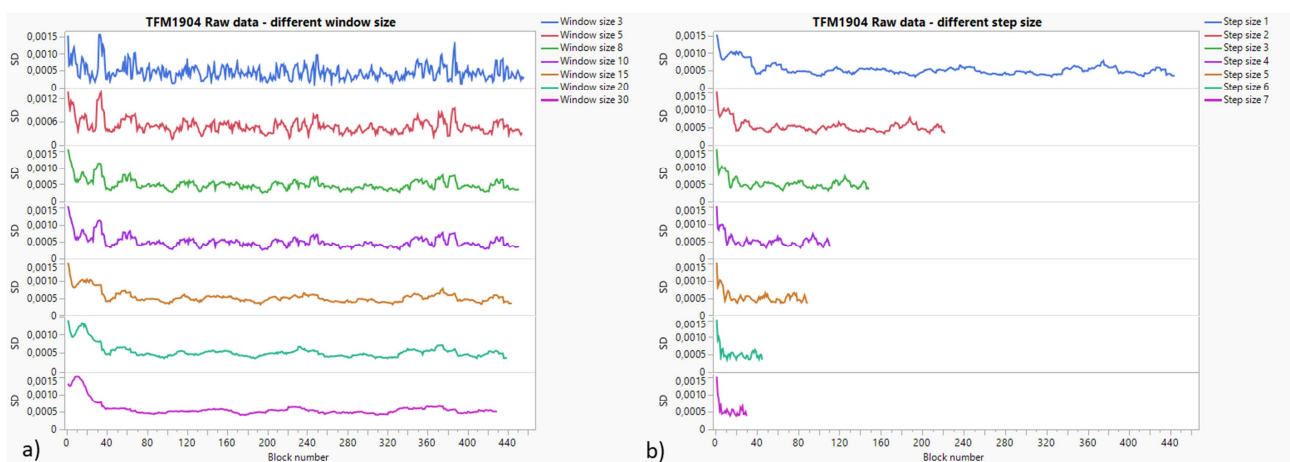


Figure 44 – MBSD calculated with step size fixed at 1 and different window sizes (picture a) and MBSD calculated with window size fixed at 15 and different step sizes (picture b).

This investigation was carried out on the raw data at first, but the same evaluation was also made on pre-processed data. In particular, the SNV pre-treatment was selected, as one of the simplest and the SNV followed by second derivative (indicated as SNV+Der2(3,9)) was selected, as the same pre-treatment used for the quantitative method (see section 4.3.2.2). In Figure 45 the MBSD (WS=15, SS=1) calculated on raw and on pre-treated data are compared. The MBSD of raw data appears noisier, respect to the ones of pre-treated data. In particular, in the MBSD of raw data, some peaks with higher SD can be seen at the beginning and also at the end of the mixing process, and they all have a similar intensity. The same is not observed when the data are pre-treated; in this case, the high SD value only appears at the beginning of the process. Therefore, the pre-treatment highlights the effective initial inhomogeneity, but not the other peaks, that in the raw data seemed to be of the same importance.

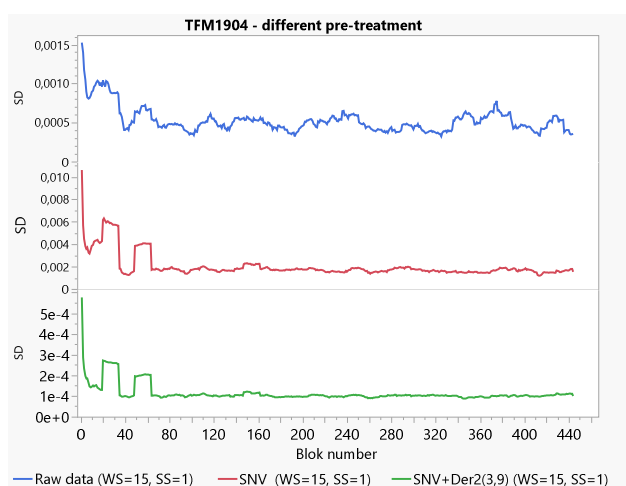


Figure 45 – MBSD of batch TFM1904 calculated on spectral data matrixes differently pre-processed. MBSD of raw data not pre-treated (upper picture), MBSD of data pre-treated with SNV (middle picture) and data pre-treated with SNV+Der2(3,9) (bottom picture).

A confirmation that the spectra pre-treatment are able to highlight the effective inhomogeneity of the system came from the observation of another laboratory batch (TFM2126). For the batch preparation the reader is sent forward to section 4.3.3.1. This batch was stopped and sampled multiple times, during the mixing process. During mixing process the powder bed incorporates air, in order to allow particle movement and the powders are in what is called “fluidized status”. As the mixer stop rotating, powder bed also stops moving, falls down on the bottom of the mixer and expels the air previously incorporated. When the bin rotation starts again, the powder bed is in a different status then it was before the rotation was stopped; therefore, an initial difference, at the re-starting, is expected. This information is evident in the MBSD of the pre-treated spectra (Figure 46, middle and bottom picture), while it is not so evident in the MBSD of raw data (Figure 46, upper picture).

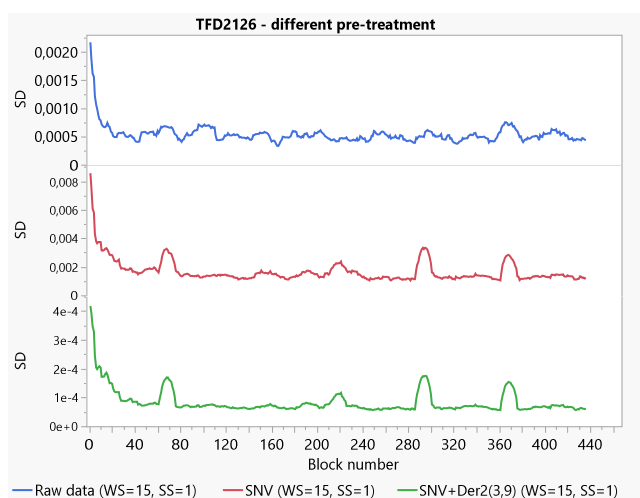


Figure 46 – MBSD of batch TFD2126, calculated on spectral data matrixes differently pre-processed. MBSD of raw data not pre-treated (upper picture), MBSD of data pre-treated with SNV (middle picture) and data pre-treated with SNV+Der2(3,9) (bottom picture).

The MBSD of the SNV and SNV+Der2(3,9) data were very similar to each other and both pre-treatments might be valid for MBSD application. The SNV+Der2(3,9) pre-treatment was preferred to the SNV one, as the same already used for the quantitative method on mixture. All the previous considerations were referred to the TFM1904 and TFD2126 laboratory batches, made by replicating the process parameters of the industrial manufacturing process (30 min of mixing at 15 rpm). During the study of the mixing process, different mixing time and rotation speed values were tested. In such cases, the WS was not 15, but it was selected on the base of the used rotation speed. The SS was always 1; the data were always pre-treated with SNV+Der2(3,9).

4.3.2.2 NIR analytical method for drug assay determination in mixture

A quantitative NIR analytical method for the in-line analysis of bilastine in powder mixture was developed. The final goal was to have an analytical PAT tool, to control the drug assay, directly during the mixing step. In fact, in the current process the control of the drug concentration is performed only on the final tablets, since the HPLC method is not applied on bulk powder mixtures. The NIR analysis represents a more effective alternative for establishing the achievement of homogeneity, respect to the blend uniformity test, performed by sampling at given interval times during mixing. It is well known, in fact, that sampling powder with probes is a procedure error affected⁸. NIR analysis, on the other hand, implies the possibility of obtaining immediate, more reliable and cost-free results, in real time, without possible demixing problems due to powder sampling.

Experimental Plan

The experimental plan, schematised in Figure 47, involved the three aforementioned steps: 1) design and experiments, 2) data elaboration and model building, 3) model verification. Once the model is developed, it can be used for prediction of an unknown sample.

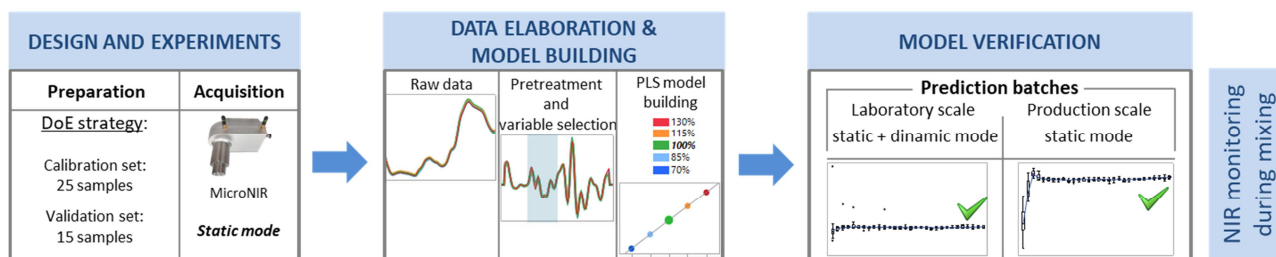


Figure 47 – Flow chart of the experimental plan for the development of the model for drug assay determination in mixture.

Design and experiments

A calibration and a validation set of samples were prepared. The calibration set should include all the usual physical and chemical variability of the process. With this purpose, the mixture components were varied in concentration. The amount of each ingredient, with the exception of MCC, was changed on five different levels, ranged between 70% and 130% of the related amount present in the registered formulation (Table 9). A DoE strategy was followed, for the selection of calibration samples. The response of interest was the bilastine assay in powder mixtures, while the studied factors were the ingredient's concentration. For sample preparation MCC, being the most abundant component, was selected as the filler and was added to keep constant the total weight of each mixture (10 g). Bilastine, MCC and sodium starch glycolate, as the most abundant ingredients have an effect on the resulting spectrum. For SiO₂ and MgSt, used in a little amount, a relevant impact on the spectra is not expected, even if MgSt has a maximum absorbance peak partially overlapped to the bilastine one. SiO₂ and MgSt variation does not cause any impediment to carrying out the experiments, but, at most, they could bring further information. For that reason, they were also included into the design space matrix. A Plackett-Burman reduced matrix was applied, which allowed to plan only 25 experiments, to investigate 5 factors at 5 levels, but still keeping the design orthogonality⁹.

With the purpose of including all the variability that really affects the manufacturing process, the API supplier was included as a further factor at two levels: supplier 1 (level 1) and supplier 2 (level -1). The effect of the API supplier was investigated with a Principal Component Analysis (PCA) on the whole calibration set. No clear distinction among bilastine samples provided by the two suppliers was highlighted in Figure 48; on the contrary, the data were in both cases randomly spread, allowing to rule out any effect attributable to the different API supplier.

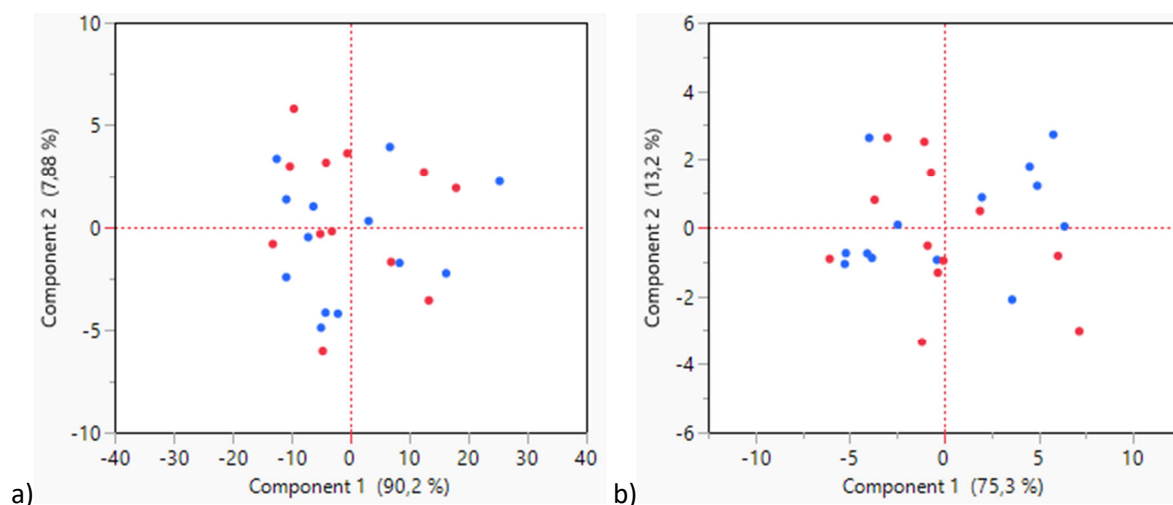


Figure 48 – a) PCA of calibration set raw data on all the wavelengths. B) PCA of calibration set of data are pre-treated with SNV and 2nd derivative, on the 1087-1217 nm wavelength interval. For both images: blue points supplier 1, red points supplier 2.

The obtained experimental matrix is shown in Table 26. Further 15 samples for external laboratory validation were prepared (Table 27). The validation set was prepared by only varying the API supplier type (2 levels) and the API concentration on eleven levels, ranged between 70% and 130% of the amount used in the manufacturing formulation (Table 9). The amount of all excipients was unchanged, respect to the formulation in Table 9, with the exception of MCC, which was added to keep constant the total weight of each sample.

RUN	Bilastine	Sodium starch glycolate	Colloidal silica	Magnesium stearate	API supplier
1	100%	100%	100%	100%	Supplier 1
2	100%	70%	70%	130%	Supplier 2
3	70%	70%	130%	85%	Supplier 1
4	70%	130%	85%	130%	Supplier 2
5	130%	85%	130%	100%	Supplier 1
6	85%	130%	100%	85%	Supplier 2
7	130%	100%	85%	85%	Supplier 1
8	100%	85%	85%	115%	Supplier 2
9	85%	85%	115%	130%	Supplier 1
10	85%	115%	130%	115%	Supplier 2
11	115%	130%	115%	100%	Supplier 1
12	130%	115%	100%	130%	Supplier 2
13	115%	100%	130%	130%	Supplier 1
14	100%	130%	130%	70%	Supplier 2
15	130%	130%	70%	115%	Supplier 1
16	130%	70%	115%	70%	Supplier 2
17	70%	115%	70%	100%	Supplier 1
18	115%	70%	100%	115%	Supplier 2
19	70%	100%	115%	115%	Supplier 1
20	100%	115%	115%	85%	Supplier 2
21	115%	115%	85%	70%	Supplier 1
22	115%	85%	70%	85%	Supplier 2
23	85%	70%	85%	100%	Supplier 1
24	70%	85%	100%	70%	Supplier 2
25	85%	100%	70%	70%	Supplier 1

Table 26 – Plackett-Burman experimental matrix (25 runs) for calibration set. The level of concentration of each single ingredient is reported for each run, as the percentage of the related amount present in the registered formulation (Table 9). These concentration levels were applied to each ingredient, with the exception of MCC, which was added to keep constant the total weight of each sample.

RUN	Bilastine	API supplier
1	100%	Supplier 1
2	130%	Supplier 2
3	130%	Supplier 1
4	85%	Supplier 2
5	85%	Supplier 1
6	115%	Supplier 2
7	115%	Supplier 1
8	70%	Supplier 2
9	70%	Supplier 1
10	90%	Supplier 2
11	105%	Supplier 1
12	110%	Supplier 2
13	80%	Supplier 1
14	120%	Supplier 2
15	95%	Supplier 1

Table 27 – Experimental matrix for validation set. The level of concentration of bilastine is reported for each run, as the percentage of the related amount present in the registered formulation (Table 9).

Laboratory calibration set (25 samples) and laboratory validation set (15 samples) were prepared as previously reported in section 4.2.2.2. Both sample sets were acquired with NIR, using a static acquisition mode, because of the small dimension of the powder samples, as previously explained in section 4.2.2.1.

Data elaboration and model building

The acquired spectra of the calibration and validation samples were elaborated using chemometric data pre-treatment, to improve the signal-to-noise ratio. At the same time a variable selection was performed, to identify the wavelength interval, containing the most suitable information with the lowest noise. As developing a quantitative method for the assay determination of bilastine, the wavelength intervals corresponding to the two maximum absorbance peaks of pure bilastine were selected on the mixture spectrum (highlighted in Figure 49, by two rectangles) and more in depth investigated, with the aim of identifying a narrower, more specific interval. With this purpose, spectra were grouped into five different colours, each one corresponding to one of the five API concentration levels. The spectral study consisted in identifying the region where spectra corresponding to samples at different concentrations are well separated and organized, according to a concentration gradient. This investigation was carried out on the SNV spectra, as the raw data did not allow a good distinction according to the concentration gradient. A previous visual investigation was made, to verify that no peak shift occurs, when applying the SNV pre-treatment¹⁰. As shown in Figure 50, the region corresponding to the first peak of maximum absorbance of bilastine exhibited a good spectra distinction, based on different API concentrations. The same trend was not found in correspondence of the second peak, which was more confused.

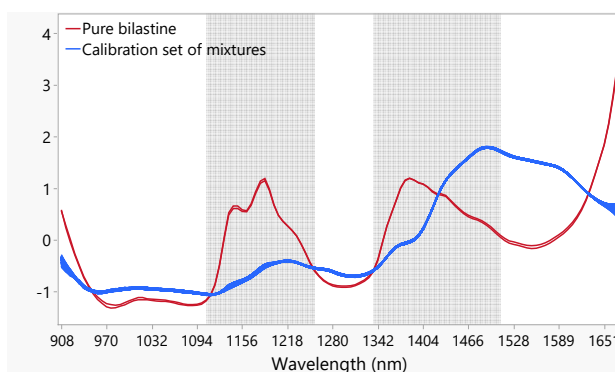


Figure 49 – Spectra of 25 mixtures of calibration set (in blue) and spectra of pure bilastine (in red). A SNV pre-treatment was applied to reduce the baseline shift noise.

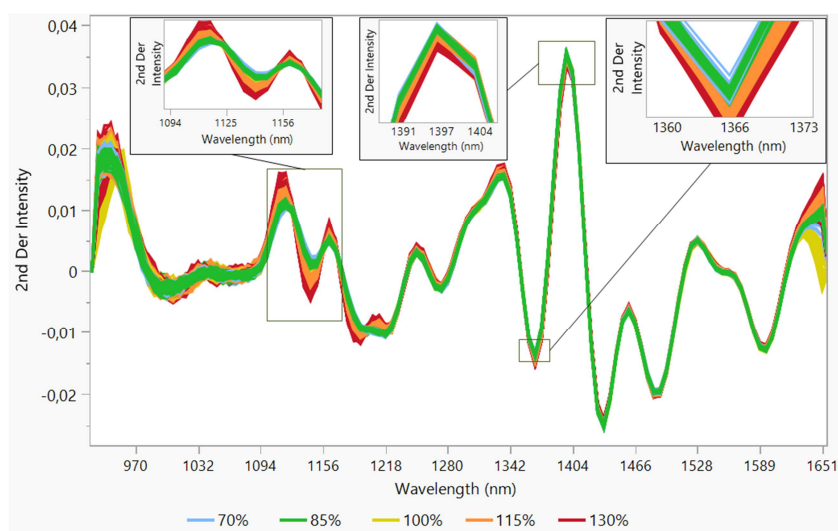


Figure 50 – Zoom of the two regions corresponding to bilastine's maximum absorbance peaks. Each colour corresponds to one of five bilastine concentration levels: 70%, 85%, 100%, 115% and 130%.

The previous visual consideration provides a first general information. However, in order to select the actual most informative interval, many different ones were investigated, all along the entire wavelength range (908-1676 nm). Particular attention was paid at the intervals which included the first peak of maximum absorbance of bilastine. All the wavelength intervals reported in Table 28 were tried in combination with different kinds of chemometric pre-treatments. A non-exhaustive list of models resulting from several wavelength interval - data pre-treatment combinations, is presented in Table 29.

Wavelength Interval (nm)	Interval ID
908-1676	Int 0
1087-1217	Int 1
1087-1304	Int 2
1807-1217+1323-1601	Int 3
1087-1601	Int 4
1323-1651	Int 5

Table 28 – Wavelength intervals taken into account for model development.

	Chemometric pre-treatment	Interval	RMSEC	RMSEP	R ² cal	R ² val
1	SNV + Der2(3,9)	Int 1	1.738	2.372	0.993	0.985
2	SNV + Der2(3,9)	Int 2	1.720	2.702	0.993	0.980
3	Der1(3,9) + SNV	Int 3	1.835	3.014	0.992	0.975
4	Der2(3,9) + SNV	Int 3	1.589	3.074	0.994	0.974
5	Der1(3,9) + SNV	Int 2	1.594	3.123	0.994	0.973
6	SNV + Der1(3,9)	Int 2	1.690	3.140	0.994	0.973
7	SNV + Der2(3,9)	Int 4	1.234	3.212	0.997	0.972
8	Der2(3,9) + SNV	Int 1	3.059	3.412	0.979	0.968
9	Der1(3,9)	Int 2	1.778	3.460	0.993	0.968
10	Der1(3,9)	Int 4	1.241	3.473	0.997	0.967
11	SNV + Der2(3,9)	Int 3	1.246	3.480	0.996	0.967
12	Der2(3,9) + SNV	Int 4	1.715	3.747	0.993	0.962
13	Der1(3,9)	Int 3	1.819	3.873	0.993	0.959
14	Der1(3,9) + SNV	Int 1	1.834	3.971	0.992	0.957
15	SNV + Der1(3,9)	Int 3	1.787	4.087	0.993	0.955
16	Der1(3,9) + SNV	Int 4	1.975	4.122	0.991	0.954
17	none	Int 1	1.419	4.307	0.996	0.950
18	SNV + Der1(3,9)	Int 1	1.970	4.438	0.991	0.947
19	Der1(3,9)	Int 1	1.454	4.533	0.995	0.944
20	SNV	Int 2	1.652	4.617	0.994	0.942
21	Der2(3,9) + SNV	Int 2	3.527	4.637	0.972	0.942
22	SNV + Der2(3,9)	Int 0	1.368	4.845	0.996	0.936
23	Der2(3,9) + SNV	Int 0	2.781	4.895	0.983	0.935
24	SNV	Int 1	1.375	5.008	0.996	0.932
25	SNV + Der1(3,9)	Int 4	1.009	5.325	0.998	0.923
26	SNV + Der1(3,9)	Int 0	1.858	5.473	0.992	0.919
27	Der1(3,9) + SNV	Int 0	1.895	5.604	0.992	0.915
28	none	Int 2	1.582	5.660	0.994	0.913
29	none	Int 3	1.341	5.893	0.996	0.906
30	SNV	Int 0	1.654	6.087	0.994	0.899
31	Der2(3,9)	Int 0	3.537	6.875	0.972	0.872
32	Der2(3,9)	Int 3	3.819	6.942	0.968	0.869
33	Der2(3,9)	Int 4	3.834	7.044	0.967	0.865
34	Der1(3,9)	Int 0	9.260	7.221	0.809	0.859
35	SNV	Int 4	1.466	7.292	0.995	0.856
36	none	Int 0	3.376	7.761	0.975	0.837
37	SNV	Int 3	1.019	8.359	0.998	0.810
38	none	Int 4	1.314	9.734	0.996	0.742
39	Der2(3,9)	Int 1	5.191	11.27	0.940	0.649

40	Der2(3,9)	Int 2	5.235	11.316	0.939	0.653
41	Der2(3,9)+ SNV	Int 5	8.281	11.589	0.847	0.636
42	SNV	Int 5	8.232	11.925	0.850	0.614
43	SNV + Der1(3,9)	Int 5	11.410	12.143	0.710	0.600
44	2° derivative (3,9)	Int 5	10.906	12.431	0.735	0.581
45	1° derivative (3,9)	Int 5	15.304	12.637	0.497	0.567
46	1° derivative (3,9) + SNV	Int 5	10.462	13.584	0.756	0.499
47	SNV + 2° derivative (3,9)	Int 5	8.152	15.318	0.852	0.364
48	none	Int 5	20.177	23.667	0.094	NA

Table 29 – A non-exhaustive list of the tried interval-pre-treatment combinations. The proposed models are ranked according to the better Root Mean Square Error of Prediction (RMSEP). The selected model is the first of the ranking.

SNV followed by Savitzky-Golay second derivative of third polynomial order and 9 smoothing points (indicated as Der2(3,9)) pre-treatment applied to the selected 1087-1217 nm (Int 1) interval was found as the combination giving the PLS model with the better predictive ability, for the intended purpose. Using the whole wavelength set (Int 0) or including a wavelength region referring also to excipients (Int 3, Int 4 and Int 5) would bring additional information, but it is not a good option, as it brings too much noise and the model shows a higher RMSEP, independently from the pre-treatment applied. The pre-treatment type is also fundamental. In fact, selecting the proper wavelength region is not sufficient to improve the RMSEP of the model, as demonstrated by the model number 17 in the table, with the selected interval (1087-1217 nm) but no pre-treatment (RMSEP=4.3). The combination of SNV and second derivative in this precise order gives the best RMSEP (2.372), in comparison to the model with only SNV (RMSEP=5.008) or second derivative treatment (RMSEP=11.27), or with both of them, but in the inverse order (Der2(3,9)+SNV, RMSEP=3.412).

The score plot of the model (Figure 51a) shows that points were well grouped into five categories, corresponding to the five bilastine concentration levels. The score plot shows how much of the total variation is explained, by each factor. The percentage value is reported next to each axis in brackets. The sum of the explained variances of bilastine content for the first and second factor is 99%. The first two factors itself allow a good group distinction, even if a point of 115% could be confused with those of 100% group. The third and fourth factors avoid this confusion and give their contribution for a better grouping. This can be seen also in Figure 51b, where the explained variance, for both calibration and validation set, is shown: all four factors were needed to explain the most of the variability observed on the response (bilastine assay). In fact, even if the first two factors explain the 99% of the total spectral variability, a model with only these two factors showed a higher deviation, during prediction. Figure 51c shows the predicted vs reference plot of the model and the statistic parameters used to assess its quality. As can be seen, good RMSEP and R^2 values were obtained for both calibration and prediction. Therefore, it can be concluded that calibration data well fit to the model and that the model has a good response on the data used for validation.

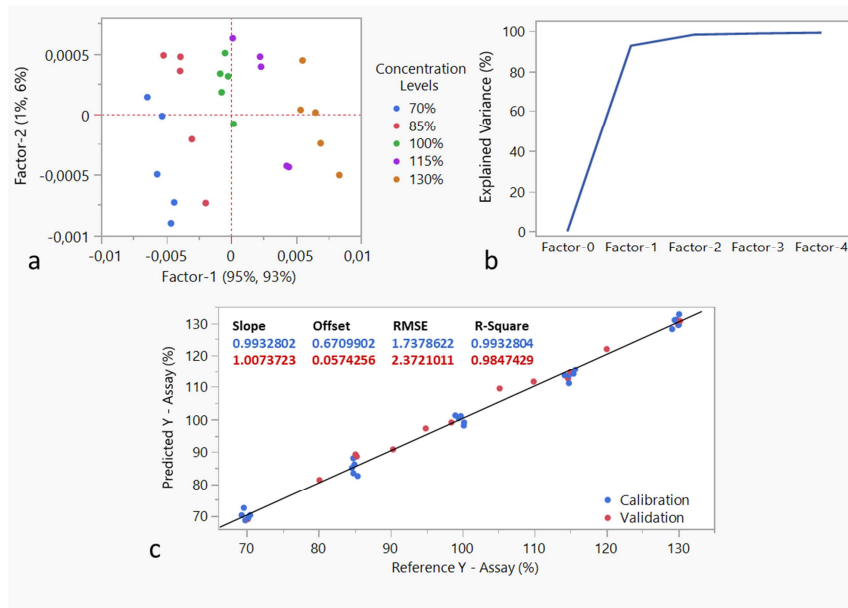


Figure 51 – PLS model outputs. Data used for the model development were pre-treated with SNV+Der2(3,9) and the selected variables interval was used (1087-1217 nm).

Model verification

Before investigating the effectiveness of the obtained PLS model on production scale batches, a preliminary trial was carried out on a laboratory batch of 2 kg (TFM1904), prepared according to the same process used for the industrial production (see section 4.2.2.2). The spectral acquisition of this batch was made in both static mode, at the end of the mixing (Figure 52a) and dynamic mode, during the mixing process (Figure 52b), in order to investigate any possible differences due to the different acquisition method. In fact, the optimal situation would be to acquire calibration and unknown sample spectra in the same way. However, this was not possible in this case, since the calibration set was acquired with static mode, because of the small amount of the samples, while the production batches can be acquired only during the mixing process, i.e. with a dynamic mode.

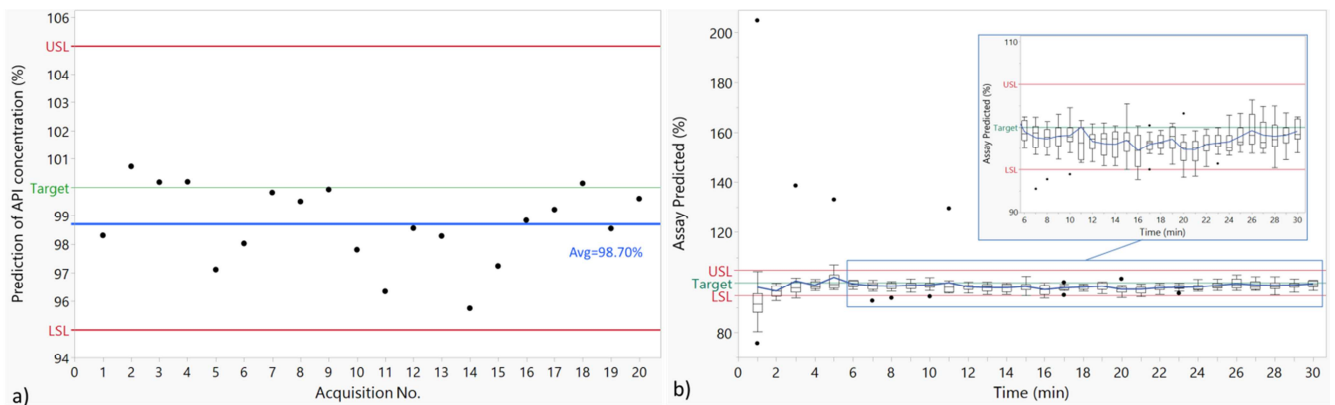


Figure 52 – Laboratory batch assay prediction. a) Assay predictions of 20 static acquisitions; assay predictions are all inside the Upper Specification Limit (USL) and Lower Specification Limit (LSL). b) Assay prediction of 450 dynamic acquisitions (1 acquisition for each revolution; 15 acquisitions per minute). The 15 acquisitions of each minute are grouped in a single box plot. The middle line of the box plot indicates the median, while the blue line connects the average value of prediction of each minute. Black points outside the box plot are probable outliers.

To better visualize and follow the trend of the mixture assay content during the mixing process, a control chart was built. As the rotation speed of the mixer was 15 rpm and the NIR instrument acquired one single spectra at every rotation, a total of 15 spectra were collected in one minute. The control chart shows summarized data for each minute, as box plots. The average, median and variability of the 15 assay values belonging to such minute are shown in Figure 52b. A line, passing through the average value, links the box plots of consecutive minutes. As shown in Figure 52a, the overall average of the 20 static acquisitions was 98.70%, i.e. very close to the target (100%) and well within the Upper Specification Limit (USL) and the Lower Specification Limit (LSL). The first 15 dynamic acquisitions during the first minute of mixing (Figure 52b) exhibited a variable oscillation of concentration values, from a maximum of 200% and a minimum of 77%, but the title value rapidly stabilized around 100%, and stayed constant and well-inside the specification limits until the end of the process.

After demonstrating the good predictive ability of the model on the laboratory scale batch, with both static and dynamic spectra acquisition modes, the model was finally applied to two manufacturing scale batches (250 kg) (batch 20-505 and batch 20-11). They were prepared as above described in section 4.2.2.2 and acquired with the dynamic mode, during the mixing process (see section 4.2.2.1). The results of model predictions for the two batches are shown in Figure 53a and Figure 53b. Also in this case, after an initial phase of about 50 rotations (less than 4 min of mixing), which showed an oscillating trend in drug assay prediction, all values were inside the specification limit and the bilastine concentration value stabilized around 100%.

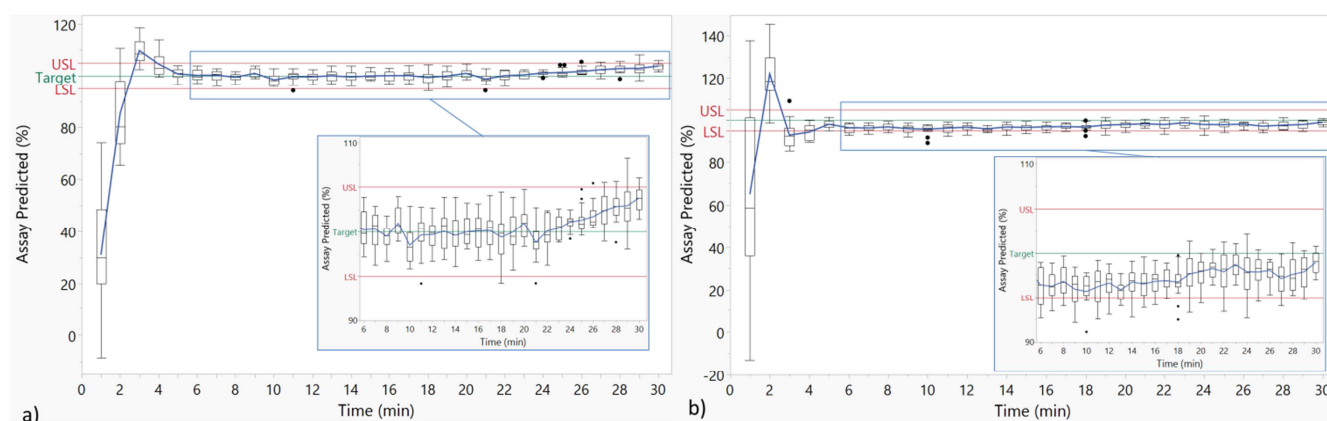


Figure 53 – Bilastine assay prediction of production batch, based on 450 dynamic acquisitions (1 acquisition for each revolution; 15 acquisitions per minute). The 15 acquisitions of each minute are grouped in a single box plot. The middle line of the box plot indicates the median, while the blue line connects the average value of prediction of each minute. Black points outside the box plot are probable outliers. a) Production batch 20-505, containing bilastine from supplier 1. b) Production batch 20-11, containing bilastine from supplier 2.

The model gave good drug assay values for both production and laboratory scale batches. Previous results cannot be compared with a reference method, since no drug assay is executed on the powder mixture, during the industrial tablet manufacturing process. However, the goodness of the model was supported by comparison with the HPLC API assay, performed on the tablets obtained from those mixtures (Table 30). The Content Uniformity is expressed in terms of Acceptance Value (AV): the lower the AV the better the uniformity content in the tablets; an acceptable AV must be lower than 15 and, according to Chodayudth¹¹, values below 8 indicate a very good content uniformity. The HPLC drug assay results are reported as the average mg of bilastine present in 10 tablets of the batch.

Batch	NIR API assay on mixtures (%)	HPLC API assay on tablets (mg/tab)	HPLC API assay on tablets (%)	Tablets content uniformity (AV)
Batch 1	103.82	19.73	98.65	3.8
Batch 2	98.98	20.09	100.45	2.0
Lab batch	99.53	20.53	102.40	5.2

Table 30 – Comparison between the in-line NIR bilastine determination in mixtures and HPLC drug assay and content uniformity (expressed in terms of Acceptance Value (AV)) on final tablets.

The results of this first series of studies have been already published¹².

4.3.2.3 NIR analytical method for drug assay determination in tablets

A quantitative NIR analytical method for the at-line bilastine drug assay determination in tablets was developed. The final goal was to have available a fast and simple method to determine the API amount in tablets, as an alternative to the destructive and off-line HPLC traditional method.

Experimental plan

The experimental plan (Figure 54), involved three steps: 1) design and experiments, 2) data elaboration and model building, 3) model verification. Once the model was developed, it was used for prediction of an unknown sample.

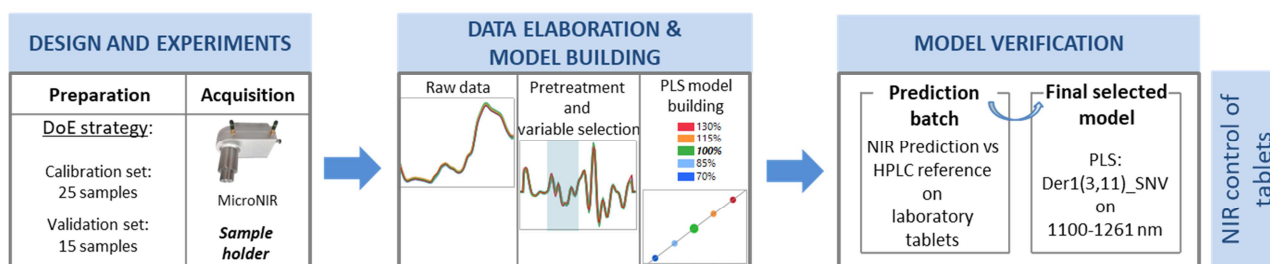


Figure 54 – Flow chart of the experimental plan for the development of the model for drug assay determination in tablets.

Design and experiments

A calibration and a validation set were prepared, by compressing the powder mixtures, previously made and used for the analytical method on mixtures. The tablets were compressed with the Natoli manual single punch press. The components variation, between $\pm 30\%$ of the labelled amount, did not have a great impact on the powder density; therefore, the filling depth of the chamber was kept constant at 9.170 mm, in order to have a tablet weight equal to 125 mg $\pm 2.5\%$. The compression force was varied between 2.6 and 3.8 kN, in order to obtain a tablet crushing strength around 130-150 N. The resulting tablets exhibited thickness variation from 3.25 to 3.45 mm, thus remained inside the acceptable limits (3.1-3.5 mm). For each batch, a total of 10 tablets were made. The calibration set had 25 powder samples, therefore 250 tablets were obtained; the validations set had 15 mixtures, therefore 150 tablets were made. All the tablets were characterized in terms of weight and thickness and, then, were acquired with the NIR spectrometer, following the previously described method (see section 4.2.2.1). All the tablets were analysed with HPLC, after completing the NIR acquisitions. Once all the data were acquired, the model research started.

Data elaboration and model building

The spectra bring a lot of important information but also a lot of noise. For that reason, the whole spectrum is not representative of the change in API concentration and a selection of a proper interval is needed. The rationale behind the choice of a spectral interval, must lead to the selection of the most diagnostic part of the spectra, which brings the more information and the lowest noise.

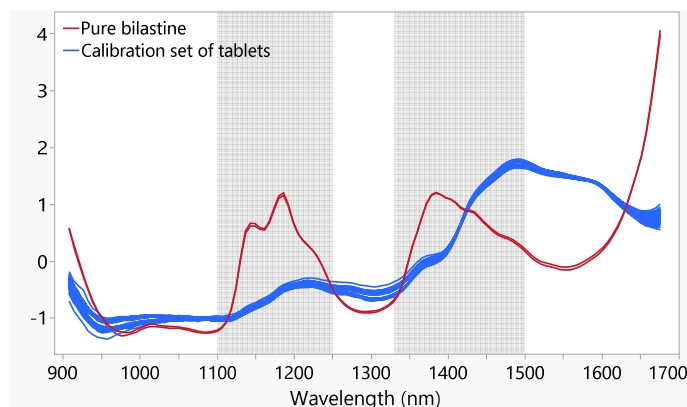


Figure 55 – Comparison between pure bilastine (in red) and bilastine tablets' spectra (in blue).

The region of bilastine absorbance can be easily found in the tablets spectra, from a direct comparison with the spectra of pure bilastine (Figure 55). The first screening was made by observing the tablets raw spectra, in order to roughly select an interval, where spectra corresponding to different concentration samples were well separated, and possibly organized according to a concentration gradient. The raw data have a lot of noise and there was no interval where the spectra were arranged according to their concentration (Figure 56a). In order to improve the visualization, the raw data were pre-treated with a SNV transformation (Figure 56b). Now, a region where the spectra are arranged according to their concentration can be seen around 1124-1186 nm. The same observation was carried out on data with other simple pre-treatments (Figure 57), giving the intervals reported in Figure 58. As a first rough interval, 1100.125-1199.235 nm was selected, because almost all the investigated pre-treatments showed linearity of concentration in such spectral region. This starting interval will be refined afterwards, once the proper pre-treatment type will be selected.

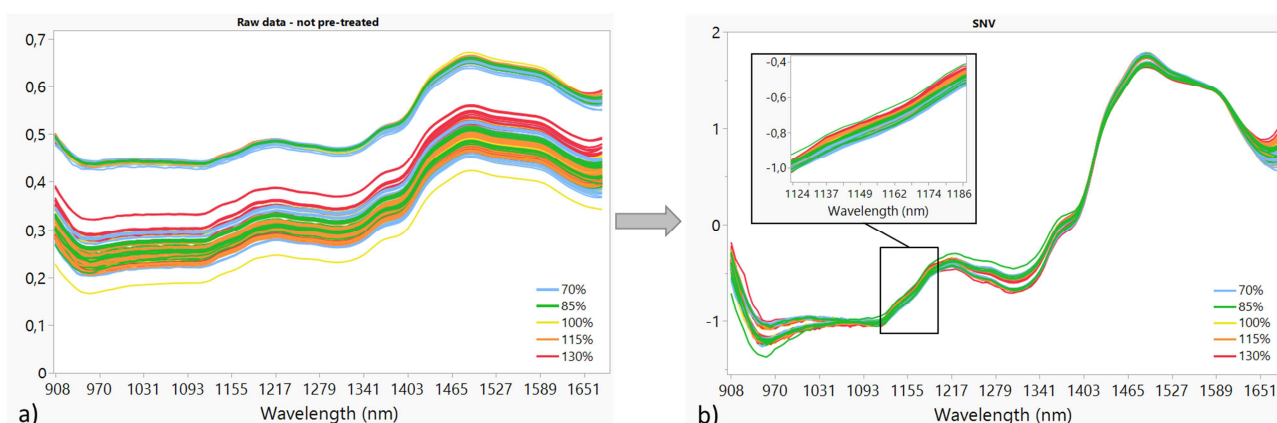


Figure 56 – a) spectra of the raw data, coloured by concentration level. b) Spectra of the SNV data; the zoomed picture is referred to the portion with a spectral organization, according to a gradient.

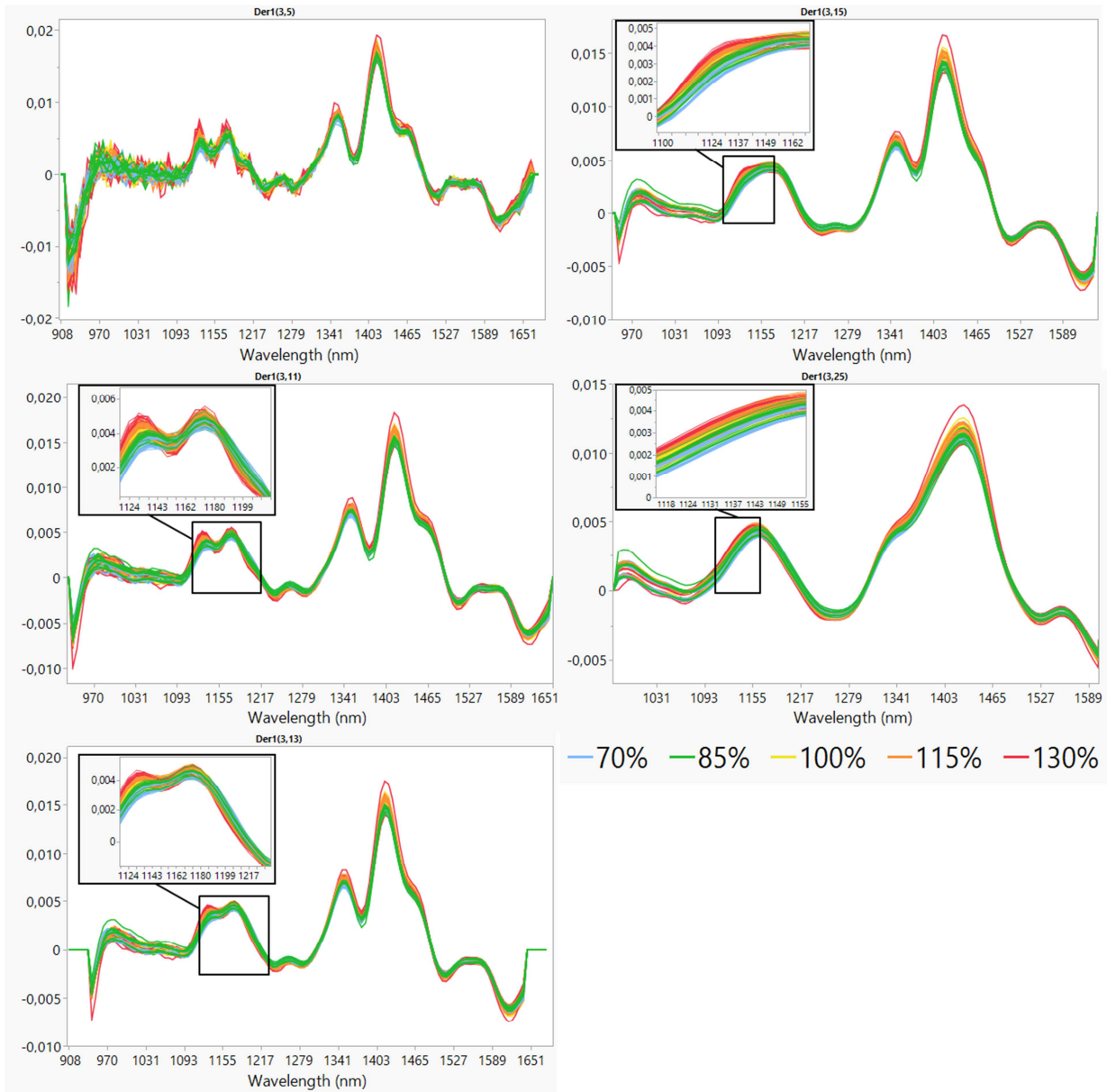


Figure 57 – Different types of pre-treatments used for finding the spectral region where data are organized according to a concentration gradient (zoomed pictures).

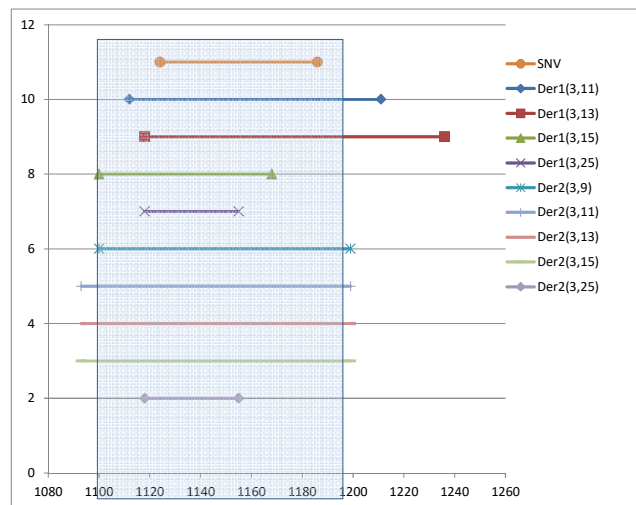


Figure 58 – Interval of linearity of concentration, individuated on spectra differently pre-treated.

The starting interval was then tried on different types of pre-treatment, in order to assess the most proper one and exclude the worst. The tried pre-treatments were Savitzky-Golay first and second derivatives (indicated as DerX(PO,SP), where X in the 1st or 2nd derivative, PO is the polynomial order and SP is the number of smoothing points used for calculation), Standard Normal Variate (SNV) and combinations of them. A total of 6 different groups were obtained from the combination of derivatives and SNV pre-treatments: 1st derivative only, 2nd derivative only, 1st derivative followed by SNV, 2nd derivative followed by SNV, SNV followed by 1st derivative and SNV followed by 2nd derivative; the SNV alone was also tested as possible pre-treatment. The first and second derivatives perform a smoothing effect on the spectra, causing the reduction of noise; however, a too deep smooth could cause also information removal. In order to select an acceptable derivative setting, without causing an excessive smoothing, the spectra of different derivative settings were visually inspected (Figure 59). Either a too low or a too high number of smoothing points was excluded. In particular, 5 smoothing points were not enough, to perform an acceptable smoothing of the spectra, which were still too noisy. On the contrary, when using more than 13 smoothing points, the spectrum resulted too smooth and the bilastine characteristic peaks merged in one single smoothed peak. In conclusion, the smoothing points taken into consideration were four: 7, 9, 11 and 13.

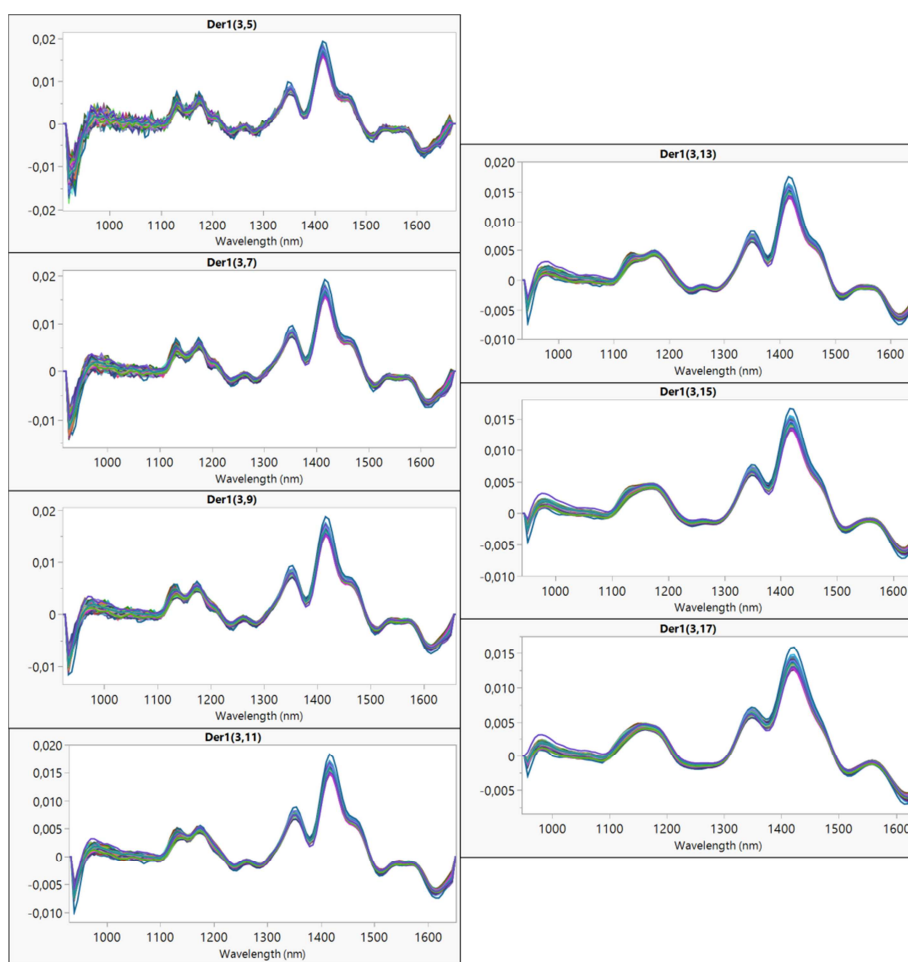


Figure 59 – Derivatives with an increasing number of smoothing points.

Four derivative settings were tried for each of the six groups, as well as the SNV alone, for a total of 25 pre-treatments combinations. Each one of them was used to build a PLS model with an external validation. The PLS models were evaluated on the base of RMSEP and R^2 ; the results are reported in Table 31.

Pre-treat.	Der1		Der2		Der1+SNV		Der2+SNV		SNV+Der1		SNV+Der2		SNV							
	RMSEP	R ² val	RMSEP	R ² val	RMSEP	R ² val	RMSEP	R ² val	RMSEP	R ² val	RMSEP	R ² val	RMSEP	R ² val						
1	Der1(3,11)	5.66	0.94	Der2(3,13)	5.48	0.94	Der1(3,11)+SNV	4.35	0.96	Der2(3,13)+SNV	5.15	0.95	SNV+Der1(3,13)	5.18	0.95	SNV+Der2(3,9)	5.37	0.94	6.56	0.91
2	Der1(3,13)	5.72	0.93	Der2(3,11)	5.61	0.94	Der1(3,13)+SNV	4.44	0.96	Der2(3,11)+SNV	6.05	0.93	SNV+Der1(3,11)	5.60	0.94	SNV+Der2(3,11)	5.41	0.94		
3	Der1(3,9)	5.93	0.93	Der2(3,9)	6.28	0.92	Der1(3,9)+SNV	4.72	0.95	Der2(3,9)+SNV	6.28	0.92	SNV+Der1(3,7)	7.13	0.90	SNV+Der2(3,13)	5.52	0.94		
4	Der1(3,7)	6.17	0.92	Der2(3,7)	6.60	0.91	Der1(3,7)+SNV	5.13	0.95	Der2(3,7)+SNV	6.43	0.92	SNV+Der1(3,9)	7.25	0.89	SNV+Der2(3,7)	5.88	0.93		

DerX(PO,SP) where X is 1st or 2nd derivative PO: Polynomial Order SP: Smoothing Points

Table 31 – PLS models resulting from the application of the 25 pre-treatments, to the calibration and validation data.

For each of the 6 groups the models were ranked, according to the lower RMSEP and the higher R². The best model of each group (corresponding to the first line of the Table 31) was selected, for further investigations. Since now, the selection was performed on the rough starting interval, but a more precise interval should be selected. Observing the spectra of Der1(3,13)+SNV data, some possible intervals have been chosen and tried, in combination with the 7 remaining pre-treatments (Table 32). A total of 49 combinations (interval-pre-treatments) were used to pre-treat data and build new PLS models.

Wavelength interval (nm)	Pre-treatment type
1100-1199	der1(3,11)
1100-1236	der2(3,13)
1100-1261	der1(3,11)+SNV
1100-1217	der2(3,13)+SNV
1100-1131+1180-1236	SNV+der1(3,13)
1180-1236	SNV+der2(3,9)
1180-1261	SNV

Table 32 – 7 wavelength intervals and 7 pre-treatments, to be tried for PLS building.

The PLS information relative to the 49 tried combination are resumed in Table 33. The pre-treatments Der2(3,13)+SNV, SNV+Der2(3,9) and Der2(3,13)+SNV (line e, f and g of Table 33) showed a RMSEP > 5 on all the intervals, thus they were excluded from further investigations. Der1°(3,11) (line d of Table 33) was equally excluded, as it always showed a higher RMSEP, respect to the Der1°(3,11)+SNV (same type of derivative, but followed by SNV). The 1100-1131+1180-1236 nm, 1180-1236 nm and 1180-1261 nm intervals were also excluded, as all the models in such intervals showed a RMSEP > 5. The remaining three models (line a, b and c of Table 33) have quite similar RMSEP and R², on all the four remaining intervals and represented the models with the lower error and the higher R². A deeper investigation was carried out, to assure the selection of the most proper model among these last 12 combinations (see Table 34).

Pre-treatment	1100-1199 nm		1100-1261 nm		1100-1236 nm		1100-1217 nm		1100-1131+1180-1236 nm		1180-1236 nm		1180-1261 nm		
	RMSEP	R ² val	RMSEP	R ² val	RMSEP	R ² val	RMSEP	R ² val	RMSEP	R ² val	RMSEP	R ² val	RMSEP	R ² val	
a	Der1(3,11)+SNV	4.35	0.96	4.60	0.96	4.46	0.96	4.49	0.96	5.56	0.94	8.47	0.85	8.66	0.85
b	SNV+Der1(3,13)	5.18	0.95	4.52	0.96	3.97	0.97	4.28	0.96	5.22	0.94	6.82	0.91	6.71	0.91
c	SNV	6.56	0.91	4.27	0.96	3.90	0.97	5.34	0.94	5.25	0.94	7.39	0.89	6.07	0.93
d	Der1(3,11)	5.66	0.94	4.96	0.95	4.98	0.95	5.21	0.95	5.77	0.93	9.09	0.83	8.66	0.85
e	Der2(3,13)+SNV	5.15	0.95	5.00	0.95	5.15	0.95	5.19	0.95	5.91	0.93	10.40	0.78	6.74	0.91
f	SNV+Der2(3,9)	5.37	0.94	5.84	0.93	5.85	0.93	5.68	0.93	7.58	0.88	9.43	0.82	9.49	0.82
g	Der2(3,13)+SNV	5.48	0.94	5.50	0.94	5.56	0.94	5.58	0.94	6.21	0.92	10.40	0.78	6.74	0.91

Table 33 – PLS models results, for the 49 interval-pre-treatment combinations.

Model verification

With the aim of selecting the final model among the remaining 12 pre-treatment-intervals combinations (Table 34), they were used to predict the drug assay of laboratory tablets and the predictions were then compared with the reference HPLC analysis.

Pre-treatment type	Wavelength Interval (nm)
Der1°(3,11)+SNV	1100-1199
Der1°(3,11)+SNV	1100-1236
Der1°(3,11)+SNV	1100-1261
Der1°(3,11)+SNV	1100-1217
SNV+Der2°(3,13)+SNV	1100-1199
SNV+Der2°(3,13)+SNV	1100-1236
SNV+Der2°(3,13)+SNV	1100-1261
SNV+Der2°(3,13)+SNV	1100-1217
SNV	1100-1199
SNV	1100-1236
SNV	1100-1261
SNV	1100-1217

Table 34 – Final 12 pre-treatment-intervals combinations, used to predict the tablet assay.

The model selection was based on the observation of the resulting tablets drug assay prediction. Since the calibration and validation sets of tablets were made with laboratory equipment and tooling, the prediction made on laboratory tablets should be more reliable and accurate. The prediction was performed on 70 laboratory tablets, made with the rotary tableting machine. They were analysed with NIR and then with HPLC. The comparison of the NIR predictions assay with the reference HPLC measured assay value was carried out with the matched pairs analysis. Three values of HPLC were excluded from the analysis, as they were too high or too low values of concentration. Such values could be probable outliers and basing the matched pair on such extreme values could be not reliable. The mean difference between the two values and the p-value were considered for all the models. In particular, the model with the lowest absolute mean difference and a high p-value was selected as the final model. In Table 35, the results of all the matched pair analysis are reported, while the matched pair of the best three models is also graphically reported in Figure 60. The PLS model selected resulted from data pre-treated with Der1(3,11)+SNV and 1100-1261 nm interval. It was the one with the better predictive ability, as demonstrated by the mean difference close to zero (0.0501).

Pre-treatment	Mean difference	p-value
Der1(3,11)+SNV_1100-1261	0.050	0.9066
Der1(3,11)+SNV_1100-1217	0.149	0.7256
Der1(3,11)+SNV_1100-1199	0.649	0.1051
SNV_1100-1236	0.861	0.0674
Der1(3,11)+SNV_1100-1236	0.876	0.0454
SNV_1100-1261	1.060	0.0229
SNV+Der1(3,13)_1100-1236	2.184	0.0001
SNV+Der1(3,13)_1100-1217	3.175	0.0001
SNV+Der1(3,13)_1100-1261	3.764	0.0001
SNV_1100-1217	4.569	0.0001
SNV+Der1(3,13)_1100-1199	5.339	0.0001
SNV_1100-1199	9.631	0.0001

Table 35 – Matched pair results of all the investigated combinations.

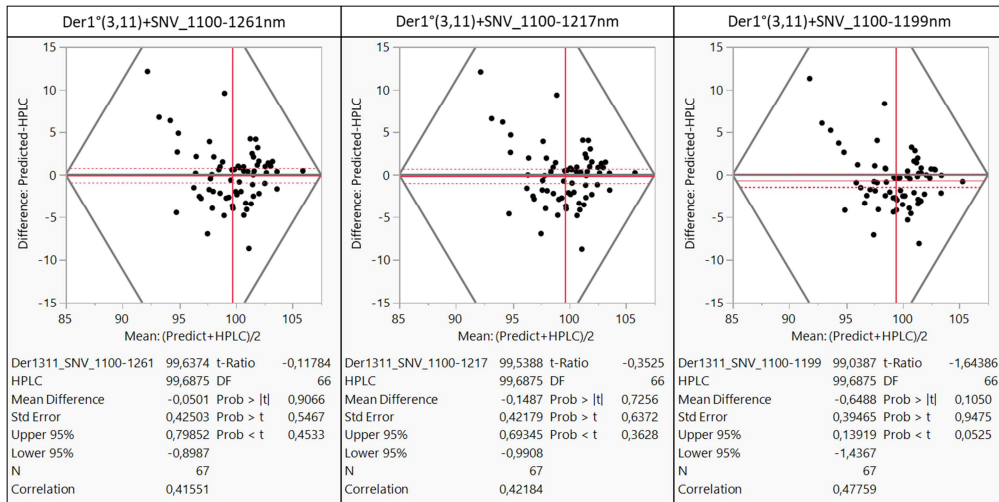


Figure 60 – Matched pair analysis, to compare the predictive ability of the three investigated models, with respect to the HPLC reference value.

The output of the selected PLS model is reported in Figure 61. The score plot (Figure 61a) showed that points were well grouped into five categories, corresponding to the five bilastine concentration levels. Since more than 96% of the total spectral variability was explained by the first two factors (see Figure 61b), only those two have been employed in the subsequent analysis. Figure 61c shows the predicted vs reference plot of the model and the statistic parameters used to assess its quality. As can be seen, good RMSEP and R² values were obtained for both calibration and prediction. Therefore, it can be concluded that calibration data well fit to the model and that the model has a good response on the data used for validation.

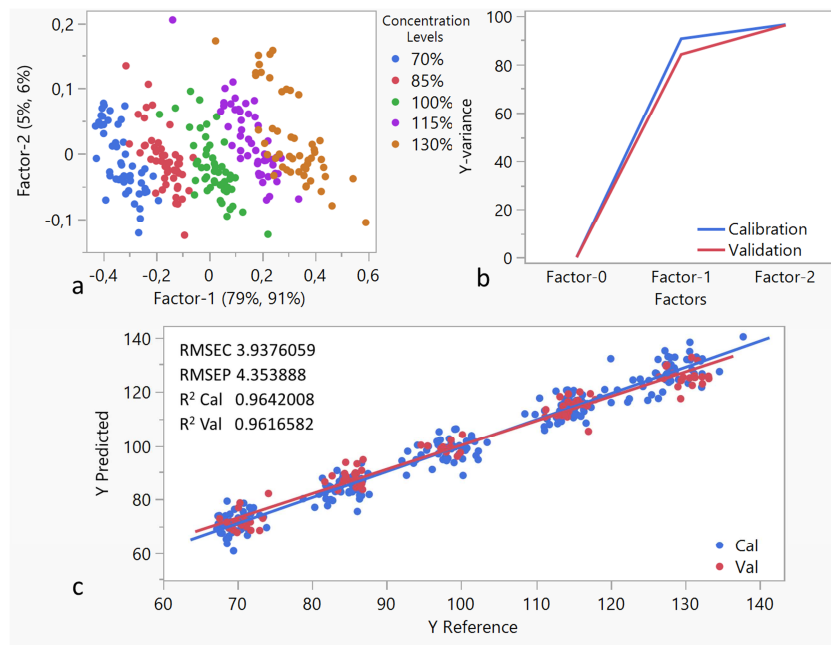


Figure 61 – PLS model outputs. Data used for the model development were pre-treated with Der1(3,11)+SNV and the 1100-1261 nm wavelength interval was used.

With the aim of having a complete evaluation of the predictive ability of the model, the NIR drug assay predictions of laboratory and manufacturing batches were compared with the reference HPLC values. Results are reported in Table 36.

	Lab Batch	Design of Experiment Batches						Manufacturing Batches			
	TFM1904	RUN 01	RUN 02	RUN 03	RUN 04	RUN 05	RUN 06	20-8	20-10	20-11	20-505
HPLC	5.2	3.7	6.2	8.0	3.5	12.0	10.5	2.3	12.2	2.0	3.8
Der1(3,11)_1100-1261nm	6.6	5.9	6.1	8.7	6.5	4.5	2.5	7.6	7.7	7.8	6.7

Table 36 – Comparison between NIR and HPLC drug assay on tablets, expressed in terms of AV, for laboratory and manufacturing tablets.

The AV were calculated for the laboratory batch TFM1904, for the batches of the first DoE (see section 4.3.3.1) and also for four manufacturing batches. All the AV values obtained with the NIR predictions are well inside the acceptable limits (<15) and showed similar values to the AV obtained from the HPLC data.

4.3.2.4 NIR analytical method for tablet crushing strength determination

The crushing strength is a destructive test and in literature, some work exists, about the development of NIR models for crushing strength determination of tablets¹³⁻¹⁵. As spectroscopic analysis is not destructive, it allows the measurement of a bigger sample of tablets.

Experimental plan

Figure 62 reports the experimental plan for the crushing strength model development; three steps have been followed: 1) design and experiments, 2) data elaboration and model building, 3) model verification. Once the model was developed, it was used for prediction of an unknown sample.

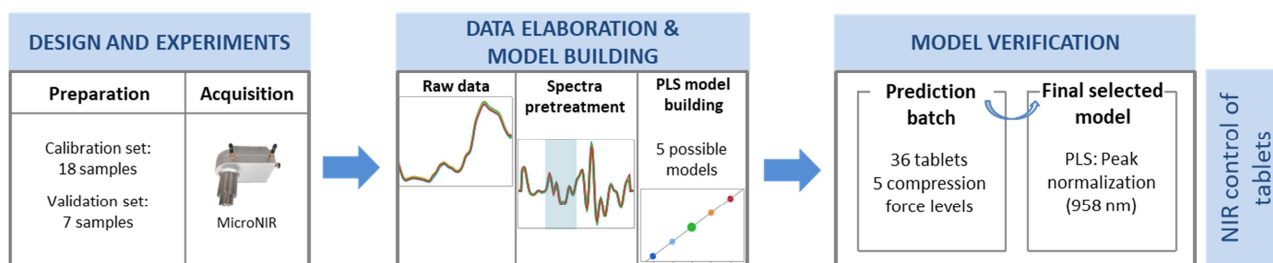


Figure 62 – Experimental plan for the development of the model for crushing strength determination.

Design and experiments

A calibration set was prepared by compressing the powders mixture at 18 different compression forces: 1, 1.5, 2, 2.5, 3, 3.5, 4, 5, 6, 7, 8, 9, 10, 11, 12, 13, 14 and 15 kN. The selection of the 18 compression force levels were based on the bilastine crushing strength target (> 60 N) and on the manufacturability plot, reported in Figure 63. Respect to the minimum compression force (equal to 1.9 kN) necessary to achieve the required crushing strength of 60 N, lower and higher level of compression force were selected. Three tablets were made, for each level and a total of 54 tablets were obtained. A validation set was also prepared by compressing the powders mixture at 7 levels of compression forces (1, 2, 3.5, 6, 9, 12 and 15 kN), and analysing three tablets for each compression level. During compression, the filling depth of the tableting machine was set at 8.5 mm and the exact applied force was measured, thanks to a strain gauge located on the machine. Each tablet was then placed into a tablet holder and scanned with NIR (see section 4.2.2.1). Only the not scored face was analysed and 10 spectral acquisitions were made, by rotating the tablet of 180° each time. Before using the spectral data to build the PLS model, the 10 acquisitions made

for each tablet were averaged, in order to have one single spectral information (averaged) for each tablet. The weight, the thickness and the crushing strength were also measured.

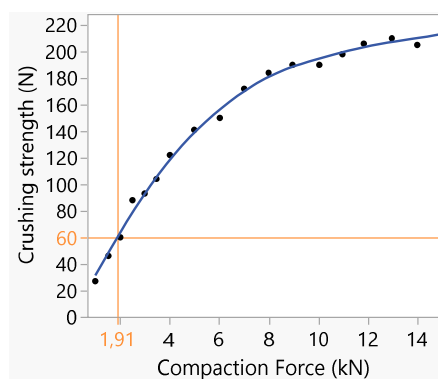


Figure 63 – Manufacturability plot: crushing strength vs compaction force, for bilastine powder mixture.

Data elaboration and model building

When interested in developing a quantitative method, as done before for mixture and tablets, all the physical differences between samples are considered as noise; therefore, they are removed with data pre-treatment. However, in this case, the information of interest is the tablet strength, which, first of all, appears as a physical difference. When applying a higher compression force a stronger tablet is obtained, which is denser and less thick. Therefore, particular attention should be paid, when selecting the type of pre-treatment, in order not to eliminate the information of interest. For this reason, all the pre-treatments generally used to reduce the baseline shift (also due to a different density or thickness) were not taken into account, in this case. No wavelength selection was performed, because the information is distributed all over the whole spectrum and not related to one specific peak. Observing the raw data, they are organized according to a gradient, which follows the compression force increase (Figure 64a). Only the pre-treatments which were able to highlight and maintain the gradient spectral organization were further investigated. As expected, the SNV reduced the baseline shift, eliminating the spectral organization (Figure 64c). On the contrary, baseline, 1st and 2nd derivative, mean normalization and peak normalization highlighted the spectral gradient and were taken into account (Figure 64b, d, e, f and g, respectively). The simplest option of no pre-treatment was equally evaluated.

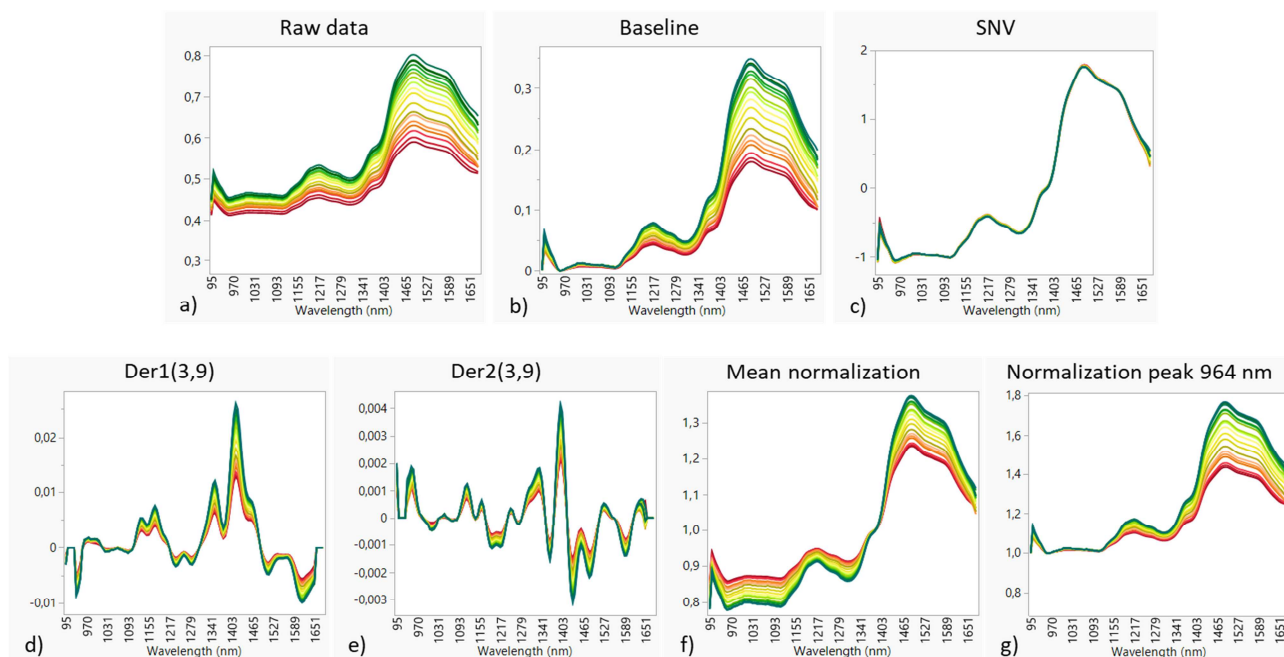


Figure 64 – Different types of pre-treatment for crushing strength quantitative method. Spectra of raw data (a); pre-treatments which increase the spectral difference (b, d, e, f and g); SNV pre-treatment eliminates the difference between spectra obtained with different compression forces (c).

When using the peak normalization, the spectra are normalized with respect to one specific wavelength. At this initial stage of the investigation, only four wavelengths, located in different positions of the first part of the spectrum, were selected. This preliminary screening helps in identifying the most suitable portion of spectrum, where to select the wavelength used for normalization. All the pre-treated data were used to build different PLS models, with an external validation (pre-treated in the same way). The goodness of the obtained model was based on the R^2 and, in particular, on the RMSEP value. PLS data are reported in the left table of Table 37. Many derivative settings were tried, but they gave very similar models, thus only the better ones are reported in the tables.

Compression force 1-15 kN					Compression force 1-6 kN				
Chemometric Pre-treatment	RMSEC	RMSEP	R^2 cal	R^2 val	Chemometric Pre-treatment	RMSEC	RMSEP	R^2 cal	R^2 val
None	8.8425	12.3704	0.9794	0.9689	None	4.5247	7.8127	0.9883	0.9766
Area normalization	11.0128	14.0041	0.9680	0.9601	Area normalization	6.4106	12.8555	0.9765	0.9367
Unit vector normalization	4.9195	7.9777	0.9936	0.9871	Unit vector normalization	5.3528	7.7198	0.9836	0.9772
Mean normalization	11.0128	14.0042	0.9680	0.9601	Mean normalization	4.9227	5.5271	0.9862	0.9883
Peak normalization (908 nm)	12.1931	15.9104	0.9608	0.9485	Peak normalization (908 nm)	5.2763	7.6628	0.9841	0.9775
Peak normalization (933 nm)	6.0417	11.1260	0.9904	0.9748	Peak normalization (933 nm)	6.7922	10.5212	0.9737	0.9576
Peak normalization (964 nm)	12.2643	18.6027	0.9603	0.9296	Peak normalization (964 nm)	5.1822	5.7786	0.9847	0.9872
Peak normalization (1026 nm)	6.3484	13.0880	0.9894	0.9652	Peak normalization (1026 nm)	5.4706	7.7036	0.9829	0.9773
Peak normalization (1150 nm)	12.1177	16.5731	0.9613	0.9441	Peak normalization (1150 nm)	4.9881	6.0893	0.9858	0.9858
Baseline	11.2621	14.1023	0.9665	0.9595	Baseline	4.6123	6.6346	0.9879	0.9831
Der1(2,11)	11.8194	14.8185	0.9631	0.9553	Der1(2,11)	4.2434	5.6668	0.9897	0.9877
Der1(3,11)	6.3558	15.0652	0.9893	0.9538	Der1(3,11)	3.6012	5.1538	0.9926	0.9898
Der2(2,11)	11.9200	15.0328	0.9625	0.9540	Der2(2,11)	-	-	-	-
Der2(3,11)	11.9200	15.0328	0.9625	0.9540	Der2(3,11)	-	-	-	-

Table 37 – RMSEP and R^2 data of the investigated pre-treatments. Left table: models built using all the initial 18 compression force levels. Right table: models built using only the compression force levels < 6 kN.

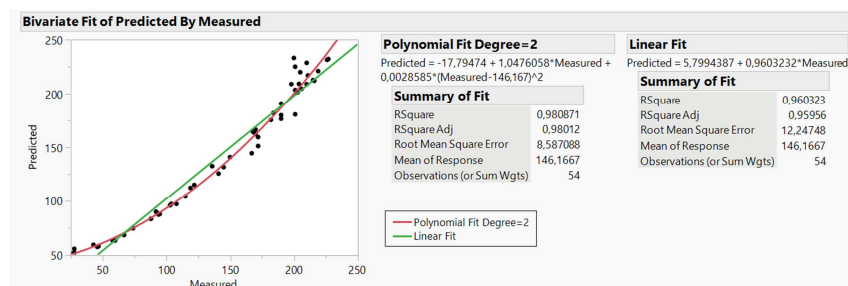


Figure 65 – Actual versus predicted plot of the PLS model pre-treated with peak normalization (964 nm).

Observing the actual vs predicted plot of the PLS models in Figure 65, an error increase can be seen for predictions relative to higher compression force levels. A linear relation is not obtained. The proposed plot refers to the PLS model obtained from data pre-treated with the peak normalization (964 nm). It is reported as an example, but similar considerations could be done for the other PLS models too. The explanation of such phenomenon comes from the tableability plot (section 3.2.2), which shows that, when increasing the compaction pressure, the tensile strength increases too (and therefore also the crushing strength). The tableability plot follows a linear relation at low compaction pressure, but the slope changes, at higher compression forces. Such behaviour traduces into confusion between the spectra of higher compaction pressure; they overlap one to another, causing the drift from linearity observed in the plot. In order to remove such confusion and to use only the linear part of the relation, only the compression force levels up to 6 kN were considered for calibration and validation set. All the previously investigated models were, therefore, recalculated with the new reduced data matrices (right table of Table 37). All the models improved, with the exception of models deriving from second derivatives pre-treated data; they gave a model of only two components, because of a not sufficient number of input data. For that reason, second derivatives were excluded. The models with a RMSEP < 6 (mean normalization, peak normalization (964 nm) and the two first derivatives) have been highlighted in Table 37 (right table). They were further assessed, in order to select the most suitable one. The others models were excluded, because of a too high error of prediction and a low R^2 . Moreover, the peak normalization pre-treatment with the lower RMSEP was related to the 964 nm, therefore, the neighbour spectral portion was investigated too. Additional models pre-treated with peak normalization were tried, by considering wavelengths equal to 945, 951, 958, 970, 976 and 982 nm for normalization. In Table 38, the models previously selected, (with a RMSEP < 6) and the new investigated models (in light green) are ranked according to the lowest RMSEP value. As the first five models have a very similar RMSEP and R^2 , a further investigation was carried out, prior to select the proper model, for tablet crushing strength measurement.

Compression force 1-6 kN				
Chemometric Pretreatments	RMSEC	RMSEP	R^2 cal	R^2 val
Der1(3,11)	3,601	5,154	0,993	0,990
Mean normalization	4,923	5,527	0,986	0,988
Der1(2,11)	4,243	5,667	0,990	0,988
Peak normalization (958 nm)	4,986	5,710	0,986	0,988
Peak normalization (964 nm)	5,182	5,779	0,985	0,987
Peak normalization (970 nm)	5,795	8,043	0,981	0,975
Peak normalization (982 nm)	5,474	8,850	0,983	0,970
Peak normalization (976 nm)	5,767	9,060	0,981	0,969
Peak normalization (945 nm)	6,991	10,509	0,972	0,958
Peak normalization (951 nm)	6,853	11,614	0,973	0,948

Table 38 – New PLS ranking, resulting from the not excluded models and the new added peak normalization pre-treatments.

Model verification

The first five models were tried on a new set of 36 tablets, done on purpose, in order to verify which of them provided the best prediction. The 36 tablets were obtained by compressing at 1.5, 2, 2.5, 3.5, and 5.5 kN. Each tablet was acquired with NIR and then broken, to measure the actual crushing strength, with a diamteral-compression test. All the five models were applied to predict the tablet crushing strength. The difference between the actual and the predicted value was calculated and it is reported in Table 39. The difference values were coloured, to better visualize the trend. Even if all the models underestimate the crushing strength, the better prediction was made by the data pre-treated with the peak normalization (958 nm). It was confirmed also by the lowest average of the residuals, equal to 3.50.

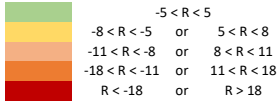
Actual Crushing strength (N)	Der1(3,11)		Mean normalization		Der1(2,11)		Peak normalization (958 nm)		Peak normalization (964 nm)		Legend
	Prediction	Residuals	Prediction	Residuals	Prediction	Residuals	Prediction	Residuals	Prediction	Residuals	
43	51	-7.95	37	6.20	48	-5.05	41	2.16	39	4.11	
44	55	-11.36	39	4.85	50	-5.63	43	1.31	41	5.93	
47	50	-3.15	38	8.83	45	2.40	48	-0.72	41	5.93	
48	55	-6.88	45	3.22	51	-2.77	51	-2.63	48	0.12	
62	59	3.10	48	13.54	58	4.30	54	7.92	51	11.41	
64	62	1.83	52	11.63	61	2.91	58	6.41	53	11.46	
64	61	2.89	53	10.56	62	2.10	58	6.39	54	9.87	
66	61	4.54	50	16.22	60	6.19	55	10.50	53	12.66	
78	82	-4.23	73	5.37	82	-3.50	79	-1.07	77	1.40	
81	77	3.56	69	12.24	78	3.13	75	5.97	73	7.85	
85	76	9.20	70	14.69	77	8.05	73	11.64	71	14.33	
87	72	15.05	68	18.92	73	13.51	71	16.15	68	18.98	
104	86	18.46	95	8.66	85	18.90	102	1.83	99	5.02	
106	90	16.08	100	6.48	88	17.63	106	0.19	105	0.52	
107	88	18.79	98	9.16	92	14.77	100	6.66	99	7.67	
108	87	21.08	98	10.37	86	22.49	109	-0.89	103	4.78	
110	97	13.39	100	9.85	91	18.53	113	-3.32	107	2.73	
110	96	14.00	103	6.57	92	17.65	112	-1.92	109	1.34	
110	101	9.08	101	9.31	102	7.81	109	1.19	108	2.16	
110	96	13.95	103	7.36	98	11.87	108	2.01	104	6.16	
110	97	13.00	105	4.92	101	8.71	110	0.34	108	2.07	
111	96	15.07	103	7.56	91	20.10	113	-1.51	110	1.32	
111	92	19.16	97	13.57	89	22.48	109	2.28	103	7.62	
112	90	21.60	101	10.79	89	23.46	111	0.59	107	4.95	
112	100	11.63	109	2.84	103	8.56	115	-2.84	111	1.46	
114	98	15.90	105	9.01	95	19.06	113	0.96	113	0.64	
117	102	14.86	106	10.59	105	12.34	115	2.12	109	7.59	
119	99	19.97	106	12.91	95	23.67	115	3.65	114	5.36	
123	106	17.01	110	13.16	106	17.21	116	7.35	111	11.71	
126	104	21.56	113	13.03	107	18.81	119	7.42	116	10.49	
127	112	15.38	115	11.79	113	13.94	120	6.55	115	11.70	
128	103	25.05	106	22.48	102	25.74	111	17.44	106	21.69	
144	145	-1.43	138	6.00	146	-2.25	144	0.50	140	4.41	
152	152	-0.04	143	9.27	151	0.65	147	4.78	141	10.81	
154	158	-3.81	148	5.79	156	-2.49	154	-0.26	148	5.52	
158	156	2.06	147	10.65	155	3.06	151	6.69	149	9.42	
Mean		9.40	9.96	10.23	3.50	6.90					

Table 39 – Difference between the actual crushing strength and the crushing strength value predicted by the five considered models. Colours reflect the residual amount respect to the measured value.

In conclusion, from the previous investigation, the final selected model was originated from data pre-treated with the peak normalization respect to wavelength 958 nm. The data of the PLS model are presented in Figure 66. The points in the score plot (Figure 66a) are not perfectly grouped, but a certain organization can be guess. The 98.5% of the total variability was explained by the first 4 factors, which have been employed for the subsequent analyses (Figure 66b). Figure 66c shows the predicted vs reference plot of the model and the statistic parameters used to assess its quality. As can be seen, good RMSEP and R² values were obtained for both calibration and prediction. Therefore, it can be concluded that calibration data well fit to the model and that the model has a good response on the data used for validation.

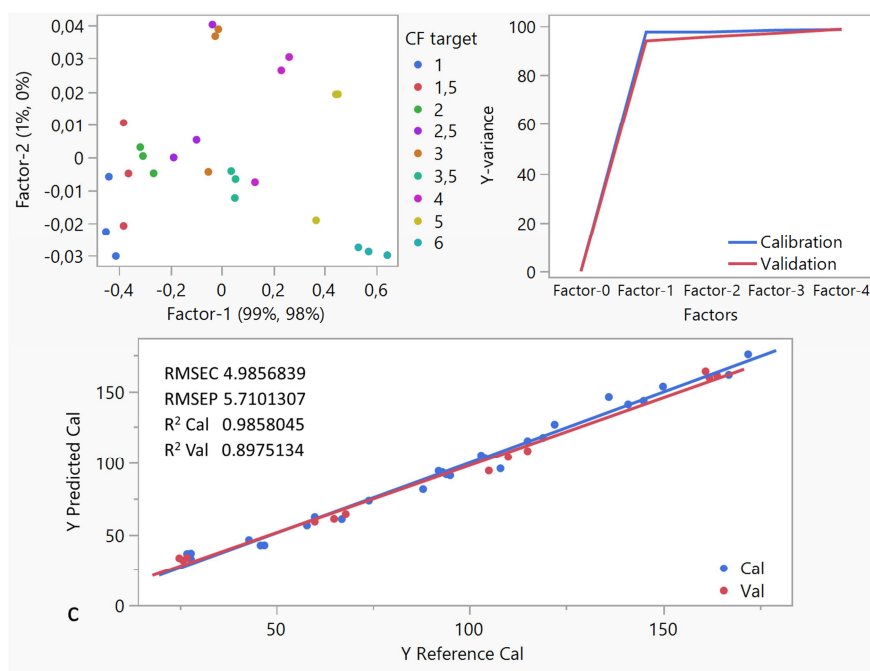


Figure 66 – PLS model obtained from the data pre-treated with a peak normalization related to the wavelength 958 nm. In blue the calibration data, in red the validation data.

The NIR method for crushing strength determination of tablets was developed in a late phase of the study; therefore, it was not applied to all the manufactured tablets. Moreover, during its use for prediction, a problem came up. The model well predicted the crushing strength of tablets obtained with the manual single station punch press, while the prediction was not accurate for tablets manufactured with the rotary tableting machine, nor for manufacturing tablets, compressed with a rotary machine.

4.3.2.5 NIR analytical method for coating process monitoring

The application of NIR spectroscopy monitoring tools, as a part of QbD approach, was actuated on the mixing and tableting step. In particular, MicroNIR was used to monitor the mixing process, to quantify the API concentration in mixture and in tablets and also to measure the tablet strength. It was nearly applied to all the single unit operation of a direct compression process. However, an additional single unit operation, commonly performed on tablets, is the coating. In order to in-line monitor the coating process of bilastine tablets, a NIR model was developed. The spectra of uncoated and coated tablets were observed, in order to verify if a difference could be seen (Figure 67). As the spectra are different, we expected to see difference during the coating process too.

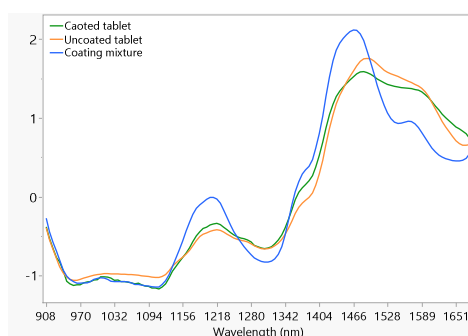


Figure 67 – Spectra of uncoated tablets (orange line), coated tablets (green line) and coating mixture of Opadry (blue line). A SNV pre-treatment was applied to improve the spectral visualization.

Experimental plan

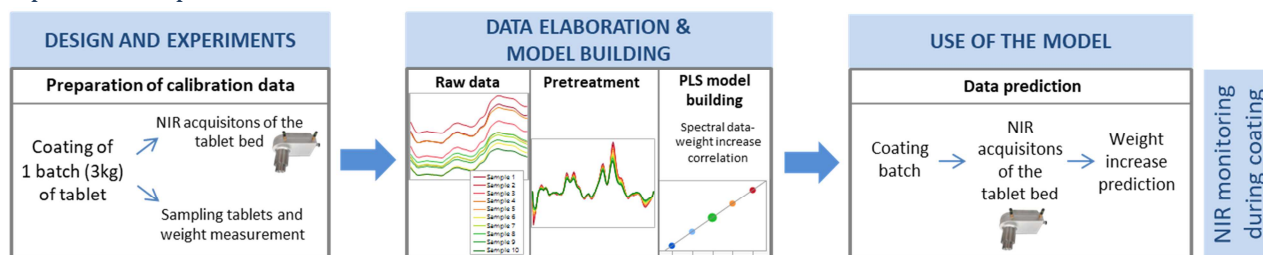


Figure 68 – Experimental plan for the development of the model for the coating monitoring.

At this early stage, a screening to verify the possibility of correlating the tablet weight gain to the NIR spectra was performed. In fact, it was necessary to verify such correlation, before planning a proper and deeper model development; therefore, a simple model was built. The literature work often monitors the coating process by acquiring spectra of single tablets, but we were interested in acquiring the entire bed of tablets. For that reason, the calibration set consisted of acquisitions made on the whole bed of tablets of one single batch (TFF2115), during the coating process. The experimental plan followed for coating model development is graphically represented in Figure 68.

Design and experiments

A batch of 3kg of tablets (TFF2115) was coated with about 1 L of Opadry OY 1-700 coating suspension at 12%, following the method previously described in section 4.2.2.4. The tablets were analysed with NIR before to start the process and, then, during the coating. The manual scan mode was used for acquisition, as described in section 4.2.2.1. The process was analysed 10 times at different time intervals (0, 3, 8, 12, 20, 30, 40, 50, 60 and 67 min), with the aim of monitoring the coating process. Three NIR acquisitions were made on the bed of tablets, each time and then averaged. At the same time, a sample of about 30 tablets was taken from the bed of tablets and then weighted. The final aim was to link the tablet weight increase, to the NIR spectral acquisitions.

Model verification

Once all the data were acquired, they were pre-treated, in order to improve the resolution and reduce the noise. The spectral changes, observed during coating, are related to both chemical and physical change. A quantitative change in peak intensity can be visualized, as a consequence of different chemical composition of coating layer and tablet core. As the API is progressively coated, it will result less and less visible to the NIR. Therefore, the API peak should reduce and peaks relative to coating components should appear. At the same time, the thickness increase can be visualized, as a change in the reflectance spectra, which does not affect the intensity, but causes an up or down shift of the entire profile. As both, chemical and physical information could be useful for the model development, particular attention should be paid when pre-processing the data with chemometrics. Any information removal should be avoided. With such premise, the spectral pre-treatment was kept as simple as possible. Only few pre-treatment types were tried: SNV, Der1(3,5), Der1(3,7), Der1(3,9), Der1(3,11), Der1(3,13), Der2(3,5), Der2(3,7) and Der2(3,9). When applying the derivative pre-treatment, an ordered progression can be seen in the spectra. In particular, an increase in tablet weight can be seen, when moving from the red to the green spectrum (Figure 69). The entire NIR wavelength interval was used to build the model: no variable selection was made. The pre-treated data matrix was used to build a PLS model. A cross-validation was used for model building, since no validation samples were available. The RMSEP and R^2 of the investigated models are reported in Table 40. The model with the lower RMSEP and the higher R^2 is the one pre-treated with the 1st

derivative and 13 smoothing points. Such model has a RMSEP of 0.702553 and a R^2 of 0.93692 and its outputs are reported in Figure 70.

Pre-treatment	RMSEP	R^2 val
Der1(3,13)	0.65	0.94
Der1(3,11)	0.66	0.94
Der1(3,9)	0.70	0.93
SNV	0.73	0.93
Der2(3,9)	0.75	0.92
Der1(3,7)	0.81	0.91
Der1(3,5)	0.81	0.91
Der2(3,7)	0.83	0.91
Der2(3,5)	1.27	0.79

Table 40 – Possible PLS models for the coating quantitative model.

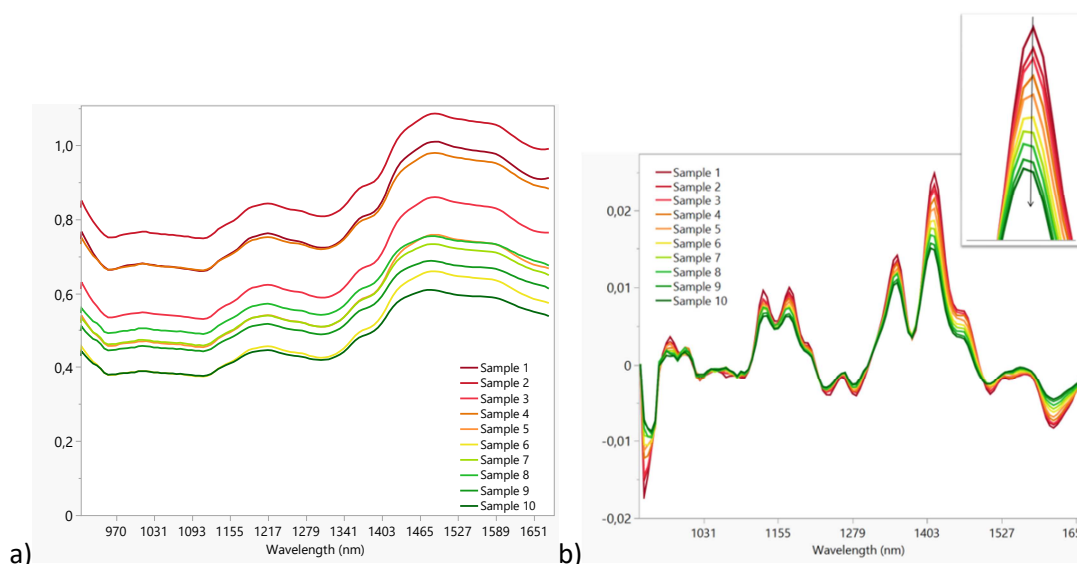


Figure 69 – Spectra of raw data (a). Spectra of pre-treated data (Der1(3,13)) (b); the zoomed frame shows how spectra are well organized according to a gradient, corresponding to the tablet weight gain.

The points in the score plot (Figure 70a) showed an ordered trend, from the top to the bottom and from the left to the right. The first two factors explain the 99% of the total spectral variability, as showed in the explained variance plot in Figure 70b. Figure 70c shows the predicted vs reference plot of the model and the statistic parameters used to assess its quality. As can be seen, good RMSEP and R^2 values were obtained for both calibration and prediction. Therefore, it can be concluded that calibration data well fit to the model and that the model has a good response on the data used for validation.

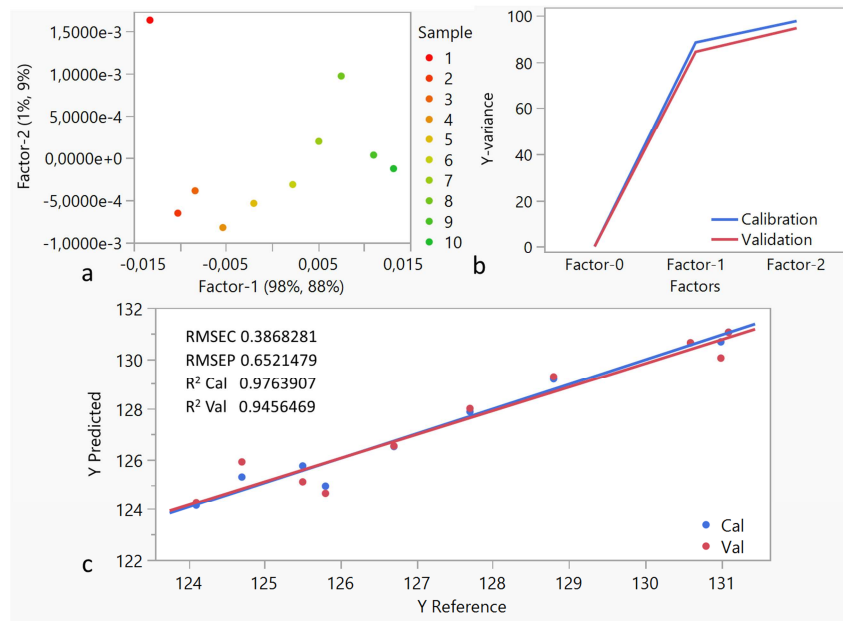


Figure 70 – PLS model for prediction of tablet weight increase; the model was built from data pre-treated with Der1(3,13).

The PLS model shows that it is possible to correlate the tablet weight gain with the NIR spectral data, acquired on the whole bed of tablets, during the coating. However, despite a good model was obtained, in order to be able to use such PAT tool during the manufacturing process, a proper model development should be performed.

4.3.3 Study of the process

4.3.3.1 Mixing

The mixing process was studied with two different kinds of investigation:

- in-line monitoring of the process, with the qualitative MBSD analysis;
- study of the process parameters variation, by planning of DoE.

In-line monitoring with Moving Block of Standard Deviation (MBSD)

The mixing process was studied, by in-line monitoring the powder blending. This investigation was aimed at describing the trend of the process and at comparing production and laboratory batches, in order to see if they presented any differences. With this purpose, two manufacturing scale batches of 250 kg and one laboratory batch of 2 kg were in-line monitored during the mixing process. The 2 kg laboratory batch (TFM1904) was prepared as described in section 4.2.2.2, replicating the manufacturing mixing conditions (mixing time: 30 min, rotation speed: 15 rpm, bin loading: 65%). The batches were monitored with the MicroNIR instrument, during the blending process and 450 spectra were recorded, one for each rotation. All the batches were acquired with a dynamic acquisition mode, using the settings corresponding to the rotation speed of 15 rpm for both, laboratory cubic 8 L mixer and manufacturing 1000 L bin (see Table 11, in section 4.2.2.1). A MBSD of WS=15 and SS=1 was calculated between the 450 spectra and plotted against the block number. In Figure 71 the three batches are compared and show a very similar trend: a high SD indicating inhomogeneity characterizes the first four minutes (about 60 rotations), then the SD decreases and a long phase of similarity between continuous spectral acquisitions appears, indicating the achievement of blend homogeneity. The rapid SD decrease is in accordance with the Fisher's law of mixing¹⁶. MBSD of laboratory (green line) and production batches (blue and red lines) were comparable to each other. The same information can be seen in the PCA plot (Figure 72): the red dots indicate the start of the process and the green ones the end of it. The groups of points have almost the same shape, indicating that all the three processes go in the same direction and have the same trend.

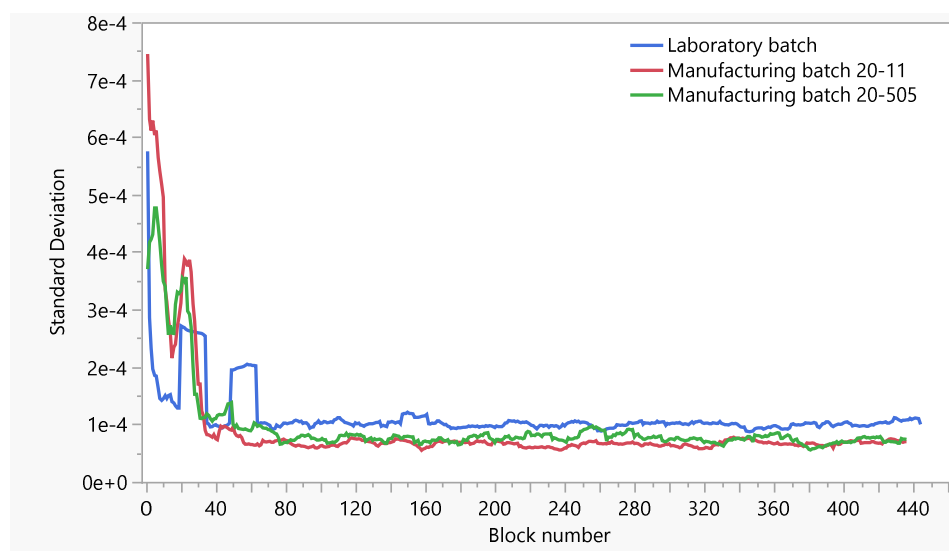


Figure 71 – Production and laboratory scale batches in-line monitored with NIR. MBSD plot of WS=15 and SS=1.

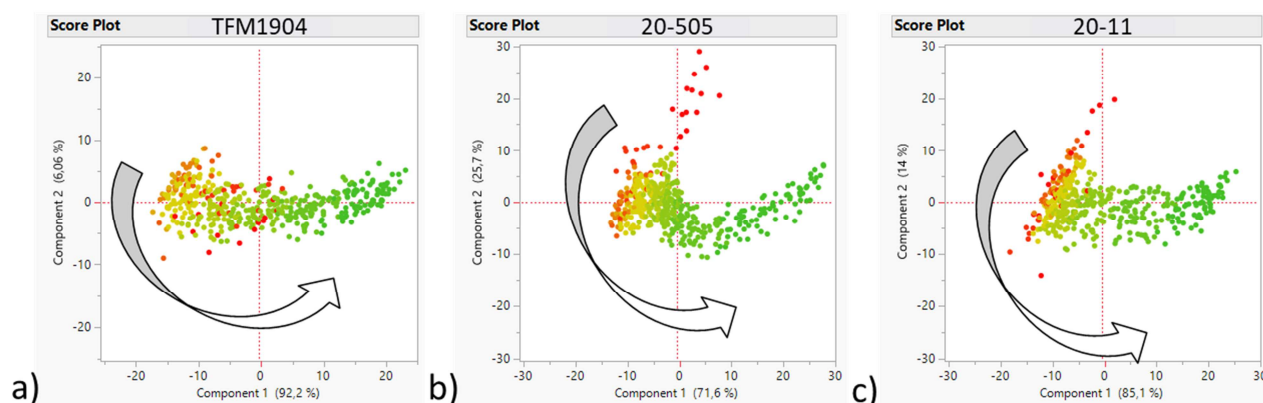


Figure 72 – PCA of the mixing process monitoring for laboratory (TFM1904) (a) and production batches: 20-505 (b) and 20-11 (c).

The quantitative model for drug assay determination in mixture¹² previously developed (see section 4.3.2.2) was applied to the same 450 spectral acquisitions of all the three batches. The quantitative PLS model was for the first time applied to these manufacturing and production batches, so this investigation represented also the confirmation of the good predictive ability of the model. The results of laboratory batch 20-505, reported as example in Figure 73, showed that the first 15 dynamic acquisitions (corresponding to the 1st minute of mixing) exhibited a variable oscillation of concentration, but the title value rapidly stabilized around 100% and stayed constant, and well inside the specification limits, until the end of the process (Figure 73, upper plot). This observation was consistent with the previous MBSD analysis: the initial phase of inhomogeneity corresponds to the oscillation of assay value, while the long phase of similarity between continuous spectral acquisitions corresponds to the equilibrium in assay value. The same conclusion is valid also for the other two batches. This concordance of results gives evidence to the possibility of mixing for a smaller time, as the powders were blended and showed the target API concentration, long before 30 min. Despite the achievement of blend homogeneity in few minutes, no demixing was seen, if mixing for a time up to 30 min. The drug assay values of each single spectrum (one spectrum was recorded for each revolution) can be compared with the MBSD as done in Figure 73, for batch 20-505. However, for an easier comparison between the three batches, a control chart was used (Figure 74), as previously done (see section 4.3.2.2). The drug assay values are grouped for minutes and represented as a box-plot. Each box-plot represents one minute of mixing and resumes the data of the 15 acquisitions made during that minute. The most of the data are inside the Upper Specification Limits (USL) and Lower Specification Limits (LSL) (blue lines at 95% and 105% in the zooms of Figure 74). In conclusion, MBSD results showed consistency with the assay prediction and the three batches were comparable to each other, thus indicating the achievement of blend homogeneity and a correct amount of API concentration.

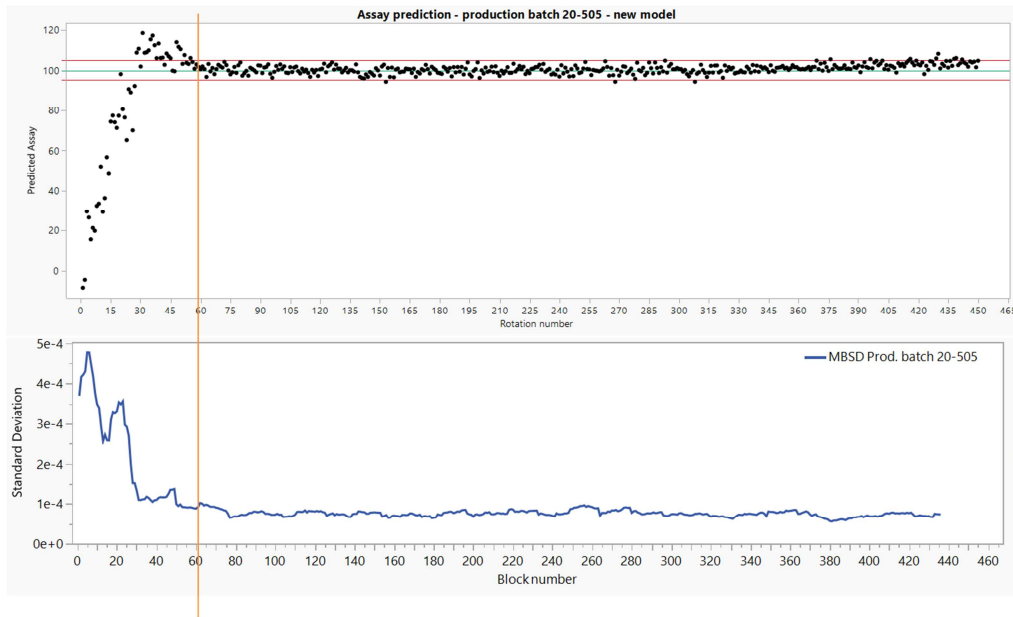


Figure 73 – Assay prediction (upper dots plot) and MBSD (bottom plot) comparison for the manufacturing batch 20-505. The orange line highlights the values oscillation of the first 60 rotations and the equilibrium after them.

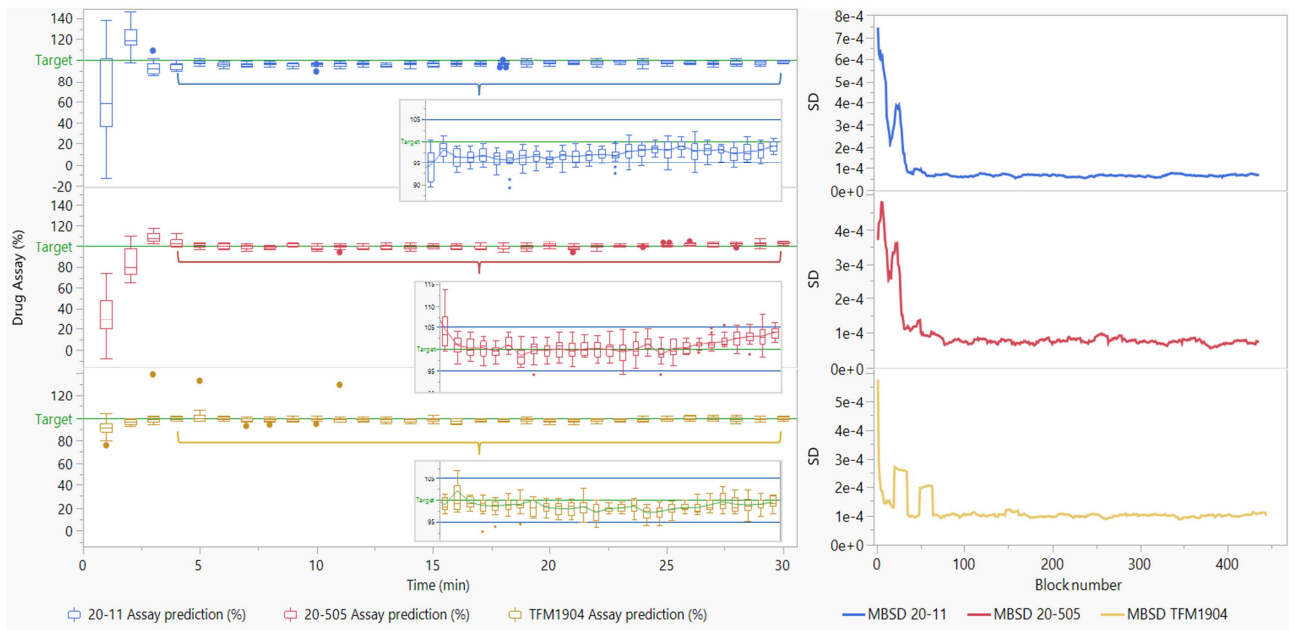


Figure 74 – On the left: drug assay predicted with the developed PLS model on mixtures. Production batches in blue and red, laboratory batch in yellow. For an easier comparison between data, the control charts in the frames were used. On the right: MDSB of the batches.

Design of Experiment: Factors (process parameters) screening

After the characterization of the mixing process, the work moved on, studying the involved process parameters. According to the risk analysis previously carried out (see section 4.3.1), the critical variables of the mixing step are the mixing time, the mixing speed rate and the bin loading. A first screening DoE was planned (Figure 75a), in order to evaluate the effect of such variables on the finished product quality. For industrial manufacturing the cost-yield ratio is of great importance; obtaining the highest yield (maximum bin loading) with the lowest energy cost (low speed rate) and time (low time) is always desirable. Currently, the powders are blended for 30 min at 15 rpm. The mixing time was varied from 10 to 30 min, as interested

in evaluating the effect of mixing for a time lower than 30 min. The rotation speed was varied from 8 to 15 rpm, as interested in evaluating the effect of mixing at speed rates lower than 15 rpm. For the reason previously explained, the bin loading was fixed at the maximum value of 65%. There is also another reason for the exclusion of bin loading from the evaluated DoE factors: at this early stage, only a small amount of the available resources has been employed for the study, as performing a screening. The effect of variation of the DoE factors was evaluated on the final tablets in terms of drug assay, standard deviation of the drug assay and content uniformity, which is expressed as the Acceptance Value (AV) index. The assay value was obtained with both, HPLC and NIR analysis. A D-optimal design was planned, for investigating two factors at two levels and their interaction, with a reduced number of trials (Figure 75a). A six runs DoE, with four vertices points and two central points, was made. The space investigated with these runs is reported in Figure 75b. The experimental matrix and experimental plan are reported in Table 41b.

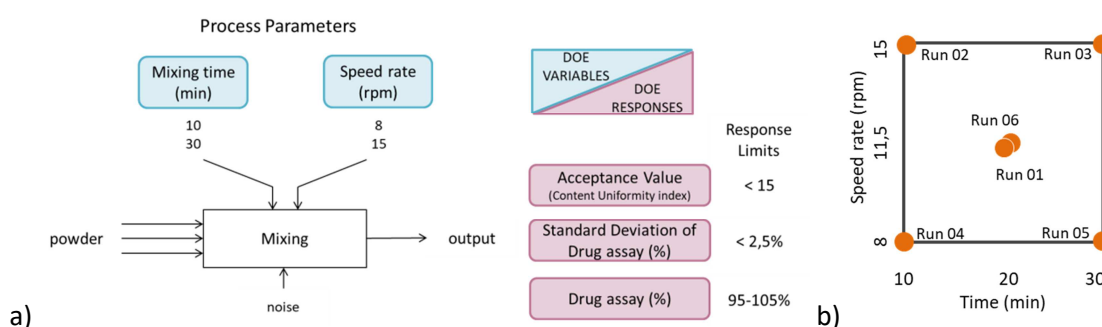


Figure 75 – a) DoE schematic view. b) Space investigated with the planned DoE.

Factors	low level	high level
Time (min)	10	30
Speed rate (rpm)	8	15

Responses	Acceptable limits
AV	< 15
Assay RSD (%)	< 2,5
Assay (%)	95-105

Run Number	Factors	
	Time (min)	Speed rate (rpm)
01	0	0
02	-1	+1
03	+1	+1
04	-1	-1
05	+1	-1
06	0	0

Run Number	Factors	
	Time (min)	Speed rate (rpm)
01	20	11.5
02	10	15
03	30	15
04	10	8
05	30	8
06	20	11.5

Table 41 – a) DoE factors and responses. b) Experimental matrix and experimental plan.

Six different runs with the same composition, reported in Table 9 (see section 4.1.2), were prepared, as described in section 4.2.2.2. The mixing process was monitored with the MicroNIR instrumentation, in order to qualitatively and quantitatively follow the trend of the mixing process, as previously done for laboratory batch TFM1904 (see section 4.3.2.1). The NIR acquisitions were made using the dynamic acquisition mode. As changing the rotation speed, different instrument settings were used. In particular, the setup correspondent to Cubic 8 L and 8 rpm, Cubic 8 L and 11.5 rpm, and Cubic 8 L and 15 rpm were employed (see Table 11, in section 4.2.2.1). As changing the mixing speed, the MBSD parameters were re-defined for each run. In particular:

- WS=11 was used for run 01 and 06, as mixed with a rotation speed of 11.5 rpm;
- WS=15 was used for run 02 and 03, as mixed with a rotation speed of 15 rpm;
- WS=8 was used for run 04 and 05, as mixed with a rotation speed of 8 rpm.

The SS was always set equal to 1 and the MBSD was calculated on the data pre-treated with SNV+Der2(3,9). The results of the in-line mixing monitoring are reported in Figure 76. The results showed that the SD rapidly reaches a low value, in all the runs. They were all similar to each other, with the exception of run 01, which showed an increase of SD, between rotation number 80 and 170. The assay

value predicted with NIR, after an initial oscillation, rapidly reaches the equilibrium (Figure 76, top). However, the model overestimates the API concentration in all the batches.

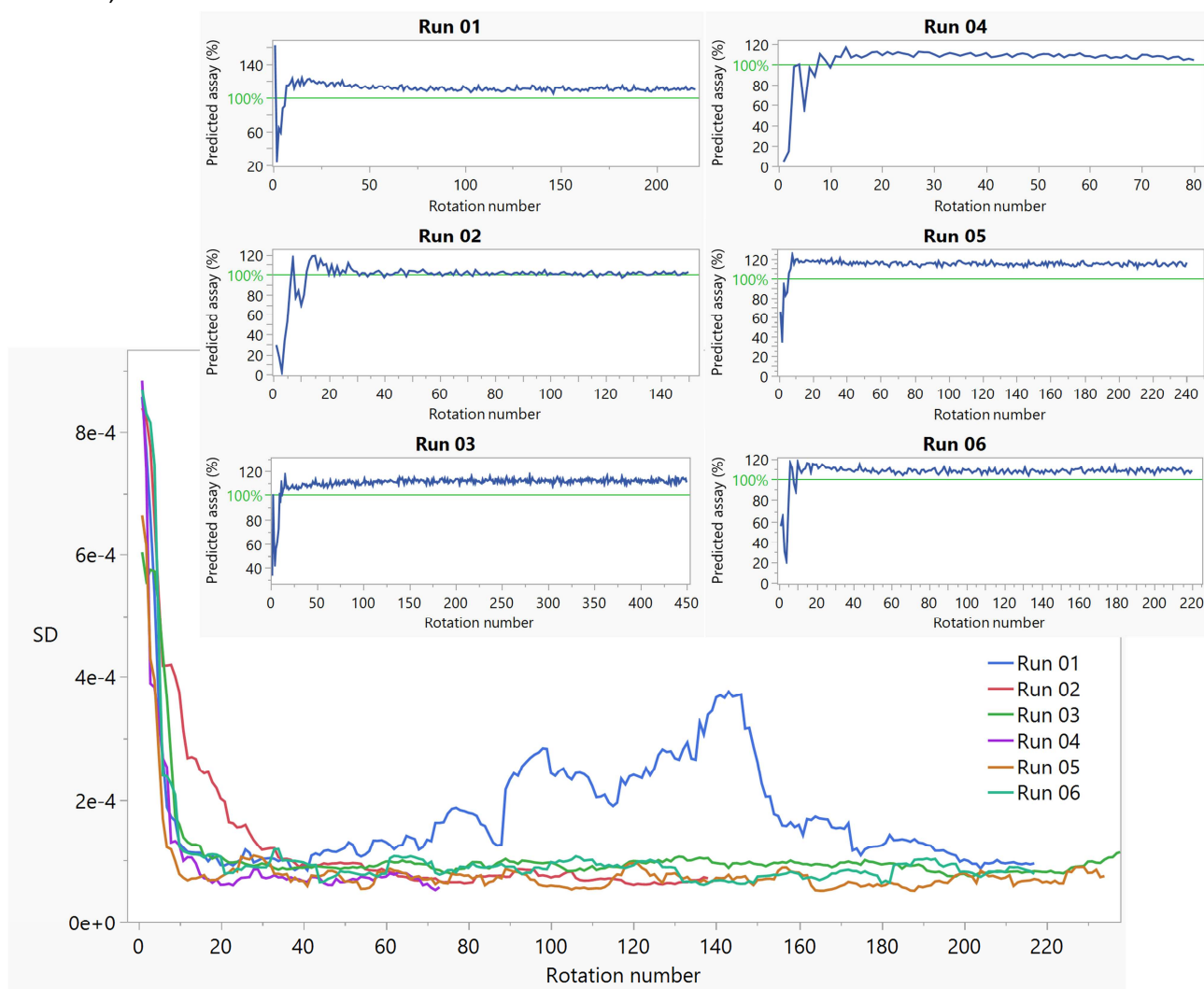


Figure 76 – MBSD and assay prediction for the six runs of DoE.

After the in-line mixing monitoring, each run was added of magnesium stearate, previously sieved, mixed for 5 further min and then compressed to give tablets. The tableting was performed with the rotary tableting machine, equipped with the bilastine dedicated tooling (compression force between 6.5 and 9.5 kN). A sample of 10 tablets was analysed for each batch. All the tablets were characterized in term of weight and thickness, acquired with NIR and, finally, analysed with HPLC. The drug assay, therefore, was measured with the reference HPLC method and also predicted with the developed NIR method (see section 4.3.2.3) All the responses measured on tablets are summarized in Table 42. The comparison between the NIR and HPLC method showed good and similar results. The NIR model overestimates the drug assay a little bit, with respect to the HPLC reference values; however, the drug assay data had the same trend, as shown by the similar AV, reported as box plot, in Figure 77. Therefore, future analyses could be performed only with the NIR method. The analysis on tablets showed an acceptable assay value (always < 15) and a low variability, indirectly confirming the homogeneity of the powder blends. Good results were obtained also for run 01, despite the higher SD in the MBSD plot.

Run Number	Responses			NIR Assay (%)	NIR Assay RSD (%)	NIR AV
	HPLC Assay (%)	HPLC Assay RSD (%)	HPLC AV			
01	100.7	1.5	4	101.0	2.4	6
02	99.5	2.6	6	99.6	2.5	6
03	101.1	3.3	8	100.5	3.6	9
04	101.2	1.4	3	99.8	2.7	7
05	98.1	4.9	12	101.5	1.8	4
06	95.3	3.2	11	98.6	1.1	3

Table 42 – Responses measured on tablets for the six runs of the DoE. The drug assay was measured with the reference HPLC analysis and also predicted with the developed NIR model.

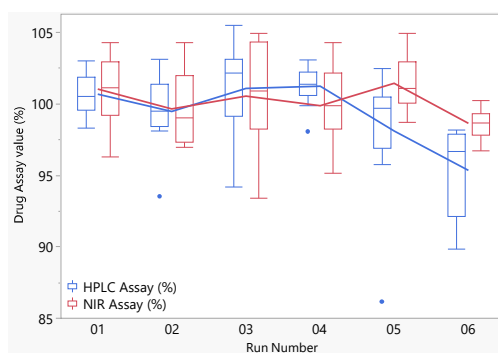


Figure 77 – Comparison between NIR and HPLC analysis of drug assay in tablets.

The results of the DoE are reported in Figure 78. The significance of the model was evaluated, by the R^2 and the RMSE (reported in the following summary of fit) and by the p-value of the ANOVA. A low R^2 and a p-value > 0.05 mean that the model is not significant enough to explain the response variation, as a function of the factors variation. The obtained results show that it was not possible to build a significant model for the AV response, as demonstrated by a not significant p-value, by the low R^2 and by the flat line in the profiler on the left. In the same way, it was not possible to build a significant model for the drug assay and for the SD of the drug assay response. Therefore, from this study, it can be concluded that the variation of factors, in the investigated range of values, does not affect the final tablet quality.

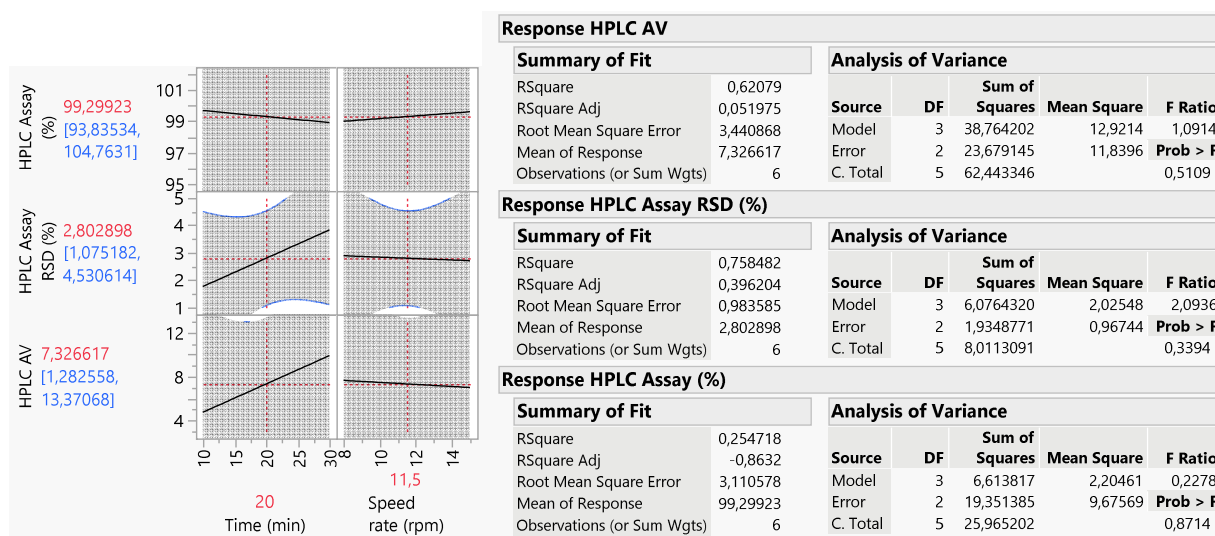


Figure 78 – Prediction profiler of DoE, on the left. Summary of fit and analysis of variance for the three DoE responses, on the right.

Design of Experiment on extended experimental domain

The range of variability of the process parameters, investigated with the previous DoE did not show any effect on the final tablet quality. A second DoE was then performed, in order to expand the range of variability of mixing time and speed rate. This second DoE is schematized in Figure 79a. The mixing time currently used in manufacturing is equal to 30 min and there is no interest in prolong it. Rather, it could be interesting to evaluate the effect of a further reduction of the time, up to 5 min of mixing. The speed rate currently used in manufacturing is equal to 15 rpm. The previous DoE showed that lower speed rate did not affect the tablet quality; therefore, in this new DoE a higher value of speed was evaluated. The bin loading was also evaluated as factor (Table 43). The DoE responses are the same of the previous DoE: the drug assay, the standard deviation of the drug assay and the content uniformity, expressed as AV. This time, the drug assay values were only predicted with NIR analysis, as good results were previously obtained, in comparison with the HPLC reference method. The previously developed model for drug assay determination in tablets were used for prediction (see section 4.3.2.3). A D-optimal design was used to investigate the effect of 3 factors at 2 levels, with a total of 8 runs, of which 7 vertices points and 1 central point (Figure 79b). The experimental matrix and the experimental plan are reported in Table 43b.

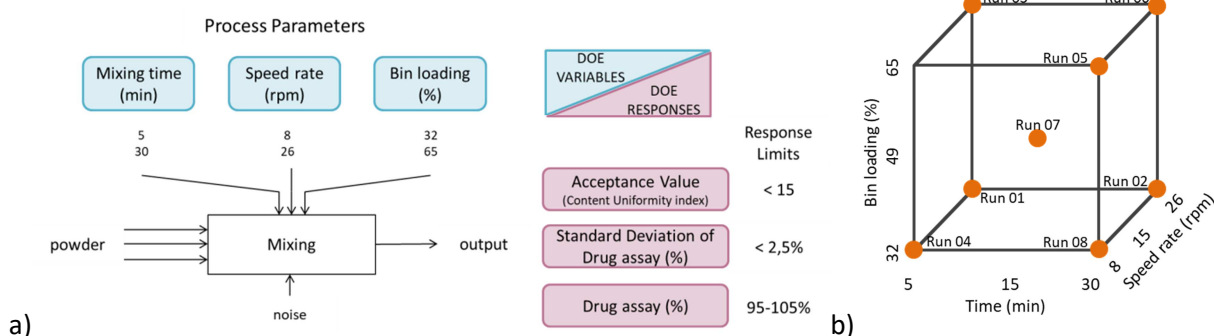


Figure 79 – a) DoE schematic view. b) Space investigated with the DoE.

Factors	low level	high level
Time (min)	5	30
Speed rate (rpm)	8	26
Bin loading (%)	32.5	65

Responses	Acceptable limits
AV	< 15
Assay RSD (%)	< 2,5
Assay (%)	95-105

Run Number	Factors		
	Time (min)	Speed rate (rpm)	Bin loading (%)
01	-1	+1	-1
02	+1	+1	-1
03	-1	+1	+1
04	-1	-1	-1
05	+1	-1	+1
06	+1	+1	+1
07	0	0	0
08	+1	-1	-1

Run Number	Factors		
	Time (min)	Speed rate (rpm)	Bin loading (%)
01	5	26	32.5
02	30	26	32.5
03	5	26	65
04	5	8	32.5
05	30	8	65
06	30	26	65
07	15	15	48.75
08	30	8	32.5

Table 43 – a) Factors investigated and responses measured. b) Experimental matrix and experimental plan.

Eight different runs were prepared. The runs composition and preparation was the same used for the first DoE. For each run, the mixing process was monitored with the MicroNIR instrumentation, in order to qualitatively follow the trend of the mixing process. The NIR acquisitions were made using the dynamic acquisition mode. As changing the rotation speed, different instrument settings were used. In particular, the setup correspondent to Cubic 8 L and 8 rpm, Cubic 8 L and 15 rpm, and Cubic 8 L and 26 rpm were employed (see Table 11, in section 4.2.2.1). As changing the mixing speed, the MBSD parameters were re-defined for each run. In particular:

- WS=8 was used for run 04, 05 and 08, as mixed with a rotation speed of 8 rpm;
- WS=15 was used for run 07, as mixed with a rotation speed of 15 rpm;
- WS=26 was used for run 01, 02, 03 and 06, as mixed with a rotation speed of 26 rpm.

The SS was always set equal to 1 and the MBSD was calculated on the data pre-treated with SNV+Der2(3,9). The results of the in-line mixing monitoring are reported in Figure 80. Despite the time and speed variation, a low SD was observed at the end of the mixing time, for all the DoE runs, indicating that the powders were blended. The drug assay value followed the same trend of the MBSD and confirmed the achievement of homogeneity (Figure 80, top).

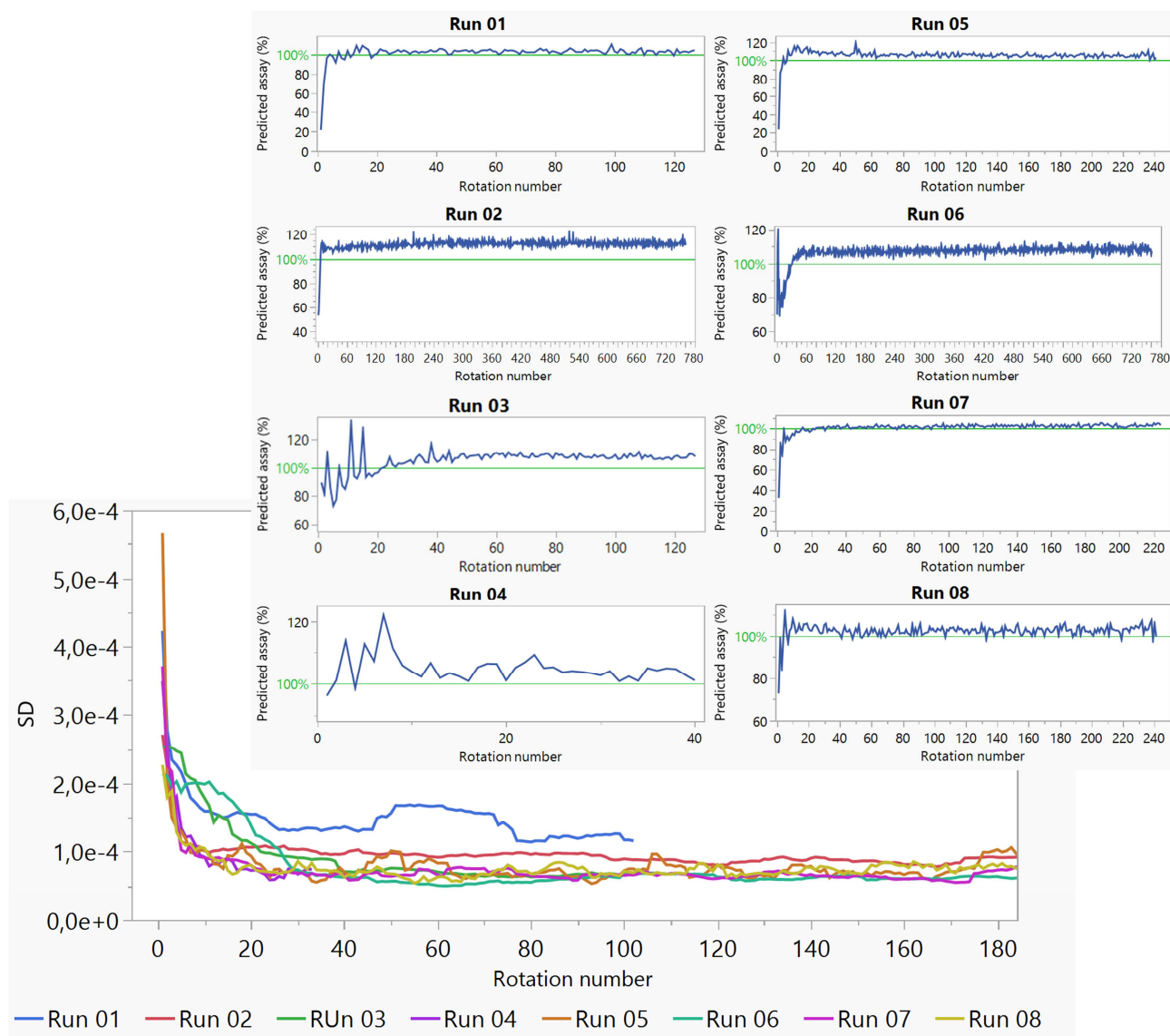


Figure 80 – MBSD and assay prediction for the eight runs of DoE.

Each run was added of magnesium stearate, previously sieved, mixed for 5 further min and then compressed to give tablets. The compression was performed with the Natoli manual single station punch press, equipped with the bilastine tooling (compression force: 3.27 - 3.94 kN and filling depth: 9.2 mm). 10 tablets were made for each run, then characterized in terms of weight and thickness and finally acquired with NIR instrument, to predict the drug assay value. All the responses measured on tablets are summarized in Table 44. The laboratory batch TFM1904, already manufactured with the currently manufacturing conditions (30 min, 15 rpm and 65% bin loading), was added, as an additional point, to the eight DoE runs, bringing more information inside the model.

Run Number	Responses		
	NIR Assay (%)	NIR Assay Std Dev (%)	NIR AV
01	99,8	2,88	6,9
02	99,53	2,36	5,65
03	101,35	3,49	8,37
04	99,88	3,93	9,42
05	99,83	2,83	6,8
06	98,48	3,14	7,56
07	97,99	2,76	7,13
08	97,74	2,17	5,97
TFM1904	103,7	1,81	6,61

Table 44 – Responses measured on tablets, for the eight runs of the DoE.

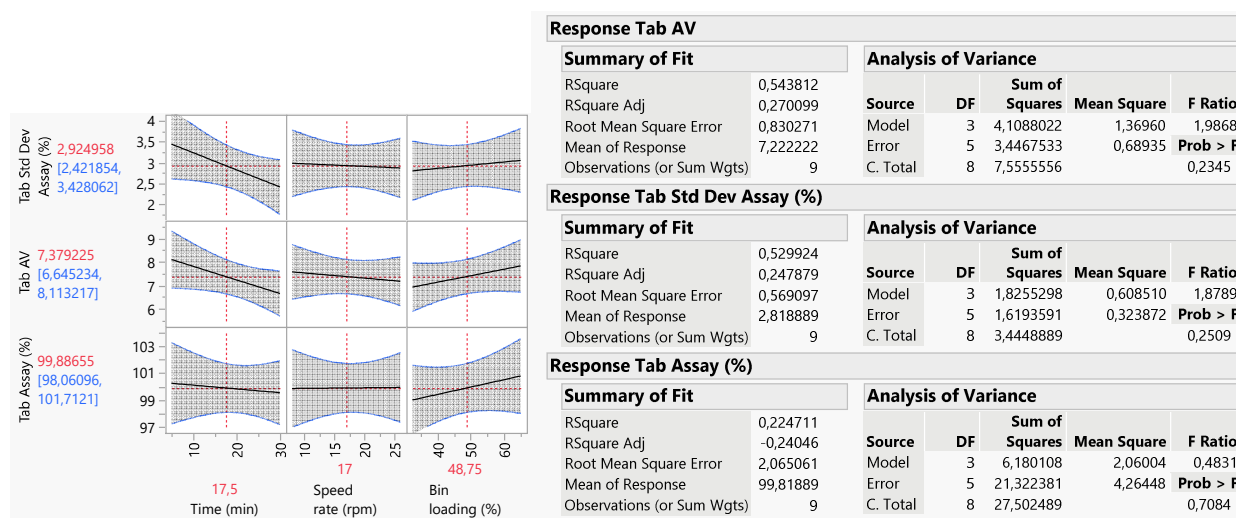


Figure 81 – Prediction profiler of DoE; summary of fit and analysis of variance for the three DoE responses.

The results of the DoE are reported in Figure 81. As for the first DoE, it was not possible to find a predictive model for the responses, by changing the factors in the evaluated range of values. A not significant p-value and a low R² were obtained for all the three responses. However, it would not be useful further expanding the variability range, as it would fall widely outside the normal setting range. The drug assay values, measured on tablets with the NIR quantitative model, are inside the acceptable limits of 95-105% and the AV is widely less than the acceptable value of 15. Therefore, the final tablet quality is not affected by the variation of the investigated factors. From this study, it can be concluded that the current mixing process setting is not critical for the tablet quality of bilastine.

Verification of mixing process setting

The results of the study of the mixing process bring to the conclusion that the powders rapidly reach homogeneity, even if mixed for 5 min at the lower speed rate, as demonstrated by the low value of SD in the MBSD plots (Figure 76 and Figure 80). An additional trial was made to confirm such observation. A 2kg laboratory batch (TFD2126) was prepared by mixing all the ingredients for 30 min at 15 rpm (standard setting). The whole mixing process was in-line monitored with NIR, with the dynamic mode acquisition (see section 4.2.2.1). As we are evaluating the effect of mixing process on the finished product, the confirmation of homogeneity was made on the final tablets. It is well known that powder sampling is affected by errors^{8,17-20}; therefore, an alternative to this approach was chosen to evaluate the homogeneity of the mixture. The mixer was stopped at certain pre-defined time intervals, corresponding to the rotation number 5, 10, 15 (1 min), 20, 25, 30 (2 min), 45 (3 min), 60 (4 min), 75 (5 min), 150 (10 min), 225 (15 min),

300 (20 min), 375 (25 min), and 450 (30 min). When the mixing was stopped, 10 powder samples were taken from the powder bed surface, in 10 different positions. No powder sample thief was used, therefore no deep sampling was performed; rather, only the powder bed surface was sampled, with a spatula and the minimum amount of powder necessary to obtain one single tablet was taken. The powder was immediately placed into the manual tableting machine, thus reducing, as much as possible, errors due to the sample handling. All the obtained tablets were then analysed with NIR, to determine the drug assay. The tablets corresponding to 3, 15 and 20 min stop were also analysed with HPLC, as reference method. The MBSD, related to the mixing process, is reported in the upper picture of Figure 82. As previously observed, the MBSD rapidly reaches a low value and stability. However, some peaks arise in correspondence of the re-starting, after the stop. The reason of such behaviour could be attribute to the difference in bulk density and other properties, between static and moving mixture powders.

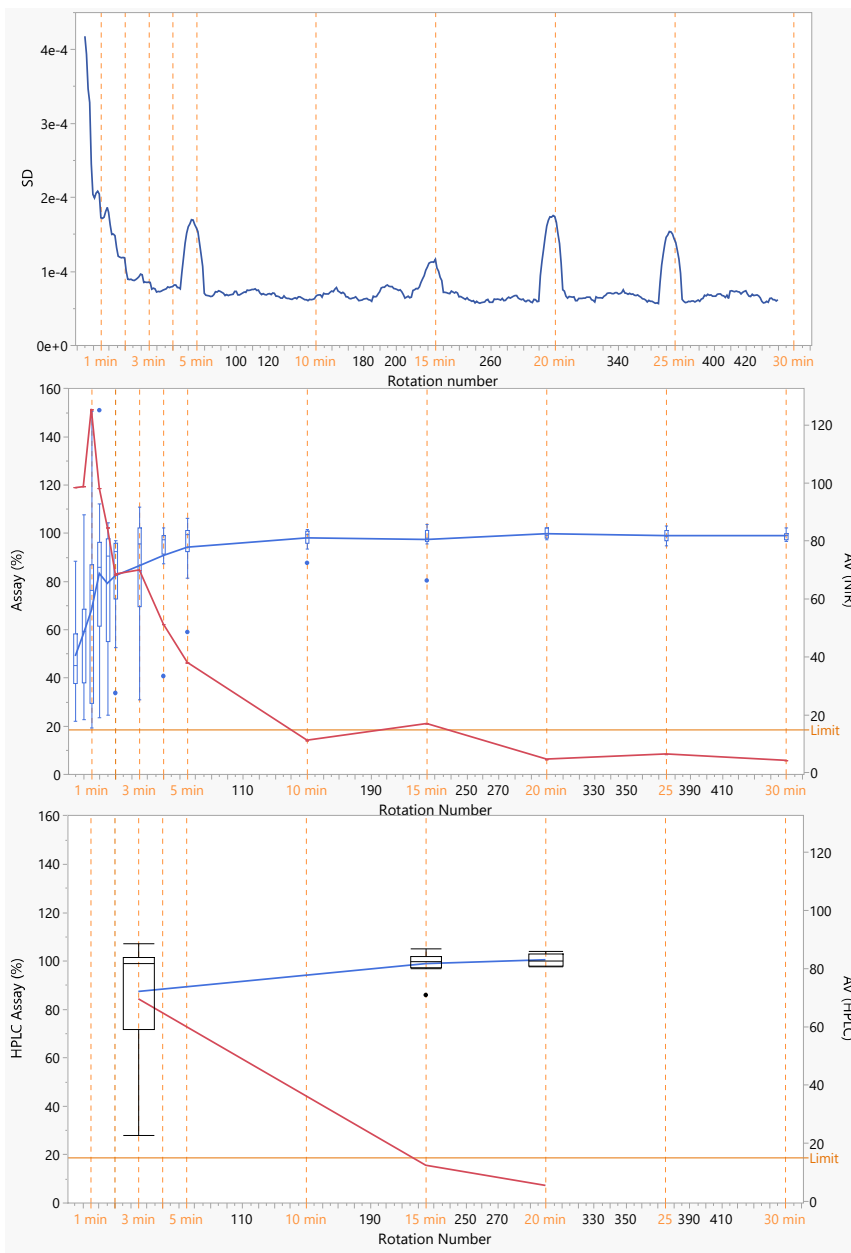


Figure 82 – Upper picture: MBSD of the batch. Middle picture: tablet NIR drug assay (blue line and boxplot) and AV calculated with the NIR predicted values (red line). Bottom picture: tablet HPLC drug assay (blue line and box plot) and the AV calculated with the HPLC measured values (red line).

The results of the NIR analysis on tablets is reported in Figure 82 (middle and bottom picture). An initial phase, of about 5 min, of low average value of API and high variability can be seen. This is followed by a phase of lower variability and an average value of API around 100%, which is the target. The AV describes the process in the same way: a high value of AV can be seen at first, then it decreases, under the threshold of 15, after 20 min. The observations were confirmed by the HPLC analysis performed on the samples at 3, 15 and 20 min, which well reflect the NIR results. From previous observation it can be concluded that the low values of SD, observed in the MBSD plot, actually reflect a situation of good homogeneity of the powder blends.

4.3.3.2 Tableting

The study of the tableting process was carried out with two approaches:

- characterization of the tableting process with a compaction study and compaction profiles;
- study of the process parameters variation, by planning a DoE.

The tableting process transforms a powder into tablets, by application of compressive force, which causes a reduction of the powder volume. In particular, when the pressure is still low, particles rearrange and pack more closely, reducing their porosity. The consequence of porosity reduction is the formation of new points of contact, between neighbour particles. As the pressure increases and the porosity cannot be reduced any further, particles change their shape and form new bonds, causing a strength increase in the new formed tablet.

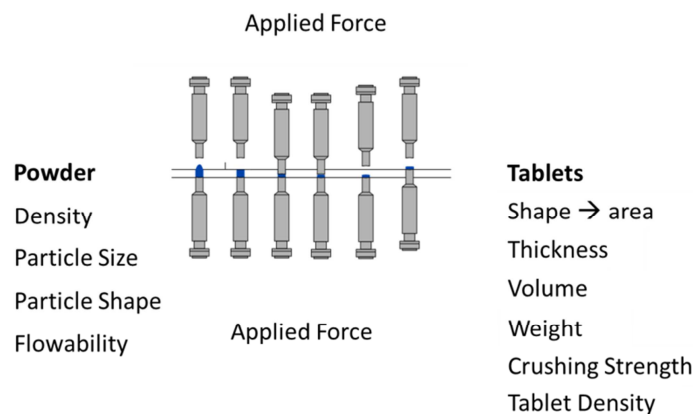


Figure 83 – Tableting p-chart.

The final tablet's characteristics depend on the input powder properties, the applied force and the equipment geometry; therefore, to better assure the tablet quality, it is necessary to gain a deeper knowledge of the tableting process and, in particular, of the relationships existing between compaction pressure, volume reduction and tablet strength. A p-chart of the tableting process is reported in Figure 83.

Compaction study

With the previously expressed purpose, the tableting process was firstly described, by performing a compaction study. Bilastine powder blend was compressed, using a round flat face punch, mounted on the manual single station punch press. Tablets were made by compressing at 18 increasing values of compaction force, from 1 up to 15 kN. All the tablets were manually made, one at a time, by changing and increasing the compaction pressure every time. For all the tablets the compaction force, weight, thickness and crushing strength were directly measured and recorded on a JMP spreadsheet, while the other necessary information (compaction pressure, tensile strength, tablet volume, true density, tablet density, solid fraction and tablet porosity) were derived with the mathematical equations and relationships reported in Table 45.

Compression parameter	
Compaction pressure (MPa)	$\frac{\text{Compaction Force}}{\text{Area}}$
	For round and flat face tablet: $\frac{2 \cdot \text{Crushing strength}}{\pi \cdot \text{Thickness} \cdot \text{Diameter}}$
Tensile strength (MPa)	For oblong bilastine tablet: $\left(\frac{2}{3}\right) \cdot \left(\frac{10 \cdot \text{Crushing strength}}{\left(\pi \cdot \text{Width} \cdot \left(\left(2.84 \cdot \left(\frac{\text{Thickness}}{\text{Width}} \right) - \left(\frac{\text{Thickness}}{\text{Wall height}} \right) \right) + 3.15 \cdot \left(\frac{\text{Wall height}}{\text{Width}} \right) + 0.01 \right) \right)} \right)$
Tablet density (g/cm³)	$\frac{(\text{Weight})}{\text{Tablet volume}}$
Solid fraction	$\frac{\text{Tablet density}}{\text{True density}}$
Powder density (g/cm³)	$\frac{\text{Weight}}{\text{Filling depth} \cdot \text{Area}}$
Porosity	$1 - \text{Solid Fraction}$

Table 45 – Equations used to obtain the tableting parameters necessary for describing tableability, compressibility and compactibility profiles.

The true density is a necessary information for calculating the solid fraction and it was estimated from the Heckel equation, as previously done by Sun²¹. The Heckel equation²² correlates the compaction pressure to the tablet density and it can be used for retrieving the true density value. When using the Heckel equation with this purpose, it can be expressed as follow:

$$P = \frac{1}{C} \left[(1 - \varepsilon_c) - \frac{\rho_{\text{tablet}}}{\rho_{\text{true}}} - \varepsilon_c \cdot \ln \left(\frac{1 - \frac{\rho_{\text{tablet}}}{\rho_{\text{true}}}}{\varepsilon_c} \right) \right]$$

where P is the compaction pressure, C is a constant indicating the deformability of the powder sample, ε_c is the critical porosity, ρ_{true} is the true density, ρ_{tablet} is the tablet density.

To retrieve the true density value, the compaction pressure was plotted versus the tablet density and, with a non-linear fitting model, solved by the Newton algorithm, all the parameters of the equation were estimated, including the true density.

The previously obtained value of true density was then used for solid fraction calculation. Once all the parameters were calculated, it was possible to express the mathematical relationship between compaction pressure, tensile strength and solid fraction, with the three plots of tableability, compressibility and compactibility (Figure 85). For a complete description of tableability, compressibility and compactibility see section 3.2.2.

The compressibility, relationship between volume reduction (or solid fraction) and compaction pressure, is described by the Kawakita equation²³:

$$\frac{\left(-100 \cdot Da \cdot \left(\frac{\text{Compaction Pressure}}{a} + \frac{1}{(a \cdot b)}\right)\right)}{\left(\text{Compaction Pressure} - \frac{(100 \cdot \text{Compaction Pressure})}{a} - \frac{100}{(a \cdot b)}\right)}$$

where *a* and *b* are parameters and *Da* is the bulk density.

Kawakita equation contains the parameters *a* and *b*, which need to be estimated, before to use it for plotting the compressibility. The parameters' estimation was carried out by plotting the solid fraction versus the compaction pressure and applying a non-linear fitting model, solved by the Newton algorithm, as previously done for the true density estimation. For parameters' estimation the bulk density (*Da*) was fixed. Once the parameters have been estimated, the Kawakita equation was used for fitting the experimental data in the compressibility plot (Figure 85a).

The compactibility expresses the strength of the tablet as a function of solid fraction, as it is a direct consequence of it. This relationship is described by the Ryshkewitch equation²⁴.

$$\text{TensileStrength (MPa)} = \sigma_0 e^{-\varepsilon(1-\text{Solid Fraction})}$$

$$\text{Log(Tensile Strength)} = \sigma_0 - \varepsilon(1 - \text{Solid Fraction})$$

where σ is the tensile strength, σ_0 the tensile strength at zero porosity and ε the tablet porosity.

The tensile strength was plotted against the solid fraction and the points were fitted, by transforming the tensile strength as logarithmic. The resulting fitting equation was then used for fitting the experimental data in the compressibility plot (Figure 85b).

The tableability describes the tensile strength as a function of pressure and this is the most used relation, even if the tensile strength directly depends only on the porosity reduction. For describing tableability profile, not many equations are available in literature. Some of the available one were tried, but did not fit the experimental data satisfactorily. For that reason, the equation was experimentally found, by substituting the term of solid fraction in the Ryshkewitch equation, with the solid fraction estimation calculated with the Kawakita equation. It is well known that the tablet tensile strength is only an indirect consequence of the compaction pressure, rather, it directly depends on the porosity, as graphically expressed by Tye et al., 2005²⁵ (Figure 84). This justifies the choice of using the direct relation of solid fraction – tensile strength and the necessity of expressing the solid fraction with the Kawakita equation (direct compaction pressure-solid fraction relation).

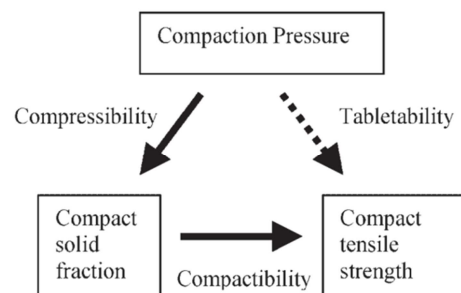


Figure 84 – Compaction pressure, tensile strength and porosity (or solid fraction), direct and indirect relationship. Figure from Tye et al., 2005²⁵.

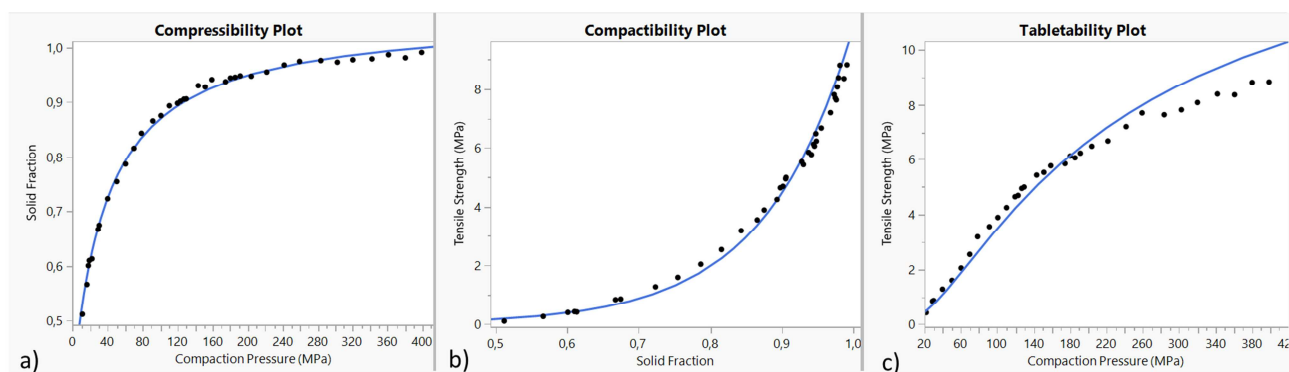


Figure 85 – a) Compressibility plot. The calculated solid fraction is plotted versus the compaction pressure and the points are fitted with the Kawakita equation (blue line). b) Compactibility plot. The points are fitted with the Ryshkewitch equation (blue line). c) Tableability plot. The points are fitted with a composite experimental equation (blue line).

The compressibility, compactibility and tableability plots are reported in Figure 85. At low values of compaction pressure (1-70 MPa) the compressibility relation is almost linear and a little increase of pressure corresponds to a rapid solid fraction increase. The region between 70 and 150 MPa is characterized by an evident change in the slope. For compaction pressure values higher than 150 MPa, the solid fraction increase is less rapid. A solid fraction of 1 corresponds to the total elimination of voids and porosity, therefore it cannot increase any further. The 90% of the porosity is eliminated when using a compaction pressure of 130 MPa. As the solid fraction increases, also the tensile strength increases, as shown by the compactibility plot (Figure 85b). A slow increase of tensile strength can be seen for low solid fraction values, as porosity is still present; then, it rapidly increases for solid fraction values higher than 0.9. This indicates that the porosity reduction actually brings to the formation of many new points of contact between neighbour particles. In fact, the intimate proximity of particles allows the development of new attractive forces, which are responsible for the formation of a solid body. However, a tensile strength of 1 MPa is, generally, considered enough for pharmaceutical tablets and it corresponds to a solid fraction of 0.7. The equation used for describing tableability, well fits the data for low compaction pressure values, but not for higher compaction pressure values (Figure 85c).

The flat face punch was used at first, for a more precise estimation of true density and other parameters. However, a second compaction profile was done, using the bilastine manufacturing oblong and convex tooling, obtaining the following plots (Figure 86). A difference from the flat face punch profiles can be seen, as the solid fraction never reaches the value 1, for the investigated range of compaction pressure. However, at higher compaction pressure (300-400 MPa), the solid fraction reaches a plateau, which indicates that the maximum value of solid fraction has been reached (Figure 86a). This is confirmed by the observation of the compactibility plot (Figure 86b); for solid fraction values equal to 0.75-0.80 the tensile strength dose not increases any further, but, rather, the points are all concentrated around a tensile strength of 7 MPa. The equation used to describe the tableability profile shows a better fit of the data obtained with the bilastine tooling, at higher compaction pressure values, even if a drift is still present in the final portion of the plot (Figure 86c).

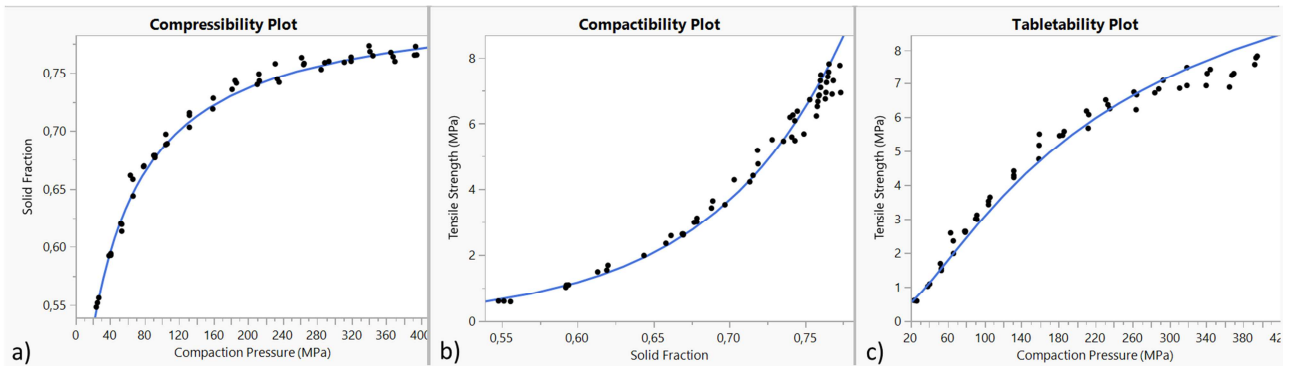


Figure 86 – Compressibility, compactibility and tableability plots obtained with the bilastine tooling.

According to the bilastine QTPP, tablet should have a strength equal or higher than 60 kN (1,54 MPa of tensile strength), which corresponds to a solid fraction of 0.63. Such value is obtained when using 55 MPa (2.5 kN) of compaction pressure. This investigation allows to describe the compaction behaviour of the powder bilastine mixture. It is also possible to extrapolate some useful information, for the definition of the design space. For example, to obtain an acceptable strength, low compaction pressures were enough; therefore, in the next part of the study, only a certain range of compaction pressure will be investigated.

Design of Experiment: Tableting Process Parameter’s study

The second part of the work was focused on the investigation of the effect of tableting process parameters variation on the final tablet quality. According to the risk evaluation carried out at the beginning (see section 4.3.1), the critical variables of the tableting process are the compression force, the rotation speed and the feeder speed level. A DoE was planned, in order to evaluate the effect of the variation of such process parameters (DoE factors), on the finished product quality. The DoE experimental plan is schematized in Figure 87a. The compression force was changed from 2 to 8 kN. This range of values was selected on the base of the previous compaction study results. The rotation speed was varied from 40 to 50 rpm; considering that 45 rpm was the usual setting of the used equipment, a lower and a higher value were investigated. The feeder speed level was varied from 5 to 9, that are usual setting values of the equipment. The effect of process parameters’ variation was evaluated on the final tablets, in terms of weight variation (CV), thickness, crushing strength and disintegration time (DoE responses). A D-optimal design was planned for investigating 3 factors at 3 levels, their 1st level interactions and the quadratic terms, with a reduced number of trials. A 20 runs DoE with all the vertices points, 6 mid-edge points and a replicated centroid was made (Figure 87b). The investigated space with these runs is reported in Figure 87b. The experimental matrix and experimental plan are reported in Table 46.

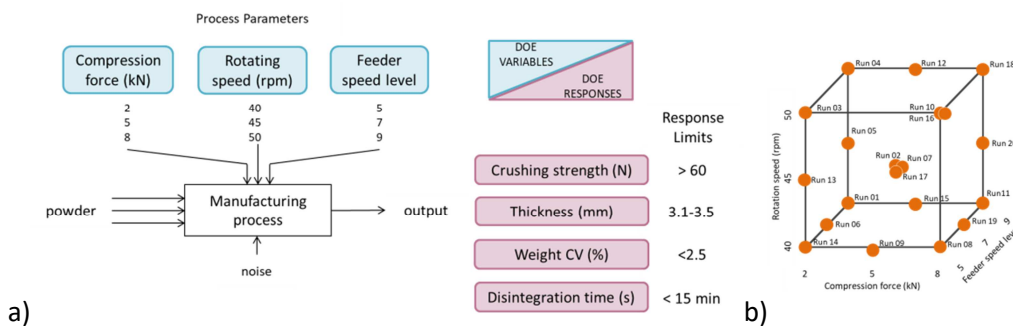


Figure 87 - a) DoE schematic view. b) Space investigated with the DoE.

Factors	low level	medium level	high level
	Compression force (kN)	2	5
Rotating speed (rpm)	40	45	50
Feeder speed level	5	7	9

Responses	Acceptable limits
	Weight CV (%)
Thickness (mm)	3.1-3.5
Crushing strength (N)	> 60
Disintegration time (s)	< 15 min

RUN	Factors		
	Compression Force (kN)	Rotation speed (rpm)	Feeder speed level
01	-1	-1	+1
02	0	0	0
03	-1	+1	-1
04	-1	+1	+1
05	-1	0	+1
06	-1	-1	0
07	0	0	0
08	+1	-1	-1
09	0	-1	-1
10	+1	+1	-1
11	+1	-1	+1
12	0	+1	+1
13	-1	0	-1
14	-1	-1	-1
15	0	-1	+1
16	+1	+1	-1
17	0	0	0
18	+1	+1	+1
19	+1	-1	0
20	+1	0	+1

RUN	Factors		
	Compression Force (kN)	Rotation speed (rpm)	Feeder speed level
01	2	40	9
02	5	45	7
03	2	50	5
04	2	50	9
05	2	45	9
06	2	40	7
07	5	45	7
08	8	40	5
09	5	40	5
10	8	50	5
11	8	40	9
12	5	50	9
13	2	45	5
14	2	40	5
15	5	40	9
16	8	50	5
17	5	45	7
18	8	50	9
19	8	40	7
20	8	45	9

Table 46 – a) DoE factors and responses. b) Experimental matrix and experimental plan.

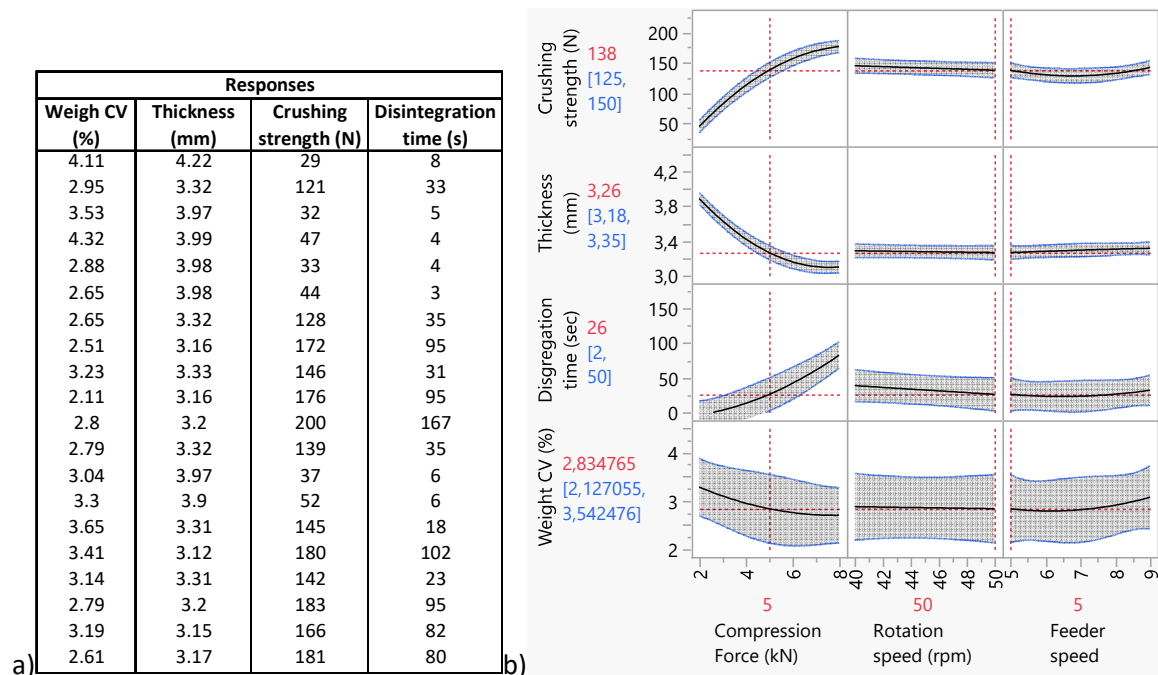


Figure 88 – Responses and results of the DoE. Tablet with numerical responses (a). Prediction profiler (b).

The results of the DoE are reported in Figure 88. The model was evaluated for each response, separately, by the R^2 and RMSE (reported in the following summary of fit) and by the p-value of the ANOVA. The most significant factors for such response have p-value <0.05 in the sorted parameters estimates. A significant model was found for crushing strength, thickness and disintegration time. In particular crushing strength was highly influenced by compression force, as expected. The compression force term leads to a crushing strength increase, as showed by the long effect bar, towards the positive values (Figure 89, sorted parameters estimates). The quadratic term of compression force, on the contrary, has a negative effect on the crushing strength. This behaviour is well represented in the tableability plot, as the tensile strength (related to crushing strength) reaches a plateau, for high values of compaction pressure (related to compression force). The thickness was influenced by the compression force and by the squared compression force terms, with an opposite effect. The thickness decreases when the compression force increases, but a plateau is reached at a certain point. The disintegration time was influenced by the compression force and by the squared compression force terms, too. In this case, however, both terms

positively affected the response. No significant model was found for the weight CV response: the R² was very low and the p-value was not significant.

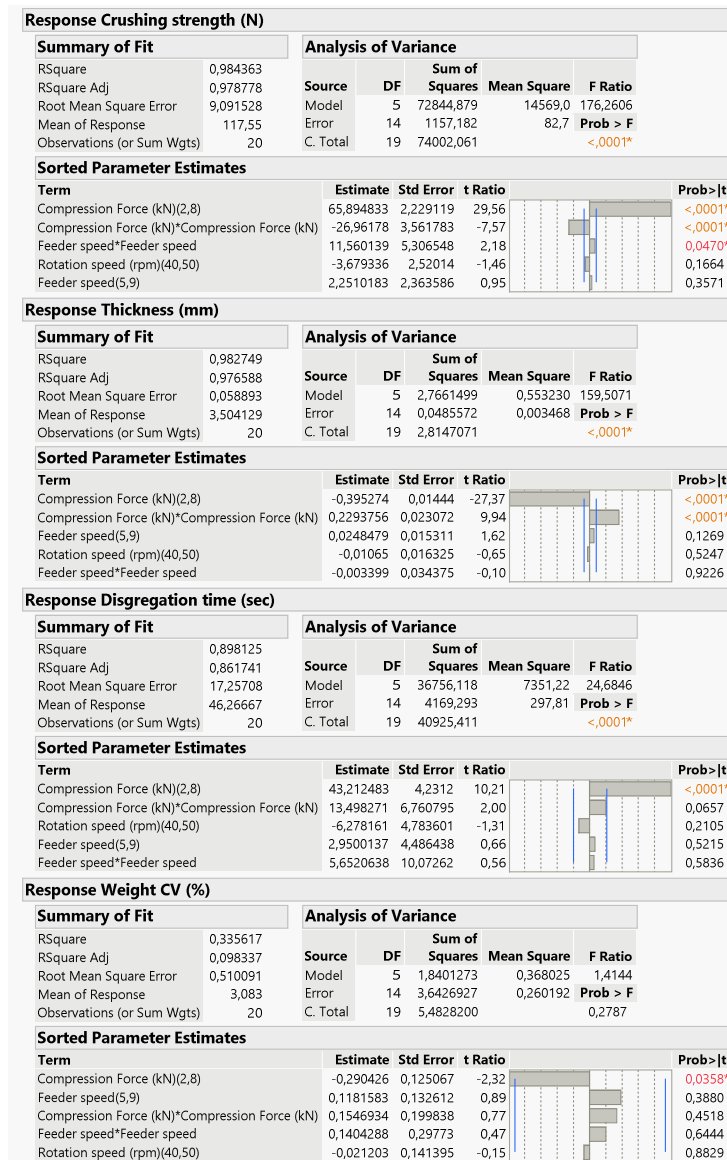


Figure 89 – Summary of fit, ANOVA and sorted parameter estimates for each DoE response.

The results are also reported in Figure 91, as a contour profiler. The three responses well described by the model are plotted one against the others, in three plots. The plot of feeder speed and compression force is reported, as exemplificative of the three plots, in Figure 90. The entire investigated space is called knowledge space (Figure 90, red square). The coloured parts refer to areas where the responses have not an acceptable value. The process parameter should never assume such values, as the ending product would not have the right quality. Inside the knowledge space, the acceptable proven range was defined (Figure 90, blue hatched area). Inside this space the process parameters can be varied in any way, as the product quality is always assured. Inside the acceptable proven range, a littler area, called normal operative range, was defined. It represents all the process parameters values, generally used for production, considering the manufacturing yield and the equipment resistance and performance (Figure 90, green hatched area).

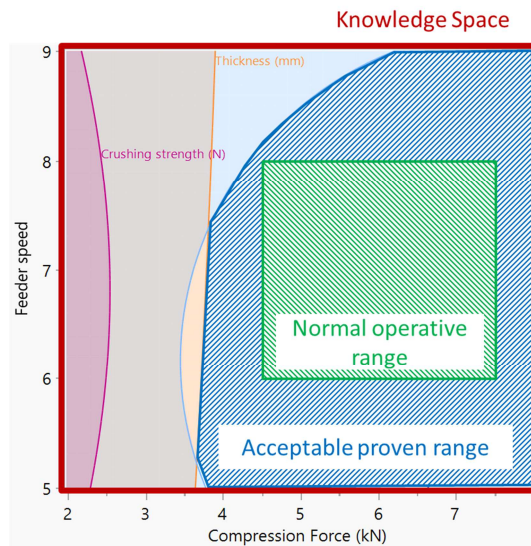


Figure 90 – Knowledge space (highlighted in red), acceptable proven range (blue hatched area) and normal operative range (green hatched area).

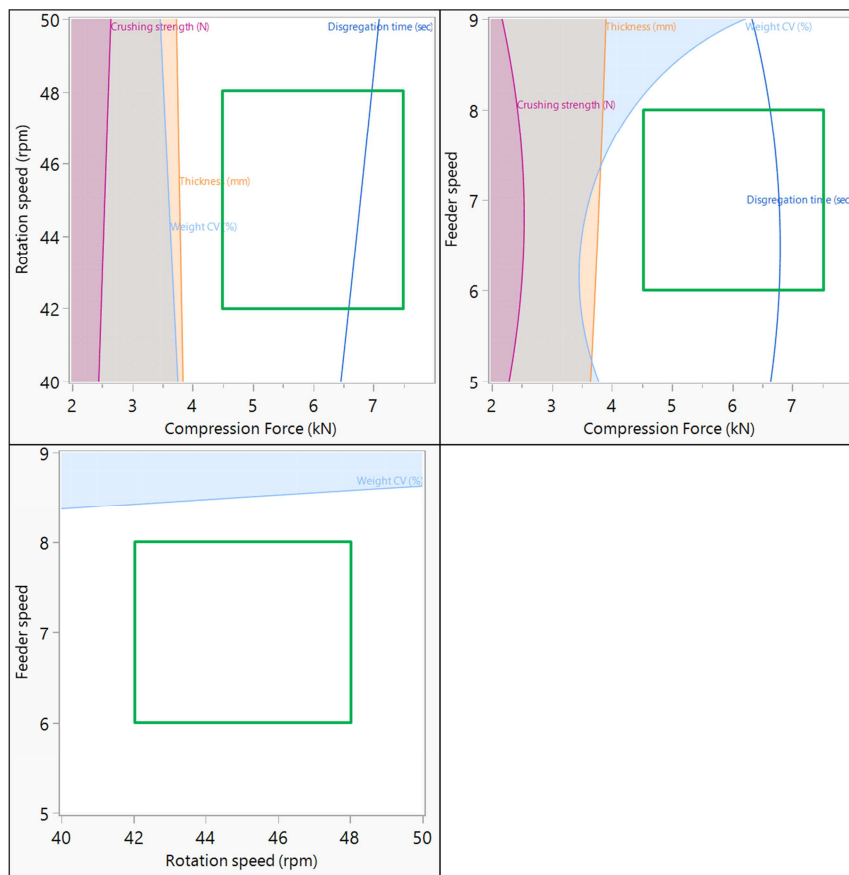


Figure 91 – Contour plot of the responses.

In conclusion, a model was found to describe the responses as a function of the factors. In particular: the rotation speed has not a great influence on the responses, the feeder speed influences only the weight variation, while the most influent parameter is the compaction force, which has an effect on all the responses, with the exception of disintegration time.

Hereafter the results of the NIR determination of crushing strength on tablets are reported.

As the model for crushing strength determination of tablets was developed in a late phase of the study, it was applied only on some tablet batches. Results showed that the model make a very good prediction of tablets manufactured with the laboratory manual alternative tableting machine (Natoli single station punch press) (Figure 92).

The laboratory powder batch TFD2126 was compressed with the manual tableting machine and the crushing strength was predicted with the developed PLS model (see section 4.3.2.4). The actual crushing strength (measured with the reference diametral-compression tester) was plotted against the crushing strength predicted with the NIR model (Figure 92). The resulting fit line showed a high R^2 (0.986) and the p-value of the ANOVA is < 0.05 , demonstrating the significance of the line fitting model and the good prediction. The two methods of measurements were also compared with the matched pair analysis, which compares the means between diametral crushing strength measurement and NIR prediction and assesses the difference among them. The lower is the mean difference, the more similar are the measurements. The matched pair analysis shows a mean difference between the two types of measurements equal to 4 N. As the actual measure is subtracted to the predicted value, the model overestimates the crushing strength a little bit.

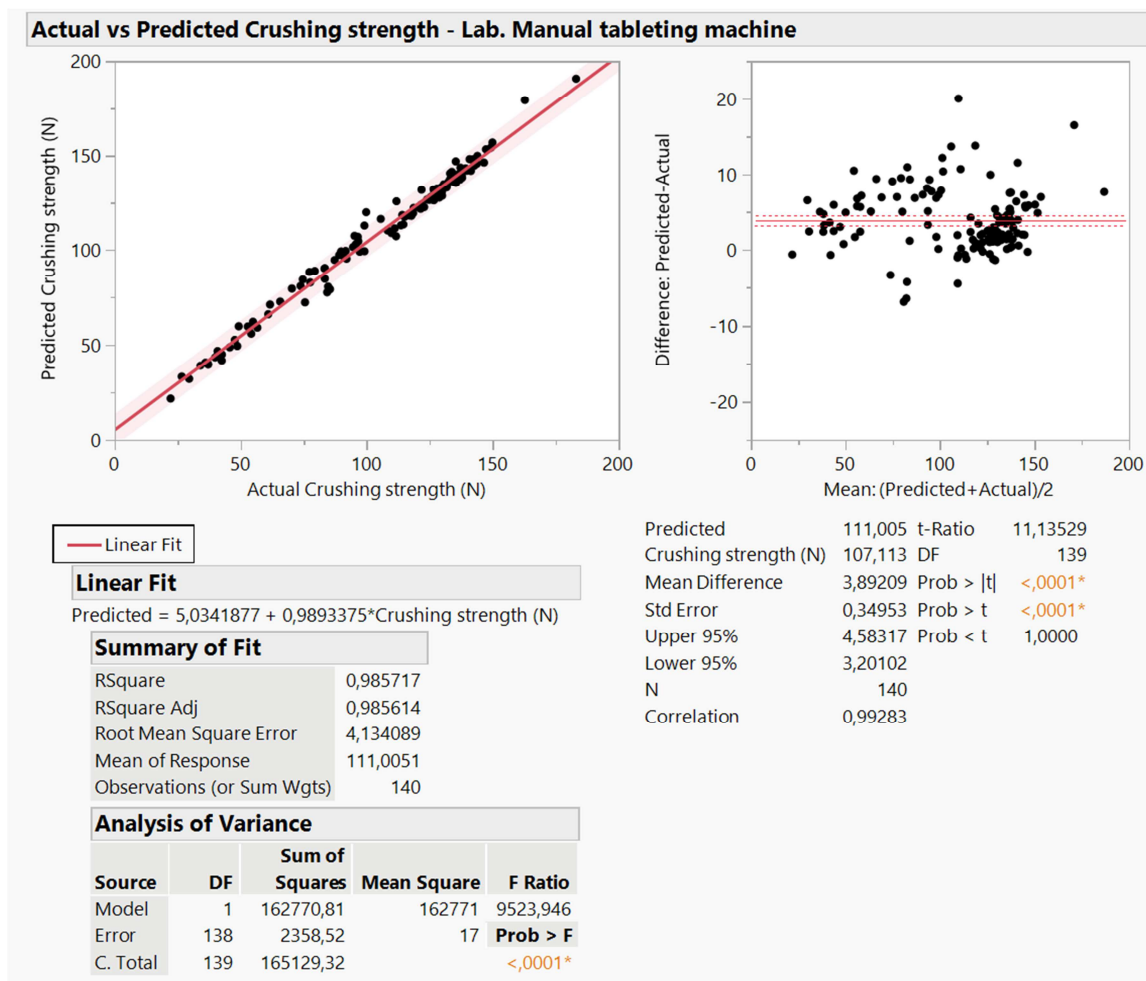


Figure 92 – Comparison between actual and predicted values of crushing strength, for the TFD2126 batch. Actual versus predicted plot on the left and matched pair analysis results on the right.

When using the model to predict the crushing strength of tablet manufactured with a rotary tableting machine, the prediction is not equally good. The same batch of powder (TFD2126) was compressed also with the laboratory rotary tableting machine, but, in this case, the model did not show a good predictive ability. The matched pair analysis shows a mean difference of 35 N, between the predicted and the actual value of crushing strength, thus indicating a big overestimation by the model (Figure 93a). A similar mean difference (33 N) was also observed, when predicting the crushing strength of production scale tablets, thus obtained with rotary tableting machine too (Figure 93b). Such observation highlights a difference in tablets obtained with the laboratory alternative tableting machine and the rotary tableting machine, of both laboratory and manufacturing type.

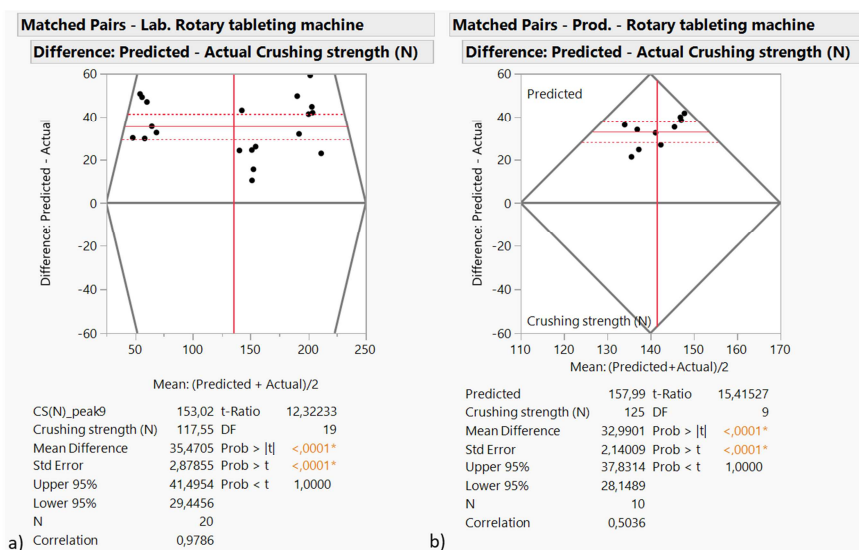


Figure 93 – Comparison between actual and predicted values of crushing strength, for laboratory tablets (a) and manufacturing tablets (b). Both groups of tablets were obtained with a rotary tableting machine.

A deeper investigation should be carried out in the future, in order to understand the observed difference. The developed NIR model should be revised, by expanding the calibration set, with addition of tablets made with a rotary tableting machine. An alternative option would be to develop another NIR model, dedicated to tablets manufactured by rotary machines.

4.3.3.3 Coating

Before planning a deeper study of the process, the possibility of monitoring the coating process with NIR was evaluated. Such exploratory investigation was necessary, as some difficulties are present and should be overcome, to perform a more structured experimental plan study. The final aim of the study was the in-line monitoring of the coating process, by measuring the tablet weight gain. However, it was not possible to place the MicroNIR instrument, as it is, inside the coating pan, because a too high temperature was present. Exposing the instrument to high temperature could cause instability in the measurement. If the present investigation turns out to be positive, a proper system to protect the MicroNIR from high temperature could be planned, in order to allow a continuous in-line monitoring, during the coating process. In the present study, the process was monitored by opening the coating pan, placing the MicroNIR probe into the tablet bed and making acquisitions with a manual scan mode (see section 4.2.2.1).

A laboratory batch (TFL2113) was prepared, as described in section 4.2.2.4. The data of the process are reported in Figure 94. The temperature of the bed of tablets was kept constant during the entire process. The spraying rate was set at 15 mL/min for the first 15 min of spraying and, then, increased to 20 mL/min. The theoretical weight gain per tablet (green line) was calculated considering the coating solution consumption and the amount of tablets. The actual weight gain (purple line) follows the trend of the theoretical one.

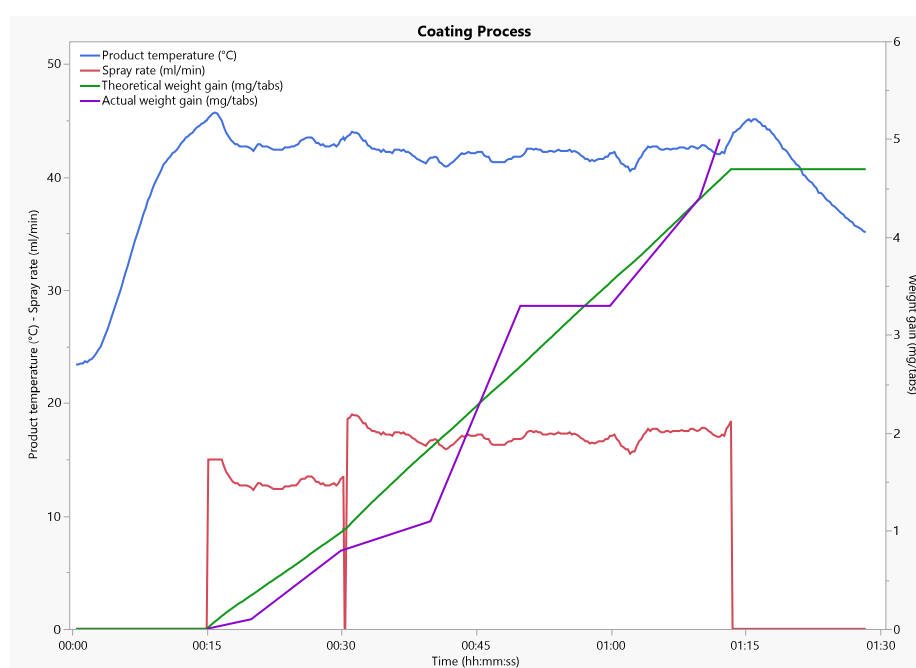


Figure 94 – Coating process data. Theoretical and actual weight gain.

At different, pre-defined time intervals (5, 10, 15, 25, 35, 45, 55 and 57 min) the coating pan was opened, to make NIR acquisitions and to take a sample of about 30 tablets. All the tablets were weighted and the weight gain is evident in Figure 95.

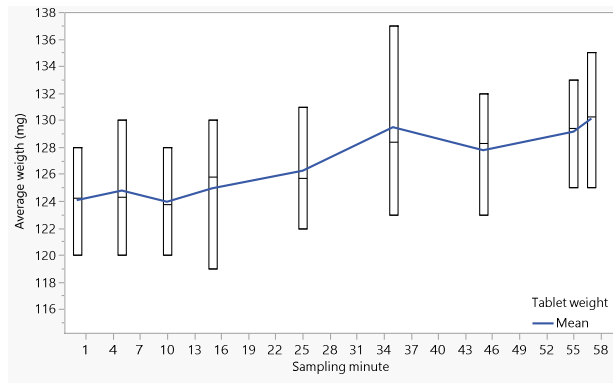


Figure 95 – Tablet weight gain of the sampled tablets.

The spectral data were pre-treated with the Savitzky-Golay first derivative of 3rd polynomial order and 13 smoothing points (Der1(3,13)), which is the same pre-processing setting used for model building. The pre-treated spectra are reported in Figure 96. The same spectral organization, according to the weight gain gradient, can be seen, indicating a good distinction between spectra corresponding to samples of different weight.

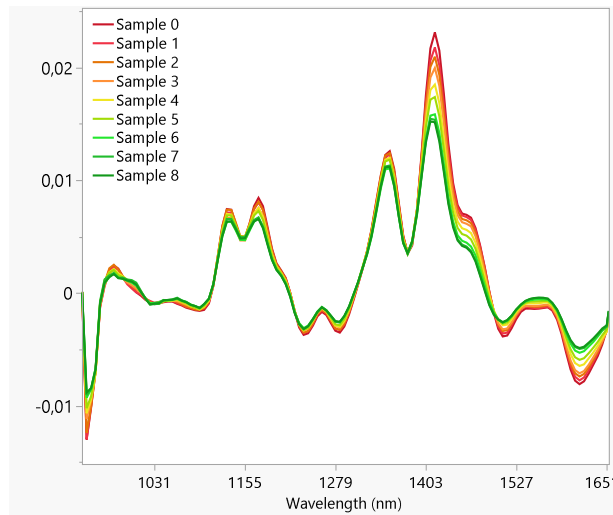


Figure 96 – Spectra pre-treated with Der1(3,13). The gradual passage from red coloured to green coloured spectra corresponds to the gradual weight gain.

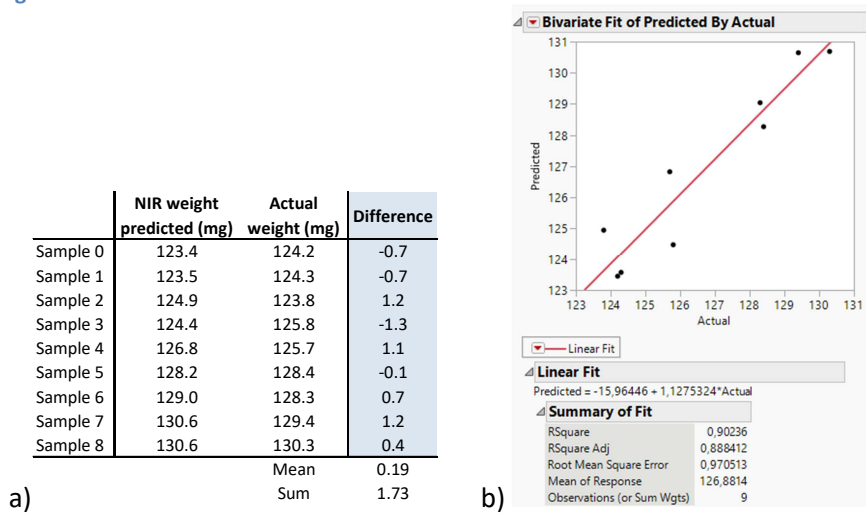


Figure 97 – a) Table of actual and predicted weight. The difference between actual and predicted weight is highlighted. b) Actual versus predicted plot. The relation shows a good R² and a low RMSE.

The previously developed model (see section 4.3.2.5) was used to predict the weight increase, corresponding to each single analysis of the process. The comparison between the predicted weight values and the actual averaged value is reported in Figure 97a. The difference calculated between the actual and the predicted values of weight of the tablets is about the zero, while the sum of all the differences, equal to 1.73, indicates that the model have a little overestimation of the weight results. The good agreement of actual and predicted results is represented by the linear fit in Figure 97b. The linear fit has a R^2 of 0.9 and a RMSE of 0.97 and the points are almost along the fitting line, especially for the samples taken in the final minutes.

In conclusion, the PLS model developed for the coating monitoring showed good results on predicting the tablet weight increase of a laboratory batch. Therefore, the exploratory investigation made to verify the possibility of using a quantitative NIR method for in-line monitoring the coating process, gave good and promising results. The work could then move on, by planning an in-line monitoring system and a deeper study of the coating process.

Conclusions

With the present work, the bilastine tablets manufacturing process, previously developed with a traditional approach, was studied and completely characterized in terms of Quality by Design. New knowledge about the product and the process was gained. The mixing and tableting process parameters that could be critical for the finished product quality were identified, with a risk assessment. The effect of their variation on the product quality was evaluated, with a Design of Experiment (DoE) strategy. In particular, for the mixing process it was not possible to define a design space, as the factors' variation, in the investigated range of values, did not affect the final tablet quality. Rather, it was assured that the current mixing process setting is not critical for product quality. For the tableting parameters, a knowledge space, an acceptable proven range and a normal operative range were defined. In particular, the compaction force was found to be the most critical process parameter.

Some spectroscopic analytical tools were developed, to satisfy the QbD requirements of real time process controls. The MBSD qualitative analysis was applied for mixing monitoring. It was used in combination with a quantitative method for drug assay determination in mixtures, in order to assure the blend homogeneity and the correct API concentration, at the end of the mixing process. The results of these studies have been already published¹².

Tablets drug assay and crushing strength were predicted with two independent NIR quantitative models; such models represent an alternative to the destructive HPLC analysis and diametral compression test, respectively. All the developed analytical tools gave good results, when applied for prediction on new samples, with the exception of crushing strength. This last model was able to give a reliable prediction only on tablets manufactured with the alternative manual tableting machine.

The possibility of in-line following the coating process by monitoring it with NIR was successfully verified, by the development of a simple quantitative NIR model for coating thickness monitoring.

In conclusion, the QbD characterization of bilastine tablets manufacturing process was realized and the PAT tools were successfully applied for real time monitoring of the process and for non destructive product characterization. Future studies should focus on the proper study of the coating process and on the improvement of the quantitative model for crushing strength determination.

References

- (1) Friedrich, D. M.; Hulse, C. A.; von Gunten, M.; Williamson, E. P.; Pederson, C. G.; O'Brien, N. A. Miniature near-infrared spectrometer for point-of-use chemical analysis. *Photonic Instrum. Eng.* **2014**, *8992*, 899203. <https://doi.org/10.1117/12.2040669>.
- (2) Garthwaite, P. H. An Interpretation of Partial Least Squares. *J. Am. Stat. Assoc.* **1994**, *89* (425), 122–127.
- (3) Geladi, P.; Kowalski, B. R. Partial least-squares regression: a tutorial. *Anal. Chim. Acta* **1986**, *185*, 1–17.
- (4) Croce, R.; Malegori, C.; Oliveri, P.; Medici, I.; Cavaglioni, A.; Rossi, C. Prediction of quality parameters in straw wine by means of FT-IR spectroscopy combined with multivariate data processing. *Food Chem.* **2020**, *305* (September 2019), 125512. <https://doi.org/10.1016/j.foodchem.2019.125512>.
- (5) Sekulic, S. S.; Ward, H. W.; Brannegan, D. R.; Stanley, E. D.; Evans, C. L.; Sciavolino, S. T.; Hailey, P. A.; Aldridge, P. K. On-line monitoring of powder blend homogeneity by near-infrared spectroscopy. *Anal. Chem.* **1996**, *68* (3), 509–513. <https://doi.org/10.1021/ac950964m>.
- (6) ICH Harmonized Tripartite Guideline. Quality Risk Management Q9 [https://database.ich.org/sites/default/files/Q9 Guideline.pdf](https://database.ich.org/sites/default/files/Q9_Guideline.pdf) (accessed Aug 11, 2021).
- (7) ICH Harmonized Tripartite Guideline. Pharmaceutical Development Q8 (R2) [https://database.ich.org/sites/default/files/Q8%28R2%29 Guideline.pdf](https://database.ich.org/sites/default/files/Q8%28R2%29_Guideline.pdf) (accessed Aug 11, 2021).
- (8) Esbensen, K. H.; Román-Ospino, A. D.; Sanchez, A.; Romañach, R. J. Adequacy and verifiability of pharmaceutical mixtures and dose units by variographic analysis (theory of sampling) - A call for a regulatory paradigm shift. *Int. J. Pharm.* **2016**, *499* (1–2), 156–174. <https://doi.org/10.1016/j.ijpharm.2015.12.038>.
- (9) Brereton, R. G. *Applied Chemometrics for Scientists*; John Wiley & Sons, Ltd, 2007.
- (10) Oliveri, P.; Malegori, C.; Simonetti, R.; Casale, M. The impact of signal pre-processing on the final interpretation of analytical outcomes - A tutorial. *Anal. Chim. Acta* **2019**, *1058*, 9–17. <https://doi.org/10.1016/j.aca.2018.10.055>.
- (11) Chalayudth, P. Establishing acceptance limits for uniformity of dosage units: part 1. *Pharm. Technol.* **2016**, *40* (12), 34–43.
- (12) Biagi, D.; Nencioni, P.; Valleri, M.; Calamassi, N.; Mura, P. Development of a Near Infrared Spectroscopy method for the in-line quantitative bilastine drug determination during pharmaceutical powders blending. *J. Pharm. Biomed. Anal.* **2021**, *204*, 1144277. <https://doi.org/10.1016/j.jpba.2021.1144277>.
- (13) Short, S. M.; Cogdill, R. P.; Wildfong, P. L. D.; Drennen, J. K.; Anderson, C. A. A near-infrared spectroscopic investigation of relative density and crushing strength in four-component compacts. *J. Pharm. Sci.* **2009**, *98* (3), 3–8. <https://doi.org/10.1002/jps>.
- (14) Blanco, M.; Alcalá, M.; Gonzalez, J. M.; Torras, E. A process analytical technology approach based on near infrared spectroscopy: tablet hardness, content uniformity, and dissolution test measurements of intact tablets. *J. Pharm. Sci.* **2006**, *95* (10), 2137–2144. <https://doi.org/10.1002/jps>.
- (15) Otsuka, M.; Yamane, I. Prediction of tablet hardness based on near infrared spectra of raw mixed

powders by chemometrics. *J. Pharm. Sci.* **2006**, *95* (7), 1425–1433. <https://doi.org/10.1002/jps>.

- (16) *Pharmaceutical Dosage Forms: Tablets*; Lieberman, H. A., Lachman, L., Schwartz, B., Eds.; Marcel Dekker Inc.: New York, 1990.
- (17) Muzzio, F. J.; Robinson, P.; Wightman, C.; Brone, D. Sampling practices in powder blending. *Int. J. Pharm.* **1997**, *155*, 153–178.
- (18) Muzzio, F. J.; Goodridge, C. L.; Alexander, A.; Arratia, P.; Yang, H.; Sudah, O.; Mergen, G. Sampling and characterization of pharmaceutical powders and granular blends. *Int. J. Pharm.* **2003**, *250*, 51–64.
- (19) Berntsson, O.; Danielsson, L.; Lagerholm, B.; Folestad, S. Quantitative in-line monitoring of powder blending by near infrared reflection spectroscopy. *Powder Technol.* **2002**, *123*, 185–193.
- (20) Sierra-Vega, N. O.; Martínez-Cartagena, P. A.; Alvarado-Hernández, B. B.; Romañach, R. J.; Méndez, R. In-line monitoring of low drug concentration of flowing powders in a new sampler device. *Int. J. Pharm.* **2020**, *583* (February), 119358. <https://doi.org/10.1016/j.ijpharm.2020.119358>.
- (21) Sun, C. C. A novel method for deriving true density of pharmaceutical solids including hydrates and water-containing powders. *J. Pharm. Sci.* **2004**, *93* (3), 646–653.
- (22) Heckel, R. W. Density-pressure relationships in powder compaction. *Trans. Metall. Soc. AIME* **1961**, *221* (4), 671–675.
- (23) Kawakita, K.; Ludde, K.H. Some consideration on powder compression equations. *Powder Technol.* **1970**, *4* (2), 61–68.
- (24) Ryshkewitch, E. Compression strength of porous sintered alumina and zirconia. *J. Am. Ceram. Soc.* **1953**, *36* (2), 65–68.
- (25) Tye, C. K.; Sun, C. C.; Amidon, G. E. Evaluation of the effects of tableting speed on the relationships between compaction pressure, tablet tensile strength, and tablet solid fraction. *J. Pharm. Sci.* **2005**, *94* (3), 465–472. <https://doi.org/10.1002/jps.20262>.

5. DEXKETOPROFEN

TROMETAMOL

PROJECT

Dexketoprofen Trometamol characterization studies

In addition to the main project, a second one was carried out. It represents a continuation of the project previously started, in occasion of the graduation thesis¹.

The considered study was about the manufacturing process transformation, from wet granulation (WG) to direct compression (DC) of dexketoprofen trometamol (DXKPT) tablets. A formulation study was performed, in order to find a suitable ingredient composition for direct compression. The final selected formulation is reported in Table 1.

Composition	x 1 tab (mg)	%
Dexketoprofen trometamol	37.5	12.5
Anhydrous Lactose (SuperTab 24AN)	132.3	44.1
Microcrystalline Cellulose Low Moisture (LM200)	88.2	29.4
Sodium starch glycolate	15.0	5.0
Magnesium stearate	9.0	3.0
Talc	15.0	5.0
Colloidal silicon dioxide (Aerosil 200VV)	3.0	1.0
	300.00	100.0

Table 1 – Composition for DC, defined with the previous thesis work.

Tablets with the formulation defined in Table 1 were made and analysed. In particular, they were tested for dissolution time and the results were compared with the dissolution time of a reference, i.e. the tablets currently obtained by WG. This comparison was done according to the EMEA Guideline on the investigation of bioequivalence², by evaluating the drug dissolution rate from the tablets at different pH values. Dissolution profiles from the new tablets at pH=4.5 and pH=7.5 (Figure 1b and Figure 1c, respectively) were similar to that from the reference ones and meet the specifications (% API > 75% in 20 min), while the profile at pH=1.2 was not (Figure 1a). In this case, tablets obtained with DC showed a lower drug dissolution rate, with respect to the reference obtained with WG.

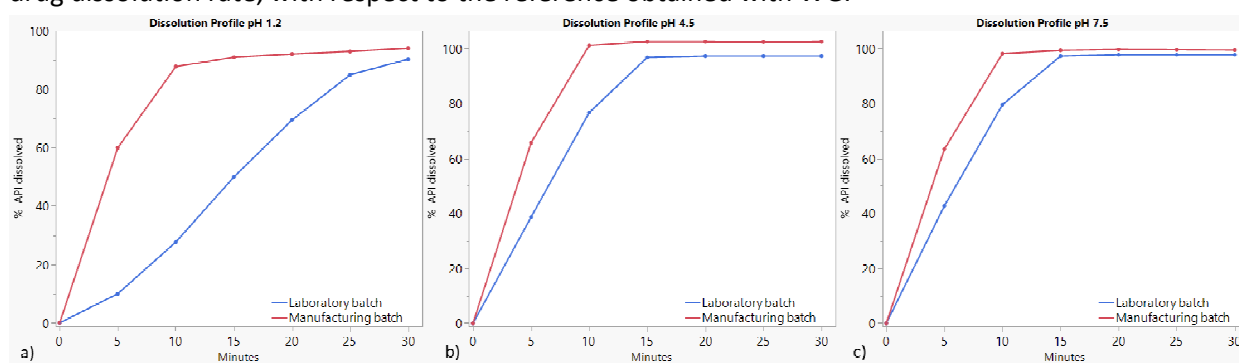


Figure 1 – Dissolution profiles comparison. a) pH = 1.2; b) pH=4.5; c) pH = 7.5. Manufacturing batch in red, laboratory batch in blue.

The cause of such unexpected behaviour was investigated. Literature data about DXKPT manufacturing reported the occurrence of a polymorphic transition of the API during the WG, but not during the DC process³. XRPD and DSC analysis demonstrated the amorphous nature of the form obtained from WG.

Considering what highlighted in this study, the different behaviour of the dissolution profiles could be attributed to the different manufacturing process (DC instead of WG). In particular, WG would lead to the modification of DKPT from solid crystalline to amorphous form and it is well known the higher dissolution rate of amorphous compounds, respect to the corresponding crystalline form. The API solubilisation is followed by its recrystallization on MCC support. One possible reason for the different dissolution behaviour, relies on the formation of an amorphous, more soluble, form in the reference product. This would explain the lower drug dissolution rate for the tablet obtained with DC. Therefore, we firstly considered this hypothesis, as a possible explanation. However, in order to investigate the cause of the different dissolution behaviour, the two manufacturing processes were compared (Figure 2). Both share the same compression and coating step; the only difference relies on the wet granulation and drying steps, only presents in the WG process. Assuming that during DC no transformation occurs, the reason of the different behaviour should depend on the wet granulation step. The occurrence of a transformation of the drug solid state was hypothesized; however, the nature of such transformation needs to be clarified. A series of studies were performed with this purpose.

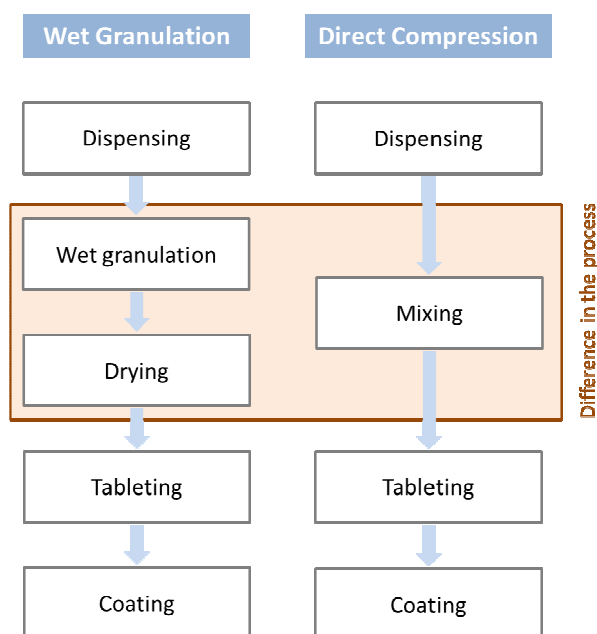


Figure 2 – Flow chart of WG and DC process; their difference is highlighted.

The DXKPT salt was, for the first time, synthesized in 1997, with a patent publication⁴. Only in 2007, the presence of polymorphism in DXKPT was disclosed, with a patent publication by Laboratorios Menarini S.A., Barcellona⁵. In particular, two polymorphic forms, denominated A and B, were synthesized and characterized with XRPD, IR and DSC. Characterization data are reported in Table 2, Figure 3 and Figure 4.

	Polymorph A	Polymorph B
Fusion peak	105.5-105.7	103.1-103.3
Onset	104.6-104.7	102.1-102.5
J/g values	125-135	110-120

Table 2 – DSC analysis on DXKPT-A and DXKPT-B. DSC was recorded between 80 and 120°C, with a heating rate of 1°C/min.

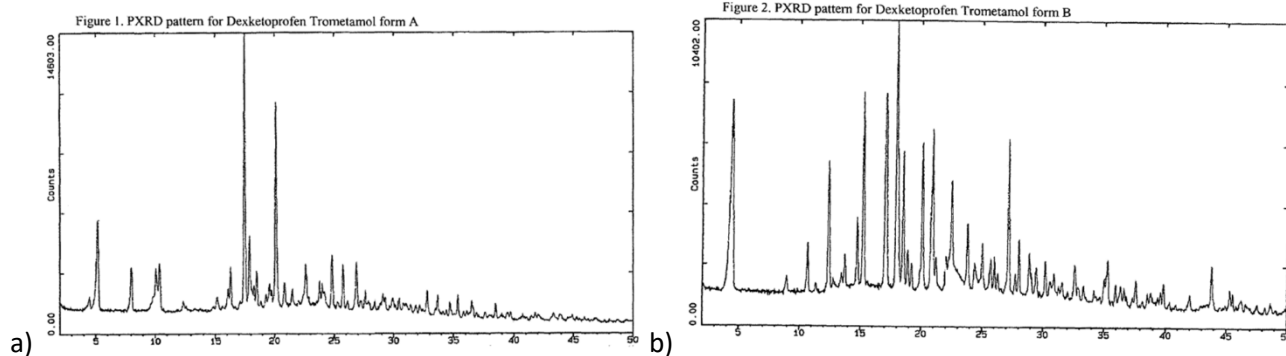


Figure 3 – XRPD of DXKPT polymorph form A (a) and polymorph form B (b).

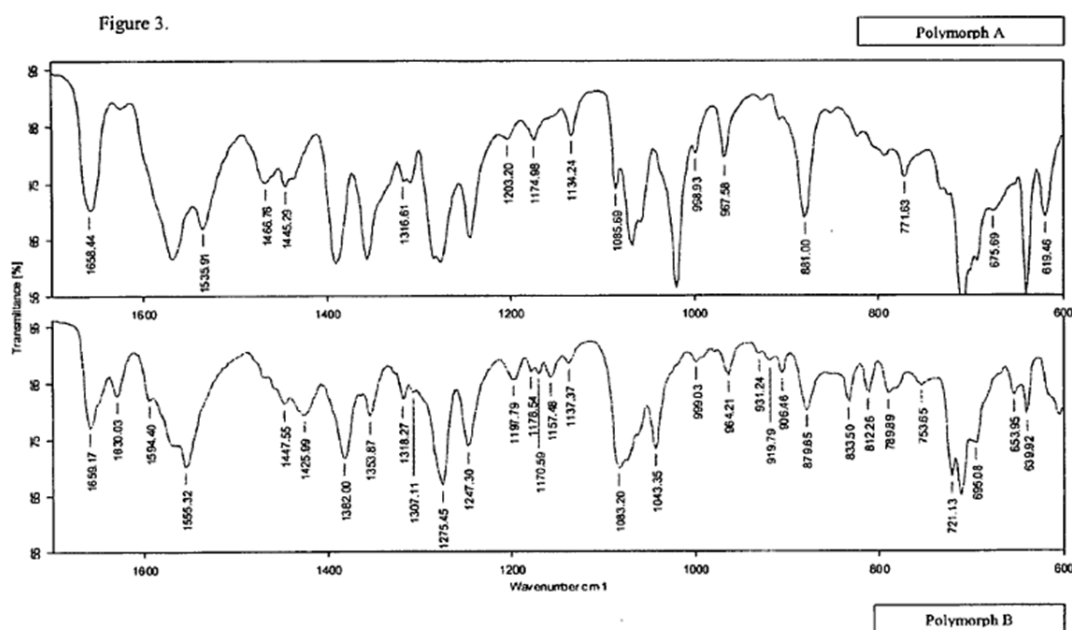


Figure 4 – IR of DXKPT polymorph A and B.

The polymorph A is the most stable form and the one employed in manufacturing. The polymorph B is metastable and tends to convert into the A stable form. The crystal structure of the racemic ketoprofen was available since 1990⁶, while the crystal structure of pure S-enantiomer, i.e. dexketoprofen, has been defined only in 2018 by Pawledzio et al., 2018⁷. As the polymorph A is predominant, respect to B, Pawledzio's crystal structure relates to the A polymorphic form. From the above cited works, the racemic compound was found to crystallize in the $P\bar{1}$ space group (triclinic lattice), with one molecule in the asymmetric unit. The S-enantiomeric (DXKPT-A) compound was found to crystallize in the $P2_12_12_1$ space group (orthorhombic lattice), with two independent molecules in the asymmetric unit. No literature's data about the crystal structure of the polymorph B were available. For that reason, a study was performed with this characterization aim by Rossi et al., 2019⁸. As the DXKPT-B form is not stable, it is quite hard to have it pure. In the proposed study, the highest content of DXKPT-B was obtained by crystallization with xylene; the identity of DXKPT-B was confirmed by a theoretical XRPD pattern, previously obtained from a single crystal X-ray determination. The results showed that DXKPT-B crystallizes in the space group $P2_1$ (monoclinic lattice), with two independent molecules in the asymmetric unit (Figure 5). These two independent molecules were similar to those of the DXKPT-A asymmetric unit. In fact, they overlap quite well in pairs. The main difference between the similar pair of molecules of DXKPT-A and DXKPT-B, concerns the carboxylic acid group orientation in one of the two molecules. The two independent molecules are

oriented in an antiparallel manner, in the crystal lattice. The aromatic ring interacts with hydrogen atoms of the CH of another aromatic ring, with CH $\cdots\pi$ interactions. The carboxylic acid group interacts with two identical molecules. The final result is a chain of identical molecules, held together by hydrogen bonds.

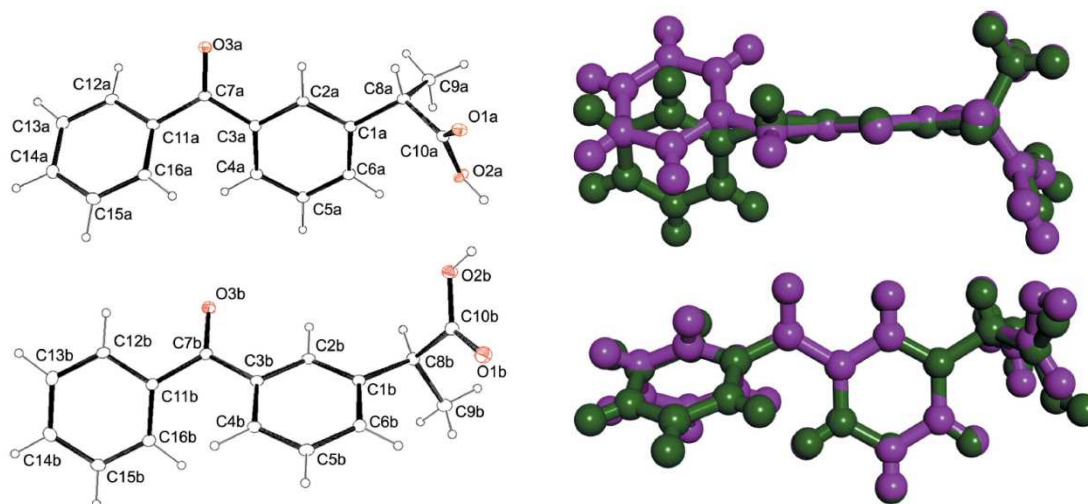


Figure 5 – Left picture: structure of the two independent molecules of the asymmetric unit of DXKPT-B. Right picture: superimposition of the two independent molecules (DXKPT molecule a in green and DXKPT molecule b in magenta).

As the transformation would occur during the WG, several hypotheses have been evaluated; in particular:

- 1) Occurrence of an amorphous transformation
- 2) Occurrence of a hydrated transformation

Amorphous transformation

The hypothesis of an amorphous transformation was taken into account, considering the work of Blanco et al., 2006³. In order to verify such hypothesis, some manufacturing (reference) and laboratory batches of DXKPT granules were prepared via WG and analysed with XRPD. The XRPD analysis of such samples showed a crystalline structure. However, the crystallinity degree was not equal to that of the pure API crystal; therefore, a small portion of amorphous compound was probably obtained.

The following samples have been analysed:

- pure API powder;
- placebo mixture (not granulated);
- physical mixture of the ingredients (not granulated);
- reference manufacturing batch: 7145395 (granulated);
- reference manufacturing batch: V9H025 (granulated);
- two laboratory batches (granulated)

The pure API raw material XRPD spectrum is superimposable with the one of polymorph form A (Figure 6, left picture); the DSC curve showed an endothermic melting peak comparable to that of the polymorphic form A (Figure 6, right picture). It can be concluded and confirmed that the API corresponds to the DXKPT polymorphic form A.

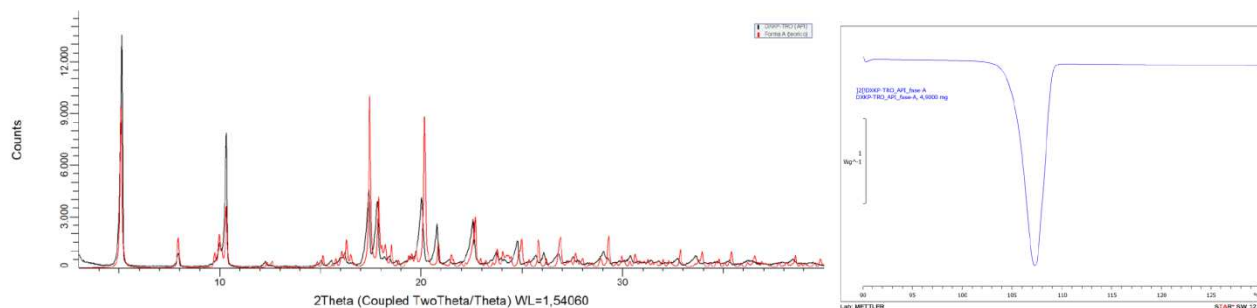


Figure 6 – Left picture: XRPD spectra of pure DXKPT API powder (in black) compared with the XRPD reference pattern of the polymorph A (in red). Right picture: DSC curve of the pure API powder sample.

The placebo mixture did not present the crystallinity peaks typical of DXKPT-A and DXKPT-B (Figure 7, left picture). On the contrary, the physical mixture showed the same peaks of the pure API powder, confirming the presence of unaltered DXKPT-A (Figure 7, left picture).

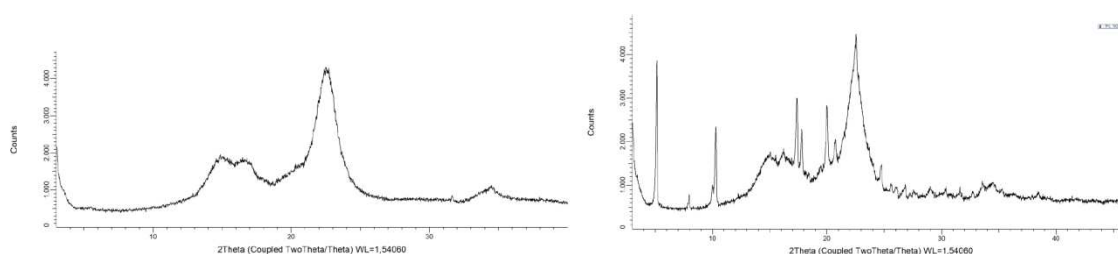


Figure 7 – Left picture: XRPD of placebo mixture. Right picture: XRPD of the physical mixture of all the ingredients.

The XRPD spectra of the reference manufacturing batch 7145395 (Figure 8, left picture) and V9H025 (Figure 8, right picture) were superimposable with that of the pure API spectrum, thus it is confirmed the presence of DXKPT-A. However, a small peak, not present in the pure API spectrum, nor in the placebo formulation, could be attributed to the polymorph DXKPT-B. Two granulated batches were also prepared, with laboratory equipment, able to replicate the manufacturing conditions. The comparison of their XRPD spectra with those of placebo mixture and pure API, highlighted, also in this case, the presence of crystalline DXKPT-A form (Figure 9).

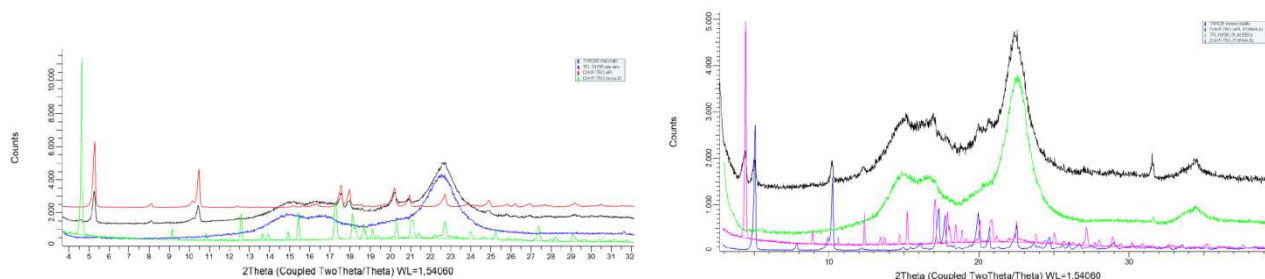


Figure 8 – Left picture: Production batch (7145395) in black, pure DXKPT in red, pure polymorphic form B in green and mixture of placebo in blue. Right picture: Production batch (V9H025) in black, pure DXKPT in blue, pure polymorphic form B in purple and mixture of placebo in green.

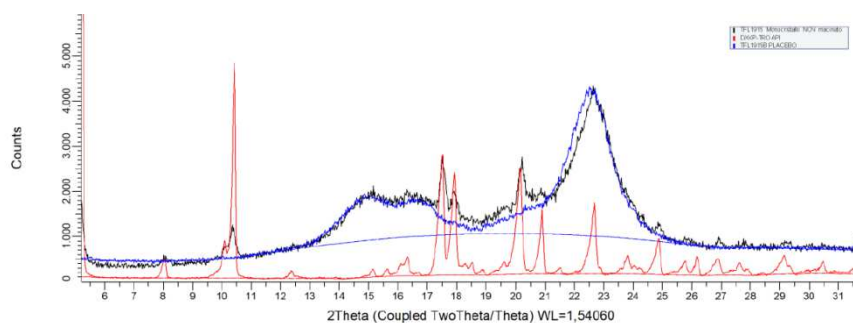


Figure 9 – Laboratory granulated batch (TFL1915) in black, pure API in red and placebo mixture in blue.

The presented results seem to contrast with the results of Blanco et al., 2006³. However, this could be explained by considering that different laboratory equipment were used. In particular, the laboratory equipment used in the present work was able to replicate the manufacturing conditions very good.

When investigating the effect of the granulation process on the formulation, an additional observation was made. A physical mixture of all the ingredients was prepared and compared with the manufacturing reference and laboratory granulates (Figure 10). It is evident that the physical mixture spectrum presents more intense and sharper peaks, with respect to the granulated batches. Such observation could confirm a partial transformation of the drug into the amorphous form. However, in this case, the amorphisation was not so predominant and immediately evident, as it was in the work of Blanco et al., 2006³.

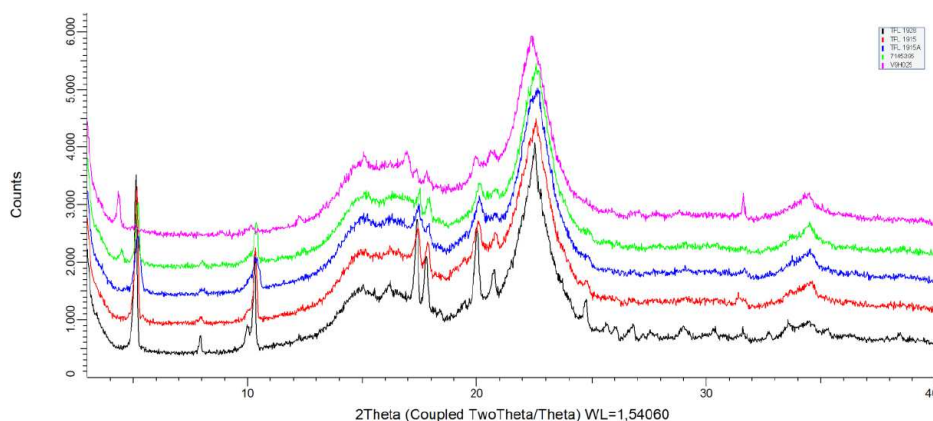


Figure 10 – Comparison between the physical mixture (black), manufacturing reference granulate: 7145395 (green), V9H025 (purple) and the two laboratory granulates (red and blue).

All the batches previously analysed with XRPD, were also analysed with DSC, in order to confirm the partial drug amorphization. The results are shown in Figure 11. The drug fusion peak was present in all the batches, but it was clearly less intense, not only with respect to that of pure API, but also to that of the simple physical mixture. This observation confirmed the hypothesis of partial drug amorphization in the batches. Moreover, in the DSC curve of the two manufacturing batches, a second peak compatible with fusion of the B polymorphic form of DXKPT is observed, confirming XRPD observations. This second peak is more evident in the V9H025 batch (Figure 11e), while in the DSC of batch 7145395 (Figure 11d) it is not well separated from the peak of the A form.

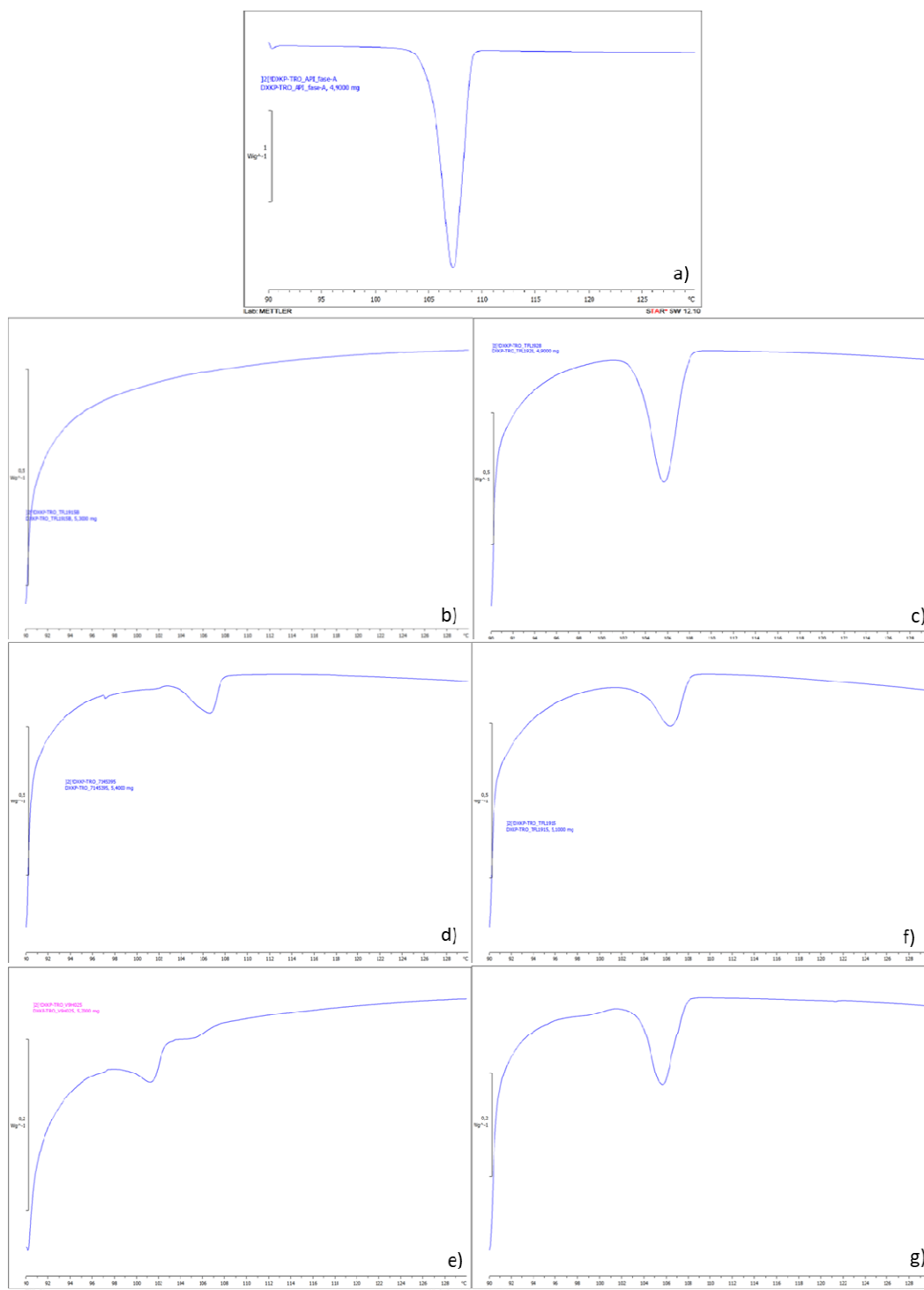


Figure 11 – DSC of pure DXKPT API powder (a), placebo powder mixture (b), physical mixture (c) manufacturing granulated batch 7145395 (d), manufacturing granulated batch V9H025 (e), and laboratory granulated batches (f and g).

Hydrated transformation

The second considered hypothesis concerns the formation of a hydrated form of DXKPT. A second study was planned by Rossi et al., 2020⁹, in order to investigate such aspects. It was firstly observed that DXKPT-A was stable to water up-take, when placed in a high humidity environment. In particular, it was stable for 30 days, kept in a close-chamber at 75% relative humidity. However, when the water was added dropwise, DXKPT-A quickly hydrated. To study the DXKPT-A behaviour, in presence of water, some samples

were prepared, by adding water in different stoichiometric ratios to the powder mixture. A total of 7 samples were prepared, by adding from 1 to 7 equivalents of water. When adding 2 or more water equivalents, the same XRPD pattern was always obtained. When adding just 1 equivalent of water, a mixture of anhydrous and hydrated form was obtained; in this case the hydrated form showed the same pattern obtained from the other samples. These results suggest the formation of a dihydrated compound. Observing the spectrum at different time points (before water addition, after 3h, 24h and 30 days), the crystallinity peaks are always present (Figure 12); therefore, the hydration transformation never involves the amorphisation of the sample.

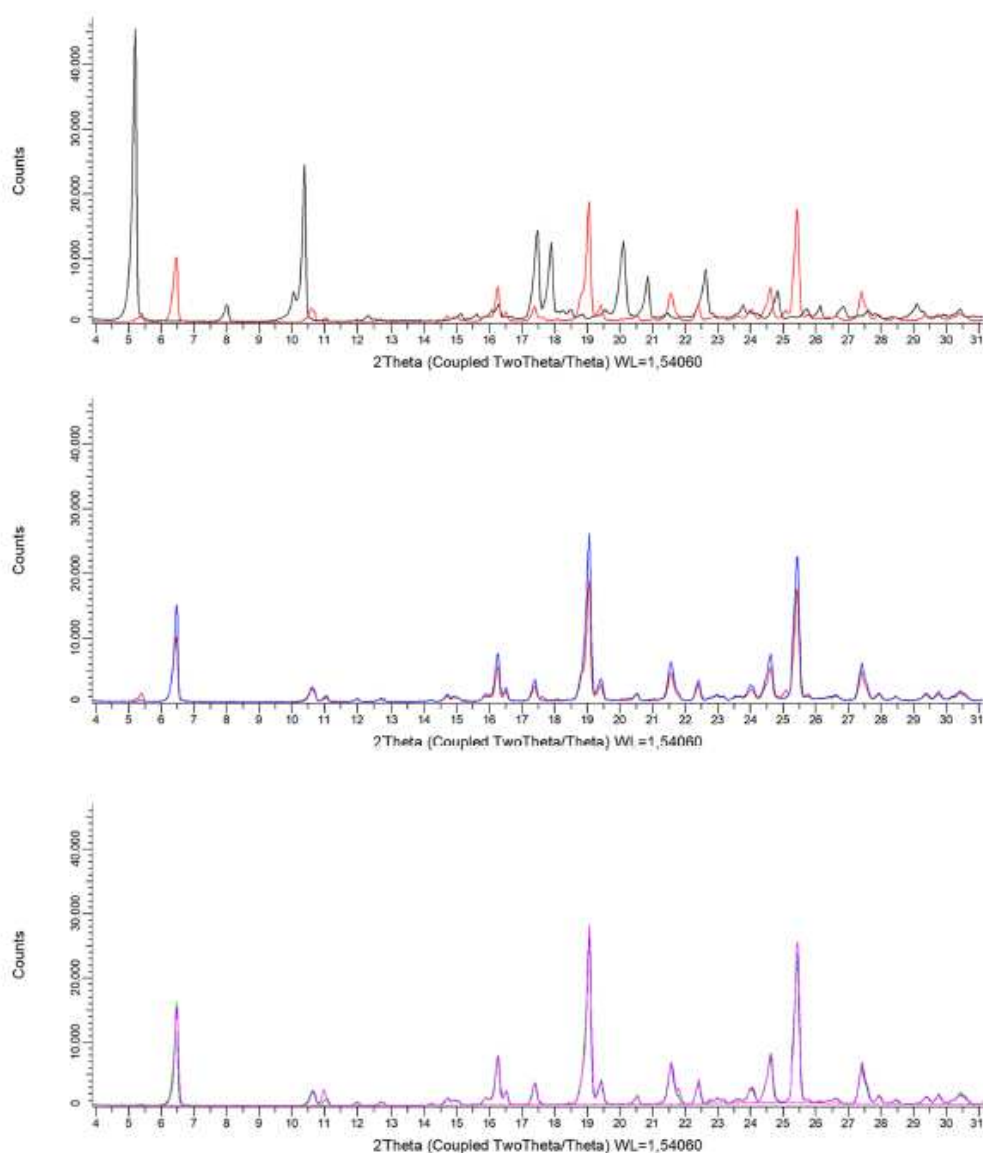


Figure 12 – XRPD spectra of the hydrated DXKPT sample (DXKPT:H₂O ratio is 1:4) at different time points. Top picture: anhydrous DXKPT-A (black) and spectrum after water addition (red). Middle picture: spectrum after water addition (red) and after 3h (blue). Bottom picture: spectrum after 3h (blue), after 24h (green) and after 30 days (purple).

To confirm such hypothesis, DXKPT was granulated with water, without addition of other excipients. The obtained sample was analysed with XRPD. The typical DXKPT-A crystallinity peaks are visible in the spectrum, but an additional peak at $2\theta=6.5$ indicates the presence of the dihydrated form, as confirmed by the comparison with the spectra of the known hydrated DXKPT form (Figure 13).

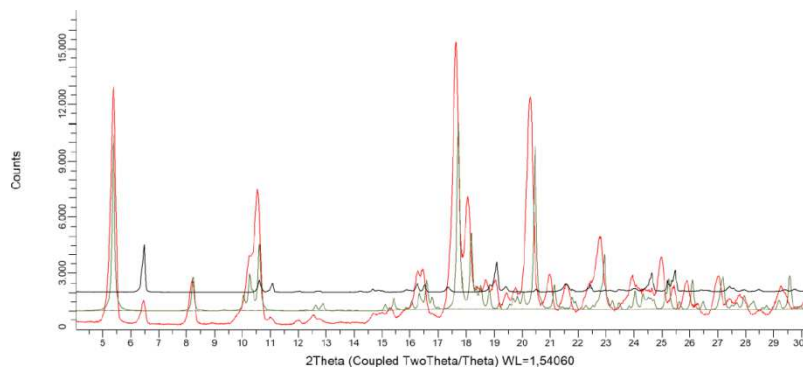


Figure 13 – PDRX of DXKPT granulated with water (red), reference DXKPT trometamol (green) and hydrated DXKPT trometamol (black).

In conclusion, some investigations were made in order to explain a discrepancy in the dissolution profiles of DXKPT tablets obtained via DC, with respect to those obtained via WG.

The first considered hypothesis, of amorphous transformation was confirmed, even if it actually occurs only in small amount, as demonstrated by the XRPD and DSC results. The presence of excipients (MCC in particular) is necessary for the transformation to occur. In fact, when performed a granulation without excipients the dehydrated form was obtained, instead of the amorphous one. In addition, the amorphous forms are more soluble than the correspondent crystalline forms, while the hydrated form are, generally, less soluble.

Such consideration brings to exclude the hydration transformation hypothesis as the possible cause of the different drug dissolution behaviour observed between tablets obtained by WG or DC. In fact, the reference granulated tablets exhibited a faster dissolution rate (and thus a higher solubility), respect to those obtained with DC. The presence of a hydrated form is not compatible with the higher solubility, while the presence of a partial drug amorphization perfectly explains it.

References

- (1) Biagi, D. Studio per la trasformazione del processo produttivo, da granulazione ad umido a compressione diretta, di compresse a base di dexketopropene trometamolo, University of Florence, 2018.
- (2) Agency European Medicines. *Guideline on the Investigation of Bioequivalence*; 2010 https://www.ema.europa.eu/en/documents/scientific-guideline/guideline-investigation-bioequivalence-rev1_en.pdf (accessed Sep 24, 2021).
- (3) Blanco, M.; Alcalá, M.; González, J. M.; Torras, E. Near infrared spectroscopy in the study of polymorphic transformations. *Anal. Chim. Acta* **2006**, *567* (2), 262–268. <https://doi.org/10.1016/j.aca.2006.03.036>.
- (4) Farshi, F.; Soylemez, S.; Koc, F.; Durmus, S. A process for preparing dexketoprofen trometamol form A and B crystals, 2009.
- (5) Bosch, M.; Mannucci, S.; Torras, E.; Falorni, R.; Gonzales, J. M. Polymorphic forms of dexketoprofen trometamol, preparation and pharmaceutical compositions thereof, 2007.
- (6) Briard, P.; Rossi, J. C. Kétoprofène. *Acta Cryst.* **1990**, *C46* (6), 1036–1038. <https://doi.org/10.1107/s0108270189004968>.
- (7) Pawledzio, S.; Makal, A.; Trzybiński, D.; Woźniak, K. Crystal structure, interaction energies and experimental electron density of the popular drug ketoprofen. *IUCrJ* **2018**, *5*, 841–853. <https://doi.org/10.1107/S2052252518013222>.
- (8) Rossi, P.; Paoli, P.; Ienco, A.; Biagi, D.; Valleri, M.; Conti, L. A new crystal form of the NSAID dexketoprofen. *Acta Cryst.* **2019**, *C75* (C75), 783–792. <https://doi.org/10.1107/S2053229619006533>.
- (9) Rossi, P.; Paoli, P.; Chelazzi, L.; Milazzo, S.; Biagi, D.; Valleri, M.; Ienco, A.; Valtancoli, B.; Conti, L. Relationships between anhydrous and solvated species of dexketoprofen trometamol: a solid-state point of view. *Cryst. Growth Des.* **2020**, *20* (20), 226–236. <https://doi.org/10.1021/acs.cgd.9b01030>.